Characterization of Nicotinic Acid Adenine Dinucleotide Phosphate (NAADP) Binding Proteins

Danni Zhu

Wolfson College

University of Oxford

A thesis submitted for the degree of

Doctor of Philosophy

Michaelmas 2018

Acknowledgement

This project could not have been successful without the help and support from many friends and colleagues. First, I would like to thank Professor Antony Galione for his mentorship and support all along, without which this project would be impossible. I am also grateful to people from Galione group and those around the department for their help. Special thanks go to Dr. Andy Lam for his valuable advice, Clive Garnham for his excellent technical support, James Bae for helping me with virtual screening and Dr. Sam Wee Khang Lin for his jack-of-all-trade 360 degrees support and companionship, both in science and in life.

I am also in debt with my numerous collaborators in Oxford and Shanghai. I would like to thank my Oxonian fellows Ming Gao, Hang Xu and Dr. Yifan Liu for helping me with NMR. My greatest gratitude goes to my collaborators in Shanghai, Dr. Bin Meng, Wu Meng, Professor Xiaolong Liu and Professor Zhijie Liu, for their help in characterizing the binding protein candidates. I am forever grateful to Dr. Yuwen Zeng, for his expertise, constructive discussion and his encouragement and support during my most difficult time.

I would also like to take this chance to thank all my friends for their companionship during my DPhil. During my time in Oxford I particularly enjoyed the regular tea sessions and Bodrum kebab trips with Faizzan and Alaa, and our witty and hilarious conversations. A big thank you to all my friends around Oxford: Ken, Maysa, Yegor, Jae, Dhivina, Mihno, Kyoko, Haruko, Cheng and Qian, Kate and Fang, Yi and Angelina, Angie, Glenn, Fusheng, Shaoyang, Hayley, and my wonderful housemates Yifei, Tilly and Jonny. Thank you so much for the camaraderie. I love you all.

Finally, I would like to express my immense gratitude to my parents, for their love and unwavering support.

Abstract

Nicotinic acid adenine dinucleotide phosphate (NAADP) is a potent intracellular second messenger capable of inducing calcium release from acidic organelles and is responsible for many important physiological activities. It has been recognized that an intermediate protein is required for NAADP to mediate its calcium-mobilizing effect through two-pore channels (TPCs). However, the identity of the intermediate NAADP binding protein remains unknown. This thesis aims to identify the elusive NAADP binding proteins to further elucidate the molecular mechanism of NAADP signalling pathway.

The first part of this thesis describes the characterization of NAADP binding protein using a chemistry approach, which includes crosslinking study in mouse embryonic fibroblasts (MEFs) and affinity isolation of binding protein via a NAADP affinity column. Crosslinking introduced significant interference to NAADP binding in MEFs. Radioligand binding assays revealed that NAADP binding in MEFs were predominantly in the membrane fraction and no high affinity binding site was detected. Affinity isolation of binding proteins by NAADP affinity columns was carried out using mouse liver cytosol. However, no high-affinity binding protein was isolated through this approach.

The second part of this thesis describes the identification of NAADP binding proteins via a combination of techniques including protein chromatography, photoaffinity labelling, mass spectrometry, virtual screen and label-free ligand binding assays. A sequential chromatography was conceived and optimized, which achieved a more than 2300-fold enrichment of high-affinity binding proteins. Photoaffinity labelling of the enriched fractions by [^{32}P]-5-azido-NAADP revealed a 27 kDa band in SDS-PAGE gel. Subsequent mass spectrometry analysis generated a list of 35 candidates. Virtual screening of candidates by AutoDock Vina and CLC Drug Discovery Workbench predicted Carbonyl Reductase 1 (CBR1), Thiopurine S-Methyltransferase (TPMT) and Cytochrome b5 Reductase 3 (CYB5R3) as promising NAADP binding protein candidates. Further experimental validation by bio-layer interferometry (BLI) and microscale thermophoresis (MST) confirmed that TPMT and CBR1 are NAADP binding proteins. CBR1 binds NAADP and NADP with similar affinities. On the other hand, TPMT showed higher affinity and high selectivity to NAADP as no binding of NADP was observed. The identification of NAADP binding protein suggests new possibility of NAADP functionality and may provide new insights into the mechanism of action of NAADP signalling pathways.

Contents

Abbreviation

AchR	Acetylcholine receptor
ADP	Adenosine diphosphate
ADPR	Adenosine diphosphate-ribose
ADPRP	Adenosine diphosphate-ribose-2'-phosphate
AMP	Adenosine monophosphate
AMPAR	α-amino-3-hydroxy-5-methyl-4-isoxazolepropionic acid receptor
AMPK	Adenosine monophosphate kinase
ATP	Adenosine triphosphate
BCA	Bicinchoninic acid
BLI	Bio-layer interferometry
BSA	Bovine serum albumin
cADPR	Cyclic ADP-ribose
cADPRP	Cyclic adenosine diphosphate-ribose
CAMKII	calmodulin-dependent kinase II
CBR1	Carbonyl reductase 1
CHAPS	3-[(3-cholamidopropyl)dimethylammonio]-1-propanesulfonate
C-IAA	Chloro-Iodoacetamide
CV	Column volume
CYB5R3	Cytochrome b5 reductase 3
DAG	Diacylglycerol
DEAE	Diethylaminoethyl
DKO	Double-knockout
DMEM	Dulbecco's Modified Eagle Medium
DMSO	Dimethyl sulfoxide
DNMT1	DNA methyltransferases 1
DPM	Disintegrations per minute
DSP	Dithiobis[succinimidylpropionate]
EC50	Half maximal effective concentration
EDTA	Ethylenediaminetetraacetic acid
ER/SR	Endo/Sarcoplasmic reticulum
FAD	Flavin adenine dinucleotide
FASP	Filter-aided sample preparation
FPLC	Fast protein liquid chromatography
GPCR	G-protein coupled receptor
GPN	Glycyl-L-phenylalanine 2-naphthylamide
GTP	Guanosine triphosphate
HA	Hemagglutinin
HIC	Hydrophobic interaction chromatography
HPLC	High performance liquid chromatography
IC_{50}	Half maximal inhibitory concentration

IEX	Ion-exchange chromatography
IMAC	Immobilized metal affinity chromatography
INMT	Indolethylamine N-methyltransferase
IP_3	Inositol-1,4,5-trisphosphate
IP_3R	IP_3 receptors
ITC	Isothermal titration calorimetry
LAMP	Lysosome-membrane associate protein
LC-MS	Liquid chromatography-mass spectrometry
LGCC	Ligand-gated calcium channel
LRRK2	Leucine-rich repeat kinase 2
MEF	Mouse embryonic fibroblast
MS	Mass spectrometry
MST	Micro-scale thermophoresis
MWCO	Molecular weight cut-off
NAAD	Nicotinic acid adenine dinucleotide
NAADP	Nicotinic acid adenine dinucleotide phosphate
NAD	Nicotinamide adenine dinucleotide
NADP	Nicotinamide adenine dinucleotide phosphate
NCX	Na^+/Ca^{2+} exchanger
NHS	N-Hydroxysuccinimide
NMDAR	N-methyl-D-aspartate receptor
NMR	Nuclear magnetic resonance
NPC1	Niemann-Pick disease type C1
PBS	Phosphate buffered saline
PEI	Polyethylenimine
$PI(3,5)P_2$	Phosphatidylinositol-3,5-bisphosphate
$PI(4,5)P_2$	Phosphatidylinositol-4,5-bisphosphate
PLC	Phospholipase C
PMCA	Plasma membrane Ca^{2+} ATPase
PPADS	Pyridoxalphosphate-6-azophenyl-2’4’-disulfonic acid
PPNDS	Pyridoxal-5-phosphate-6-(2-naphthylazo-6-nitro-4,8-disulfonate)
PRMT5	Protein arginine methyltransferases 5
RMSD	Root-mean-square deviation
RyR	Ryanodine receptor
SAH	S-adenosyl-L-homocysteine
SAM	S-adenosyl-L-methionine
SDS	Sodium dodecyl sulfate
SDS-PAGE	Sodium dodecyl sulfate polyacrylamide gel electrophoresis
SEC	Size-exclusion chromatography
SEM	Standard error mean
SERCA	Smooth endoplasmic reticular Ca^{2+} ATPase
SOC	Store-operated channel
SPR	Surface plasmon resonance

STIM	Stromal interaction molecule
TCEPERE	Tris(2-carboxyethyl)phosphine)
TEAB	Tetraethylammonium bromide
TEV	Tobacco etch virus
TFA	Trifluoroacetic acid
TGN	Thioguanine nucleotide
TLC	Thin layer chromatography
TPC	Two-pore channel
TPMT	Thiopurine S-methyltransferase
TRP	Transient receptor potential
UV	Ultraviolet
VGCC	Voltage-gated calcium channel
WT	Wild type

Chapter 1 Introduction

1.1. Calcium as a signalling messenger

Calcium is the fifth abundant element in humans and the majority is deposited in bones and teeth. The role of calcium as a signalling messenger was first discovered in 1883. While studying the contraction of isolated rat hearts, Ringer acknowledged the importance of including calcium salts into the medium, as saline made from distilled water cannot maintain the heartbeat as effectively as saline made from tap water (Ringer, 1883). Calcium is now recognized as an essential messenger that regulates a variety of cellular processes and functions such as exocytosis, muscle contraction, gene transcription and fertilization, etc. (Berridge *et al.*, 2003). Unlike many other signalling molecules which can be regulated by their synthesizing and degrading enzymes, calcium ions (Ca^{2+}) cannot be chemically altered and can easily precipitate with phosphate. Cells maintain intracellular Ca^{2+} concentrations at around 100 nM, mainly by three routes: extrusion of Ca^{2+} to extracellular space via various pumps and exchangers on the plasma membrane, buffering of Ca^{2+} via binding to numerous

calcium-binding proteins and Ca^{2+} compartmentalization into internal calcium storages (Clapham, 2007). This creates a concentration gradient across the membranes as Ca^{2+} concentration in intracellular storages and extracellular domain could be as high as millimolar level.

1.2. Calcium efflux

In cells, much of the energy is spent on maintaining a low cytoplasmic calcium concentration. Cytosolic Ca^{2+} can be translocated either to the extracellular domain via pumps and exchangers located on the plasma membrane, or into intracellular calcium storages through various mechanisms. The extrusion of Ca^{2+} into extracellular spaces is carried out primarily by plasma membrane Ca^{2+} ATPase (PMCA) and Na^{+}/Ca^{2+} exchanger (NCX). One ATP is hydrolyzed for each Ca^{2+} ion that PMCA transports, while NCX exchanges three Na^{+} ions inwards for every Ca^{2+} ion it extrudes (Carafoli, 1991; Blaustein and Lederer, 1999). PMCA possesses high affinity for Ca^{2+} ions but due to its relatively low transport capacity, it is more effective at maintaining a low cytoplasmic Ca^{2+} concentration in resting cells. The NCX, on the other hand, is of low affinity but high capacity and can rapidly expel Ca^{2+} in the event of a substantial cytosolic Ca^{2+} elevation (Carafoli, 1991; Carafoli et al., 2001).

Alternatively, Ca^{2+} can be compartmentalized into internal organelles that serve as intracellular calcium stores. For instance, smooth endoplasmic reticular Ca^{2+} ATPase (SERCA) is responsible for the calcium uptake of endo/sarcoplasmic reticulum (ER/SR), which hydrolyzes one ATP for every 2 Ca^{2+} ions that get pumped into the lumen of ER/SR meanwhile exchanges 2-3 protons as counterions (Yu *et al.*, 1993). Also, Ca^{2+}

can be transported into mitochondria through a Ca^{2+} uniporter located on the inner membrane of the mitochondria. The uniporter can be activated by mitochondrial membrane potential and possesses immense Ca^{2+} transport capacity as well as extreme affinity for Ca^{2+} ions (Kirichok *et al.*, 2004). Furthermore, it has been proposed that lysosomes also function as calcium stores in addition to their conventional role as digestive and recycling organelles, since it has been demonstrated that osmotic lysis of lysosomes by glycyl-L-phenylalanine 2-naphthylamide (GPN) would result in the elevation of cytosolic [Ca^{2+}] (Haller *et al.*, 1996). The presence of a putative Ca^{2+}/H^{+} antiporter, whose function as a Ca^{2+} transporter is dependent on the proton gradient maintained by V-type ATPase, has been suggested since inhibition of V-type ATPase with bafilomycin A1 has been shown to reduce lysosomal calcium content (Churchill *et al.*, 2002).

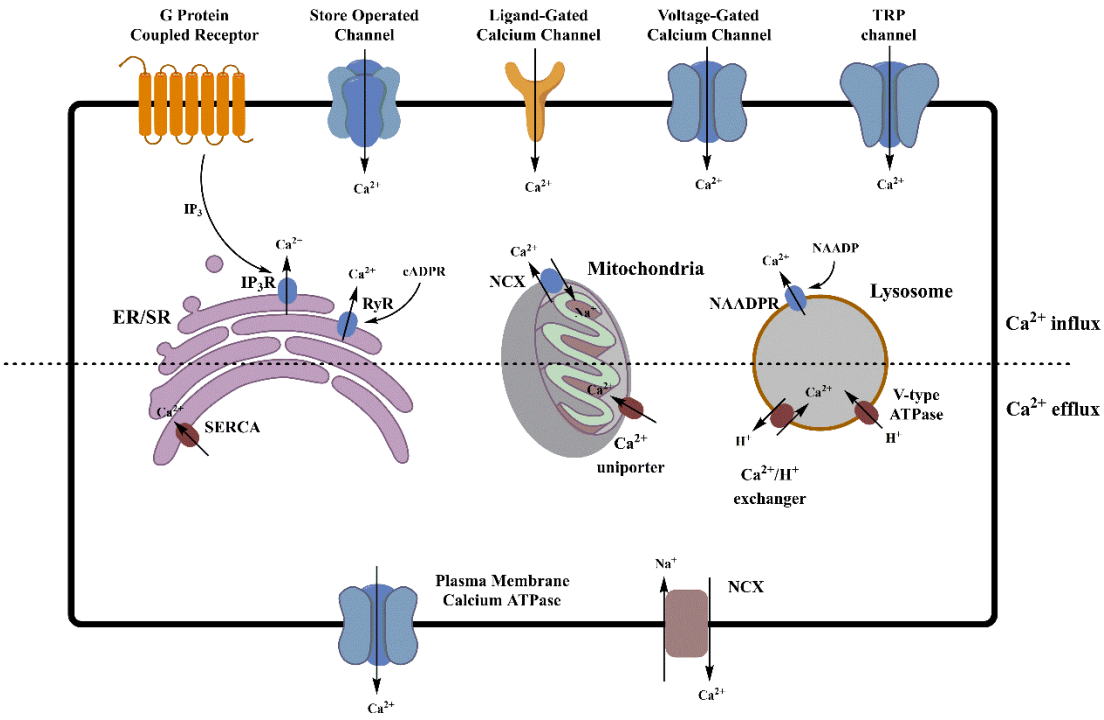

Figure 1.1. Simplified diagram of Ca^{2+} homeostasis regulation.

1.3. Calcium influx

1.3.1. Calcium influx via plasma membrane channels

Several classes of Ca^{2+} selective channels are present on the plasma membrane and readily conduct calcium influx in response to various physiological events. Voltage-Gated Calcium Channels (VGCCs) are triggered by changes of the plasma membrane potential and subsequently open up, initiating the movement of a vast number of Ca^{2+} ion down the concentration gradient that dramatically changes cytoplasmic [Ca^{2+}]. Another class of plasma membrane calcium channel is the Ligand-Gated Calcium Channels (LGCCs), which mediate extracellular Ca^{2+} entry upon binding of specific ligands such as neurotransmitters and growth factors. This includes, for example, α-amino-3-hydroxy-5-methyl-4-isoxazolepropionic acid receptor (AMPAR), N-methyl-D-aspartate receptor (NMDAR), P2X receptors and acetylcholine receptor (AchR) (Burnashev, 1998; Pankratov and Lalo, 2014). In addition, transient receptor potential (TRP) channel can be found on the plasma membrane in the form of tetramers and increases intracellular Na^{+} and Ca^{2+} in response to environmental stimulus such as temperature, pH, mechanical force and various chemicals (Ramsey *et al.*, 2006). Moreover, Store-Operated Channels (SOCs), typically Stim/Orai channel complex, induce Ca^{2+} influx in the event of ER calcium depletion. Situated on the ER membrane, STIM1 monitors ER lumen Ca^{2+} content and multimerizes when sensing exhaustion of luminal Ca^{2+}, which then migrates and couples to plasma membrane-bound Orai1 channel in proximity and initiates replenishment of ER Ca^{2+} content (Lewis, 2007).

1.3.2. Calcium influx via intracellular Ca^{2+}-mobilizing pathways

Mobilization of Ca^{2+} from intracellular calcium stores can be initiated by the activation of G-Protein Coupled Receptors (GPCRs) that are coupled with G_q or G_{11} protein, resulting in dissociation of the G proteins that trigger a downstream signalling pathway and eventually mediate Ca^{2+} release from intracellular stores via PLCβ. Alternatively, Ca^{2+} release from intracellular stores can be triggered by intracellular second messengers including inositol-1,4,5-trisphosphate (IP_3), cyclic ADP-ribose (cADPR), and nicotinic acid adenine dinucleotide phosphate (NAADP). IP_3 can be generated by a variety of phospholipase C while cADPR and NAADP are synthesized by ADP-ribosyl cyclase or CD38. Among them, NAADP emerged as the most potent second messenger that evokes Ca^{2+} release from novel intracellular calcium stores, the acidic organelles (i.e. endolysosomes), at low nanomolar concentration (Calcraft *et al.*, 2009).

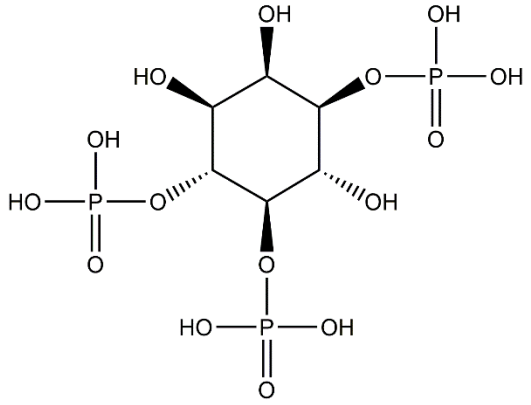

Inositol 1,4,5-triphosphate (IP_3)

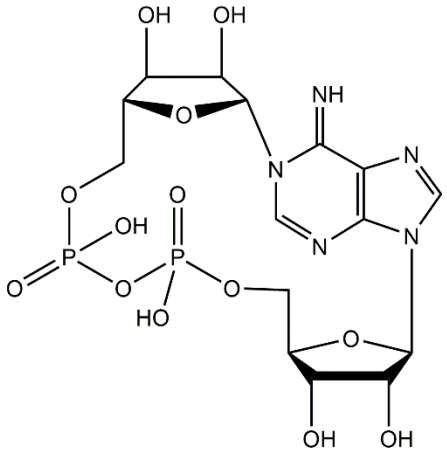

Cyclic ADP-ribose (cADPR)

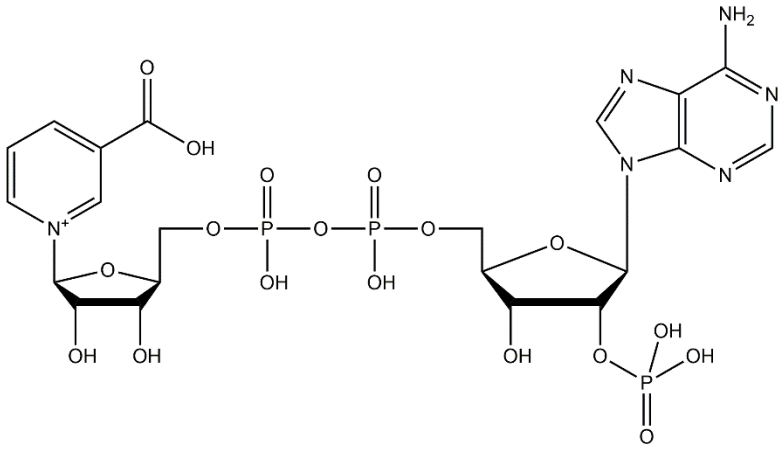

Nicotinic Acid Adenine Dinucleotide Phosphate (NAADP)

Figure 1.2. Structures of intracellular second messengers: inositol-1,4,5-trisphosphate (IP_3), cyclic ADP-ribose (cADPR) and nicotinic acid adenine dinucleotide phosphate (NAADP).

1.3.3. IP_3-mediated calcium signalling

1.3.3.1. Inositol-1,4,5-trisphosphate (IP_3)

Inositol-1,4,5-trisphosphate (IP_3) was the first identified calcium-mobilizing intracellular second messenger. The synthesis of IP_3 is carried out by phospholipase C (PLC) located on the plasma membrane. Several isoforms of PLC exist and are activated by different stimulus: PLCβ is activated by G_q and G_{11} protein dissociated from GPCR; PLCγ has been shown to be coupled with tyrosine-kinase-coupled receptors activation; PLCδ activation has been linked to cytosolic [Ca^{2+}] increase; PLCε responds to Ras activation; PLCζ, a recently discovered new isoform, has been involved in the generation of Ca^{2+} oscillations that are necessary for mammalian egg activation during fertilization (Berridge *et al.*, 2003; Kashir *et al.*, 2010). Activation of PLC results in hydrolysis of membrane-bound phosphatidylinositol-4,5-bisphosphate ($PI(4,5)P_2$), which produces IP_3 and diacylglycerol (DAG).

1.3.3.2. IP_3 receptor

There are three subtypes of IP_3 receptors (IP_3R1, IP_3R2, IP_3R3) and they form homo- and hetero-tetrameric receptor complexes (Taylor et al, 1999). IP_3 has been demonstrated to bind all IP_3R subtypes with high affinity, showing K_d values of 49.5 ± 10.5 nM for IP_3R1, 14.4 ± 3.5 nM for IP_3R2 and 163.0 ± 44.4 nM for IP_3R3 (Iwai *et al.*,2007). With the exception of IP_3R1 being expressed predominantly in neurons, the expression of all three IP_3 receptors subtype can be detected in most cell lines and tissue preparations (Newton *et al.*, 1994; Taylor et al, 1999). IP_3Rs are primarily

localized on the ER/SR (Ehrlich *et al.*, 1988, Ross *et al.*, 1989). Nevertheless, localization of IP_3Rs in other subcellular locations such as plasma membrane, nuclei and Golgi apparatus has also been observed (Stehno-Bittel *et al.*, 1995; Pinton *et al.*, 1998; Dellis *et al.*, 2006). All IP_3Rs have preferential permeability for divalent cations and more selectivity to Ca^{2+} as several reports observed P_{Ca}/P_K values from 4.3 to 10 (Foskett *et al.*, 2007). The channel activity of IP_3R can be modulated by many factors, including calmodulin-dependent kinase II (CAMKII), cAMP/cGMP-dependent kinase, protein kinase C and most notably, Ca^{2+} itself (Foskett *et al.*, 2007). Ca^{2+} regulates the IP_3 sensitivity of different IP_3Rs to various extents. IP_3 activation of IP_3R1 and cytosolic Ca^{2+} concentration displays a bell-shape relationship: Ca^{2+} increases IP_3R1 open probability at concentrations below 300 nM whereas the opposite effect is observed at Ca^{2+} concentration more than 300 nM (Bezprozvanny *et al.*, 1991). However, whether the same bell-shape pattern exists for IP_3R2 and IP_3R3 remains debatable (Thrower *et al.*, 2001). IP_3Rs can be antagonized by heparin, which inhibits the binding of IP_3 to IP_3Rs as well as Ca^{2+} release from intracellular stores (Kobayashi *et al.*, 1988; Supattapone *et al.*, 1988).

1.3.4. cADPR-mediated calcium signalling

1.3.4.1. Cyclic ADP-ribose (cADPR)

In addition to IP_3, cyclic ADP-ribose (cADPR) is also a second-messenger capable of inducing Ca^{2+} release from intracellular calcium stores. It was first discovered by Clapper *et al.* as an enzymatic metabolite of NAD which evoked Ca^{2+} responses in sea urchin egg homogenate that was distinct from IP_3-mediated Ca^{2+} release (Clapper *et*

al., 1987). cADPR is synthesized via cyclization of β-NAD, a reaction that can be catalyzed by Aplysia ADP-ribosyl cyclase or its mammalian equivalent, CD38 (Lee and Aarhus, 1995). It is believed that the calcium-mobilizing activity of cADPR is mediated through the ryanodine receptor (RyR) as RyR antagonists such as ryanodine and ruthenium red inhibit cADPR response (Galione *et al.*, 1991).

1.3.4.2. Ryanodine receptors

Ryanodine receptors (RyRs) are localized on the ER/SR and are named after their specificity for ryanodine, a plant alkaloid that blocks Ca^{2+} release through the channel at high concentrations. Like the IP_3 receptor, there are three isoforms of RyR (RyR1-3), and they function as homotetramers consisting of four subunits, each with a molecular weight of approximately 565 kDa (Marks *et al.*, 1989; Takeshima *et al.*, 1989). Also, RyRs are divalent cation selective channels permeable to Ca^{2+} as revealed by lipid bilayer experiments, showing a permeability ratio of P_{Ca}/P_K around 6 (Smith *et al.*, 1988). Isoforms of RyR exhibit differential expression across tissues: RyR1 expression is mostly restricted to skeletal muscle whereas RyR2 is predominantly localized in the heart, and RyR3 is expressed in the brain but can also be found in many other tissues (Ledbetter *et al.*, 1994). Similar to IP_3R, the RyRs are also modulated by cytosolic Ca^{2+} in a bell-shape pattern. Single channel recording suggests that low micromolar free Ca^{2+} activates RyR whereas millimolar concentration of free Ca^{2+} produces an inhibitory effect (Zalk *et al.*, 2007). Interestingly, photoaffinity labelling of cADPR binding protein indicated that cADPR may not bind to RyR directly but to an accessory protein instead (Walseth *et al.*, 1993). This prompted the subsequent discovery of FK506-binding proteins, which has been suggested to be a key regulator of RyR activity

during cADPR-mediated Ca^{2+} release (Noguchi *et al.*, 1997). In addition to previously mentioned RyR antagonists, cADPR, cytoplasmic Ca^{2+} and FK506-binding proteins, RyR activity can also be modulated by many other regulators, these include voltage-gated L-type calcium channels, small molecules and ions like ATP and Mg^{2+}, accessory proteins such as calmodulin and calsequestrin, kinases including protein kinase A and CAMKII, and reactive oxygen and nitric oxide that affects RyR gating properties through oxidation and nitrosylation (Zalk *et al.*, 2007; Lanner *et al.*, 2010).

1.4. Nicotinic Acid Adenine Dinucleotide Phosphate (NAADP) as a calcium signalling messenger

1.4.1. Discovery of NAADP

In 1987, Clapper *et al.* investigated the Ca^{2+} release by pyridine nucleotides in sea urchin egg homogenate and purified microsomes. It was discovered that alkaline-treated NADP was 30-fold more effective than NADP in evoking a Ca^{2+} response and could induce Ca^{2+} release from sea urchin egg homogenate desensitized to cADPR and IP_3 (Clapper *et al.*, 1987). It was not until 1995 that the identity of this molecule was finally confirmed as nicotinic acid adenine dinucleotide phosphate (NAADP) by High Performance Liquid Chromatography (HPLC), ^1H NMR, mass spectrometry and the sea urchin egg homogenate calcium release assay (Lee and Aarhus, 1995). The ^1H NMR spectra of NAADP was almost identical to that of NADP and their mass spectra showed that NAADP is only one atomic mass unit higher than NADP. However, the retention of NAADP was apparently different than NADP or NADPH in HPLC. Sea urchin egg

homogenate calcium release assay also revealed that the EC_{50} of NAADP was about 30 nM whereas NAADP analogs NADP and NAAD did not evoke any Ca^{2+} release at concentrations of 1.1 µM and 4 µM, respectively. This makes NAADP a much more potent calcium signalling messenger than IP_3 and cADPR.

1.4.2. Synthesis and degradation of NAADP

It has been demonstrated that NAADP can be synthesized by incubating β-NADP with nicotinic acid in multiple tissue homogenates (Chini and Dousa, 1995). Aarhus *et al.* suggested that two enzymes, *Aplysia* ADP-ribosyl cyclase and mammalian CD38, catalyze the synthesis of NAADP via base exchange reaction (Aarhus *et al.*, 1995). Sequence comparison of Aplysia ADP-ribosyl cyclase and human CD38 revealed that the two proteins share 27% homologous sequence, suggesting that CD38 could be functionally equivalent to ADP-ribosyl cyclase in mammalian systems (States *et al.*, 1992). Both enzymes have been shown to synthesize cADPR and NAADP (Lee and Aarhus, 1991; Howard *et al.*, 1993; Aarhus *et al.*, 1995). The production of NAADP by these enzymes *in vitro* is dependent on acidic pH and the presence of appropriate substrates. The rate of NAADP synthesis for both ADP-ribosyl cyclase and CD38 reaches maximum at pH 4-5. When incubated with 1 mM NADP at pH 5, both enzymes manifested a half-maximal concentration of 5 mM nicotinic acid for NAADP production (Aarhus *et al.*, 1995). Such acidity and high concentration of nicotinic acid seems not in the physiological range, yet the extreme Ca^{2+} release potency of NAADP could make up for the suboptimal NAADP production in physiological conditions.

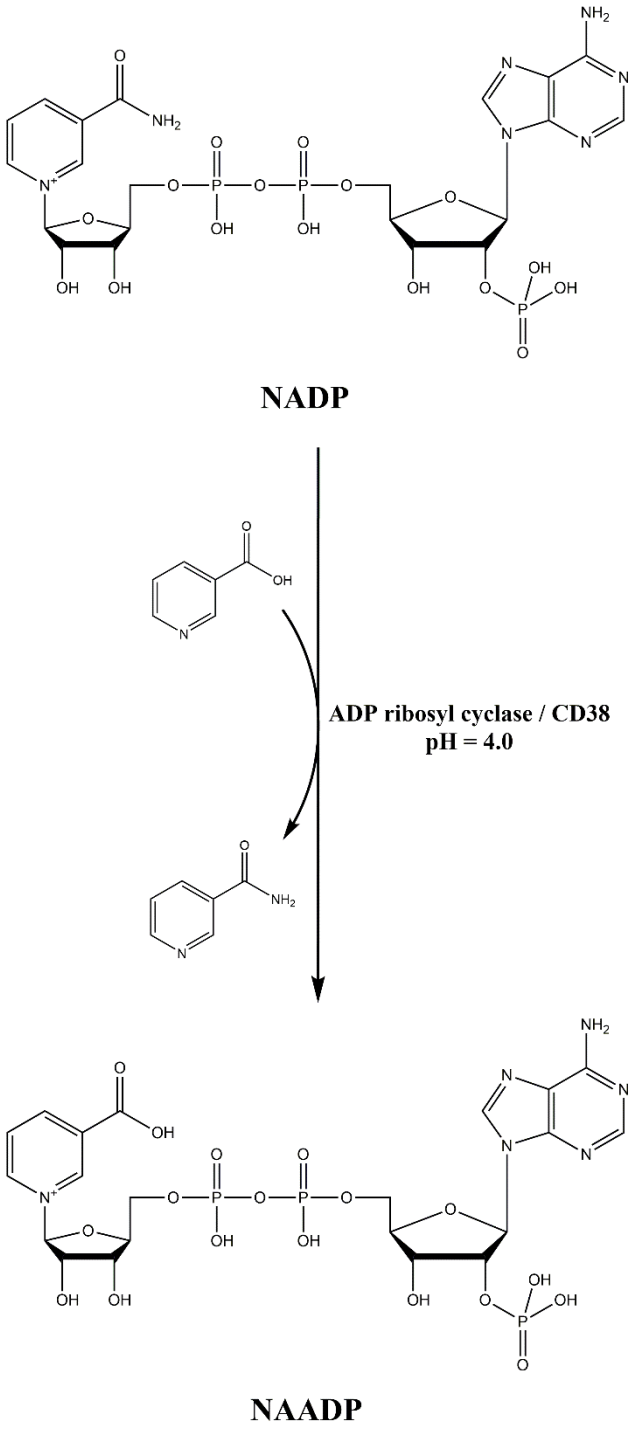

Figure 1.3. Synthesis of NAADP via base exchange reaction.

Degradation of NAADP has been observed in various preparations, including several rat tissue homogenates (Chini and Dousa, 1995; Bak *et al.*, 1999; Cheng *et al.*, 2001), mouse brain membrane (Berridge *et al.*, 2002), sea urchin sperm extract (Billington *et al.*, 2002) and sea urchin egg homogenate (Wilson *et al.*, 1998). Several enzymes have been linked to NAADP inactivation. Chini and Dousa suggested that the extremely high NAADP inactivation capability observed in rat kidney extract could be attributed to the abundance of acid phosphatase and alkaline phosphatase in the proximal tubules (1995), indicating that the dephosphorylation of NAADP to NAAD by phosphatase could be one of the NAADP inactivation pathways. This has been proven to be the major NAADP inactivation pathway in mouse brain (Berridge *et al.*, 2002) and a few reports also demonstrated the inactivation of NAADP by alkaline phosphatase (Lee *et al.*, 1997; Schmid *et al.*, 2012). In addition, NAADP can be cleaved by nucleotide pyrophosphatase, presumably into nicotinic acid mononucleotide and 2,5-ADP (Lee *et al.*, 1997; Berridge *et al.*, 2002). Reduction of NAADP to NAADPH by reductases such as glucose-6-phosphate dehydrogenase is also a possible route of inactivation since NAADPH failed to elicit Ca^{2+} release in sea urchin egg homogenate at concentrations up to 200 nM, which is far less potent than NAADP (Billington *et al.*, 2004). Finally, the NAADP synthases, CD38 and ADP-ribosyl cyclase, are also capable of hydrolyzing NAADP and thereby inactivate it. Graeff and colleagues showed that the hydrolase activity of CD38 peaks at pH 5 and converts NAADP to nicotinic acid and ADPRP (2006). The hydrolysis of NAADP by CD38 was observed in Jurkat T cells as well (Schmid *et al.*, 2011). Similarly, it has been noted that ADP-ribosyl cyclase breaks down NAADP into nicotinic acid and cADPRP (Graeff *et al.*, 2006).

1.4.3. NAADP targets acidic organelles for calcium release

NAADP targets an internal organelle that is distinct from the target of IP_3 or cADPR. This was discovered even before the identification of NAADP as it evoked Ca^{2+} release from a group of Percoll-separated microsomes that were rather insensitive to IP_3 and cADPR (Clapper *et al.*, 1987). Later, the experiment on stratified sea urchin eggs provided the direct visual evidence of Ca^{2+} release from different internal calcium stores (Lee and Aarhus, 2000). ER Ca^{2+} depletion by SERCA inhibitor thapsigargin prevents further Ca^{2+} response caused by IP_3 or cADPR while NAADP-induced Ca^{2+} release only showed a minor reduction (Genazzani and Galione, 1996). Photolysis of caged NAADP and cADPR revealed that the calcium stores targeted by cADPR were located on the same pole as egg nucleus, endoplasmic reticulum and IP_3-sensitive stores, while the NAADP-sensitive calcium stores were segregated with mitochondria to the other pole of the stratified egg. Further investigation showed that NAADP induces Ca^{2+} release from reserve granules in sea urchin eggs, which is equivalent to lysosomes and can be labelled by the fluorescent acid organelle marker lysotracker red (Churchill *et al.*, 2002). In addition, glycyl-L-phenylalanine 2-naphthylamide (GPN) caused osmotic lysis of lysosomes and effectively eliminated the Ca^{2+} response by NAADP in intact sea urchin eggs whereas the responses to IP_3 and cADPR remained relatively unaffected. Moreover, inhibition of the ATP-dependent vacuolar proton pump by bafilomycin A1 abolished the Ca^{2+} uptake of NAADP-sensitive stores, indicating that the primary target of NAADP in sea urchin egg homogenate is the

lysosomal-related acidic organelles and these require a proton gradient to maintain luminal Ca^{2+} content.

In addition to sea urchin egg homogenate, NAADP has been shown to mobilize Ca^{2+} from acidic organelles in various mammalian cell preparations. For instance, the Ca^{2+} response evoked by the photorelease of NAADP in pancreatic MIN6 cells was rather insensitive to thapsigargin but could be abolished by GPN and bafilomycin A1, which targets the acidic organelles (Yamasaki *et al.*, 2004). On the other hand, Ca^{2+} release resulting from photolysis of caged IP_3 or cADPR was not significantly affected by GPN or bafilomycin A1. Moreover, bafilomycin A1 has also been demonstrated to inhibit NAADP-induced Ca^{2+} release in many other mammalian system, such as bovine coronary arterial smooth muscle cells (Zhang *et al.*, 2006), peritubular smooth muscle cells (Gambara *et al.*, 2008), guinea pig ventricular myocytes (Macgregor *et al.*, 2007) and rat cortical neurons (Brailoiu *et al.*, 2005). These pieces of evidence agree with the findings in sea urchin eggs and indicate that the primary target of NAADP in mammalian cells is also lysosome-related acidic organelles.

1.4.4. Characteristics of NAADP signalling and its physiological roles

A key characteristic of NAADP-induced Ca^{2+} release is that there is no cross-desensitization between NAADP and IP_3 or cADPR. It has been described in many studies that that homologous desensitization induced by any of these three intracellular Ca^{2+}-releasing messengers has little influence on the Ca^{2+} response elicited by the other two, suggesting that they operate on different receptors. This is

supported by the dissection of the NAADP signalling pathway using pharmacological tools. In sea urchin egg homogenate, the cADPR antagonist 8-amino-cADPR, and the IP_3 receptor blocker heparin inhibited Ca^{2+} release by cADPR or IP_3, respectively, yet NAADP-evoked Ca^{2+} release was hardly affected (Lee and Aarhus, 1995). On the other hand, the NAADP antagonist Ned-19 specifically blocked the Ca^{2+} response from NAADP in sea urchin egg but had little effect on IP_3- and cADPR-induced Ca^{2+} release (Naylor *et al.*, 2009).

Another characteristic of NAADP signalling is that NAADP-evoked Ca^{2+} release operates on a two-pool model via organelle crosstalk: initial local Ca^{2+} release from acidic organelles elicited by NAADP is propagated into global Ca^{2+} waves by recruiting other Ca^{2+}-mobilizing pathways, such as IP_3- and cADPR-dependent pathways, through Ca^{2+}-induced Ca^{2+} release (Churchill and Galione, 2001a). This hypothesis has been supported by the fact that lysosomes may cluster and form tight coupling junctions with SR, hence allowing the amplification of a local Ca^{2+} burst evoked by NAADP (Kinnear *et al.*, 2004) which subsequently transforms into the biphasic NAADP Ca^{2+} release demonstrated by Calcraft *et al.* in TPC2-overexpressing cells (2009).

NAADP also exhibits unique self-desensitization characteristics in sea urchin egg homogenate and mammalian cells. In both intact sea urchin egg and egg homogenate, preincubation of subthreshold concentrations of NAADP was found to block a subsequent Ca^{2+} response induced by NAADP in a time- and concentration-dependent manner (Genazzani *et al.*, 1996; Aarhus *et al.*, 1996). Moreover, Dickey *et al.* discovered that the inhibitory effect of thio-NADP on the NAADP-mediated Ca^{2+} response in sea urchin egg homogenate was caused by self-desensitization triggered

by a trace amount of NAADP contamination (Dickey *et al.*, 1998). On the other hand, NAADP desensitization in mammalian cells requires much higher concentrations and follows a bell-shaped pattern (Masgrau *et al.*, 2003; Zhang and Li, 2007; Zong *et al.*, 2009). An initial increase of NAADP concentration up to 100 nM results in an increase of the Ca^{2+} released (Cancela *et al.*, 1999). A further increase of NAADP concentration reduces the Ca^{2+} response and no response was observed at concentrations above 1 µM (Masgrau *et al.*, 2003).

The distinctive homologous desensitization pattern of NAADP also forms a unique spatiotemporal Ca^{2+} memory. In intact sea urchin eggs, local photolysis of caged NAADP induces local self-desensitization, which renders the calcium stores in the affected area irresponsive to subsequent global photorelease of NAADP. This makes the global Ca^{2+} release pattern complimentary to the first local Ca^{2+} signals triggered by NAADP, which has not been seen in the case of caged-IP_3 or caged-cADPR (Churchill and Galione, 2001b). These observations underline a novel mechanism of spatiotemporal regulation of Ca^{2+} signals.

NAADP has been suggested to have pivotal roles in many physiological processes. Fertilization of sea urchin eggs is marked with a dramatic increase of NAADP concentration, which is subsequently involved in many early Ca^{2+} responses during fertilization such as the cortical flash (Churchill *et al.*, 2003). NAADP has also been suggested to facilitate Ca^{2+} oscillations that contribute to insulin secretion in pancreatic beta-cells in response to glucose (Masgrau *et al.*, 2003; Naylor *et al.*, 2009) and may induce fluid secretion in pancreatic acinar cells (Cancela *et al.*, 1999; Yamasaki *et al.*, 2004). Brailoiu *et al.* also reported that the presence of NAADP

promotes the differentiation of PC12 cells (2006). Moreover, NAADP has been suggested to cause depolarization of rat medulla oblongata neurons by triggering Ca^{2+} release from intracellular stores and recruitment of non-selective cation channels on the plasma membrane (Brailoiu *et al.*, 2009b). NAADP-mediated Ca^{2+} release has also been associated with smooth muscle contraction (Kinnear *et al.*, 2004) and activation of T lymphocytes (Berg *et al.*, 2000). Furthermore, a study performed by Morgan and Galione revealed that NAADP-induced Ca^{2+} release from acidic organelles is accompanied by concentration-dependent alkalization of the luminal compartment (Morgan and Galione, 2007). Also, since Ca^{2+} signals are critical for lysosomal biogenesis, autophagy, and vesicle trafficking, NAADP may influence these processes by regulating local Ca^{2+} release (Piper and Luzio, 2004). Finally, impaired NAADP signalling has been observed in several lysosomal storage disorders. For instance, Niemann-Pick disease type C1 (NPC1) is a neurodegenerative lysosomal storage disorder caused by mutation of NPC1 protein, featuring excessive accumulation of lipid in lysosomes and disruption of lysosomal Ca^{2+} homeostasis (Lloyd-Evans *et al.*, 2010). In human NPC1 mutant fibroblasts, the lysosomal Ca^{2+} content is profoundly reduced by roughly 70%, and Ca^{2+} transients triggered by NAADP-AM are reduced by approximately 69% compared to the WT human fibroblast homeostasis (Lloyd-Evans *et al.*, 2008). These abnormalities could have significant impact in endolysosomal fusion and trafficking in NPC1 disease.

1.4.5. NAADP antagonists

The [^{32}P]-NAADP binding assay and a series of NAADP receptor antagonists allowed extensive investigation of NAADP binding properties in many cells and tissue

preparations. At first, it was believed that thio-NADP is a specific antagonist of NAADP receptor due to its selective inhibitory effect on NAADP-induced Ca^{2+} release in sea urchin egg homogenate (Chini *et al.*, 1995), but this later proved to be self-desensitization elicited by NAADP contamination in commercially available thio-NADP (Dickey *et al.*, 1998).

Later, Billington and Genazzani discovered that PPADS and its structural analog PPNDS could reversibly compete with [^{32}P]-NAADP in a radioligand binding assay with apparent IC_{50}s of 4.20 ± 0.34 µM and 3.02 ± 0.25 µM, respectively (2007). PPADS is also capable of inhibiting Ca^{2+} release evoked by 100 nM NAADP in sea urchin egg homogenate, showing an IC_{50} of 20.6 ± 1.0 µM. However, the specificity of PPADS as an antagonist for NAADP receptors was questioned since PPADS is also a competitive antagonist of P2X and P2Y purinergic receptors (Lambrecht *et al.*, 2002).

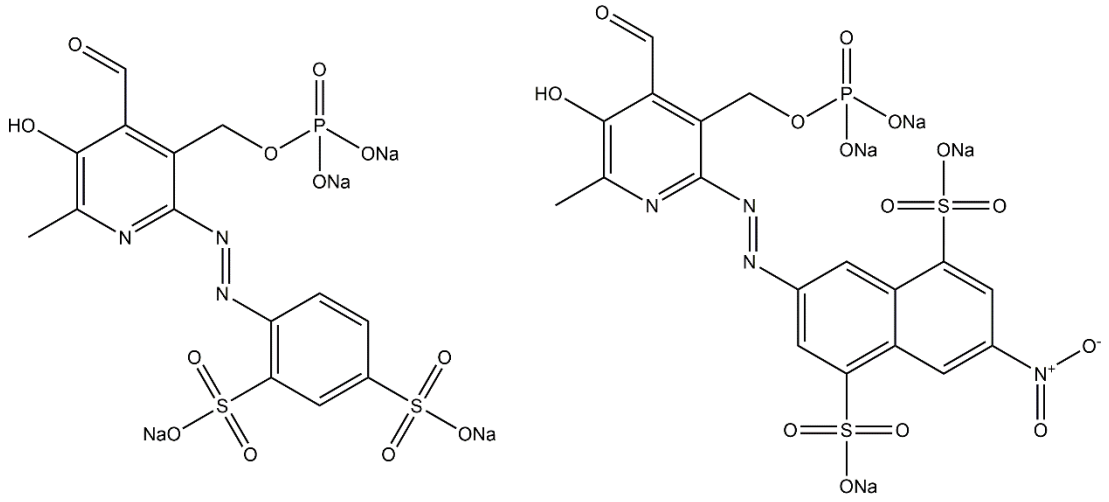

Figure 1.4. Structures of NAADP antagonists PPADS (pyridoxalphosphate-6-azophenyl-2'4'-disulfonic acid) and PPNDS (pyridoxal-5-phosphate-6-(2-naphthylazo-6-nitro-4,8-disulfonate)).

Some other attempts of searching for NAADP antagonists focused on the membrane-permeant nicotinic acid derivatives, since the nicotinic acid moiety is the most critical

part that bestows the potency and selectivity of NAADP. One of the first described compounds of this kind, CMA008, was reported by Dowden *et al* (2006). The Ca^{2+} response in sea urchin egg homogenate elicited by 250 nM NAADP was effectively antagonized by CMA008, which has an IC_{50} of approximately 15 µM. Binding competition was also observed in [^{32}P]-NAADP binding in the presence of CMA008, but at a higher IC_{50} of 90 µM. However, when used at concentrations higher than 30 µM, CMA008 seemed to induce Ca^{2+} release from sea urchin egg and the effect became more pronounced when its concentration was increased to more than 100 µM, indicating that CMA008 could be a partial agonist rather than an antagonist (Dowden et al, 2006). On the other hand, BZ194 was discovered during a screen for NAADP antagonists from an alkylated nicotinic acids library (Dammermann *et al.*, 2009). BZ194 dose-dependently reduced the amplitude of the Ca^{2+} peak and Ca^{2+} plateau in Jurkat T cells upon injection of NAADP, showing an IC_{50} at low micro molar concentrations. The suppression of the Ca^{2+} response by BZ194 has also demonstrated to be independent of the IP_3 and cADPR pathways (Dammermann *et al.*, 2009).

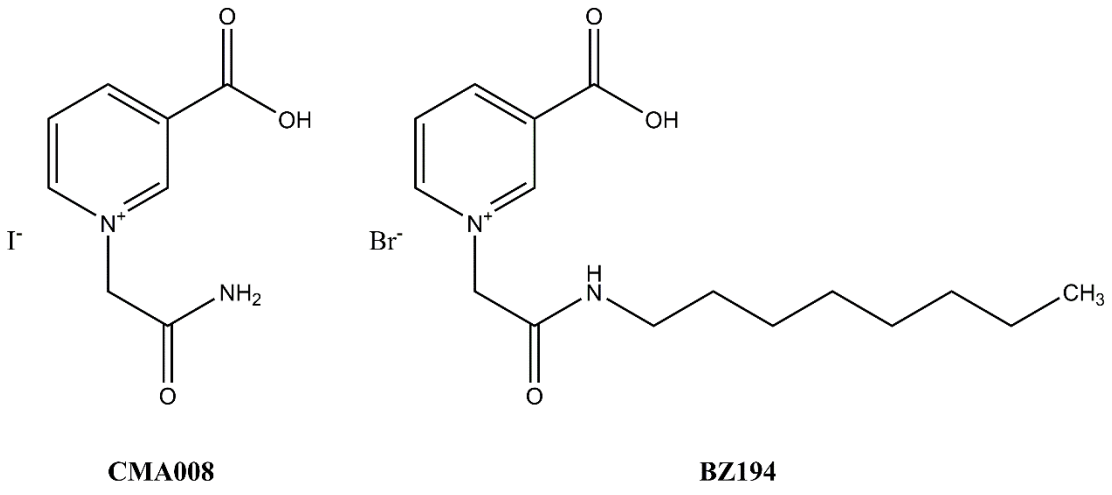

Figure 1.5. Structures of nicotinic acid derivatives CMA008 and BZ194 that act as NAADP antagonists.

More recently, Naylor *et al.* searched for NAADP-like molecules based on a ligand-based virtual screen and electrostatic similarity and discovered the NAADP antagonist Ned-19, which is a non-competitive NAADP antagonist that decreases the maximal Ca^{2+} release induced by NAADP, increases the EC_{50} of NAADP and can fully displace [^{32}P]-NAADP binding in sea urchin egg homogenate (2009). On the other hand, Ned-20, an analog of Ned-19 which has an altered position for a fluoride atom on the benzene ring, did not have any impact on the Ca^{2+} response elicited by NAADP but could block homologous desensitization in sea urchin egg homogenate by subthreshold concentrations of NAADP (Rosen *et al.*, 2009). Moreover, Ned-19.4, the methyl ester form of Ned-19, did not show competition of binding in the [^{32}P]-NAADP binding assay. However, it causes reduction of NAADP-induced Ca^{2+} release in sea urchin homogenate in a dose-dependent manner without affecting the EC_{50} of NAADP. The evidence provided by synthetic antagonists of NAADP signalling suggested the possible existence of an inhibitory allosteric binding site on the NAADP receptor in sea urchin eggs in addition to the NAADP binding site.

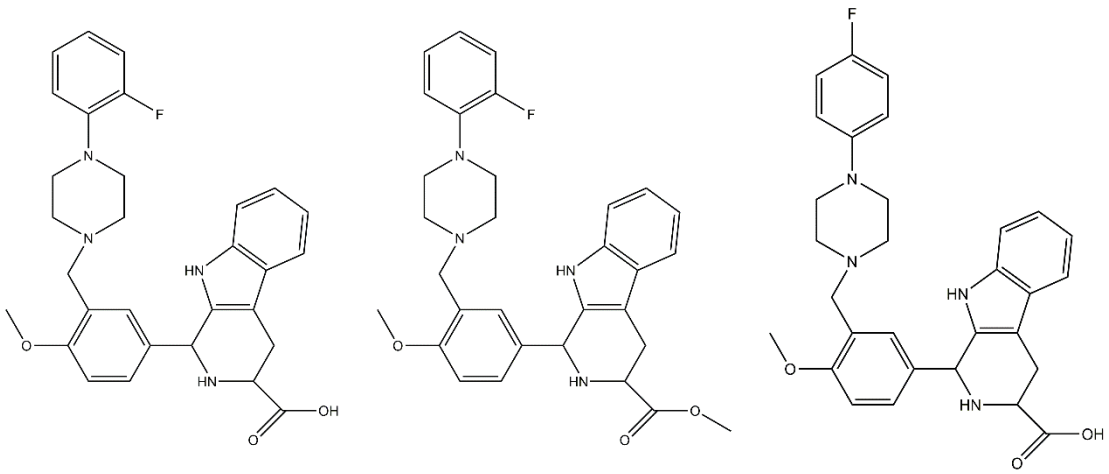

Figure 1.6. Structures of NAADP antagonists Ned-19, Ned-19.4 and Ned-20.

1.4.6. Modification of NAADP and structural determinants of NAADP calcium-release activity

Recently, a vast number of NAADP analogs have been synthesized to gain insight into the structural-activity relationships of NAADP in NAADP-induced Ca^{2+} signalling.

Structural modification on the pyridine moiety has been extensively investigated. The 3-position of the pyridine is necessary for NAADP recognition and requires an acid that is directly attached to the pyridine ring and is negatively charged in the physiological environment to maintain its potency (Billington *et al.*, 2005). Shifting the 3-carboxyl group to a 4-position also results in loss of Ca^{2+}-release activity shown as a 200-fold increase of EC_{50} in sea urchin egg homogenate (Lee and Aarhus, 1997). Substitution on the 4- and 5-positions of the pyridine ring has been examined as well. Jain *et al.* synthesized NAADP analogs from 4- and 5-substituted nicotinic acid using the base-exchange reaction and characterized their potency to trigger a Ca^{2+} response as well as propensity to bind to NAADP receptors in sea urchin egg homogenate (Jain *et al.*, 2010). It has been observed that NAADP analogs synthesized from 4-substituted nicotinic acid is associated with loss of potency, as even a small substitution like an amino group on the 4-position resulted in a 235-fold increase in EC_{50} in sea urchin egg homogenate Ca^{2+} release and an 88-fold increase of IC_{50} in a competitive binding assay. In contrast, substitution on the 5-position of the nicotinic acid moiety is well tolerated and only a slight loss of potency has been observed. Some 5-substituted NAADP derivatives, such as 5-amino- and 5-metyl-NAADP, have an almost identical potency as NAADP itself. Similar studies have been performed in mammalian cells using

photolysis of caged 4- and 5-substituted NAADP derivatives (Ali *et al.*, 2014). Unlike in sea urchin egg homogenate, most tested NAADP derivates were almost equally potent as NAADP in inducing Ca^{2+} release in SKBR3 cells. This suggests that the structural-activity correlation could vary in different systems. What is worth noting is that the positive charge of the pyridinium is also crucial for the Ca^{2+}-release efficacy. NAADPH generated from reduction of the pyridine ring shows a similar binding affinity to NAADP in a homologous binding assay yet has a 40-fold increase in EC_{50} compared to NAADP (Billington *et al.*, 2004).

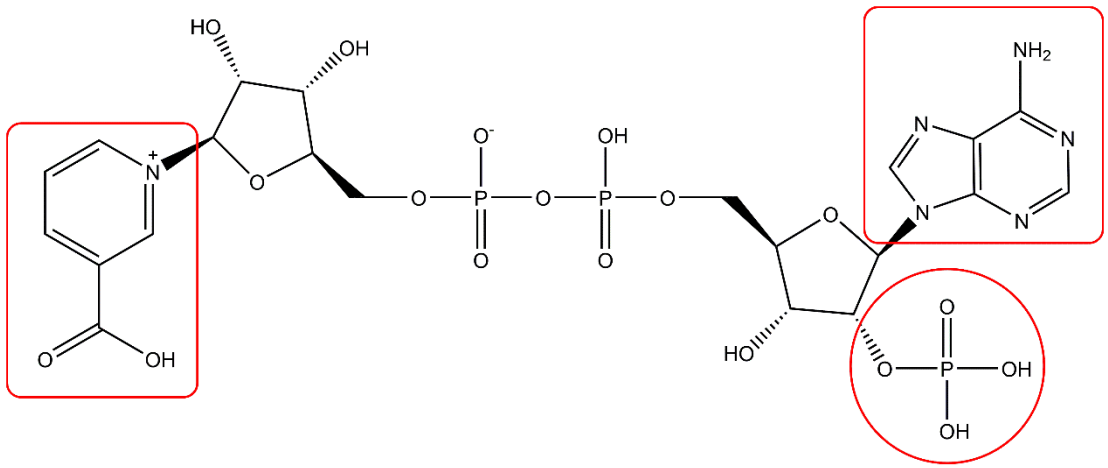

NAADP

Figure 1.7. Structural determinants of NAADP biological activity. Functional groups marked in red have been identified as critical determinants for NAADP calcium-mobilizing activity.

The 2'-phosphate on adenosine is another essential determinant of NAADP activity. The removal of phosphate results in complete loss of potency and binding capability as exemplified by NAAD in many reports (Lee and Aarhus, 1995; Billington and Genazzani, 2000; Walseth *et al.*, 2012a; Walseth *et al.*, 2012b; Lin-Moshier *et al.*, 2012). Caged NAADP, in which the 2'-phosphate is made inaccessible by the formation of NPE- or DMNPE-ester, also possesses no Ca^{2+}-releasing activity (Lee *et al.*, 1997; Cancela *et al.*, 1999; Churchill *et al.*, 2002). Furthermore, shifting the 2'-phosphate to

a 3-position on adenosine or forming a 2',3'-cyclic phosphate reduces its binding affinity (Lee and Aarhus, 1997).

Finally, the adenine moiety of NAADP is also one of the important determinants for the NAADP-mediated Ca^{2+} response. Conversion of the purine base to an inosine base through modification of the adenine ring resulted in a 1000-fold less potent product, NAIDP (Trabbic *et al.*, 2012). In addition, fluorescent NAADP derivatives, etheno-NAADP and etheno-aza-NAADP, are also synthesized by adenine ring modifications and are roughly 100-fold less effective than NAADP since their EC_{50}s are about 5 and 2.5 µM in sea urchin egg homogenate, respectively (Lee and Aarhus, 1998).

1.4.7. NAADP receptors

Many known receptors have been proposed as potential NAADP receptor candidates. Some of the major candidates are TRPML-1, TRPM2, P2 purinergic receptors, RyRs and two-pore channels (TPCs).

1.4.7.1. TRPML-1

TRPML-1 is a member of the TRP channels localized on the late endosomal and lysosomal membrane and was first discovered through its involvement in the lysosomal storage disorder Mucolipidosis Type IV (Bargal *et al.*, 2000). TRPML-1 can be activated by phosphatidylinositol-3,5-bisphosphate ($PI(3,5)P_2$) and is essential in the regulation of lysosomal trafficking (Dong *et al.*, 2010; Xu and Ren, 2015). Various reports have implicated its identity as a cation channel but there has been debate about its ion selectivity: while some suggested that TRPML-1 is permeable to Na^+, K^+

and Ca^{2+}, others demonstrated that it is also a proton and Fe^{2+} permeable channel. TRPML-1 was first purposed as a candidate for the NAADP receptor by Zhang and Li (2007). They demonstrated that incorporation of purified rat liver lysosomes into planar lipid bilayers could reconstitute calcium channel activity sensitive to NAADP. The open probability of the channel also correlated with NAADP concentration in a bell-shape pattern typically seen in mammalian preparations (Zhang and Li, 2007). In addition, an antibody targeting the C-terminus of TRPML-1 effectively blocked NAADP-induced channel activity. Similar observations were also reported in bovine coronary arterial myocytes. Calcium channel activation by NAADP was significantly reduced by treatment with TRPML-1 antibody or depletion of TRPML-1, either through immunoprecipitation or si-RNA knock-down (Zhang *et al.*, 2009). Re-expression of TPML-1 in a human fibroblast cell line with TRPML-1 deficiency also restored the cell line's sensitivity to NAADP (Zhang *et al.*, 2011).

However, there has been reports of contradictory observations. TRPML-1 expressing SKBR3 cells did not show responsiveness to NAADP whereas NAADP-induced Ca^{2+} release was observed in TPC1/TPC2-expressing cells and their lysosomal preparations (Yamaguchi *et al.*, 2011). In addition, knock-out of TRPML-1 did not significantly alter the frequency and amplitude of NAADP-evoked Ca^{2+} oscillations in mouse pancreatic acinar cells. Pryor *et al.* also reported that the overexpression of TRPML-1 did not result in an increase in NAADP binding in NRK cells (Pryor *et al.*, 2006). Finally, NAADP-induced Ca^{2+} signals in TPC1/TPC2 double-knockout (DKO) MEFs were not recovered by over-expression of TRPML-1, but were by re-expression of TPC1 or TPC2 (Ruas *et al.* 2015).

1.4.7.2. TRPM2

TRPM2 is a non-selective cation channel permeable to Ca^{2+}. It is widely expressed among different tissues, predominately in the brain (Beck *et al.*, 2006). Subcellular localization of TPRM2 has been seen on the plasma membrane as well as on lysosomal membranes since immunofluorescence showed overlapping staining of TRPM2 and the lysosome marker LAMP-1 (Lange *et al.*, 2009). Apart from the well-recognized agonist ADPR, TRPM2 can also be activated by several other molecules, including H_2O_2, cADPR and NAADP (Sano *et al.*, 2001; Kolisek *et al.*, 2005; Beck *et al.*, 2006). Ca^{2+}, on the other hand, cannot directly activate TRPM2 but exerts its modulatory effect by sensitizing TPRM2, thus allowing activation at a lower concentration of ADPR (Perraud *et al.*, 2001). TRPM2 signalling can be antagonized by AMP, which is a degradation product of ADPR (Kolisek *et al.*, 2005). TRPM2 has been suggested by Beck *et al.* as a potential candidate for the NAADP receptor since NAADP was found to activate TRPM2 currents in Jurkat T lymphocytes and TRPM2-expressing HEK293 cells (2006). However, the NAADP concentration required to achieve half-maximal activation was 730 µM, which indicates a quite low affinity since such high concentrations of NAADP normally would inhibit Ca^{2+} release in mammalian cells (Masgrau *et al.*, 2003).

1.4.7.3. P2 purinergic receptors

The effects of extracellular ATP are mediated through P2 purinergic receptors on the plasma membrane. There are two types of the P2 receptors: P2X receptors are ligand-gated non-selective cation channels, and P2Y receptors are G-protein coupled receptors (Qureshi *et al.*, 2007). They both respond to the binding of extracellular ATP

and mobilize Ca^{2+} from intracellular calcium stores upon activation (Dubyak and El-Moatassim, 1993). It has been demonstrated that the P2 purinergic receptor antagonist PPADS competes with NAADP binding in sea urchin egg homogenate and blocks NAADP-induced Ca^{2+} release in a concentration-dependent manner (Billington and Genazzani, 2007). Moreschi *et al.* also showed that NAADP activates the human $P2Y_{11}$ receptor in transfected 1321N1 astrocytoma cells (2008). A potential candidate for the NAADP receptor, $P2X_4$, was found to be expressed on lysosomes, as immunofluorescence showed overlapping of staining with the lysosome marker LAMP-1 (Qureshi *et al.*, 2007). However, the activation mechanism of $P2X_4$ receptor in lysosomes is not clear. Since the ATP-binding site was predicted to be facing the lumen of the lysosome (Qureshi *et al.*, 2007), a cytosol-facing nucleotide binding site must also be present if NAADP is to active the receptor.

1.4.7.4. RyR

As one of the quintessential calcium channels, RyR has also been proposed as a potential NAADP receptor by many independent reports.

The first evidence was revealed by Mojzisova *et al.* during electrophysiology recordings of planar lipid bilayers incorporated with RyR2 from rat heart and it was found that NAADP increased the channel open probability (Mojzisova *et al.*, 2001). Similar studies were also performed by Hohenegger *et al.* and they concluded that the probability of RyR1 opening increased in proportion to the NAADP concentration, with an EC_{50} of approximately 30 nM (Hohenegger *et al.*, 2002). Moreover, NAADP was found to cause Ca^{2+} release by activating RyR on the nuclear envelope, and the Ca^{2+} response could be abolished by application of thapsigargin, ryanodine and ruthenium

red but not bafilomycin A1 or nigericin (Gerasimenko *et al.*, 2003). The authors also reported similar observations in pancreatic acinar cells (Gerasimenko *et al.*, 2006). In addition, NAADP-mediated Ca^{2+}-signals were inhibited by ruthenium red and knock-down of RyR in Jurkat T cells (Langhorst *et al.*, 2004; Dammermann and Guse, 2005). Interestingly, expression of RyRs has been found on secretory granules in the pancreatic beta cell line MIN6 (Mitchell *et al.*, 2003). However, it has been demonstrated from lipid bilayer studies that low luminal pH has an inhibitory effect on RyR activity (Laver *et al.*, 2000). Therefore RyR is unlikely to function as a lysosomal calcium channel that accounts for the NAADP-mediated Ca^{2+} response. Furthermore, the NAADP-induced Ca^{2+} release in MIN6 cells was not sensitive to the RyR inhibitors ryanodine and dantrolene, suggesting that another distinct receptor from RyR may be responsible for the Ca^{2+}-releasing effects of NAADP (Mitchell *et al.*, 2003). Numerous studies also confirmed that the inhibition of RyRs has little effect on NAADP-induced Ca^{2+} release (Lee and Aarhus, 1995; Chini *et al.*, 1995).

The role of RyRs in NAADP signalling is more likely to be attributed to the amplification of the Ca^{2+} signal from lysosomal Ca^{2+} and subsequent global Ca^{2+}-induced Ca^{2+} release. Immunocytochemistry has revealed that lysosomes can form clusters that co-localize with SR expressing RyRs and form tight lysosome-sarcoplasmic reticulum junctions, which facilitates the amplification of local Ca^{2+} into global Ca^{2+} waves upon activation by NAADP (Kinnear *et al.*, 2004; Kinner *et al.*, 2008).

1.5. Two-pore channels (TPCs)

The first reported two-pore channel isoform, TPC1, was discovered in a rat kidney cDNA library during screening for voltage-gated ion channels (Ishibashi *et al.*, 2000). Unlike conventional voltage-gated calcium and sodium channels that are comprised of four homologous domains with six transmembrane segments in each, TPC1 has only two of these domains and contains two conserved positively charged voltage sensor segments (Ishibashi *et al.*, 2000). Currently, three mammalian isoforms of TPC have been identified. While expression of TPC1 and TPC2 seems to be more universal, TPC3 is not found in several prominent mammalian models, such as mouse and rat, or in humans. (Zhu *et al.*, 2010).

In 2005, Peiter *et al.* discovered that in Arabidopsis Thaliana, TPC1 is located on the membrane of vacuoles, which is a lysosomal equivalent in plants, and knockout of TPC1 resulted in impaired Ca^{2+}-dependent slow-vacuolar channel activity (Peiter *et al.*, 2005). Later, northern blot analysis revealed the wide distribution of TPC1 and TPC2 in mouse and human tissues (Zong *et al.*, 2009; Calcraft *et al.*, 2009). Subsequent investigation uncovered that TPCs are expressed within the endolysosomal system. Immunofluorescent labelled hemagglutinin (HA)-tagged human TPC2 showed a punctate distribution in the cytoplasm that overlapped with lysosomal-membrane associated protein 1 and 2 (LAMP-1 and LAMP-2) in HEK293 cells but not with markers of early/late endosomes, ER, Golgi or mitochondria (Calcraft *et al.*, 2009). This is consistent with another study of TPC2 subcellular localization in SKBR3 cells (Brailoiu *et al.*, 2009a). Conversely, TPC1 and TPC3 have a more diffuse distribution in the

endolysosomal system and only show infrequent colocalization with lysosomal markers (Brailoiu *et al.*, 2009a; Calcraft *et al.*, 2009).

Expression of TPCs has been linked to the NAADP-induced Ca^{2+} response. Calcraft *et al.* demonstrated that TPC2-overexpressing HEK293 cells showed a modest increase of [^{32}P]-NAADP binding and the photolysis of caged NAADP in those cells elicited a biphasic Ca^{2+} response: an initial slow ramp-like (10-180s) Ca^{2+} transient followed by a larger subsequent Ca^{2+} release. However, the biphasic Ca^{2+} response was not observed in wild-type HEK293. Furthermore, the second phase Ca^{2+} transient in TPC2 cells could be suppressed by thapsigargin and heparin and the Ca^{2+} response in both phases could be completely abolished by bafilomycin A1. These pieces of evidence indicate that the biphasic Ca^{2+} transient is a result of Ca^{2+} release from two different intracellular calcium stores: NAADP induces Ca^{2+} release from lysosomes, creating a slow and subtle Ca^{2+} transient which is followed by Ca^{2+}-induced Ca^{2+} release from ER. These findings are in line with the hypothesis proposed by Churchill and Galione that NAADP induces Ca^{2+} oscillations via recruitment of other Ca^{2+} release pathways (Churchill and Galione, 2001a). In addition, pancreatic β-cells from TPC2 knockout mice failed to show any inward cation current that could be observed in wild-type pancreatic β-cells upon stimulation by NAADP (Calcraft *et al.*, 2009). Moreover, in mouse embryonic fibroblasts (MEFs), NAADP-induced Ca^{2+} signals were attenuated by TPC1 or TPC2 single-knockout and were completed eliminated by TPC1/TPC2 double-knockout (DKO) (Ruas *et al.*, 2015). Interestingly, the NAADP-mediated Ca^{2+} release in DKO MEFs could be restored by re-expression of recombinant TPC1 and TPC2, but not TRPML-1 or pore-dead TPC2 mutants. These observations demonstrated the indispensable role of TPCs in the NAADP-induced Ca^{2+} response.

Despite compelling evidence suggesting that TPCs are crucial for NAADP-mediated Ca^{2+} signals, dispute over whether TPCs are indeed NAADP-gated calcium channels arose recently. Wang *et al.* claimed that TPCs are NAADP-insensitive sodium channels that are activated exclusively by phosphatidylinositol-3,5-bisphosphate ($PI(3,5)P_2$) but not other phosphoinositides (Wang *et al.*, 2012). The glucose-triggered Ca^{2+} response was hardly affected in TPC1/TPC2 DKO mouse pancreatic islets but the response could still be reduced by the NAADP antagonist Ned-19. Another study by Cang *et al.* also supported the proposal by Wang *et al.* (Cang *et al.*, 2013). However, it was surprising that while Wang *et al.* demonstrated NAADP-induced Ca^{2+} release from lysosomes in intact INS1 cells, no measurable whole-endolysosomal current was detected upon addition of NAADP in their endolysosomal patch recording (Wang *et al.*, 2012). This suggests that their preparation could be lacking one or more crucial factors of the NAADP-mediated signalling pathway. In contrast, Jha *et al.* studied the electrophysiology of TPC2 using the same approach and stated that TPC2 can be activated by NAADP and the NAADP-mediated current is regulated in a Mg^{2+}-sensitive manner (Jha *et al.*, 2014).

Meanwhile, it has been noticed that the TPC DKO mice generated by Wang *et al.* by deletion of first 69 and 49 amino acid of TPC1 and TPC2, respectively (Wang *et al.*, 2012), may not be the *bona fide* TPC-null mice. It has been demonstrated that TPC expression is not abolished by N-terminus truncations and functional TPCs may still exist in their knockout mice (Brailoiu *et al.*, 2010; Yamaguchi *et al.*, 2011; Churamani *et al.*, 2013). Ruas *et al.* also showed that re-expression of N-terminus truncated TPC1 and TPC2 used by Wang *et al.* could rescue the NAADP-responsiveness in TPC1/TPC2 DKO MEFs and manifested a strong localization within the endolysosomal

compartment (Ruas *et al.*, 2015). Moreover, the Ca^{2+}-permeability of TPCs has been confirmed by many independent studies using single channel recordings of planar lipid bilayers incorporated with TPCs (Pitt *et al.*, 2010; Rybalchenko *et al.*, 2012; Pitt *et al.*, 2014), whole lysosome recording (Schieder *et al.*, 2010) and whole cell recording of cells expressing TPC variants that are redirected to the plasma membrane (Brailoiu *et al.*, 2010; Yamaguchi *et al.*, 2011; Jha *et al.*, 2014).

In summary, although controversy over TPC properties has been reported, current evidence still strongly suggests a link between TPCs and NAADP-induced Ca^{2+} release from lysosomes. However, a consensus has been reached that TPCs may be only one of the participants in a vast signalling network regulated by NAADP. Further investigation into the unknown auxiliary proteins is necessary to thoroughly understand the role of TPCs in NAADP-mediated Ca^{2+} signalling.

1.6. TPC interactomes

As TPCs have become centered in the NAADP-mediated calcium signalling pathway, a number of TPC interacting proteins have emerged as possible regulators of TPC channel properties. The anti-apoptotic protein Hax-1 was the first identified TPC interactor identified by yeast two hybridization screening from a human heart cDNA library, indicating a potential apoptosis inhibition mechanism through Hax-1-TPC interaction (Lam *et al.*, 2013). Leucine-rich repeat kinase 2 (LRRK2) was also found to co-immunoprecipitate with GFP-TPC2 (Gomez-Suaga *et al.*, 2012). Mutation of LRRK2 has been associated with the onset of Parkinson's Disease. Intriguingly, LRRK2 seems to mimic the effects of NAADP, which could be antagonized by the NAADP antagonist

Ned-19 or expression of TPC mutants (Gomez-Suaga *et al.*, 2012). Moreover, interaction of TPC and mTOR was confirmed by co-immunoprecipitation, suggesting a possible role of TPCs in nutrient sensing (Cang *et al.*, 2013; Lin-Moshier *et al.*, 2014). Jha also showed that MAP kinase JNK and p38 also exert their regulatory effects on TPCs (2014). More recently, a systematic investigation of TPC interactomes by co-immunoprecipitation and mass spectrometry analysis was carried out by Lin-Moshier *et al.* and discovered three major groups of TPC interactors. The first group is proteins relevant to Ca^{2+} homeostasis, such as calcium binding proteins like annexins and calreticulin as well as interactors of STIM1 and IP_3 receptor, etc. The second group is consisted of endolysosomal dynamics regulators including Rab GTPases and syntaxins. Interestingly, TPC expression in Xenopus oocytes caused disruption of the pigment distribution and can be reversed by incubation with Rab7 nucleotide binding inhibitor (Lin-Moshier *et al.*, 2014). Pigmentation disruption was also observed with Rab-binding defective TPC2-expressing Xenopus oocytes but to a less extent, suggesting strong dependency of the pigmentation defect on a TPC-Rab interaction. The third group of TPC interactomes encompasses many autophagy regulators. It has been demonstrated recently that TM9SF1, one of the nonaspanin proteins identified as a TPC interactor, co-expressed with TPCs on lysosomes and facilitates the formation of autophagosomes (Sun, 2016). Interestingly, TPCs act through an inhibitory mechanism and suppress autophagosome formation induced by TM9SF1. Finally, NAADP binding proteins discovered using the photolabelling probe [^{32}P]-5-azido-NAADP have been found in the TPC immunocomplexes in sea urchin egg and multiple mammalian cells and tissue preparations, which may potentially serve as modulators of the TPC channel

activities (Walseth *et al.*, 2012a; Walseth *et al.*, 2012b; Lin-Moshier *et al.*, 2012; Ruas *et al.*, 2015).

1.7. NAADP binding proteins

The NAADP binding properties of sea urchin egg homogenate have been well characterized. In sea urchin eggs, NAADP binds to a membrane-bound site with an extremely high affinity of 193 ± 35.7 pM (Billington and Genazzani, 2000). Structural analogs of NAADP, such as NADP and NADPH, bind with significantly lower affinity, as their K_ds are 500- and 25000-fold higher than NAADP. Other NAADP derivatives like NAD, NAAD and ADP did not show affinity to the NAADP binding site as determined by the [^{32}P]-NAADP binding assay. What is worth mentioning is that although study of NAAPD binding sites using the Ned series antagonists suggested multiple bindings sites (Rosen *et al.*, 2009), the reported [^{32}P]-NAADP binding assay results to date could only detect one high affinity binding site in sea urchin egg homogenate (Billington and Genazzani, 2000; Rosen *et al.*, 2009; Ruas *et al.*, 2010). Moreover, it has been reported that in sea urchin egg homogenate, potassium ions inhibit the dissociation of NAADP from its binding site in a concentration-dependent manner (Dickinson and Patel, 2003). NAADP binding is essentially irreversible in sea urchin egg homogenate when 250 mM K^+ is present in the medium.

In contrast to sea urchin eggs, the NAADP binding in mammalian cells and tissues has been demonstrated to be reversible, with multiple binding sites and lower affinities, though the high affinity binding site is usually within the nanomolar range. For example, the radioligand binding assay detected only one binding site in brain

microsomes with an IC_{50} of 200 ± 17 nM (Patel *et al.*, 2000). However, the possibility of multiple binding sites exists as indicated by negative cooperativity (Hill coefficient = 0.76 ± 0.04). On the other hand, three NAADP binding sites were found in rabbit heart microsomes with dissociation constants of 130 pM, 4 nM and 4.2 ± 0.71 nM (Bak *et al.*, 2001). Interestingly, a low concentration of unlabelled NAADP promoted the binding of [^{32}P]-NAADP, suggesting positive cooperativity. In addition, two binding sites were revealed in MIN6 pancreatic cell membrane preparations by a homologous displacement study (Masgrau *et al.*, 2003). These two binding sites can be distinguished as high affinity and low affinity binding sites with dissociation constants of 130 ± 31 nM and 12 ± 0.6 µM, respectively. Similarly, two binding sites were found in mouse liver homogenate with K_ds of 5.0 ± 4.2 nM and 7.2 ± 0.8 µM (Calcraft *et al.*, 2009). The above pieces of evidence suggest that either multiple binding sites may be present on NAADP receptors, or multiple NAADP binding proteins exist in mammalian systems.

Although being the most promising candidates for the NAADP receptor, study shows that TPCs may not directly bind NAADP. Overexpression of TPC2 in HEK293 cells increased NAADP specific binding by more than 200%, yet this increase was incomparable to the 250-fold increase of TPC mRNA levels (Calcraft *et al.*, 2009). The unbalanced increase of TPC mRNA levels and NAADP specific binding indicates that TPC may be one component of a larger complex that functions as the NAADP receptor. This is supported by the fact that immunopurified endogenous sea urchin egg TPC complexes retained high affinity and selectivity for NAADP as well as K^+-dependent irreversible binding (Ruas *et al.*, 2010). Furthermore, liver homogenate from TPC1/TPC2 DKO mice retained similar NAADP binding capacity and affinity in

comparison to WT liver homogenates, suggesting that TPCs are not essential for NAADP binding (Ruas *et al.*, 2015). The advent of a synthetic NAADP probe, [^{32}P]-5-azido-NAADP, finally allowed the visual authentication of the NAADP binding protein. Photoaffinity labelling of sea urchin egg homogenate by [^{32}P]-5-azido-NAADP revealed three populations of possible NAADP binding proteins with sizes of approximately 45, 40 and 30 kDa (Walseth *et al.*, 2012a). The labelling of these bands can be effectively displaced by NAADP with an IC_{50} of 0.7 nM. Conversely, 10 µM NADP could only reduce the labelling of bands by roughly 30%. Proteins from labelled bands also exhibited irreversible binding to NAADP in high K^+ concentrations, a hallmark of NAADP binding property in sea urchin egg homogenate. Intriguingly, the 45 and 40 kDa band was found in immunocomplexes pulled down by TPC1 and TPC3 antibodies, indicating interaction between the binding protein and TPCs.

NAADP binding proteins in mammalian cells have also been discovered by photoaffinity labelling and the labelling profiles are in general more complicated than sea urchin egg homogenate. Photoaffinity labelling in Jurkat T cells, SKBR3, HEK293, mouse liver and pancreas all identified unique sets of proteins labelled by [^{32}P]-5-azido-NAADP (Walseth *et al.*, 2012a; Walseth *et al.*, 2012b; Lin-Moshier *et al.*, 2012; Ruas *et al.*, 2015). However, a 22/23 kDa doublet was revealed that bound NAADP with high affinity in all mammalian cells tested so far and possessed selectivity for NAADP over NADP. The doublet was found in both cytosol and membrane fractions of SKBR3 and Jurkat T cells (Walseth *et al.*, 2012b; Lin-Moshier *et al.*, 2012). Interestingly, it has been demonstrated that the 22/23 kDa doublet has a preferential cytosolic localization since around 75% of the photolabelled doublet was recovered in the cytosolic fraction (Lin-Moshier *et al.*, 2012). Nevertheless, the doublet from the

membrane fraction has a higher affinity towards NAADP as shown by homologous displacement study. The IC_{50} of NAADP in a SKBR3 P100 (membrane) fraction was 22 ± 4 nM, which is significantly lower than the IC_{50} of NAADP in the S100 (cytosol) fraction (134 ± 23 nM, Lin-Moshier *et al.*, 2012). It is also worth noting that in Jurkat T cells, the photolabelling of some bands in the S100 fraction was intensified when a low concentration (3-100 nM) of unlabelled NAADP was present, which is reminiscent of the positive cooperativity observed in rabbit heart microsomes (Bak *et al.*, 2001; Walseth *et al.*, 2012b). In summary, the above findings validated the existence of an NAADP binding protein, which could be one of the crucial components of the NAADP-mediated signalling pathway.

1.8. Aim of this thesis

This thesis is dedicated to tackling one of the unsolved puzzles in the field of NAADP signalling: the identification of the NAADP binding protein. For almost three decades, numerous attempts have been made to characterize the NAADP binding protein(s), yet none has decisively unravelled the identity of this elusive protein(s). Understanding how NAADP acts at the molecular level is paramount to expand our knowledge of the NAADP signalling pathway and would prompt the discovery of unknown players in NAADP signalling as well as their possible physiological roles. Based on our current knowledge of NAADP signalling as reviewed in this introductory chapter, this thesis set out to uncover the identity of the NAADP binding protein(s) using different approaches. The results are discussed in chapter 3 and 4. In chapter 3, an attempt to characterize the NAADP binding protein(s) using chemical crosslinking and NAADP affinity column is described. Chapter 4 is a comprehensive report of NAADP binding protein identification using an interdisciplinary approach, which consisted of four sections: enrichment of NAADP binding by sequential chromatography, visualization of NAADP binding protein(s) by photoaffinity labelling, identification of NAADP binding protein(s) via mass spectrometry-docking tandem analysis and the experimental validation of NAADP binding protein(s).

Chapter 2 Methods and Materials

2.1. Material

All chemicals and reagents were purchased from either Sigma Aldrich or Thermo Scientific unless otherwise stated. Magnetic hydrazide beads were purchased from Bioclone Inc.. [γ-^{32}P]-ATP was purchased from PerkinElmer Inc.. C57BL/6 mice were obtained either from the Harlan Laboratory Inc. or Biomedical Services, University of Oxford.

2.2. Tissue homogenization and fractionation

All tissues used in this study were obtained from freshly sacrificed C57BL/6 mice using Schedule 1 killing (CO_2/cervical dislocation). Tissues were harvested from mice and washed with Phosphate Buffer Saline (PBS) three times to remove blood, and blood clots were taken out later. The tissues were then weighed and diced. Every gram of tissue was mixed with 4 ml hypotonic buffer (20 mM bis-Tris, 1 mM EDTA (ethylenediaminetetraacetic acid), pH 7.0, with protease inhibitor cocktail supplement (Roche)), and homogenized using a IKA Ultra-Turrax T8 Disperser (Homogenizer) at

6,000 rpm for 2 minutes on ice. The homogenate was then centrifuged at 2,000 rpm for 10 minutes at 4 °C using a Beckman GPR centrifuge and the supernatant was transferred to a new tube. The pellet was mixed 1:1 (v/v) with hypotonic buffer, homogenized and centrifuged again with the same setting. The resulting supernatant was combined with the supernatant previously collected after the first spin and this is referred to as the crude homogenate of the corresponding tissue in this study.

The fractionation of the tissue homogenates was carried out using a Sorvall Discovery M120 SE ultra-centrifuge. The crude homogenates were centrifuged in a vacuum at 100,000xg for 1 hour at 4 °C. The resulting supernatant is regarded as the cytosolic fraction and the pellet was resuspended and referred as the membrane fraction of the corresponding tissue.

2.3. Cell culture

Wild type (WT) and TPC1/TPC2 double-knockout (DKO) mouse embryonic fibroblasts (MEFs) were maintained in Dulbecco's Modified Eagle Medium (DMEM) with the supplement of 10% fetal bovine serum (Biosera), 2 mM glutamine, 100 U/ml penicillin and 100 µg/ml streptomycin. MEFs were kept in a humidified cell culture incubator at 37 °C with 5% (v/v) CO_2. Confluent cells were digested with 0.05% trypsin, diluted with fresh DMEM and propagated into new flasks. For crosslinking experiments, WT and DKO MEFs were propagated into 150 mm petri-dishes and maintained in DMEM until reaching 100% confluency.

2.4. Protein quantification

Protein concentration was quantified by the bicinchoninic acid (BCA) assay. The assay reagent was prepared by mixing bicinchoninic acid solution with 160 mM (4% w/v) copper sulphate solution at a 50:1 (v/v) ratio. 10 µl of protein sample or bovine serum albumin (BSA, Roche) standards (0-2000 µg/ml) was added into 200 µl assay reagent and incubated at 37 °C for 30 minutes. The absorption of assay mix was measured at 595 nm by TECAN SunRise Remote Control Plate Reader (TECAN Life Sciences). A standard curve was generated by plotting absorption of BSA standards against their concentrations. The protein concentrations of samples were then calculated by interpolation from the BSA standard curve.

2.5. Protein electrophoresis and staining

Protein samples were mixed with Laemmli sample buffer (63 mM Tris-HCl, 2% (w/v) sodium dodecyl sulfate (SDS), 0.1% (v/v) 2-mercaptoethanol, 0.0005% (w/v) bromophenol blue, 10% (v/v) glycerol, pH 6.8), heated at 95 °C for 10 minutes and then centrifuged at 20,000xg for 10 minutes. The pellets were discarded and the supernatants were loaded onto a 4-20% Tris-Glycine precast gel (NuSep). The electrophoresis was performed using a Mini-PROTEAN 3 vertical electrophoresis system (BioRad) at 150 V in Tris-Glycine running buffer (25 mM Tris, 192 mM glycine, 0.1% (w/v) SDS, pH 8.3) until the blue dye front reached the end of the gel. For electrophoresis of ^{32}P photolabelled proteins, samples were not heated but incubated with Laemmli sample buffer at room temperature for 10 minutes instead.

Proteins separated by sodium dodecyl sulfate polyacrylamide gel electrophoresis (SDS-PAGE) were stained with Imperial Protein Stain (Thermo Scientific) once the electrophoresis was completed. The precast gel was removed from the electrophoresis chamber and placed in a clean tray. Then the Tris-Glycine gel was taken out from the gel cassette and washed three times in 50 ml deionized water for 5 minutes each. After that, 20 ml Imperial Protein Stain was applied to completely cover the gel, and kept on gentle shaking for one hour in the dark. The stained gel was transferred to fresh deionized water and washed extensively to remove residual staining solution, and was kept in 200 ml deionized water overnight to reduce the background staining as much as possible. Scanning of the gel was performed with a Typhoon 9410 Variable Mode Imager, using the following settings: Acquisition Mode: Fluorescence; Excitation: Red 633 nm; PMT: 650V; Pixel size: 100 microns; Normal sensitivity.

2.6. Crosslinking

WT and DKO MEFs were cultured in 150 mm petri dishes. First, the culture medium was discarded and the cells were washed three times with PBS. Dithiobis[succinimidylpropionate] (DSP) was dissolved in PBS containing 10% DMSO (v/v) to a final concentration of 1 mM, and 10% DMSO in PBS (v/v) was used as the control. The percentage of DMSO was chosen since DSP slowly precipitates when DMSO constitutes less than 10% volume in solution. Crosslinking was initiated by incubating WT and DKO MEFs with 10 ml of control or crosslinking solution at room temperature for 30 minutes. After that, the control/crosslinking solution was discarded and the reaction was quenched by a 15-minute incubation with 10 ml

quench buffer (20 mM Tris, 150 mM sodium chloride). Cells were then washed with PBS. 1 ml hypotonic buffer was subsequently added to each petri dish to aid cell scraping and collection. Collected cells were further disrupted by sonication (15 amplitudes, 4 cycles with 2 minutes intervals, three 15-second sonication with 30 seconds interval in each cycle). After sonication, unbroken cells and cell debris were spun down by centrifugation and discarded, and the cell lysate was carried on to the subsequent [^{32}P]-NAADP binding assay.

2.7. Thin-Layer Chromatography

Thin-Layer Chromatography (TLC) was used to monitor the production of oxidized NAADP. TLC plates coated with silica gel or polyethylenimine-modified cellulose (PEI-cellulose) were cut into adequate sizes before development. For PEI-cellulose, plates were pre-developed in deionized H_2O and the impurities shown as a yellow stain at the top of the fully-developed plate were cut off. The samples were applied onto the TLC plates along the pencil-marked starting line using capillaries. Briefly, samples were loading into capillaries and made transient contacts to the plates to allow sample application while maintaining minimal spot sizes. This was repeated several times until a sufficient amount was applied. The plates were then air-dried until all sample solvent had been evaporated.

The development of the TLC plates was carried out in a twin-trough chamber. Both troughs were filled with the solvent of choice and allowed 30 minutes to reach vapour equilibrium with the lid on. After that, the TLC plates were swiftly placed into the trough vertically. Solvent slowly moved up the plates as the development continues.

When the solvent front almost reached the top of the plate, the plates were taken out and air-dried in a chemical hood. As all plates contained a fluorescent indicator, visualization was carried out by directly illuminating the plates with UV at 254 nm in the dark.

2.8. Oxidation of NAADP and the preparation of NAADP affinity column

35 mg NAADP was dissolved in 1 ml 0.1 M sodium phosphate, pH 7.0. 10 mg sodium periodate was added to the NAADP solution and incubated in the dark at room temperature for 30 minutes. The reaction was monitored by thin-layer chromatography (TLC) on a PEI-cellulose plate. Once the reaction was completed, the remaining periodate was quenched by the addition of ethylene glycol to a final concentration of 50 mM, followed by 15 minutes incubation in the dark.

Oxidized NAADP was then purified by Sep-Pak C18 cartridge (Waters). Saturated sodium diphosphate solution was added to the sample to a final concentration of 2 M and the pH was adjusted to 2 using 1 M phosphoric acid. A Sep-Pak C18 cartridge was conditioned with 5 ml methanol and equilibrated with 5 ml water prior to separation. Sample was loaded onto the C18 column using a syringe, washed with 1 ml 1 M phosphoric acid and eluted with 3 ml water. Periodate contamination was tested using 0.5 M potassium iodide. The fractions collected from the C18 column were tested on a PEI-cellulose TLC plate and those that contained oxidized NAADP while free from periodate contamination were combined and its concentration was measured by absorption at 254 nm using a spectrophotometer (IMPLEN). 15 mg hydrazide-coated

magnetic beads were subsequently added to the oxidized NAADP solution and incubated with gentle agitation overnight at room temperature. The amount of oxidized NAADP coupled to the beads was calculated from the reduction of absorption at 254 nm. The beads were then treated with 0.1 M glyceraldehyde to quench any free hydrazine groups. Finally, the NAADP affinity column prepared from oxi-NAADP coupled magnetic beads was washed extensively until ready to use.

2.9. Affinity pull-down of NAADP binding proteins

Freshly prepared mouse liver cytosol was added to the NAADP affinity column and incubated for one hour with gentle shaking. The total protein input was 500 µg for each experiment. 500 µM NAADP was added to the reaction mixture for competition of specific NAADP binding. After the incubation, column beads were isolated from the reaction mixture by strong magnets and washed three times with PBS to remove any residual mouse liver cytosol or weakly bound proteins. Proteins bound to the column were then eluted with Laemmli buffer (sample loading buffer). Protein samples were loaded onto a precast 4-20% Tris-Glycine gel after 10 minutes heating at 95 °C and were separated by SDS-PAGE using methods described in section 2.5.

2.10. Fast Protein Liquid Chromatography (FPLC)

Fast Protein Liquid Chromatography (FPLC) was performed using an Akta FPLC workstation. In this study three types of chromatography were performed, namely ion-exchange chromatography (IEX), hydrophobic interaction chromatography (HIC) and size-exclusion chromatography (SEC).

For ion-exchange chromatography, separation was performed in HiTrap DEAE FF (Diethylaminoethyl FastFlow, GE Healthcare Life Sciences). The separation started in a low-salt buffer and proteins were eluted based on their surface charges by a gradient of high-salt buffer. Buffer A: 20 mM bis-Tris, 1 mM EDTA, pH 7.0. Buffer B: 20 mM bis-Tris, 1 mM EDTA, 1 M KCl, pH 7.0. The gradient ran at 2.5 ml/min and was setup as follows: 4 column volume (CV) 0% buffer B, 3 CV 2% buffer B and 5 CV 5% buffer B, then the column was cleaned with 5 CV 100% buffer B and re-equilibrated with 7 CV buffer A.

For hydrophobic interaction chromatography, HiTrap Butyl HP (Butyl HighPerfromance, GE Healthcare Life Sciences) and Phenyl FF (high substitution) (Phenyl FastFlow, GE Healthcare Life Sciences) were used for separation. Phenyl FF (high substitution) column has a similar ligand density as the Butyl HP column (40 µM/ml and 50 µM/ml, respectively), hence the protein binding capacity of these two columns are comparable. The separation started in a high-salt buffer and proteins were eluted by a low-salt buffer gradient based on their surface hydrophobicity. For Phenyl FF, the chromatography buffers are listed as follows: Buffer A: 50 mM potassium phosphate, 1 mM EDTA, 1.5 M ammonium sulfate, pH 7.0. Buffer B: 50 mM potassium phosphate, 1 mM EDTA, pH 7.0. The gradient ran at 2.5 ml/min and was setup as follows: 6 CV 0% buffer B, 0-100% buffer B in 10 CV, then the column is cleaned with 15 CV 100% buffer B and re-equilibrated with 5 CV buffer A. For Butyl HP column, the concentration of ammonium sulfate in both buffer A and B was reduced from 1.5 M to 1.3 M. Flow rates were 1 ml/min for 1 ml column and 2.5 ml/min for 5 ml column. Elution gradient was optimized on Butyl HP 5 ml column. The slope-step gradient was set as follows: 0% buffer B for 5 CV, 15% buffer B for 5 CV and 15-100%

B in 10 CV. Then the column was cleaned with 15 CV 100% buffer B and re-equilibrated with 5 CV buffer A. For the final optimized step gradient, the gradient was set to 0% buffer B for 5 CV, 15% buffer B for 6 CV, cleaning with 100% buffer B for 10 CV and re-equilibrated with 5 CV buffer A.

For size-exclusion chromatography, purification of the protein was performed using a Superdex 200 HR 10/30 column (GE Healthcare Life Sciences). The buffer used was 50mM potassium phosphate, pH 7.0 or 50mM potassium phosphate, 150 mM potassium chloride, pH 7.0. The size-exclusion chromatography was carried out with 1.5 CV isocratic elution at 0.5 ml/min.

In some experiments, buffer exchange was performed on FPLC using a HiTrap desalting column (GE Healthcare Life Sciences) and the desired buffer. This was performed with 1.5 CV isocratic elution at 2 ml/min.

2.11. Synthesis of NAADP, [^{32}P]-NAADP and their azido analogs

In this study, NAADP and [^{32}P]-NAADP were used to measure NAADP binding in various samples.

The synthesis of NAADP is a one-step reaction using NADP and excessive nicotinic acid. The reaction was carried out at pH 4.0 in the presence of *Aplysia* ADP-ribosyl cyclase and later the NAADP was purified with an AGMP-1 anion exchange column (Bio-Rad) using a 40-minute 150 mM trifluoroacetic acid (TFA) gradient.

[^{32}P]-NAADP was synthesized in the lab routinely in a two-step reaction modified from what has been described previously (Aarhus *et al.*, 1996). In the first step, [^{32}P]-ATP was converted to [^{32}P]-NADP by incubating with NAD and human NAD kinase overnight. [^{32}P]-NADP was then mixed with nicotinic acid and ADP-ribosyl cyclase at pH 4.0 to produce [^{32}P]-NAADP. When the reaction was completed, [^{32}P]-NAADP was purified with an AGMP-1 anion exchange column using the 40-minute 150 mM TFA gradient and the radioactive signal was detected using an in-line radiation detector (Bioscan Flow Count B-FC-1000, Bioscan). The collected [^{32}P]-NAADP was neutralized with 1 M Tris, pH 7.1 and stored at 4°C.

The synthesis of 5-azido-NAADP and [^{32}P]-5-azido-NAADP is similar to that of NAADP except that 5-azido-nicotinic acid was used as the reactant instead of nicotinic acid. 5-azido-nicotinic acid was synthesized at the Shanghai Institute of Organic Chemistry, Chinese Academy of Sciences using previously described methods (Jain *et al.*, 2010).

2.12. Radioligand binding assay

Nitrocellulose filters were moistened using 0.1% CHAPS (3-[(3-cholamidopropyl)dimethylammonio]-1-propanesulfonate) and incubated with 200 µl protein solution overnight at 4 °C to allow protein absorption onto the filter. The protein solution was removed and the filters were incubated with 200 µl control (no NAADP) or NAADP of various concentrations in binding buffer (20 mM HEPES, 250 mM potassium acetate, pH 7.2) for 15 minutes, followed by the addition of 50 µl 1 nM [^{32}P]-NAADP (final concentration 0.2 nM) and a further incubation of 1 hour. Nitrocellulose filters were then washed with 1.5 ml ice-cold binding buffer 4 times and

subsequently transferred to a storage phosphor screen (GE Healthcare Life Sciences). The screen was scanned the next day to acquire the image of radioactive signals of the samples.

2.13. Nuclear Magnetic Resonance (NMR)

Structural characterization of 5-azido-nicotinic acid and 5-azido-NAADP by NMR (nuclear magnetic resonance) was kindly performed by Dr. Yuwen Zeng from the Shanghai Institute of Organic Chemistry, and Mr. Hang Xu and Mr. Ming Gao from the Chemistry Research Laboratory, University of Oxford. 5-azido-nicotinic acid was dissolved in deuterated methanol and the ^{1}H NMR analysis was carried out by Bruker AV500 (500MHz) at the Shanghai Institute of Organic Chemistry, Chinese Academy of Sciences. 5-azido-NAADP was dissolved in deuterated water prior to ^{1}H NMR analysis by Bruker AVF400 (400MHz) at the Chemistry Research Laboratory, University of Oxford.

2.14. In-gel photoaffinity labelling

Proteins were pre-incubated with either deionized water or 4 µM NAADP for 10 minutes. After that, [^{32}P]-5-azido-NAADP was added to the mix to a final concentration of 0.2 nM and incubated for an additional 20 minutes to allow the sample to reach binding equilibrium. The solution was then exposed to 365 nm UV irradiation for 20 minutes in the dark. After UV irradiation, samples were incubated with Lammeli buffer for 10 minutes and then loaded onto a 4-20% Tris-Glycine precast gel for

electrophoresis, using settings described in the previous section (see section 2.5 Protein electrophoresis and staining).

2.15. Mass Spectrometry (MS)

Protein liquid chromatography-mass spectrometry (LC-MS) was performed at the Advanced Proteomics Facility, University of Oxford. Protein samples were processed according to FASP (Filter-Aided Sample Preparation) protocol before analysis. Fractions collected from FPLC were concentrated using a Vivacon 10 KDa MWCO centrifugal concentrator at 15,900xg until most material had gone through the filter. 200 µl reduction buffer (8 M Urea, 100 mM TEAB (tetraethylammonium bromide), and 10 mM TCEP (tris(2-carboxyethyl)phosphine)) was then added to the filter and incubated for 30 minutes with gentle shaking. After that, the reduction buffer was removed by centrifugation at 15,900xg and the filter was incubated with 200 µl of alkylation buffer (8 M Urea, 100 mM TEAB, 20 mM C-IAA (Chloro-Iodoacetamide)) in the dark with gentle shaking for 30 minutes at room temperature. When the alkylation was complete, the alkylation buffer was discarded by centrifugation at 15,900xg and the filters were washed with 200 µl 1 M Urea, 50 mM TEAB, pH 8 twice followed by trypsin digestion. Trypsin buffer was added to the filter to an enzyme:protein ratio (w/w) of 1:20. The digestion was carried out at 37 °C for one hour with gentle shaking.

When the digestion was finished, the filters were centrifuged at 15,900xg for 30 minutes and washed with 200 µl 0.1% TFA using the same settings. Digested peptides were eluted with 200 µl 50% acetonitrile in 0.1% TFA. All flowthrough was combined and dried down using a speed vacuum centrifuge.

The peptides were then further purified on C18 membranes. Desiccated peptides were resuspended in 8 M Urea and sonicated for 5 minutes. Meanwhile, C18 membranes were placed in pipette tips, wetted with 30 µl 100% acetonitrile and washed with 30 µl 0.1% TFA. The tips were then placed in a new Eppendorf tube. Sonicated samples were added to the tips and centrifuged at 2,000 rpm until all liquid had gone through the C18 membrane, followed by washing with 30 µl 0.1% TFA. All flow through was collected in the same tube at this point. After washing with TFA, the tips were transferred to another new Eppendorf tube and the peptides bound to the C18 membranes were eluted with 20 µl 50% acetonitrile in 0.1% TFA to minimize the volume and slowly spun at 1,000 rpm until the membrane was dry. The eluent was desiccated in a speed vacuum centrifuge until ready for LC-MS analysis.

2.16. Virtual screening

In this study, virtual screening of potential NAADP binding protein candidates was carried out by two independent pieces of software, AutoDock Vina (The Scripps Research Institute) and CLC Drug Discovery Workbench (Qiagen). X-ray crystallography structures of shortlisted protein candidates were downloaded from The European Bioinformatics Institute (EMBL-EBI) or The Protein Data Bank (RCSB PDB) in pdb format. The 3D structure of NAADP was downloaded from PubChem.

For docking simulation using AutoDock Vina, the pdb files were first processed by PyMOL software (Schrödinger). Ligands, cofactors and water molecules were removed from the protein structure. The structures were then visualized using AutoDockTools-1.5.6 (The Scripps Research Institute), polar hydrogens were added, and saved in

pdbqt format. The NAADP 3D structure was also converted into pdbqt format in a similar way. The grid box for docking simulations was set in AutoDockTools to cover the entire protein structure. This setting was adjusted for each individual protein. The coordinates of the grid box were noted and subsequently used as input parameters in AutoDock Vina, together with the structures of both protein and NAADP in pdbqt format. The docking simulation was carried out in command prompt and results were returned in text files containing affinity (kcal/mol), RMSD l.b. (RMSD lower bound) and RMSD u.b (RMSD upper bound).

For docking simulation with CLC Drug Discovery Workbench, the preparation of the structures was performed by excluding the ligands, cofactors and water molecules from the protein crystallography structures. The binding site of the protein was setup by 'Setup Binding Site' function, which covered all or most of the protein structure. The results were returned in 3D-conformation and optimized using a built-in function to get the final docking score.

2.17. Protein expression

Based on the result of protein-ligand docking, three protein candidates were selected from the list and expressed in *E. Coli*. Expression and purification of the protein candidates was carried out by Dr Bing Meng from the Institute for Advanced Immunochemical Studies, ShanghaiTech University. In short, the protein amino acid sequences were obtained and searched for their cDNA sequence from EMBL. The sequences were then cloned into a pET-28b vector with a 10x histidine tag and a TEV

(Tobacco Etch Virus) cleavage sequence (ENLYFQS) to allow removal of the His-tag by TEV protease. A serine residue would be fused with the N-terminal after the cleavage.

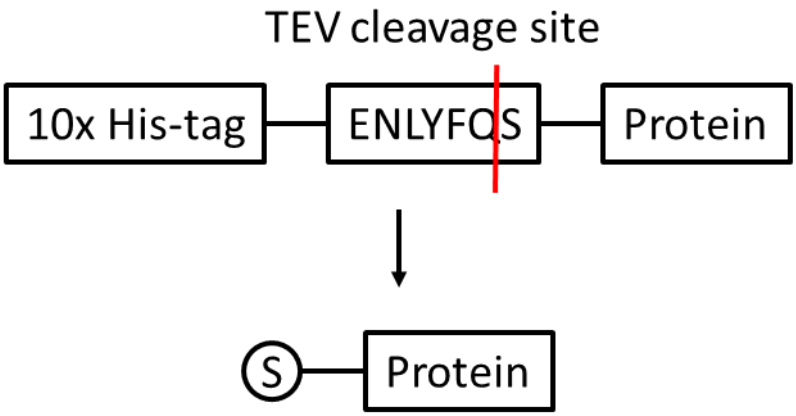

Figure 2.1. TEV cleavage of His-tag from target protein. A serine residue would remain fused to the N-terminal of the protein after the cleavage by TEV protease.

The three protein candidates expressed are: human carbonyl reductase [NADPH] 1, human NADH-cytochrome b5 reductase 3, isoform 2 and human thiopurine S-methyltransferase. The amino acid sequences and corresponding plasmid maps are listed as follow:

UniProtKB - P16152 (CBR1_HUMAN): Human Carbonyl reductase [NADPH] 1 (hCBR1):

MSSGIHVALVTGGNKGIGLAIVRDLCRLFSGDVVLTARDVTRGQAAVQQLQAEGLSPRFHQLDI
DDLQSIRALRDFLRKEYGGLDVLVNNAGIAFKVADPTPFHIQAEVTMKTNFFGTRDVCTELLPLIK
PQGRVVNVSSIMSVRALKSCSPELQQKFRSETITEEELVGLMNKFVEDTKKGVHQKEGWPSSAY
GVTKIGVTVLSRIHARKLSEQRKGDKILLNACCPGWVRTDMAGPKATKSPEEGAETPVYLALLPP
DAEGPHGQFVSEKRVEQW

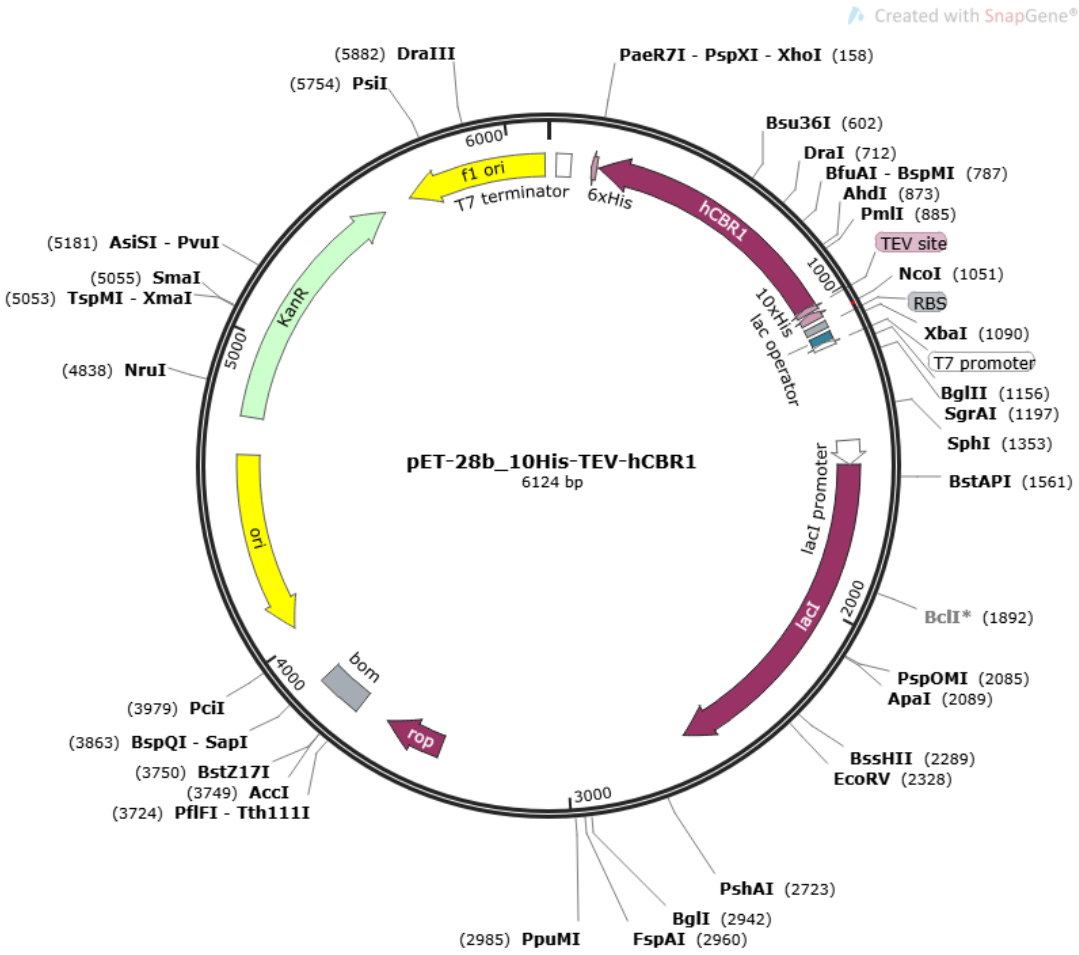

Figure 2.2. Plasmid map of recombinant hCBR1.

UniProtKB - P00387-2 (NB5R3_HUMAN): Human NADH-cytochrome b5 reductase 3 (hCYB5R3), isoform 2:

MKLFQRSTPAITLESPDIKYPLRLIDREIISHDTRRFRFALPSPQHILGLPVGQHIYLSARIDGNLVVR
PYTPISSDDDKGFVDLVIKVYFKDTHPKFPAGGKMSQYLESMQIGDTIEFRGPSGLLVYQGKGKF
AIRPDKKSNPIIRTVKSVGMIAGGTGITPMLQVIRAIMKDPDDHTVCHLLFANQTEKDILLRPELE
ELRNKHSARFKLWYTLDRAPEAWDYGQGFVNEEMIRDHLPPPEEEPLVLMCGPPPMIQYACLP
NLDHVGHPTERCFVF

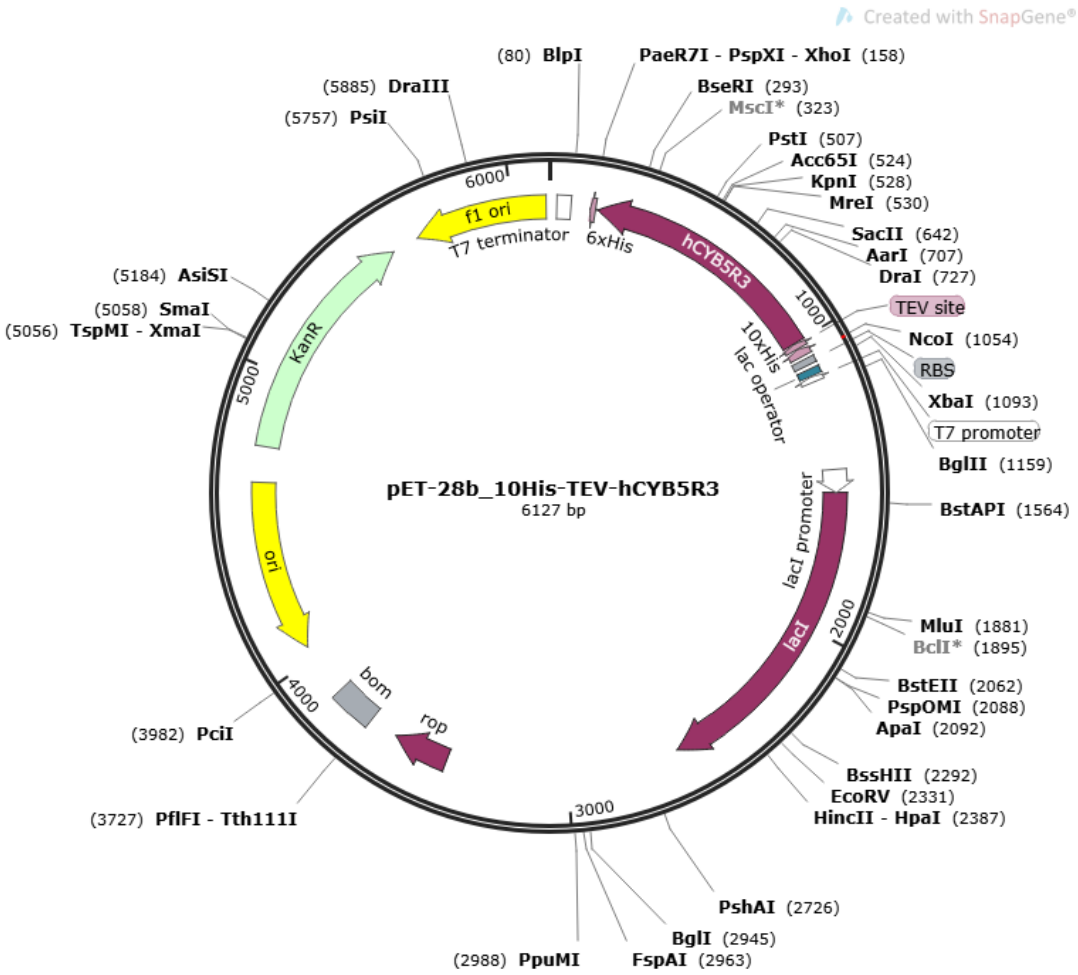

Figure 2.3. Plasmid map of recombinant hCYB5R3.

UniProtKB - P51580 (TPMT_HUMAN): Human Thiopurine S-methyltransferase (hTPMT):

MDGTRTSLDIEEYSDTEVQKNQVLTLEEWQDKWVNGKTAFHQEQGHQLLKKHLDTFLKGKSG
LRVFFPLCGKAVEMKWFADRGHSVVGVEISELGIQEFFTEQNLSYSEEPITEIPGTKVFKSSSGNIS
LYCCSIFDLPRTNIGKFDMIWDRGALVAINPGDRKCYADTMFSLLGKKFQYLLCVLSYDPTKHPG
PPFYVPHAEIERLFGKICNIRCLEKVDAFEERHKSWGIDCLFEKLYLLTEK

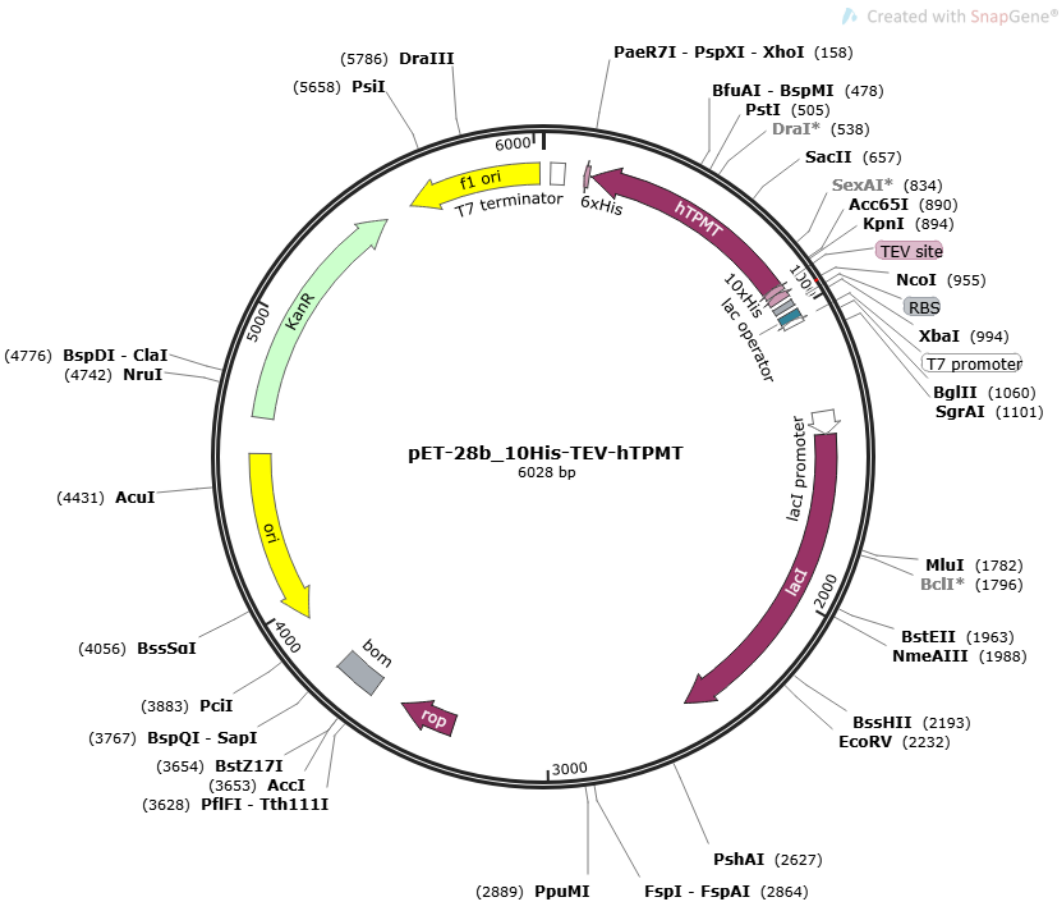

Figure 2.4. Plasmid map of recombinant hTPMT.

The recombinant proteins expressed in *E. Coli* were purified by sequential chromatography. His-tagged recombinant proteins in E. Coli lysate were first captured by TALON metal affinity resin, then digested with TEV protease to remove the histidine tags and passed through the TALON metal affinity resin again to remove any undigested protein. Later the proteins were further purified in apo- and holo-enzyme

form via ion-exchange chromatography and size-exclusion chromatography and their purity was checked by SDS-PAGE.

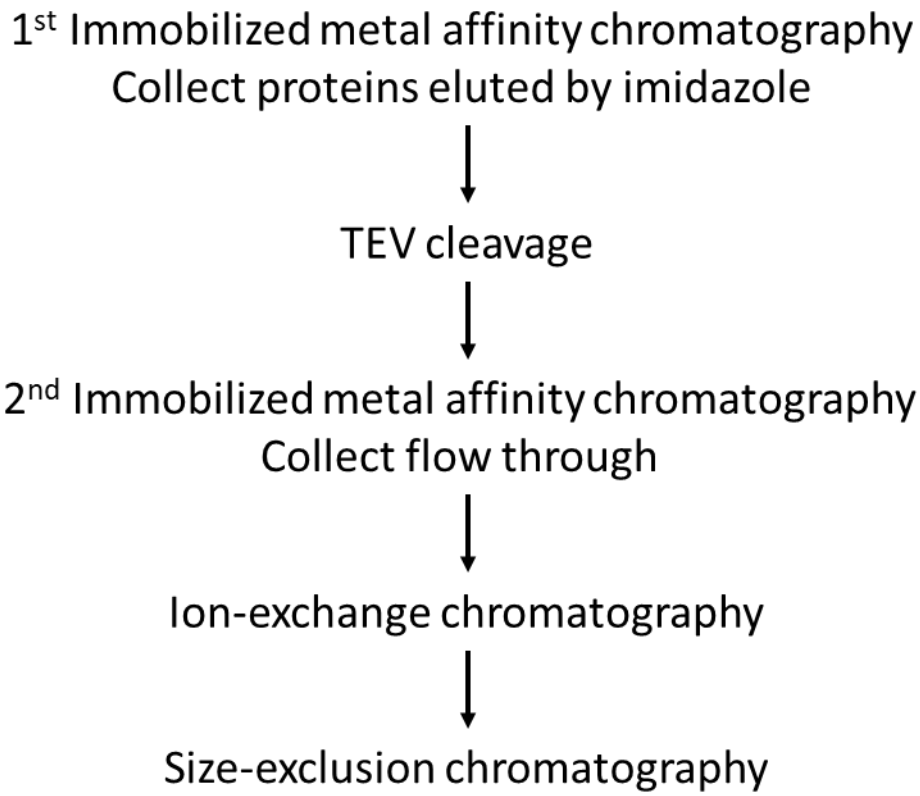

Figure 2.5. Recombinant protein purification strategy.

2.18. Bio-Layer Interferometry

All Bio-Layer Interferometry (BLI) experiments were performed by Ms. Meng Wu at the Institute of Biochemistry and Cell Biology, Shanghai Institutes for Biological Sciences, Chinese Academy of Sciences.

Proteins (apo-hCBR1, holo-hCBR1, apo-hCYB5R3, holo-hCYB5R3 and hTPMT) were diluted to a concentration of 2 mg/ml, biotinylated by mixing with 10 mM biotin at 1:1 molar ratio and incubated at room temperature for 1 hour. Excess biotin was removed by desalting (Zeba Spin Desalting Column, Pierce). A BLI experiment was carried out on Octet RED 96 System (Pall ForteBio) using Super Streptavidin biosensors (SSA

biosensors, Pall ForteBio) and a 96-well plate. 50 µg/ml biotinylated protein was immobilized onto the SSA biosensors and any free streptavidin was then blocked by 5 µM biocytin to reduce background signal. The experiment phases are described in the following table:

Table 2.1. Procedure of Bio-layer Interferometry experiment.

No.	Phase	Duration (s)	Description
1	Baseline	60	Baseline equilibrium of biosensor in buffer.
2	Loading	900	Immobilization of biotinylated protein onto biosensor.
3	Quenching	180	Elimination of free streptavidin by 5 µM biocytin.
4	Baseline2	120	Baseline equilibrium of biosensor with immobilized protein.
5	Association	600	Association of the ligand with immobilized protein on biosensor.
6	Dissociation	600	Dissociation of the ligand from immobilized protein on biosensor.

All measurements were done in HEPES buffer (25 mM HEPES, 250 mM sodium chloride, pH 7.8) with various concentrations of NAADP. In addition, double referencing was used to minimize the background signal and to achieve a better signal-to-noise ratio. One reference sample and one reference biosensor were included in every BLI experiment. The reference sample refers to the biosensor that had protein immobilized but was run in the association phase with buffer that contained no ligand, whereas the reference biosensor did not have protein immobilized but the experiment was run normally. This allowed subsequent subtraction of baseline drift and non-specific ligand-sensor binding from the signal detected. The signal of protein-ligand interaction was thus obtained by subtracting the signal of the reference sample and reference biosensor from the original signal observed in the experiment. The data was analyzed by software provided by the system manufacturer (Data anaylsis-10 version, Pall ForteBio), including curve fitting, K_{on}, K_{off} and K_d calculation.

For heat-inactivated hTPMT experiments, hTPMT (2 mg/ml) was heated at 99 °C for 2-3 hours until substantial precipitation was observed. The precipitated protein was removed by centrifugation and the supernatant was then biotinylated and later tested using the methods described above.

2.19. Micro-Scale Thermophoresis

Micro-Scale Thermophoresis (MST) was performed on a Monolith NT. 115 system (NanoTemper Technologies) by Ms. Meng Wu at Institute of the Biochemistry and Cell Biology, Shanghai Institutes for Biological Sciences, Chinese Academy of Sciences. NT-647-NHS (Protein Labelling Kit RED-NHS, NanoTemper Technologies) was first dissolved in DMSO then diluted in HEPES buffer to make a dye solution of ~28 µM. 100 µl dye solution was then mixed with 10 µM protein in HEPES buffer at 1:1 volume ratio and incubated in dark for 30 minutes. Meanwhile, gravity flow purification Column B (Protein Labelling Kit RED-NHS, NanoTemper Technologies) was conditioned and equilibrated with HEPES buffer. Once the incubation was finished, labelled protein was purified by Column B and any free dye was removed during the process. Labelled protein was eluted from Column B in about 500 µl HEPES buffer, which gave approximately 2 µM protein concentration. 3-4 µl eluent was loaded into Monolith NT Series Premium Capillaries (NanoTemper Technologies) and tested by Monolith NT.115 to measure the efficiency of the labelling. After that, the eluent was diluted 10-fold in HEPES buffer to make the sample solution for the experiment while NAADP stock was diluted with HEPES buffer at 1:1 volume ratio to generate 16 concentrations from 6 mM to 183 nM. NAADP dilutions were mixed with the same volume of sample solution and incubated at room temperature for 20-30 minutes before loading into

capillaries for MST testing. MST power was set to medium and LED power was set to 20-60% depending on the labelling efficiency. Data analysis, curve fitting and K_d calculation was performed in MO. Affinity Analysis 2.2.4.

Chapter 3 Characterization of NAADP binding protein by chemistry approaches

NAADP-induced Ca^{2+} release has been discovered as one of the key intracellular calcium signalling pathways featuring high potency. However, it remains elusive how NAADP evokes Ca^{2+} responses inside cells. Previously, it has been proposed that the Two-Pore Channels (TPCs) could be the NAADP receptor since their presence is essential for NAADP to cause Ca^{2+} release from acidic organelles, and the overexpression of TPCs results in an increase in NAADP binding in the membrane compartment of the cells. Nevertheless, in contrast to the 250-fold increase of TPC mRNA in the overexpression system, NAADP binding only increased by 3-fold, which indicates that there might be intermediate proteins that bind NAADP in the signalling cascade (Calcraft *et al.*, 2009).

This chapter describes an attempt to characterize NAADP binding protein(s) using two chemical approaches: crosslinking and an affinity column made from chemically modified NAADP.

3.1. Crosslinking of NAADP binding proteins in mouse embryonic fibroblasts (MEFs)

3.1.1. Introduction

It has been shown by the [^{32}P]-NAADP binding assay that significant NAADP binding is present in the cytosolic compartment of MEFs (unpublished data), which suggests a link to the robust NAADP-mediated calcium release in MEFs (Ruas *et al.*, 2015). Our hypothesis is that the cytosolic NAADP binding protein(s) could bind NAADP and interact with TPCs on the lysosomal membrane to evoke subsequent Ca^{2+} release from lysosomes. Therefore, chemical crosslinking of NAADP binding protein in MEFs was conceived to dissect the interaction between cytosolic NAADP binding proteins and TPCs in MEFs.

3.1.2. [^{32}P]-NAADP binding in mouse embryonic fibroblast

To see whether the transient interaction between cytosolic NAADP binding proteins and TPCs could be captured, an amine-reactive and cleavable chemical crosslinker, DSP (dithiobis (succinimidyl propionate)) was used to perform crosslinking in both wildtype (WT) and TPC1/TPC2 double-knockout (DKO) MEFs.

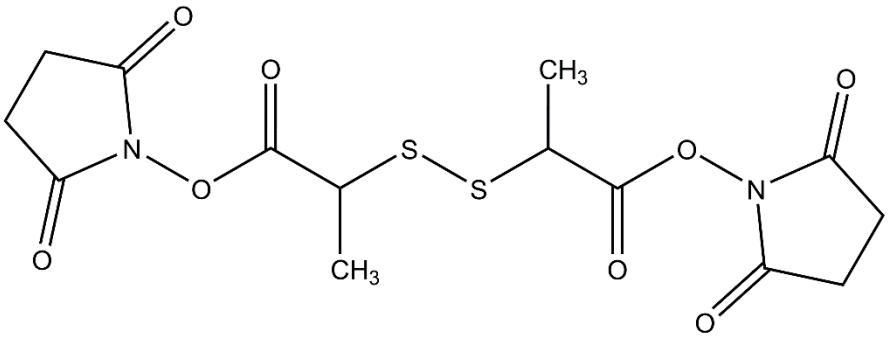

Figure 3.1. Structure of DSP. Molecular weight 404.42. Spacer Arm 12.0 Å.

The initial plan was to adopt a reversible cross-linking immunoprecipitation (ReCLIP) strategy, in which proteins of interests are isolated by immunoprecipitation after crosslinking with the bait protein, then analyzed by mass spectrometry (MS) following cleavage of the crosslinker (Smith *et al.*, 2011). In a preliminary study, immunoprecipitation was performed in DSP-crosslinked WT and DKO MEF homogenates to pull down TPC2, and the NAADP binding of the pull-downed protein complexes were tested by [^{32}P]-NAADP binding assay. However, the radioactive signals recovered from the assay were poor and almost indistinguishable from background radiation (data not shown). Since the TPC2 antibodies used had been rigorously tested in the lab, the problem could be attributed to insufficient protein capture by immunoprecipitation or interference of the NAADP binding by crosslinker.

To validate our assumption, a new set of experiments was conceived using MEF membranes as study subjects to achieve a better signal to noise ratio. In this scenario, our hypothesis is that the crosslinking by DSP would result in a shift of the NAADP binding profile, from the cytosolic compartment to the membrane compartment. After homogenization of MEFs by sonication, a [^{32}P]-NAADP binding assay was performed to examine whether the crosslinking would cause an overall reduction of

NAADP binding since non-specific crosslinking is very likely to cause protein denaturation or steric occlusion of the ligand binding site.

The procedure of the radioligand binding assay is illustrated in Figure 3.2. Nitrocellulose filters were washed with 0.1% CHAPS and incubated with protein samples. The next day, samples were discarded and filters were incubated with [^{32}P]-NAADP in the presence or absence of unlabelled NAADP to measure the NAADP binding of the proteins that were immobilized onto the filter.

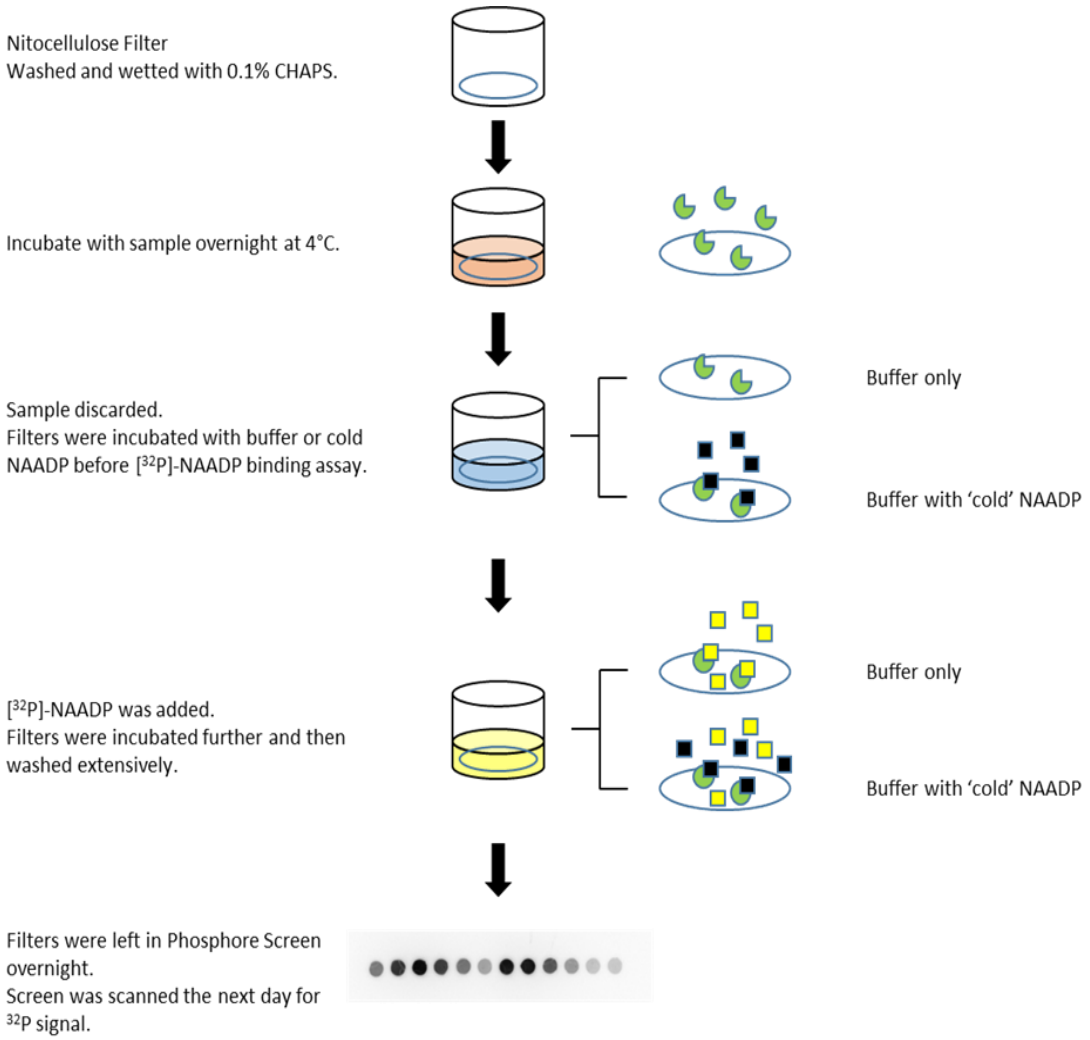

Figure 3.2. Procedures of [^{32}P]-NAADP radioligand binding assay.

The results of the binding assay on MEF homogenate is shown in Figure 3.3. The overall [^{32}P]-NAADP binding of MEFs crosslinked by DSP is higher than their non-

crosslinked counterparts while the proportion of non-specific binding remained similar. It is possible that the crosslinking made the protein or protein complexes more resistant to disruption by sonication and hence preserved the NAADP binding.

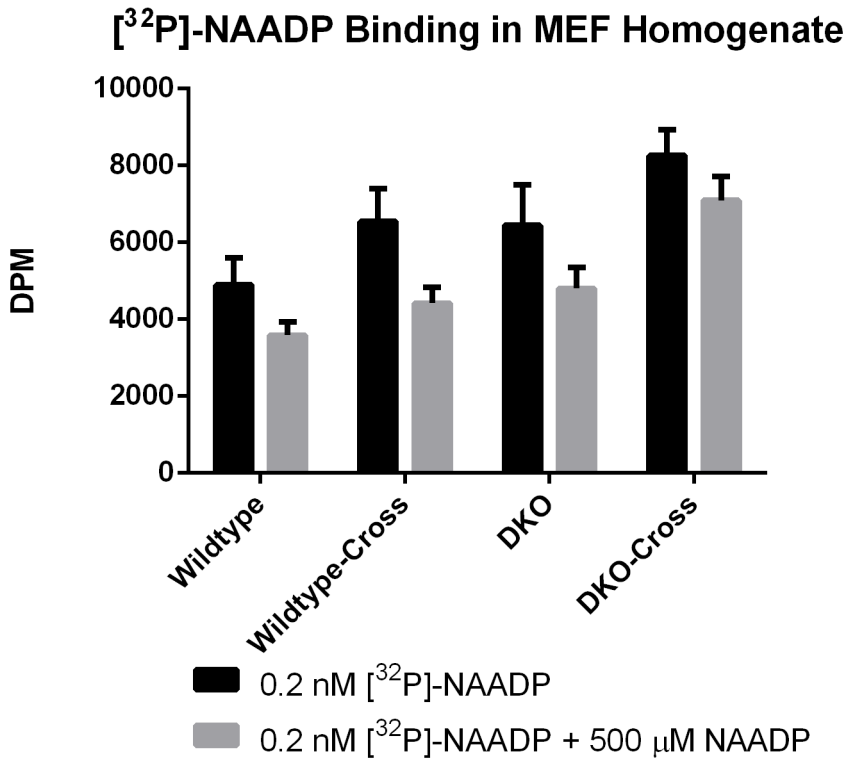

Figure 3.3. Effect of crosslinking on NAADP binding in WT/DKO MEF homogenate. Each column represents results from 80 μg protein. 500 μM unlabelled NAADP was used to determine the non-specific binding. Crosslinked MEFs showed slightly higher binding than the non-crosslinked MEFs. Each bar represents the mean DPM value of the duplicates ± SEM (n=4).

Next, the NAADP binding pattern was further investigated by determination of the [^{32}P]-NAADP binding in the corresponding cytosolic or membrane fractions (Figure 3.4). To our surprise, the [^{32}P]-NAADP binding in the membrane fraction was about 1- to 4-fold higher than the cytosolic fraction depending on cell type and treatment. Both WT and DKO MEFs cytosol exhibited very little specific binding and DSP crosslinking did not seem to affect [^{32}P]-NAADP binding in the cytosol. On the other hand, only around 40% of the [^{32}P]-NAADP binding in the membrane fractions of WT and DKO MEFs turned out to be specific, and crosslinking by DPS reduced both specific and non-

specific [^{32}P]-NAADP binding on the membrane fraction by almost 50%. These pieces of evidence suggested that crosslinking would impose significant detrimental effects on NAADP binding and may not be the best approach to study the interaction between NAADP binding protein and TPCs in MEFs.

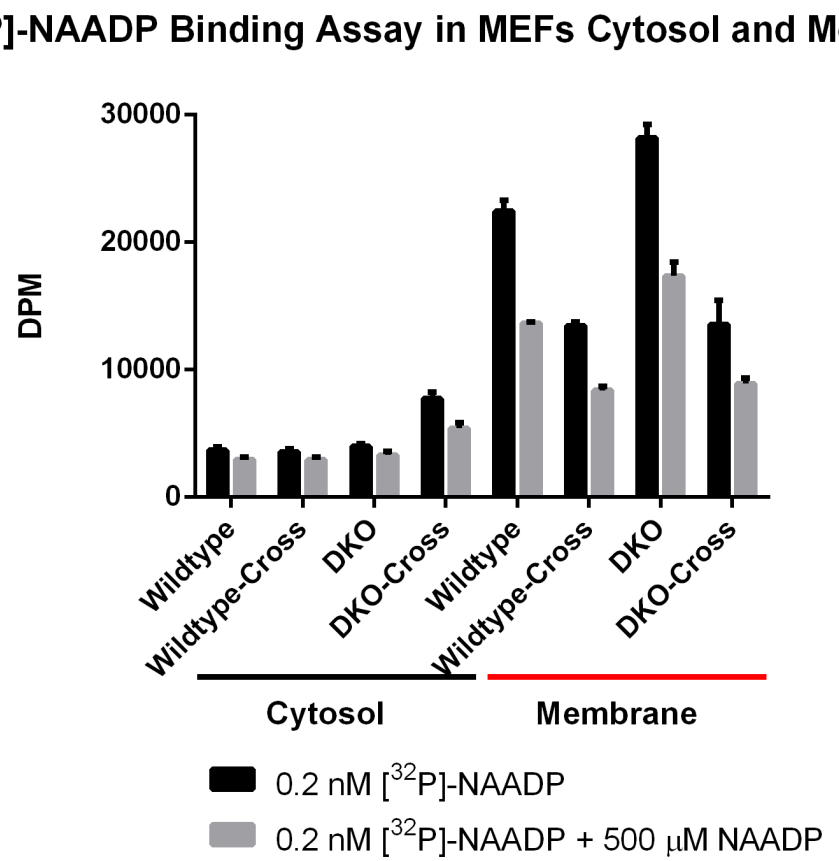

Figure 3.4. Effect of crosslinking on NAADP binding in WT/DKO MEF cytosol and membrane fractions. Each column represents result from 80 μg protein. 500 μM unlabelled NAADP was used to determine the non-specific binding. In MEFs, the NAADP binding is predominantly on the membrane fraction. Crosslinking causes a significant reduction of NAADP binding in the membrane fraction of both WT and DKO MEFs. Each bar represents the mean DPM value of the duplicates ± SEM (n=4).

3.1.3. NAADP binding affinity in mouse embryonic fibroblast membranes

In the previous set of experiment, it was found that although MEFs had high total NAADP binding, a considerable amount of non-specific binding was observed. To further characterize the NAADP binding in MEFs, the affinity of NAADP binding was determined using a [^{32}P]-NAADP competitive binding assay. In both WT and DKO membrane preparations only one low affinity binding site was discovered. As illustrated in Figure 5.4, the IC_{50} of WT membrane was approximately 121.2 µM while the DKO membrane had an IC_{50} of about 73.3 µM.

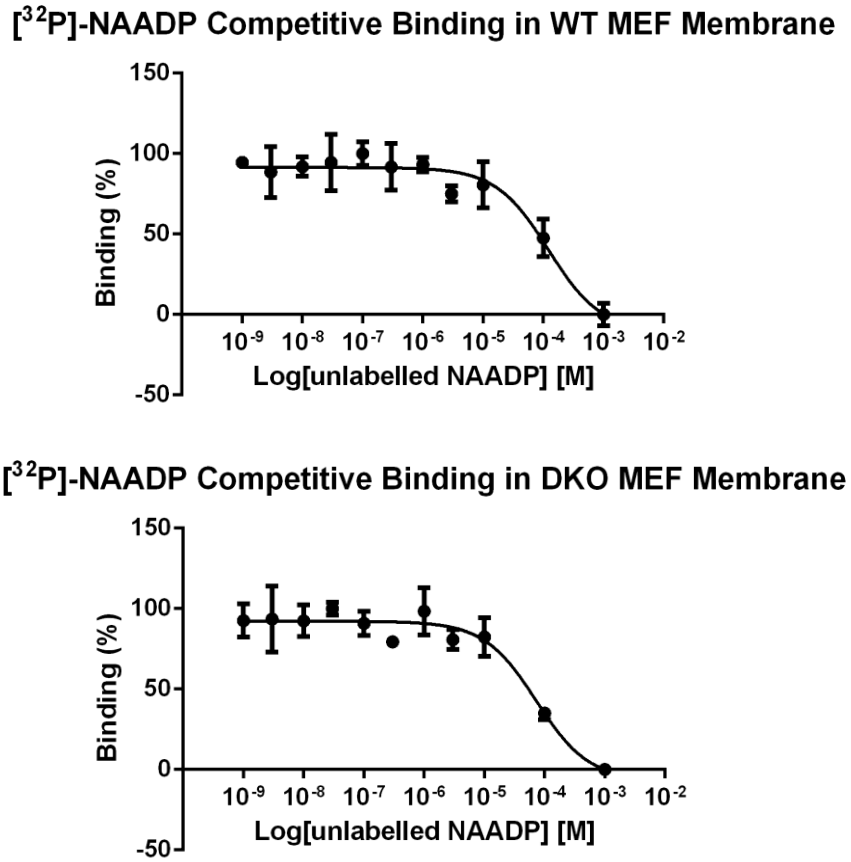

Figure 3.5. [^{32}P]-NAADP binding on WT/DKO MEF membrane. Each dot represents result from 80 µg protein. Competition of 0.2 nM [^{32}P]-NAADP with a gradient of unlabelled NAADP revealed only one low affinity binding site on the WT/DKO MEF membrane. Each bar represents the mean DPM value of the duplicates ± SEM (n=4).

3.1.4. Discussion

In this section, chemical crosslinking was employed to explore the possibility of capturing the interaction between the cytosolic NAADP binding protein and TPCs. Crosslinking has been proven to be a valuable tool in studying protein-protein interactions in transient protein complexes as those complexes are often lost during extensive handling (Vasilescu *et al.*, 2004). DSP is an amine-reactive crosslinker and is well-suited for the ReCLIP strategy due to its long spacer arm length, membrane permeability and cleavability by reducing agents such as SDS-PAGE reducing buffer. However, the binding assay using immunoprecipitated TPC2 beads in the preliminary study did not recover much of the signal, possibly due to the site occlusion of the crosslinker at the interaction site of binding protein on TPC2 since later experiments showed that DSP treated membranes had significant reduction of NAADP binding. Therefore, the ReCLIP strategy could not be implemented and had to be revised and substituted with a membrane preparation instead to enhance the ^{32}P signal. Nevertheless, the crosslinking experiments in MEFs proved that promiscuous chemical crosslinking is not the best approach to dissect NAADP signalling pathway due to its interference with NAADP binding.

Ruas *et al.* demonstrated that NAADP-AM could elicit calcium response in MEFs, which could be inhibited by many agents such as bafilomycin A1, GPN, nigericin and the NAADP inhibitor Ned-19 (Ruas *et al.*,2015). It is now widely accepted that NAADP does not directly bind to TPCs but to an intermediate protein. Recent pieces of evidence revealed that NAADP has two binding sites in various tissues (Calcraft *et al.*, 2009; Zhu, 2012; Ruas *et al.*,2015) and proteins showing high affinity binding at nanomolar

concentrations are believed to be involved in the NAADP signalling cascade since [^{32}P]-NAADP binding that occurred at the low affinity can be displaced by NADP (Calcraft *et al.*, 2009). Contrary to the popular idea of an intermediate cytosolic protein being responsible for the NAADP binding, our result showed that in WT and DKO MEFs, the NAADP binding on the membrane is 1 to 4 times more than that in the cytosol. A high concentration (10%) of DMSO was used to dissolve the crosslinker and this may have caused the disruption of the plasma membrane. It has been demonstrated by molecular dynamics (MD) that 10% DMSO would create transient water pores, but this would not be large enough to cause the loss of cytosolic proteins via leakage (Gurtovenko and Anwar, 2007). Thus, it is likely that the subcellular distribution of NAADP binding protein in MEFs is predominantly on the membrane.

Surprisingly, high affinity NAADP binding protein could not be detected using the radioligand binding assay in both WT and DKO MEF membrane preparations, suggesting its exceedingly low abundance since the radioligand binding assay can detect protein even at picogram levels (Weiss *et al.*, 2009). Moreover, only a low affinity binding site was detected in MEF membranes, and its affinity was even poorer than most of the low affinity sites identified in other preparations. The IC_{50} of the low affinity site on WT MEF membranes was 121.2 µM, which is 10-fold and 30-fold higher than that in MIN6 membranes (12 ± 0.6 µM, Masgrau *et al.*, 2003) and mouse liver membranes (4.6 ± 2.4 µM, Calcraft *et al.*, 2009). The fact that MEFs could still robustly respond to NAADP stimulus, combined with the evidence above, suggests that the scarcity of binding protein could be compensated for by its extreme efficacy. It is also possible that the disruption of MEFs via homogenization caused the denaturation of its high-affinity NAADP binding protein(s), thus leading to the absence of the high

affinity binding protein population in the radioligand binding assay. The observation of NAADP binding in WT and DKO MEFs also reiterated the existence of cell and tissue-specific variations of NAADP binding properties in mammalian systems.

3.2. NAADP Affinity Column

3.2.1. Introduction

Affinity columns have long been used as an effective method to isolate proteins or macromolecules of interests from complex mixtures or extracts. Unlike many other types of chromatography which rely on the chemical or physical interaction between the proteins and solid phase, affinity chromatography is dependent on the specific interaction between the molecules. Matrix crosslinked with nucleotides like ATP, GTP, NAD and NADP has been used as affinity column to isolate or purify various enzymes or kinases (Lamed *et al.*, 1973; Low *et al.*, 1992).

Previously, an ATP-coupled matrix was prepared by using periodate to oxidize the cis-glycol groups on the ribose ring of ATP and convert them into aldehydes, which then spontaneously react with the hydrazides on the chemically modified matrix and form stable hydrazone bonds (Lamed *et al.*, 1973).

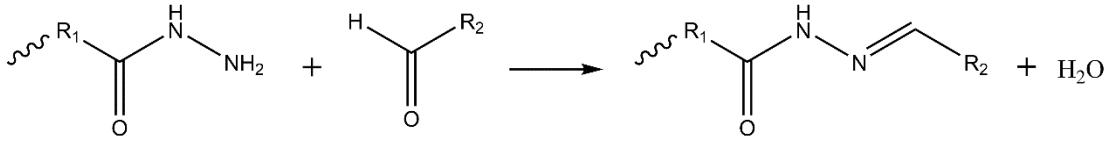

Figure 3.6. Principle of hydrazone bond formation.

Periodate oxidation is widely used in carbohydrate chemistry to perform 1,2-glycol scission. The periodate reaction is mild and simple as it often requires only an aqueous environment, and is highly selective under appropriate condition which limits the oxidation to 1,2-glycols, 2-amino alcohols, α-hydroxy ketones and aldehydes, α-amino aldehydes, 1,2-diketones, and some activated methylene groups (Bobbitt, 1956). NAADP has one cis-glycol group next to the nicotinic acid moiety, and hence might be

suitable for this approach (Figure 3.7). In this study, periodate has been used to oxidize NAADP to open the cis-glycol groups so that it could be immobilized onto the hydrazide magnetic beads (Figure 3.6) to generate an NAADP affinity column potentially capable of capturing NAADP binding protein(s) from crude mouse liver homogenate.

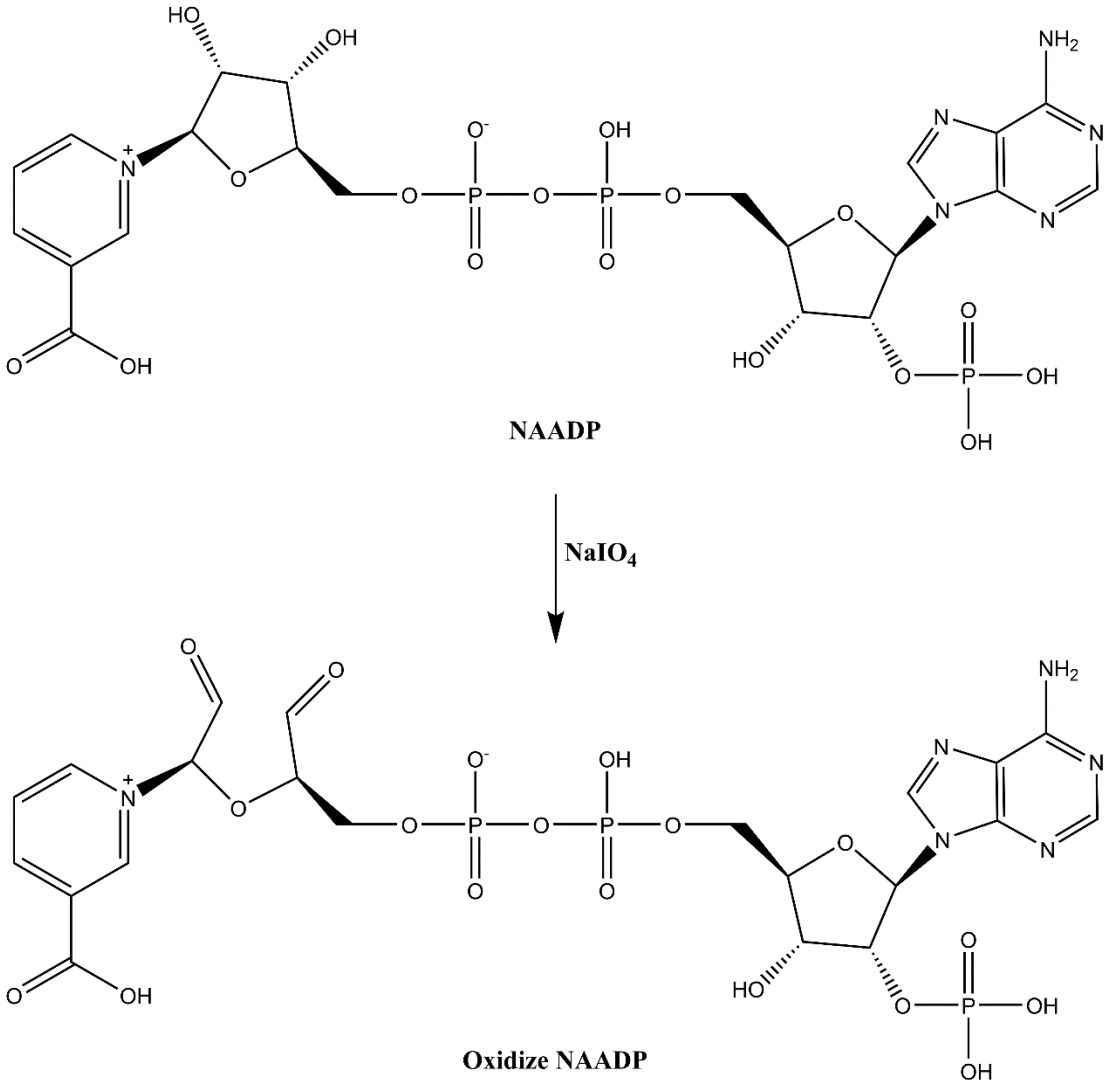

Figure 3.7. Principle of periodate oxidation of NAADP.

3.2.2. NAADP oxidation by sodium periodate

NAADP was oxidized by sodium periodate at neutral pH in the dark. Initial attempts to detect oxidized NAADP (abbreviated as oxi-NAADP) formation by HPLC using a strong anion exchange column AGMP-1, 150 mM trifluoroacetic acid (TFA) and a 12-minute gradient did not see separation of oxi-NAADP from NAADP (data not shown). A 40-minute gradient using 700 mM sodium acetate as elution buffer did not yield any satisfactory separation either (data not shown). Later the reaction was monitored by Thin-Layer Chromatography (TLC). Combinations of stationary and mobile phases were tested (Table 3.1) to determine the best setting for separation. All mobile phase combinations with silica gel plates did not result in distinct retardation factors of oxi-NAADP and NAADP, whereas with polyethylenimine-modified cellulose (PEI-cellulose) plates normally reasonable separations could be observed.

Table 3.1. Thin-Layer Chromatography of oxidized NAADP separation.

Stationary phase	Mobile phase	Composition	Separation
Silica gel			
	H_2O:MeOH: HOAc	10:3:0.2 (v/v)	No
	NH_4HCO_3	0.4 M	No
	MeOH:$CHCL_3$:H_2O: HOAc	13:10:3.5:0.2 (v/v)	Poor
	MeOH:DCM	15:85 (v/v)	No
PEI-cellulose			
	EtOAc/Butanol/HOAc/H_2O	80:10:5:5 (v/v)	No
	KH_2PO_4	0.75 M pH 3	Streaking
	KH_2PO_4	0.75 M pH 4.3	Streaking
	KH_2PO_4	0.75 M pH 4.7	Streaking
	LiCl	1 M	Good

As show in Figure 3.8, the best separation was achieved on the PEI-cellulose plate using 1 M LiCl as solvent.

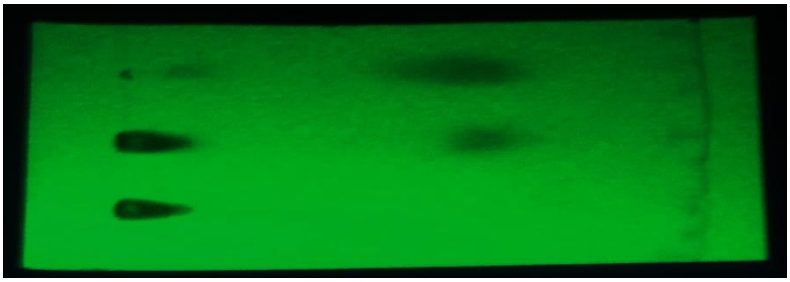

Figure 3.8. TLC result of periodate oxidation. Sample from top to bottom: NAADP, oxi-NAADP + NAADP, oxi-NAADP. Stationary Phase: PEI-Cellulose. Mobile Phase: 1 M LiCl. Solvent front is marked with pencil on the right side of the TLC plate.

Using potassium dihydrogen phosphate solution as mobile phase also yielded acceptable separation but was troubled by substantial sample streaking. This was possibly caused by Schiff base formation, in which aldehyde or ketone group reversibly reacts with the amine group on the plate (Figure 3.9). In contrast, only minor streaking was observed when the plate was developed in 1 M LiCl, illustrating the importance of solvent in achieving satisfactory separation.

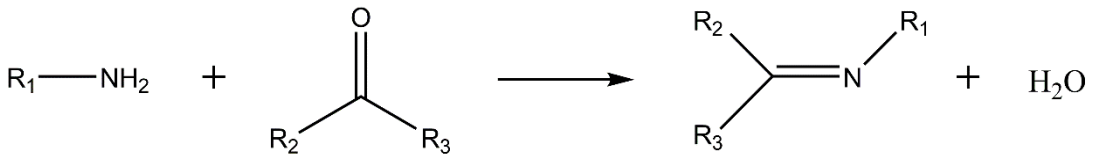

Figure 3.9. Principle of Schiff Base formation.

When the reaction was completed, oxi-NAADP was purified by C18 cartridge to remove residual periodate and its concentration was calculated from the extinction co-efficient (17440 $M^{-1}cm^{-1}$ at 254 nm) using an absorption reading from the spectrophotometer. After that, oxi-NAADP was mixed with magnetic hydrazide beads to initiate coupling. To measure the amount of oxi-NAADP coupled to the magnetic beads, the concentration of oxi-NAADP was checked again using the same method. Upon completion of coupling, the free hydrazide groups on the beads were eliminated by incubation with glyceraldehyde and the NAADP affinity column was then ready to use.

3.2.3. Affinity pull-down of mouse liver cytosol using NAADP affinity column and mass spectrometry analysis

Mouse liver cytosol has been chosen as the source of protein as it has been previously demonstrated to have substantial total binding as well as high affinity NAADP binding (Calcraft *et al.,* 2009). The liver cytosol was incubated with the NAADP affinity column and the proteins bound to the column were eluted by Lammeli buffer. SDS-PAGE of the eluent revealed that the intensity of multiple bands within 35-70 kDa decreased and one band around 45 kDa was completely displaced when free NAADP (500 μM) was present during the incubation. This suggests that the column could indeed isolate proteins that bind NAADP from a complex mixture. The bands from both control and NAADP treated sample were excised from the gel and submitted to protein mass spectrometry for analysis.

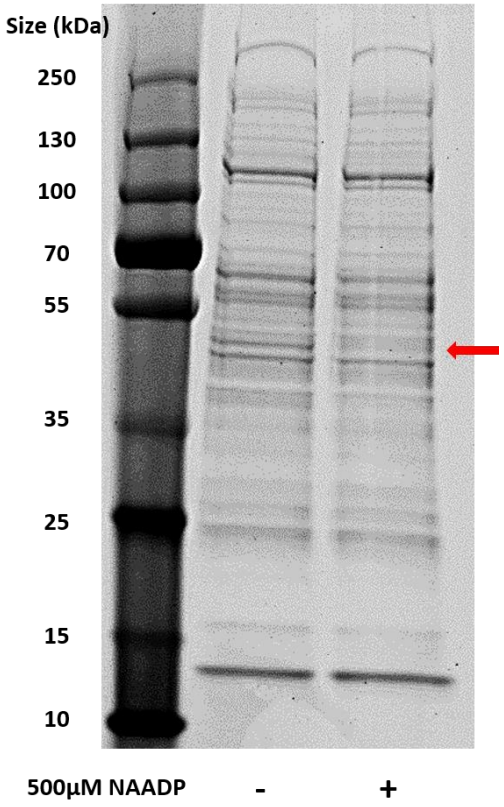

Figure 3.10. SDS-PAGE profile of eluent from NAADP affinity column.

The quantitative MS analysis revealed the identities of proteins that were absent in the NAADP treated sample group. Table 3.2 is a summary of all proteins from MS analysis that were more enriched in the control group (Control/NAADP > 1). Several intriguing protein candidates were found in the table, such as isocitrate dehydrogenase [NADP] and 6-phosphogluconate dehydrogenase. These proteins are known to bind NADP.

Table 3.2. Mass spectrometry analysis of protein candidate from NAADP affinity column.

Protein	Description	mw (Da)	% Coverage	Control/NAADP
sp|Q6IME9|K2C72_MOUSE	Keratin, type II cytoskeletal 72 OS=Mus musculus GN=Krt72 PE=3 SV=1	56805	5.60	Control Only
sp|P62737|ACTA_MOUSE	Actin, aortic smooth muscle OS=Mus musculus GN=Acta2 PE=1 SV=1	42078	37.00	Control Only
sp|P68373|TBA1C_MOUSE	Tubulin alpha-1C chain OS=Mus musculus GN=Tuba1c PE=1 SV=1	49950	50.30	Control Only
sp|P70694|DHB5_MOUSE	Estradiol 17 beta-dehydrogenase 5 OS=Mus musculus GN=Akr1c6 PE=1 SV=1	37078	13.00	Control Only
sp|Q8CII2|CD123_MOUSE	Cell division cycle protein 123 homolog OS=Mus musculus GN=Cdc123 PE=2 SV=2	38846	7.10	Control Only

sp|Q8CHS8-3|VP37A_MOUSE	Isoform 3 of Vacuolar protein sorting-associated protein 37A OS=Mus musculus GN=Vps37a	44445	7.80	Control Only
sp|Q8VCR7|ABHEB_MOUSE	Alpha/beta hydrolase domain-containing protein 14B OS=Mus musculus GN=Abhd14b PE=2 SV=1	22473	15.70	17.81
sp|P04919-2|B3AT_MOUSE	Isoform Kidney of Band 3 anion transport protein OS=Mus musculus GN=Slc4a1	103232	2.20	8.47
sp|P22907-2|HEM3_MOUSE	Isoform 2 of Porphobilinogen deaminase OS=Mus musculus GN=Hmbs	39374	32.50	7.43
sp|P16858|G3P_MOUSE	Glyceraldehyde-3-phosphate dehydrogenase OS=Mus musculus GN=Gapdh PE=1 SV=2	35841	25.80	6.75
sp|P54071|IDHP_MOUSE	Isocitrate dehydrogenase [NADP], mitochondrial OS=Mus musculus GN=Idh2 PE=1 SV=3	50946	39.80	4.40
sp|Q3UV17|K22O_MOUSE	Keratin, type II cytoskeletal 2 oral OS=Mus musculus GN=Krt76 PE=2 SV=1	62896	10.40	3.83
sp|P01837|IGKC_MOUSE	Ig kappa chain C region OS=Mus musculus PE=1 SV=1	11789	28.30	3.74
sp|Q9DCD0|6PGD_MOUSE	6-phosphogluconate dehydrogenase, decarboxylating OS=Mus musculus GN=Pgd PE=1 SV=3	53285	47.00	3.32
sp|Q99JY0|ECHB_MOUSE	Trifunctional enzyme subunit beta, mitochondrial OS=Mus musculus GN=Hadhb PE=1 SV=1	18972	24.90	3.22
sp|O55229|CHKB_MOUSE	Choline/ethanolamine kinase OS=Mus musculus GN=Chkb PE=1 SV=3	45151	11.70	3.02
sp|Q61239|FNTA_MOUSE	Protein farnesyltransferase/geranylgeranyltransferase type-1 subunit alpha OS=Mus musculus GN=Fnta PE=1 SV=1	44040	21.20	2.99
sp|Q9Z0E6|GBP2_MOUSE	Interferon-induced guanylate-binding protein 2 OS=Mus musculus GN=Gbp2 PE=1 SV=1	66787	9.30	2.92
sp|Q64345|IFIT3_MOUSE	Interferon-induced protein with tetratricopeptide repeats 3 OS=Mus musculus GN=Ifit3 PE=2 SV=1	47264	25.10	2.84
sp|P0CG49|UBB_MOUSE	Polyubiquitin-B OS=Mus musculus GN=Ubb PE=2 SV=1	26639	32.80	2.84
tr|G5E8V9|G5E8V9_MOUSE	MCG18094 (Fragment) OS=Mus musculus GN=Arfip1 PE=4 SV=1	41547	16.90	2.79
sp|P14094|AT1B1_MOUSE	Sodium/potassium-transporting ATPase subunit beta-1 OS=Mus musculus GN=Atp1b1 PE=1 SV=1	35226	10.50	2.76
sp|O88844|IDHC_MOUSE	Isocitrate dehydrogenase [NADP] cytoplasmic OS=Mus musculus GN=Idh1 PE=1 SV=2	46717	84.10	2.43
sp|P97855|G3BP1_MOUSE	Ras GTPase-activating protein-binding protein 1 OS=Mus musculus GN=G3bp1 PE=1 SV=1	51869	15.10	2.06
tr|D3Z3J6|D3Z3J6_MOUSE	Polyadenylate-binding protein-interacting protein 1 OS=Mus musculus GN=Paip1 PE=2 SV=1	42088	17.20	2.05
sp|Q922H4|GMPPA_MOUSE	Mannose-1-phosphate guanyltransferase alpha OS=Mus musculus GN=Gmppa PE=2 SV=1	46287	18.10	2.02
sp|Q8C5W3-2|TBCEL_MOUSE	Isoform 2 of Tubulin-specific chaperone cofactor E-like protein OS=Mus musculus GN=Tbcel	48074	29.50	2.01

sp|Q9JII6|AK1A1_MOUSE	Alcohol dehydrogenase [NADP(+)] OS=Mus musculus GN=Akr1a1 PE=1 SV=3	36618	8.30	1.96
sp|P02535-2|K1C10_MOUSE	Isoform 2 of Keratin, type I cytoskeletal 10 OS=Mus musculus GN=Krt10	57097	13.40	1.94
sp|Q8BTY1|KAT1_MOUSE	Kynurenine--oxoglutarate transaminase 1 OS=Mus musculus GN=Ccbl1 PE=1 SV=1	42262	14.40	1.92
sp|P49443|PPM1A_MOUSE	Protein phosphatase 1A OS=Mus musculus GN=Ppm1a PE=1 SV=1	42460	31.90	1.91
sp|Q61074|PPM1G_MOUSE	Protein phosphatase 1G OS=Mus musculus GN=Ppm1g PE=1 SV=3	58782	5.40	1.88
sp|P07724|ALBU_MOUSE	Serum albumin OS=Mus musculus GN=Alb PE=1 SV=3	68756	8.10	1.84
sp|Q8BNU0|ARMC6_MOUSE	Armadillo repeat-containing protein 6 OS=Mus musculus GN=Armc6 PE=2 SV=1	50723	11.80	1.83
sp|Q922U2|K2C5_MOUSE	Keratin, type II cytoskeletal 5 OS=Mus musculus GN=Krt5 PE=1 SV=1	61819	22.90	1.83
sp|P03995-2|GFAP_MOUSE	Isoform 2 of Glial fibrillary acidic protein OS=Mus musculus GN=Gfap	49942	6.10	1.79
sp|Q9DBR1-2|XRN2_MOUSE	Isoform 2 of 5'-3' exoribonuclease 2 OS=Mus musculus GN=Xrn2	108780	3.50	1.77
sp|O89023|TPP1_MOUSE	Tripeptidyl-peptidase 1 OS=Mus musculus GN=Tpp1 PE=1 SV=2	61394	3.70	1.76
sp|Q3U5Q7|CMPK2_MOUSE	UMP-CMP kinase 2, mitochondrial OS=Mus musculus GN=Cmpk2 PE=2 SV=2	50077	16.10	1.73
sp|Q8C5W0-2|CLMN_MOUSE	Isoform 2 of Calmin OS=Mus musculus GN=Clmn	117335	10.80	1.72
sp|P42227-2|STAT3_MOUSE	Isoform Stat3B of Signal transducer and activator of transcription 3 OS=Mus musculus GN=Stat3	84953	12.20	1.67
sp|P97384|ANX11_MOUSE	Annexin A11 OS=Mus musculus GN=Anxa11 PE=1 SV=2	54135	25.20	1.66
sp|Q8R123-2|FAD1_MOUSE	Isoform 2 of FAD synthase OS=Mus musculus GN=Flad1	54804	19.50	1.64
sp|P15105|GLNA_MOUSE	Glutamine synthetase OS=Mus musculus GN=Glul PE=1 SV=6	42146	14.50	1.58
sp|P43883|PLIN2_MOUSE	Perilipin-2 OS=Mus musculus GN=Plin2 PE=2 SV=2	16967	24.80	1.57
sp|Q3TYX3|SMYD5_MOUSE	SET and MYND domain-containing protein 5 OS=Mus musculus GN=Smyd5 PE=2 SV=2	47137	7.50	1.54
sp|Q8C5H8-2|NAKD2_MOUSE	Isoform 2 of NAD kinase 2, mitochondrial OS=Mus musculus GN=Nadk2	50899	11.20	1.54
sp|O88544|CSN4_MOUSE	COP9 signalosome complex subunit 4 OS=Mus musculus GN=Cops4 PE=1 SV=1	46328	70.00	1.53
sp|P11679|K2C8_MOUSE	Keratin, type II cytoskeletal 8 OS=Mus musculus GN=Krt8 PE=1 SV=4	54604	71.20	1.50
sp|Q63932|MP2K2_MOUSE	Dual specificity mitogen-activated protein kinase kinase 2 OS=Mus musculus GN=Map2k2 PE=1 SV=2	44329	27.60	1.49
sp|Q3TMH2|SCRN3_MOUSE	Secernin-3 OS=Mus musculus GN=Scrn3 PE=1 SV=1	47703	20.30	1.48
sp|P29341|PABP1_MOUSE	Polyadenylate-binding protein 1 OS=Mus musculus GN=Pabpc1 PE=1 SV=2	70734	27.50	1.45
sp|P00329|ADH1_MOUSE	Alcohol dehydrogenase 1 OS=Mus musculus GN=Adh1 PE=1 SV=2	39800	17.90	1.45
sp|P21614|VTDB_MOUSE	Vitamin D-binding protein OS=Mus musculus GN=Gc PE=1 SV=2	53637	12.00	1.45

sp|P99024|TBB5_MOUSE	Tubulin beta-5 chain OS=Mus musculus GN=Tubb5 PE=1 SV=1	49711	62.20	1.37
sp|Q9QYF9|NDRG3_MOUSE	Protein NDRG3 OS=Mus musculus GN=Ndrg3 PE=1 SV=1	43009	13.60	1.37
tr|E9Q0F0|E9Q0F0_MOUSE	Protein Krt78 OS=Mus musculus GN=Krt78 PE=4 SV=1	112374	2.00	1.34
sp|Q3UI43|BABA1_MOUSE	BRISC and BRCA1-A complex member 1 OS=Mus musculus GN=Babam1 PE=2 SV=1	36824	8.70	1.33
sp|Q8VDI7|UBAC1_MOUSE	Ubiquitin-associated domain-containing protein 1 OS=Mus musculus GN=Ubac1 PE=2 SV=2	45574	33.70	1.32
sp|Q9DBG7|SRPR_MOUSE	Signal recognition particle receptor subunit alpha OS=Mus musculus GN=Srpr PE=1 SV=1	69687	9.90	1.31
sp|Q8CCS6-2|PABP2_MOUSE	Isoform 2 of Polyadenylate-binding protein 2 OS=Mus musculus GN=Pabpn1	34037	9.20	1.28
sp|P52430|PON1_MOUSE	Serum paraoxonase/arylesterase 1 OS=Mus musculus GN=Pon1 PE=1 SV=2	39594	11.00	1.27
sp|Q99P30-3|NUDT7_MOUSE	Isoform 3 of Peroxisomal coenzyme A diphosphatase NUDT7 OS=Mus musculus GN=Nudt7	26876	18.70	1.25
sp|Q9DCH4|EIF3F_MOUSE	Eukaryotic translation initiation factor 3 subunit F OS=Mus musculus GN=Eif3f PE=1 SV=2	38014	15.80	1.25
sp|Q8R3H9|TTC4_MOUSE	Tetratricopeptide repeat protein 4 OS=Mus musculus GN=Ttc4 PE=2 SV=1	44365	4.90	1.24
sp|P49429|HPPD_MOUSE	4-hydroxyphenylpyruvate dioxygenase OS=Mus musculus GN=Hpd PE=1 SV=3	45080	37.90	1.24
sp|Q8VC97|BUP1_MOUSE	Beta-ureidopropionase OS=Mus musculus GN=Upb1 PE=2 SV=1	43963	51.90	1.22
sp|O35685|NUDC_MOUSE	Nuclear migration protein nudC OS=Mus musculus GN=Nudc PE=1 SV=1	38388	59.30	1.22
sp|P63260|ACTG_MOUSE	Actin, cytoplasmic 2 OS=Mus musculus GN=Actg1 PE=1 SV=1	41820	65.60	1.21
sp|Q3UM45|PP1R7_MOUSE	Protein phosphatase 1 regulatory subunit 7 OS=Mus musculus GN=Ppp1r7 PE=1 SV=2	41321	69.30	1.20
sp|Q9CZ30|OLA1_MOUSE	Obg-like ATPase 1 OS=Mus musculus GN=Ola1 PE=1 SV=1	44755	46.50	1.19
sp|Q8VCA8|SCRN2_MOUSE	Secernin-2 OS=Mus musculus GN=Scrn2 PE=2 SV=1	46643	22.80	1.18
sp|P18572-2|BASI_MOUSE	Isoform 2 of Basigin OS=Mus musculus GN=Bsg	24137	27.90	1.18
sp|Q9QYG0|NDRG2_MOUSE	Protein NDRG2 OS=Mus musculus GN=Ndrg2 PE=1 SV=1	40817	72.20	1.18
sp|Q920E5|FPPS_MOUSE	Farnesyl pyrophosphate synthase OS=Mus musculus GN=Fdps PE=1 SV=1	40610	22.90	1.16
sp|A3KMP2|TTC38_MOUSE	Tetratricopeptide repeat protein 38 OS=Mus musculus GN=Ttc38 PE=2 SV=2	52262	9.70	1.16
sp|P62196|PRS8_MOUSE	26S protease regulatory subunit 8 OS=Mus musculus GN=Psmc5 PE=1 SV=1	45669	43.60	1.16
sp|Q99KQ4|NAMPT_MOUSE	Nicotinamide phosphoribosyltransferase OS=Mus musculus GN=Nampt PE=1 SV=1	55485	11.80	1.15
sp|Q8VCN5|CGL_MOUSE	Cystathionine gamma-lyase OS=Mus musculus GN=Cth PE=1 SV=1	43593	21.90	1.14
sp|Q8VCM7|FIBG_MOUSE	Fibrinogen gamma chain OS=Mus musculus GN=Fgg PE=2 SV=1	49432	18.80	1.14

sp|P63037|DNJA1_MOUSE	DnaJ homolog subfamily A member 1 OS=Mus musculus GN=Dnaja1 PE=1 SV=1	44894	20.20	1.14
sp|O54804-2|CHKA_MOUSE	Isoform 2 of Choline kinase alpha OS=Mus musculus GN=Chka	26254	13.00	1.13
sp|P30416|FKBP4_MOUSE	Peptidyl-prolyl cis-trans isomerase FKBP4 OS=Mus musculus GN=Fkbp4 PE=1 SV=5	51612	15.90	1.13
sp|P25799-2|NFKB1_MOUSE	Isoform 2 of Nuclear factor NF-kappa-B p105 subunit OS=Mus musculus GN=Nfkb1	105711	10.70	1.12
sp|P28656|NP1L1_MOUSE	Nucleosome assembly protein 1-like 1 OS=Mus musculus GN=Nap1l1 PE=1 SV=2	41109	7.60	1.11
sp|Q9CZU6|CISY_MOUSE	Citrate synthase, mitochondrial OS=Mus musculus GN=Cs PE=1 SV=1	51775	18.50	1.11
sp|P19157|GSTP1_MOUSE	Glutathione S-transferase P 1 OS=Mus musculus GN=Gstp1 PE=1 SV=2	23630	36.20	1.10
sp|Q99L47|F10A1_MOUSE	Hsc70-interacting protein OS=Mus musculus GN=St13 PE=1 SV=1	41684	35.30	1.09
sp|P97807-2|FUMH_MOUSE	Isoform Cytoplasmic of Fumarate hydratase, mitochondrial OS=Mus musculus GN=Fh	54412	36.80	1.09
sp|Q9JLI6|SCLY_MOUSE	Selenocysteine lyase OS=Mus musculus GN=Scly PE=1 SV=1	47216	49.50	1.08
sp|Q3THS6|METK2_MOUSE	S-adenosylmethionine synthase isoform type-2 OS=Mus musculus GN=Mat2a PE=2 SV=2	43715	39.20	1.08
sp|P32020|NLTP_MOUSE	Non-specific lipid-transfer protein OS=Mus musculus GN=Scp2 PE=1 SV=3	59178	41.90	1.07
sp|Q71RI9-2|KAT3_MOUSE	Isoform 2 of Kynurenine--oxoglutarate transaminase 3 OS=Mus musculus GN=Ccbl2	51165	25.50	1.07
sp|P08730-2|K1C13_MOUSE	Isoform 2 of Keratin, type I cytoskeletal 13 OS=Mus musculus GN=Krt13	47796	11.30	1.07
sp|P09411|PGK1_MOUSE	Phosphoglycerate kinase 1 OS=Mus musculus GN=Pgk1 PE=1 SV=4	44594	30.90	1.07
sp|Q9WVL0|MAAI_MOUSE	Maleylacetoacetate isomerase OS=Mus musculus GN=Gstz1 PE=1 SV=1	24296	11.10	1.06
sp|Q922D8|C1TC_MOUSE	C-1-tetrahydrofolate synthase, cytoplasmic OS=Mus musculus GN=Mthfd1 PE=1 SV=4	101298	23.10	1.06
sp|P70441|NHRF1_MOUSE	Na(+)/H(+) exchange regulatory cofactor NHE-RF1 OS=Mus musculus GN=Slc9a3r1 PE=1 SV=3	38631	32.70	1.05
sp|Q8K3W0|BRE_MOUSE	BRCA1-A complex subunit BRE OS=Mus musculus GN=Bre PE=1 SV=2	43776	23.00	1.04
sp|Q7TMM9|TBB2A_MOUSE	Tubulin beta-2A chain OS=Mus musculus GN=Tubb2a PE=1 SV=1	49947	57.50	1.02
sp|Q07076|ANXA7_MOUSE	Annexin A7 OS=Mus musculus GN=Anxa7 PE=2 SV=2	49965	55.50	1.02
sp|P05784|K1C18_MOUSE	Keratin, type I cytoskeletal 18 OS=Mus musculus GN=Krt18 PE=1 SV=5	47581	86.80	1.01
sp|Q3THG9|AASD1_MOUSE	Alanyl-tRNA editing protein Aarsd1 OS=Mus musculus GN=Aarsd1 PE=1 SV=2	60559	29.90	1.01
sp|Q61081|CDC37_MOUSE	Hsp90 co-chaperone Cdc37 OS=Mus musculus GN=Cdc37 PE=2 SV=1	44619	17.70	1.01

To investigate whether the displacement of the protein band is due to low affinity interaction between the protein and immobilized NAADP, another set of affinity pull-down experiments was carried out using various concentrations of NAADP and NADP.

As shown in Figure 3.11, the band could not be displaced by NAADP or NADP at a concentration as high as 10 µM. At higher concentrations, NADP also showed a similar effectiveness as NAADP in displacing the protein band, suggesting that the ligand-protein interaction here was not exclusive to NAADP, but also nucleotides with structural similarity.

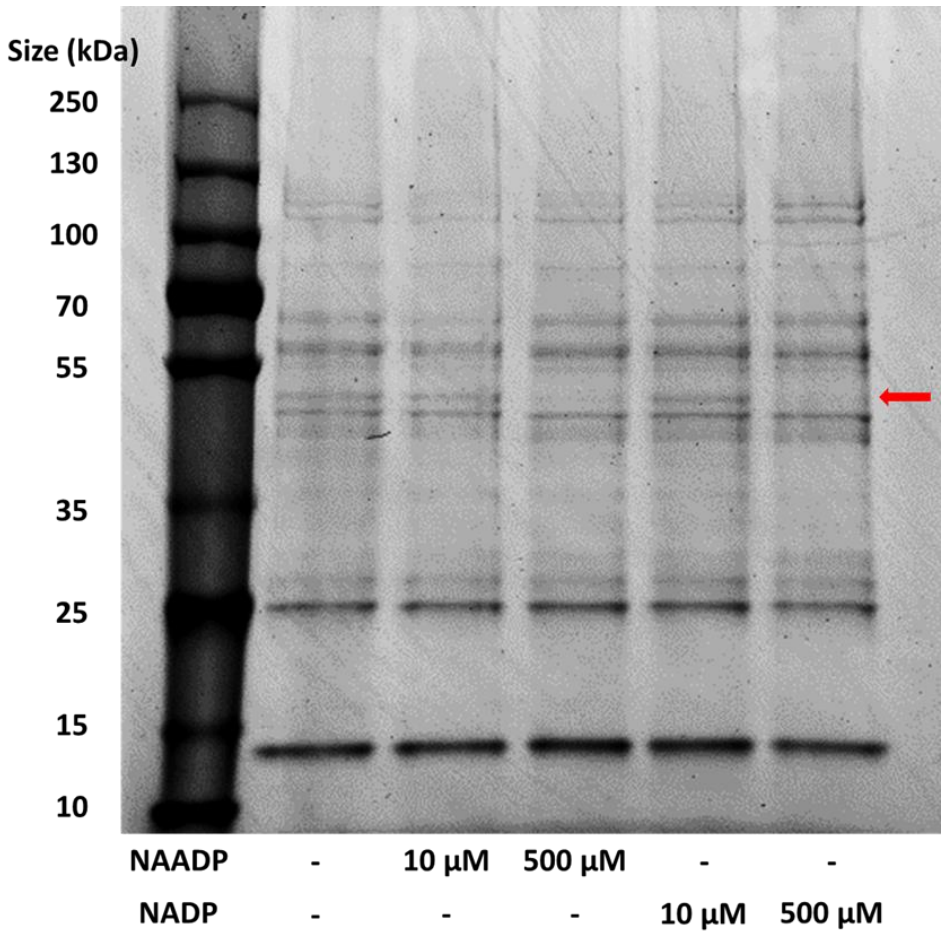

Figure 3.11. SDS-PAGE profile of affinity column eluent in the presence or absence of NAADP or NADP.

3.2.4. Discussion

In this section, the possibility of isolating NAADP binding protein from mouse liver cytosol via affinity column has been explored.

The initial thin-layer chromatography separation of NAADP and oxi-NAADP on unmodified silica gel TLC plate was not successful. Silica gel is by far the most popular and widely used TLC sorbent. It is prepared by acid precipitation of silicate solution, during which particles develop and form three-dimensional network that creates a highly polar absorbent (Wall, 2005). The absorptive characteristics of silica gel, which separates a mixture of compound by their polarity, is attributed to the residue hydroxyl group on the surface (Wall, 2005). Although silica gel is highly versatile, it could not separate NAADP and oxi-NAADP on the TLC plate. The retardation factors of both compounds are either 0 or 1 despite using several combinations of solvents with various polarities. This suggests that though oxidation of NAADP resulted in structural changes, these changes were not significant enough to cause profound polarity variation to be seen on silica gel. Hence silica gel was not the best stationary phase for monitoring NAADP oxidation. The alternative stationary phase used here was the PEI-cellulose. Polyethylenimine modification of cellulose makes it a strong anion exchanger suitable for nucleic acid, nucleotide and nucleoside (Wall, 2005). However, the different mechanism of action was not the only the factor that accounted for the successful separation. Although the choice of solvent is paramount in improving the resolution of the TLC, the formation of a Schiff base during the development of the PEI-cellulose plate played an even more essential role in providing distinct retardation factors of two compounds. The aldehyde groups on the oxi-NAADP, a product of the

periodate oxidation, reacted with the primary amines on the polyethylenimine and formed a Schiff base, which effectively locked down oxi-NAADP while NAADP traveled freely along with the solvent. A previous attempt to monitor the reaction using HPLC via ion-exchange chromatography did not lead to a satisfactory separation. The ion-exchange column used in HPLC contained AGMP-1, a strong anion exchange resin with quaternary ammonium functional groups. However, no primary amines are available on the AGMP-1 resin, hence Schiff base formation would not occur and a similar separation as on PEI-cellulose was not observed.

Affinity chromatography is probably one of the finest approaches to isolate and purify the NAADP binding protein as its principle relies on the specific interaction between the immobilized functional groups on the matrix and the target of interest in the mobile phase. However, studies of the structure-activity relationships of NAADP analogs revealed that modifications of NAADP is normally not well tolerated and results in significant activity loss. Common coupling approaches via carboxylic acid group on the 3-position of the pyridine ring or via 6-amine group on the adenine moiety is not feasible since these groups have been shown to be critical for NAADP potency and modification would causes significant loss of biological activity (Lee and Aarhus, 1997; Trabbic *et al.*, 2012). An alternative approach to immobilize NAADP is via the ribose ring through periodate oxidation coupled with hydrazide modified surface, which has been described previously in developing nucleotide-immobilized matrix (Wilchek and Lamed, 1974). Although NAADP could be coupled onto the magnetic beads through this method, pull-down of the high affinity NAADP binding protein was not successful as demonstrated by NAADP/NADP displacement of protein bands in SDS-PAGE. The oxidized NAADP is reported to have an IC_{50} of roughly 15 µM

in sea urchin egg homogenate (Yee, 2002), which is an almost 10000-fold decrease in affinity compared to NAADP, indicating that the integrity of the ribose ring is critical for recognition of and binding to the NAADP binding protein. The coupling of oxi-NAADP to the beads may also restrict the access of the molecule to NAADP binding protein and hence further lower its apparent binding affinity. In Chapter 4, the importance of cis-glycol groups in determining the affinity of NAADP for binding protein will be discussed based on the results of docking simulation.

This is also the first reported attempt to isolate NAADP binding protein from mammalian cells using an NAADP affinity column. Previously, a similar approach was adopted in the affinity purification of NAADP binding protein in sea urchin egg homogenate (Billington *et al.*, 2004), and the authors reported distinct bands that corresponded to the molecular weights of glucose-6-phosphate dehydrogenase and 6-phosphogluconate dehydrogenase. 6-phosphogluconate dehydrogenase was also found in the list of the proteins identified through MS analysis of affinity pull-downed complexes in this study, which is in good agreement with the literature mentioned above and proved that the method is valid in mammalian systems as well. However, it is worth mentioning that more recently, Lin-Moshier *et al.*, and Walseth *et al.*, reported the photoaffinity labelling of NAADP binding protein in mammalian cells and sea urchin egg (Lin-Moshier *et al.*, 2012; Walseth *et al.*, 2012a). Walseth and his colleague discovered three protein bands at 30-, 40- and 45 kDa in sea urchin egg homogenate that could be labelled with [^{32}P]-5-azido-NAADP and determined their K_ds to be around 10 nM (Walseth *et al.*, 2012a). In comparison, protein eluted from an NAADP affinity column using sea urchin egg homogenate as input did not see such specific bands in their SDS-PAGE result (Billington *et al.*, 2004). On the other hand, a

22/23-kDa doublet was photolabelled in SKBR3 cells, HEK293 cells, mouse pancreas and mouse liver (Lin-Moshier *et al.*, 2012; Ruas *et al.*, 2015). The IC_{50}s of the doublet varies from 10 to 198 nM depending on cell type and subcellular localization. Nonetheless, the doublet was not observed in this study despite using an excessive amount (500 µM) of free NAADP to identify specific protein bands. Although Billington and his colleagues stated that the specific bands corresponding to the sizes of glucose-6-phosphate dehydrogenase and 6-phosphogluconate dehydrogenase could also be eluted from their affinity column using only 4 nM NAADP (Billington *et al.*, 2004), the K_ds of these proteins for NAADP have not been reported. In addition, the protein band that corresponds to 6-phosphogluconate dehydrogenase in the present study did not see attenuation of the band intensity in the presence of NAADP up to 10 µM. Furthermore, one would wonder if these dehydrogenases represent the high affinity NAADP binding protein as they are known for binding NADP or NAD as substrates for catalytic purposes. Studies have indicated that in mammalian cells only the low-affinity site can be displaced by NADP whereas the high-affinity site could not (Calcraft *et al.*, 2009). Indeed, the SDS-PAGE analysis in the present study revealed that neither NAADP or NADP could cause any significant displacement of the target protein band at 10 µM concentration. Together with the other NADP binding proteins found in the MS analysis, such as isocitrate dehydrogenase and alcohol dehydrogenase, all these evidences suggest that affinity column generated from chemical modification and coupling of NAADP may not be able to distinguish high and low-affinity NAADP binding and therefore is not suitable for isolating high affinity NAADP binding proteins.

Chapter 4 Identification of NAADP binding proteins

The preceding chapter described an attempt to isolate and identify high affinity NAADP protein(s) using chemical approaches. However, neither crosslinking or an NAADP affinity column was able to successfully isolate the high affinity NAADP binding protein(s). Given the complexity of this mission, it was perceived that a single method alone would not be sufficient to achieve the ultimate goal. Therefore, a new strategy using fast protein liquid chromatography, photoaffinity labelling, mass spectrometry, docking simulation, bio-layer interferometry and microscale thermophoresis in tandem was conceived and is explained in this chapter.

4.1. Purification of NAADP binding protein by Fast Protein Liquid Chromatography (FPLC)

4.1.1. Introduction

Years of effort had been made in search of the NAADP binding protein(s), yet its identity remained unclear despite many promising leads. It is believed that finding a source of protein with prevalent abundance of NAADP binding protein(s) would increase the chance of its identification. Thus, the FPLC was exploited as the step of this grand campaign to enrich the high affinity NAADP binding protein(s).

The material for the chromatography purification is mouse liver cytosol. Mouse liver was chosen as the source of the protein due to its relatively large tissue size and reasonable amount of NAADP binding. The livers were harvested from freshly sacrificed C57BL/6 mouse and homogenized, and the cytosol was obtained by collecting the supernatant from the subsequent ultracentrifugation. Protein separation was performed on Akta FPLC (GE Healthcare Life Sciences). Fractions were collected and their NAADP binding was tested using a radioligand binding assay. The fractions with enriched NAADP binding were combined and proceeded to the next step.

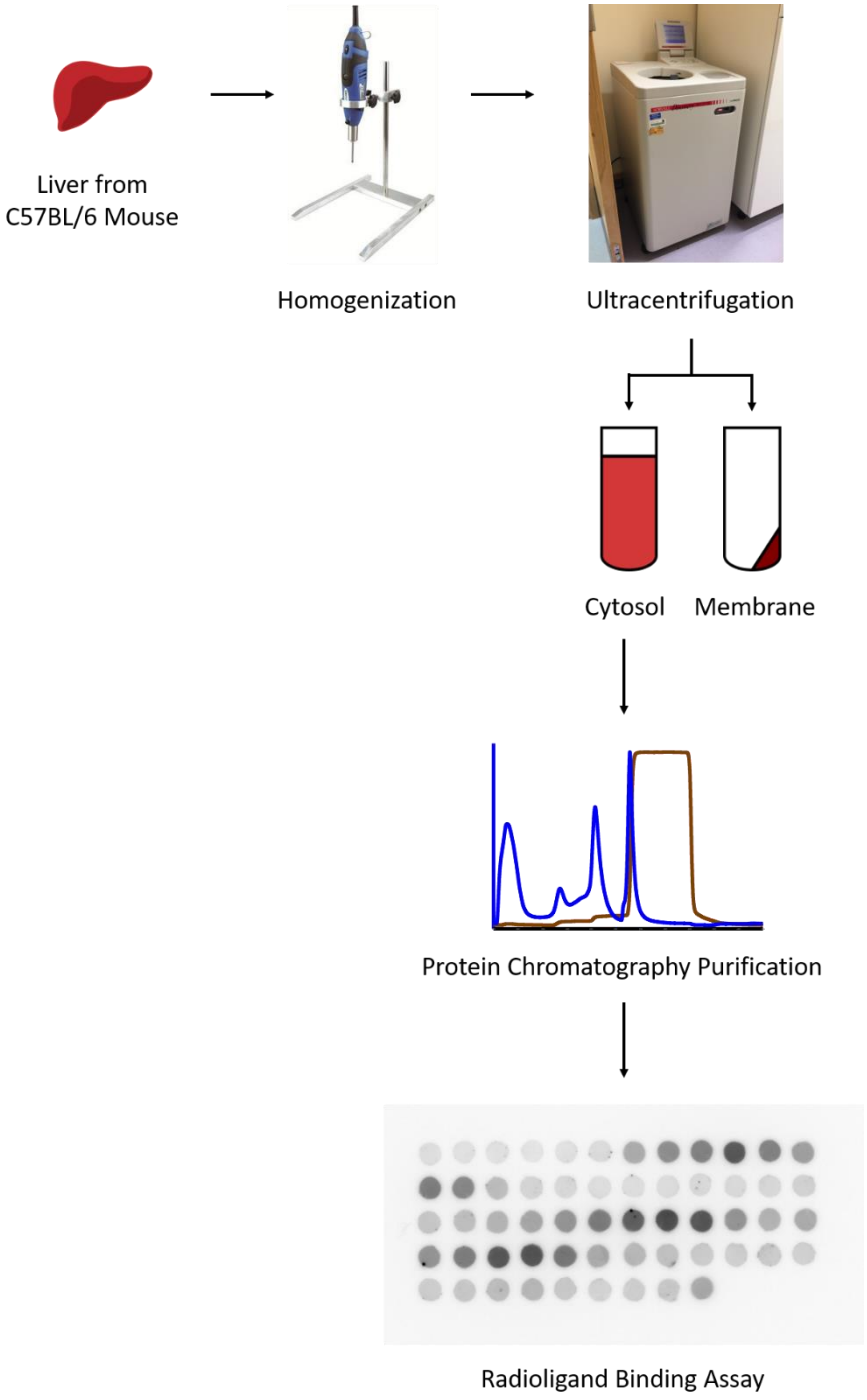

Figure 4.1. Schematics of chromatographic purification of NAADP binding protein from mouse liver cytosol.

Chromatography operates through different principles. It separates components that partition differently between stationary and mobile phases, which in turn migrate at differential speed through the chromatography medium (Carta and Jungbauer, 2010). The partitioning of the components is usually based on the molecular attraction between components and functional groups on the surface of the stationary phase,

including electrostatic interaction, Van der Waals forces and bio specificity. Size-exclusion chromatography, however, relies solely on steric exclusion to achieve separation of components of various sizes (Carta and Jungbauer, 2010). The development of the protein purification strategy was a process which consisted of three attempts. The first attempt was a strategy that combines ion-exchange chromatography (IEX) with size-exclusion chromatography (SEC). The enrichment was achieved through this process yet was not enough to remove the bulk of the non-target proteins. As a result, a list of more than 700 candidates was acquired from the mass spectrometry (MS) analysis. The second attempt that used ion-exchange and hydrophobic interaction (HIC) did not yield satisfactory enrichment of the binding protein(s). In the third attempt, ion-exchange, hydrophobic interaction and size-exclusion chromatography was performed in tandem and resulted in an astounding 2300-fold enrichment of the NAADP binding protein(s), which became the foundation of the subsequent photoaffinity labelling, mass spectrometry analysis and in-silico docking simulation.

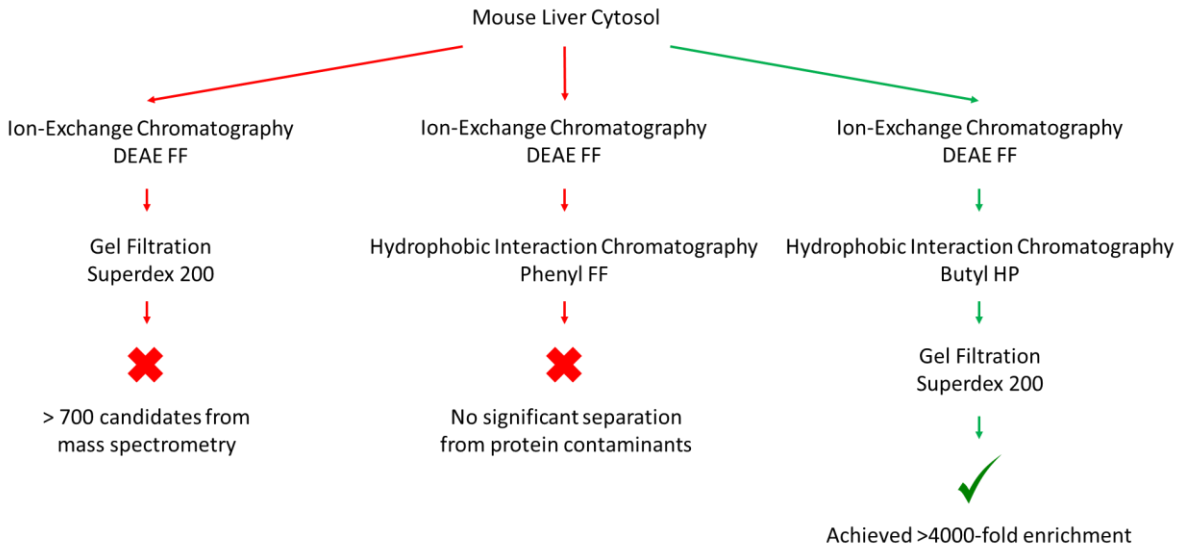

Figure 4.2. Development of FPLC purification strategy.

4.1.2. Sequential chromatographic purification of NAADP binding protein

4.1.2.1. Purification of NAADP binding protein by ion-exchange chromatography

As the first step of the purification, the goal is to remove as many impurities as possible. Here ion-exchange chromatography was chosen since it requires fewer prerequisites of the sample and the elutants can be used for the following steps (hydrophobic and size-exclusion chromatography) with minimal sample handling. DEAE FF (Diethylaminoethyl Fast Flow) is a weak anion-exchange column with a 6% highly crosslinked agarose beads matrix, which provides a broad selectivity and a balance between scale and resolution and is best suited for clarifying the crude sample.

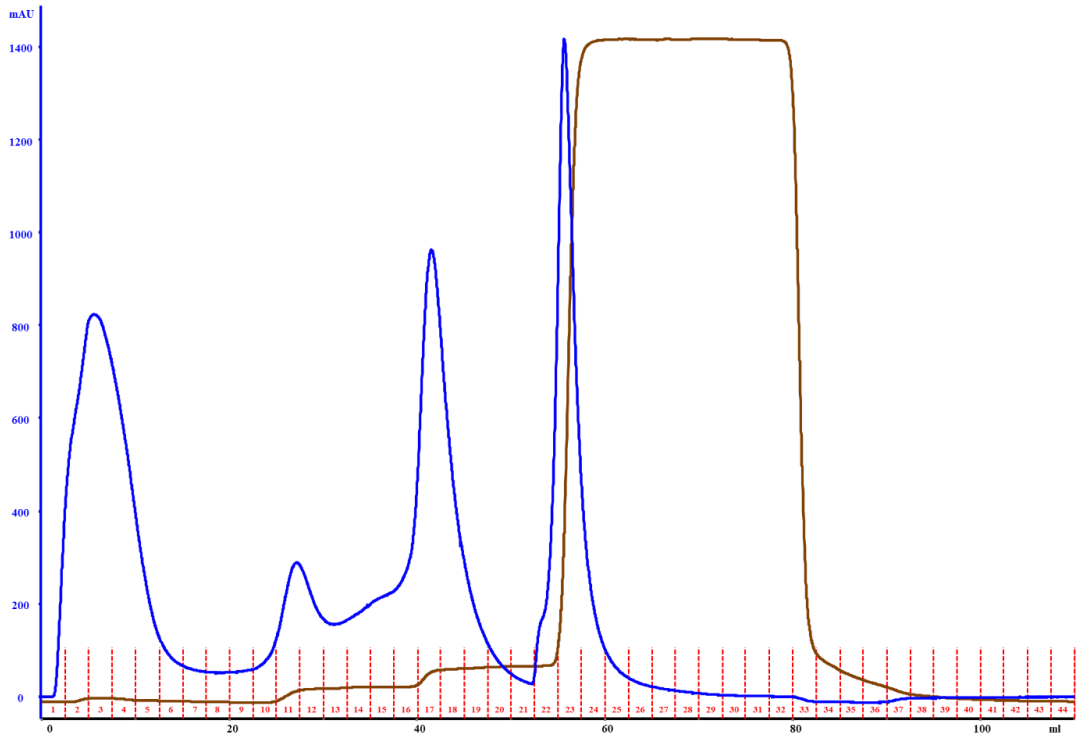

Figure 4.3. Representative chromatogram of ion-exchange chromatography by DEAE FF. Traces: Blue: UV; Brown: conductivity.

A step gradient was used to shorten the time course of the chromatography while maintaining resolution. The DEAE FF effectively isolated a group of NAADP binding protein, which can be found as the third UV peak from the left in Figure 4.3, from bulk impurities. Most of the NAADP binding was found in fraction 15-20, as illustrated by the result of the radioligand binding assay shown in Figure 4.4.

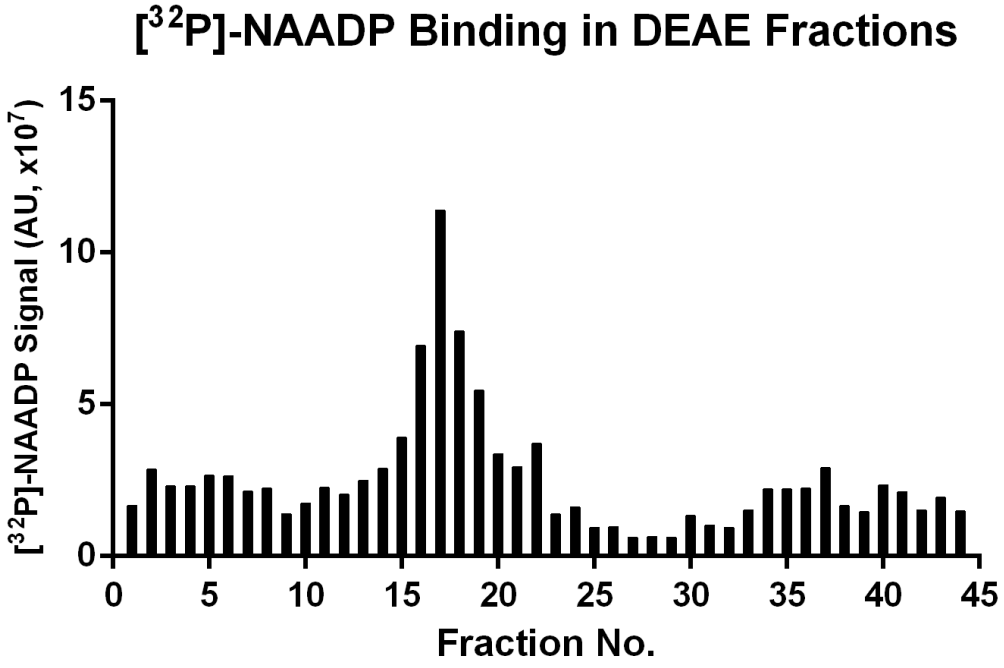

Figure 4.4. Representative ^{32}P signal of collected DEAE FF fractions.

To estimate the affinity of fractions 15-20 to NAADP and NADP, another radioligand assay was carried out using 500 nM and 500 µM NAADP or NADP (Figure 4.5) to examine the high/low/non-specific binding of NAADP or NADP in the corresponding fractions. The results, as summarized in Table 5.1, revealed that fractions 15 and 16 have higher affinity for NADP than NAADP since NADP could displace [^{32}P]-NAADP more effectively. Therefore, only fractions 17-20 were collected and combined for the next step.

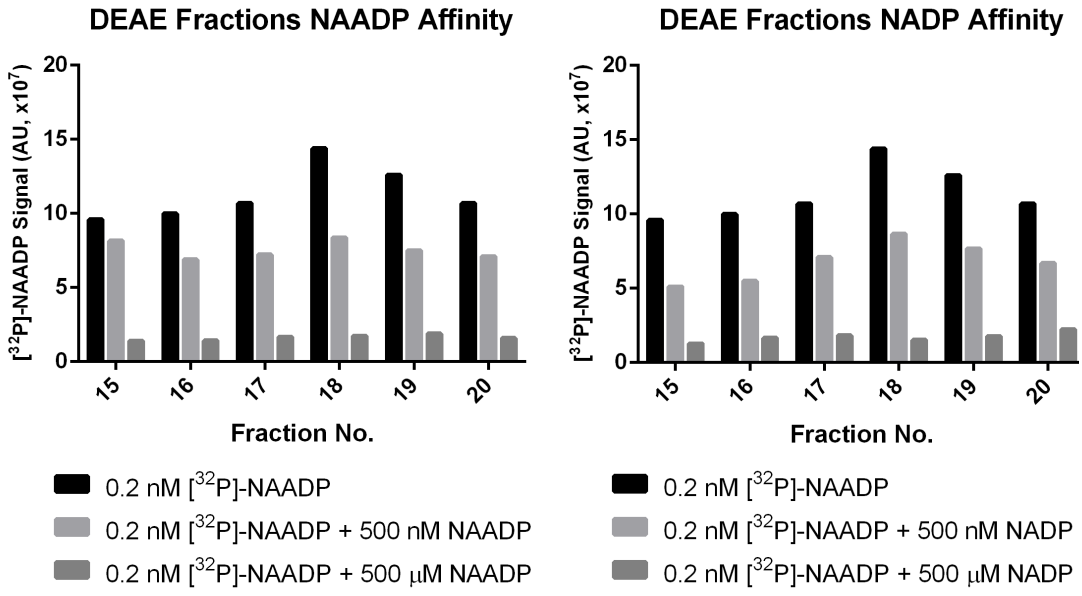

Figure 4.5. NAADP and NADP affinity of DEAE FF fraction 15-20.

Table 5.1. Remaining ^{32}P signal in DEAE fraction 15-20 in the presence of 500 nM NAADP or NADP.

Fraction	Remaining radioactivity in the presence of:	
	500 nM NAADP	**500 nM NADP**
15	84.9%	53.2%
16	68.9%	55.0%
17	67.8%	66.6%
18	58.2%	60.1%
19	59.3%	60.7%
20	66.6%	62.7%

4.1.2.2. Purification of NAADP binding protein(s) by hydrophobic interaction chromatography

Columns with various hydrophobic functional groups are commercially available. The hydrophobic groups of choice are phenyl, octyl and butyl, and the column can be either high or low substitution depending on the quantity of functional groups coupled to the matrix, which offer various strengths of hydrophobic interaction. For preliminary probing of the most suitable column, the fractions collected from DEAE FF were transferred to Phenyl FF (high substitution) for separation. However, the resolution of the separation was not satisfactory since no distinct protein population could be distinguished, as illustrated in both the chromatogram (Figure 4.6) and radioligand binding assay (Figure 4.7).

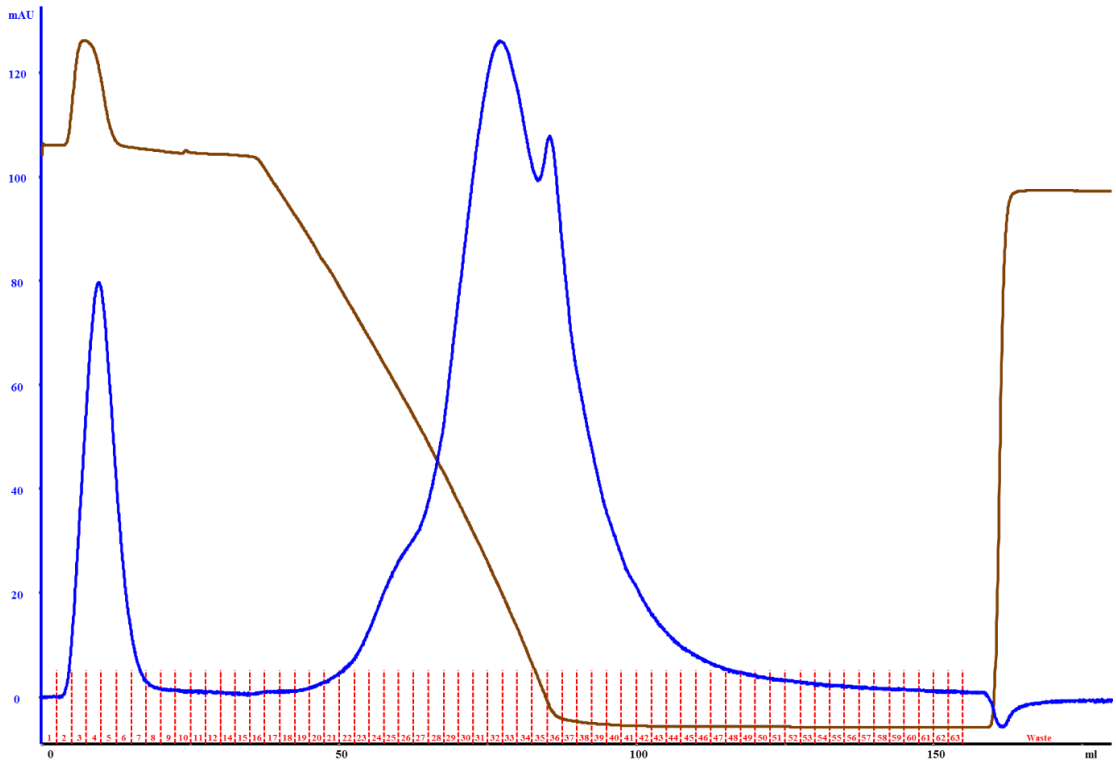

Figure 4.6. Representative chromatogram of hydrophobic interaction chromatography by Phenyl FF. Traces: Blue: UV; Brown: conductivity.

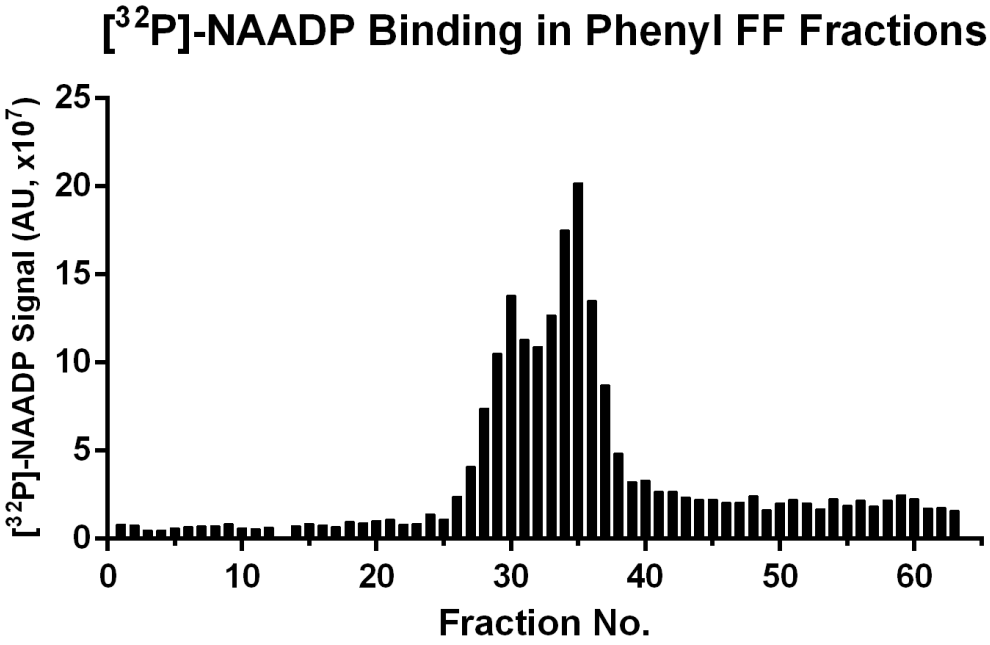

Figure 4.7. Representative ^{32}P signal of collected Phenyl FF fractions.

Another attempt using a Butyl HP (Butyl High Performance) 1 ml column showed reasonable separation of various protein populations using a slope gradient. As demonstrated in Figure 4.9, there were two groups of proteins that had relatively high NAADP affinity (Fractions 10-12 and Fractions 15-16), which corresponded to the second and fourth peak from the left in Figure 4.8. However, further attempts could not reliably reproduce the binding profiles of fractions 15-16, as it varied dramatically between batches. Therefore the optimization of the Butyl HP gradient was focused on isolating fractions 10-12.

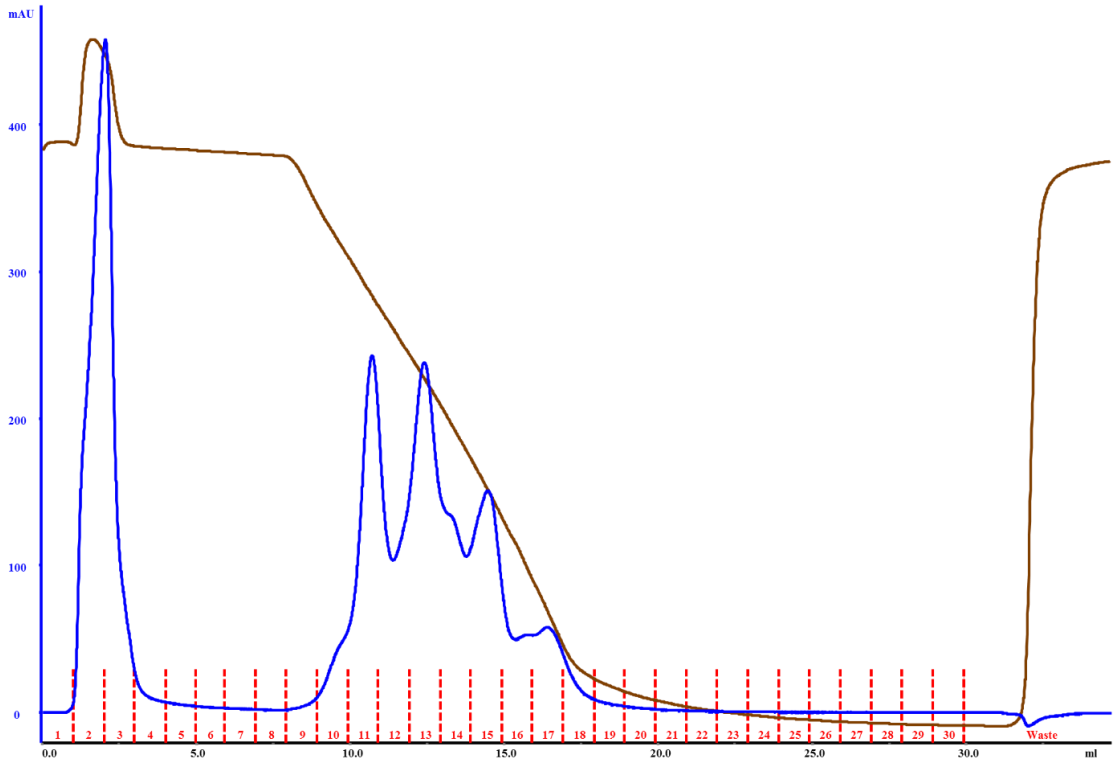

Figure 4.8. Representative chromatogram of hydrophobic interaction chromatography by Butyl HP with slope gradient. Traces: Blue: UV; Brown: conductivity.

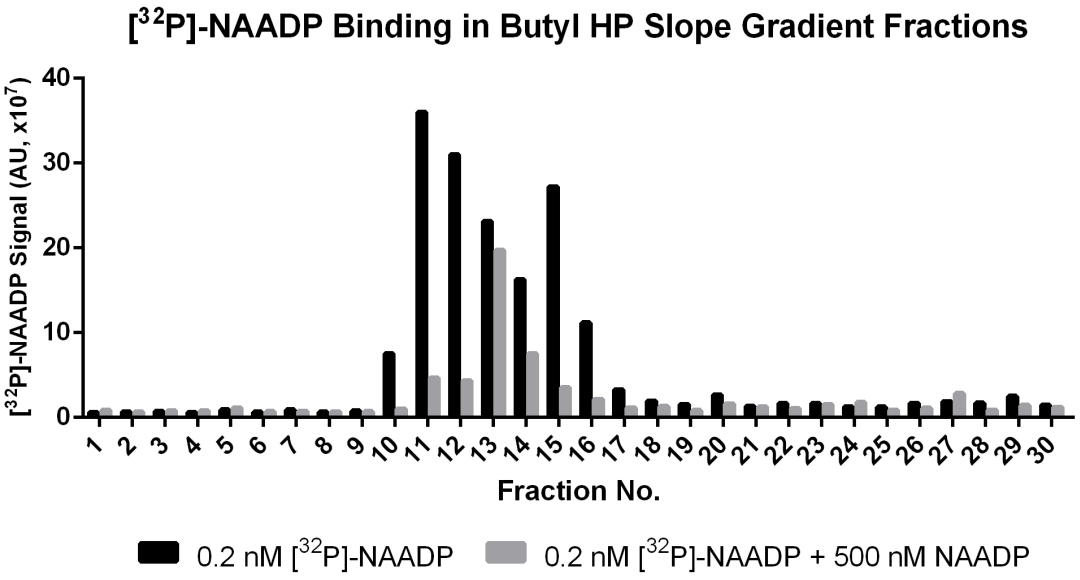

Figure 4.9. Representative ^{32}P signal of collected Butyl HP fractions in the presence or absence of 500 nM NAADP.

Fraction 10-12 eluted very early in the slope gradient, almost at the beginning of the gradient. Hence, the first optimization of the Butyl HP gradient introduced a step gradient in the original slope gradient. The Butyl HP column used in the

chromatography was also scaled up from 1 ml to 5 ml, thus allowing a larger amount of the protein to be processed. The step gradient holds at 13% buffer B, which effectively isolated the minimal amount of protein from the input while retaining the majority of the NAADP binding (Fraction 14-24, Figure 4.10, Figure 4.11). Fractions 10-12 from the slope gradient now correspond to fractions 14-24 in the optimized step gradient. It is worth noting that fractions 14 and 15 in the new gradient had the most protein eluted in fractions 14-24, but had little NAADP binding compared to the other fractions within the range (Figure 4.11).

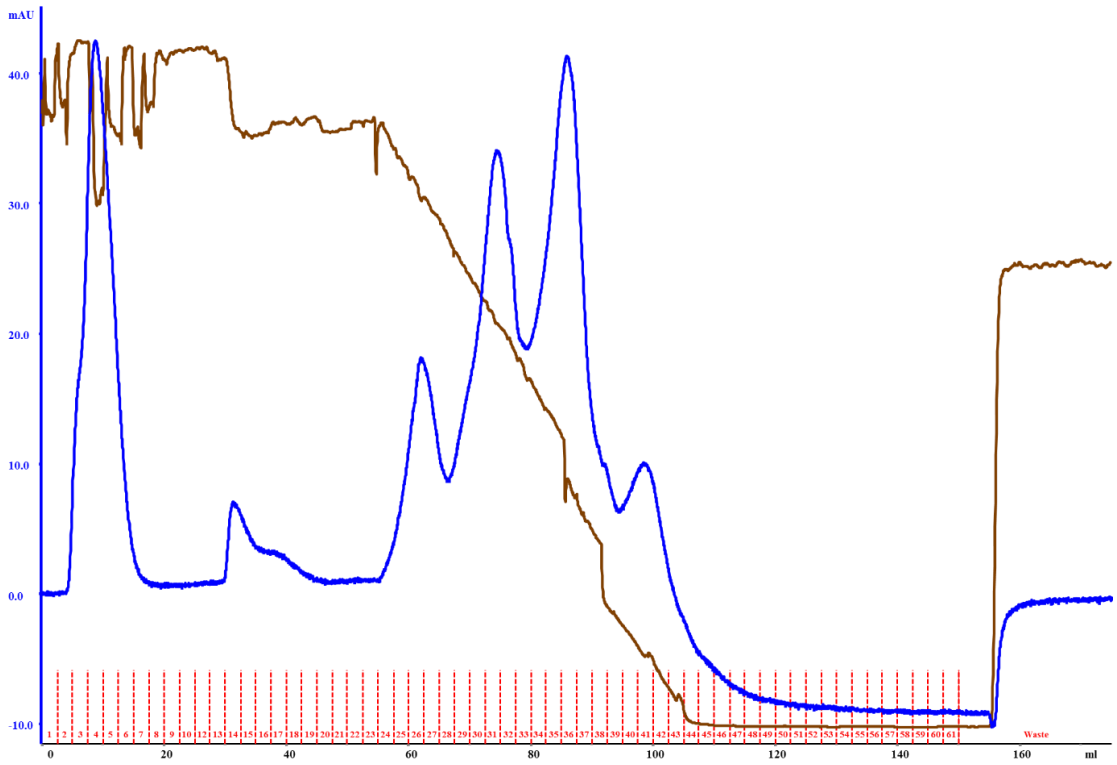

Figure 4.10. Representative chromatogram of hydrophobic interaction chromatography by Butyl HP with refined slope gradient. Traces: Blue: UV; Brown: conductivity.

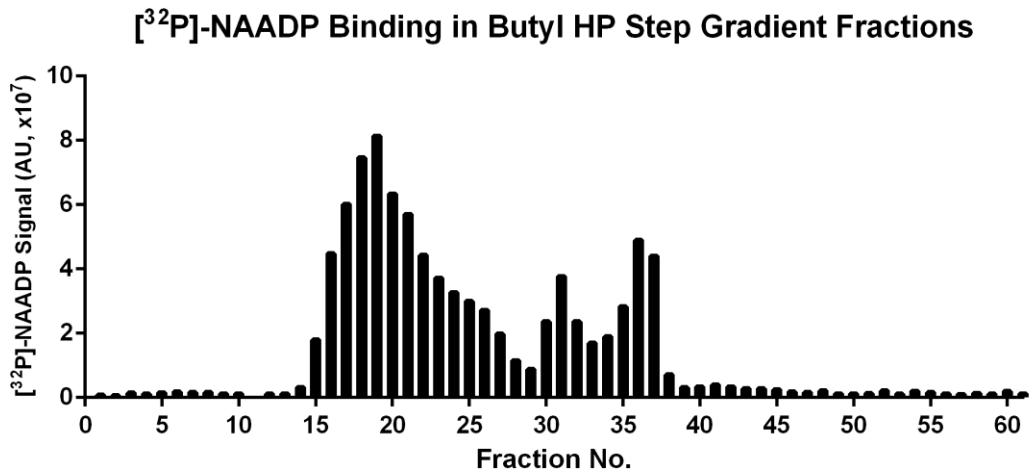

Figure 4.11. Representative ^{32}P signal of collected Butyl HP fractions.

The second optimization of the separation aimed to reduce the operation time for each run. Judging from the NAADP binding profile in Figure 4.11, the fractions other than 16-24 offer little value as their binding/protein ratios were significantly lower than that of fractions 16-24. Thus, the second optimization of the gradient transformed it into a complete step gradient to improve the speed of the separation.

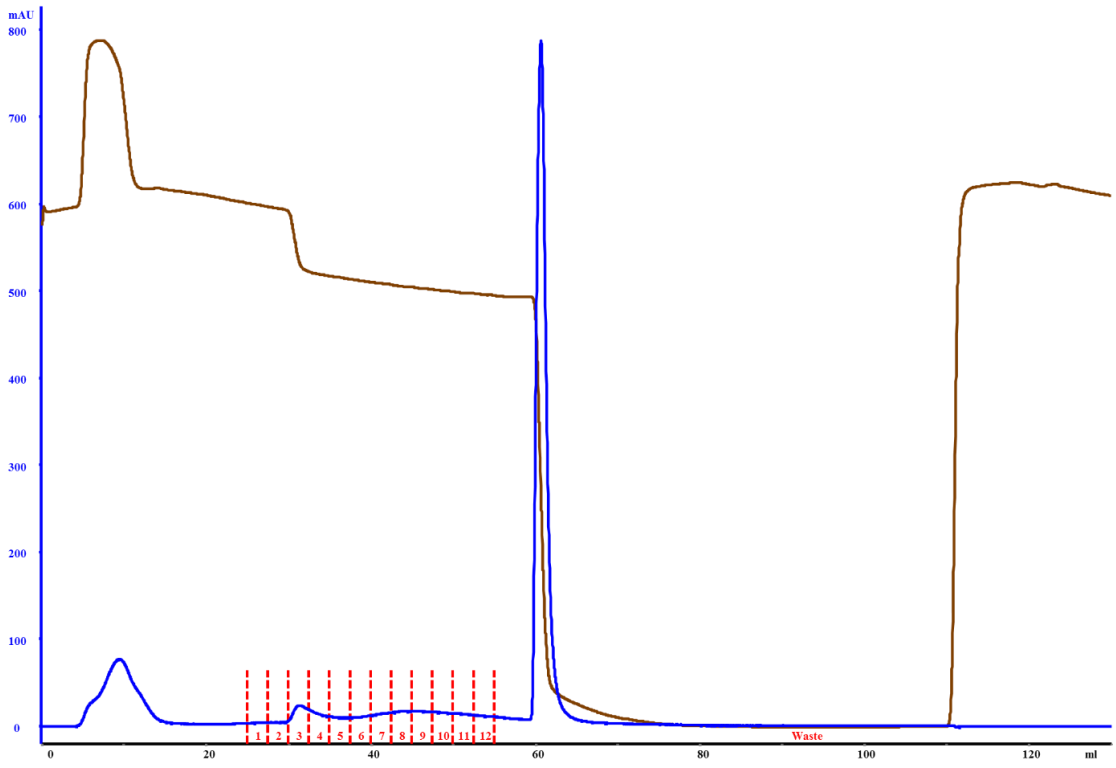

Figure 4.12. Representative chromatogram of hydrophobic interaction chromatography by Butyl HP with optimized step gradient. Traces: Blue: UV; Brown: conductivity.

Finally, after two optimizations, the chromatography profile of the Butyl HP separation is shown in Figure 4.12 and fractions 5-12 were collected, combined and proceeded to the next stage of the purification.

4.1.2.3. Purification of NAADP binding protein(s) by size-exclusion chromatography

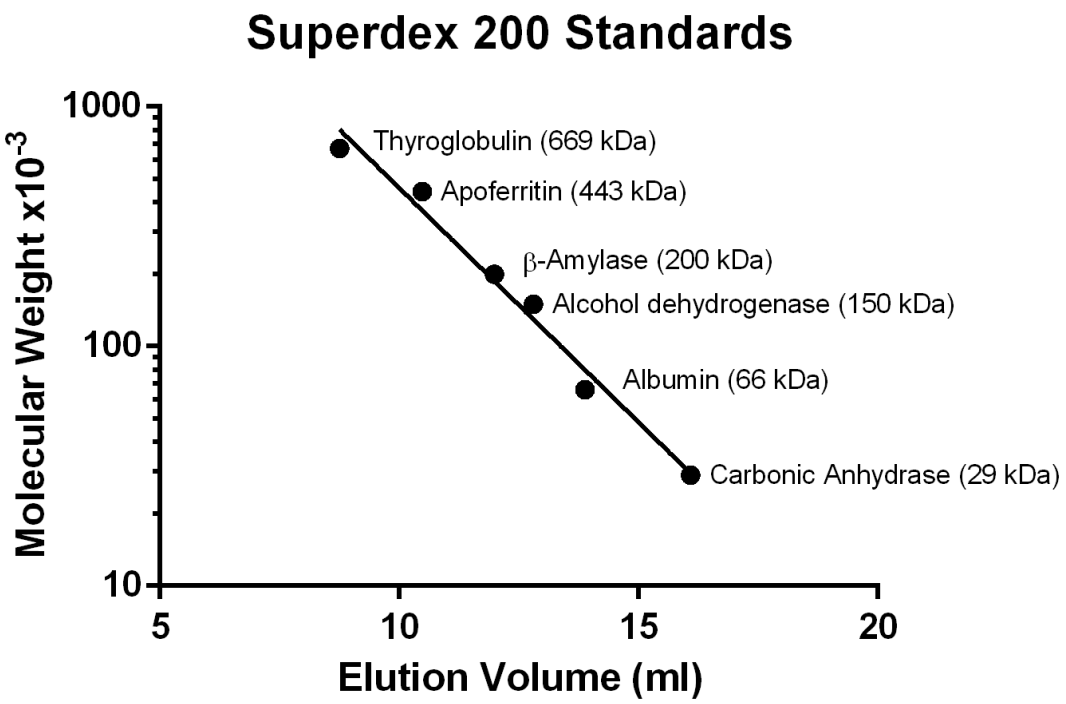

Figure 4.13. Standard curve of Superdex 200 HR 10/30. All proteins from Molecular Weight Ladder (Sigma Aldrich) were mixed and loaded onto Superdex column for separation and the volume at which their peak emerged were plotted against their molecular weight on a semi-log scale. A linear regression was performed on all data points. R^2=0.9811.

Superdex 200 HR 10/30 has an exclusion limit of 1300 kDa and an optimal separation range from 10-600 kDa. The resolution of Superdex 200 column was measured by a Molecular Weight Ladder for size-exclusion chromatography from Sigma Aldrich (Figure 4.13). Protein of different sizes were loaded onto the Superdex 200 column and separated with isocratic elution using 50 mM potassium phosphate, pH 7.0. The elution volumes of peaks were plotted against their molecular weights on a semi-log

scale. The coefficient of determination (R^2) was 0.9811, demonstrating good resolution of the column within its effective range.

The size-exclusion chromatography, in general, requires adequate ionic strength to prevent non-specific ionic interaction between protein and matrix. Non-specific ionic interaction between protein and matrix often manifests as delayed elution of protein. The influence of ionic strength on the elution of high affinity NAADP binding protein(s) was also investigated. The fractions collected from Butyl HP column were combined and concentrated using an Amicon Centrifugal Concentrator and separated by Superdex 200 using buffer with different ionic strength. The protein input was divided into two portions, and separated in 50 mM potassium phosphate, pH 7.0 in the presence or absence of 150 mM potassium chloride. The result of the radioligand binding assay of fractions from these two approaches were compared in Figure 4.15. The NAADP binding was enriched in fractions that eluted almost at the lower end of the effective separation range, suggesting that the potential high affinity NAADP binding protein(s) could be of relatively low molecular weight. Although the chromatograms of those two runs virtually had very little difference (Figure 4.14), the radioligand binding assay showed that the elution of the high-affinity NAADP binding protein(s) was delayed by one fraction number. The shift in the peak location is beneficial since the collecting fraction 30 and 31 would result in a much lower protein content than collecting fraction 29 and 30, which may in turn greatly reduce the contaminants. Therefore, the buffer composition was set for 50 mM potassium phosphate, pH 7.0 for size-exclusion chromatography to minimize the protein contaminants while capturing much of the high affinity NAADP binding protein.

Fractions 30-32 were collected and designated as the highly enriched NAADP binding protein fractions, and were subsequently sent for MS analysis.

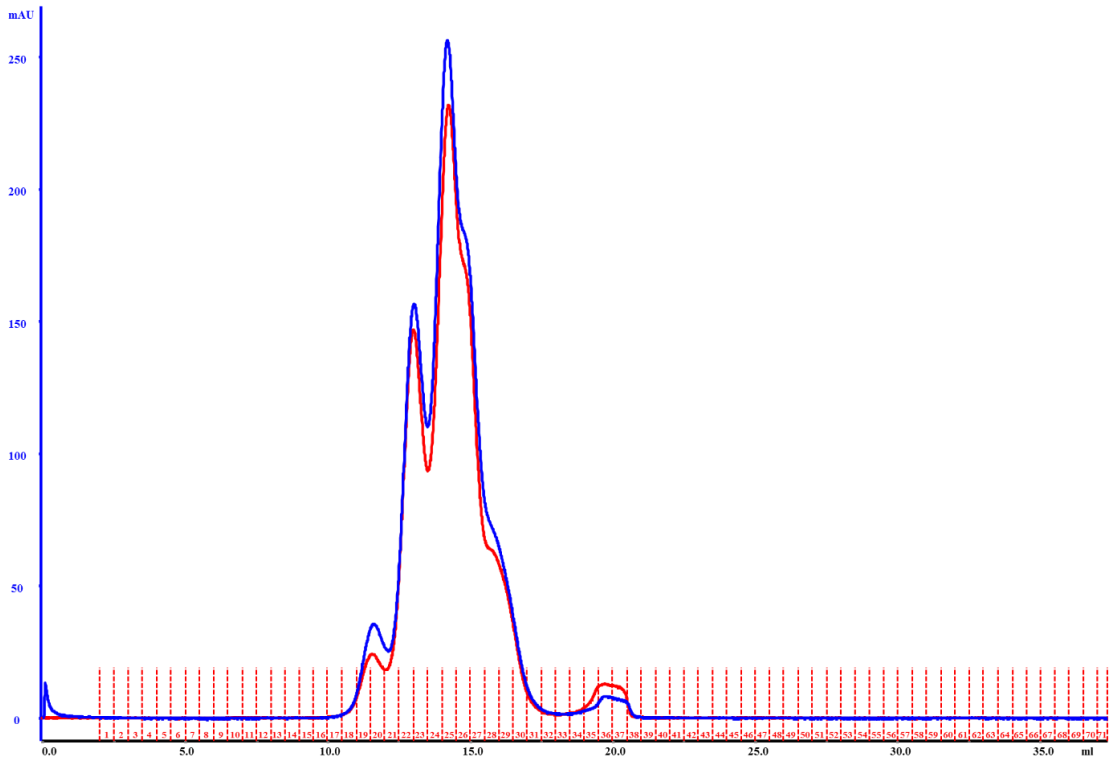

Figure 4.14. Representative chromatogram of size-exclusion chromatography by Superdex S200 HR10/30. Traces: Blue: UV in 50 mM potassium phosphate, pH 7.0; Red: UV in 50 mM potassium phosphate and 150 mM potassium chloride, pH 7.0.

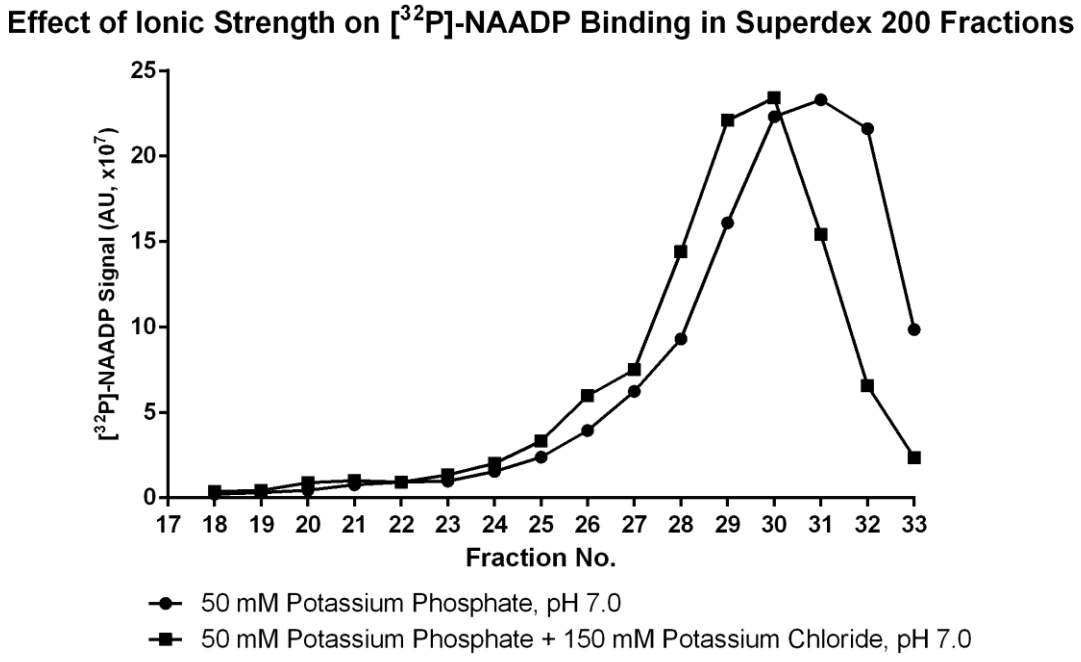

Figure 4.15. Influence of buffer ionic strength on ^{32}P signal of Superdex 200 fractions.

4.1.3. Enrichment of NAADP binding protein by sequential chromatographic purification

After the condition of each chromatography had been set, a large scale NAADP binding protein(s) purification was carried out. The NAADP binding affinity of the collected fractions and the enrichment of each step was determined by the radioligand binding assay.

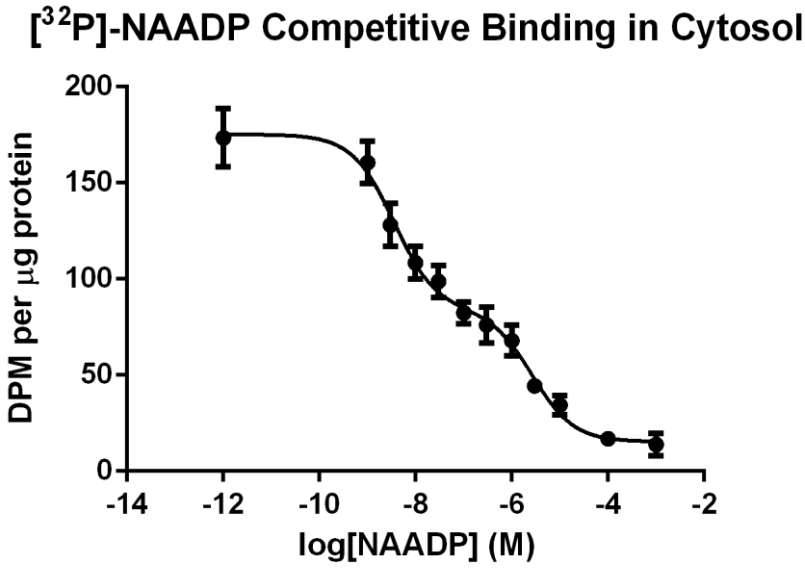

Figure 4.16. [^{32}P]-NAADP competitive binding curve in mouse liver cytosol.

The [^{32}P]-NAADP binding profile of mouse liver cytosol fraction (Figure 4.16) was consistent with the published literature (Calcraft *et al.*, 2009; Ruas *et al.*, 2015). The binding curve could be fitted with a two-site homologous binding model, suggesting that there were two populations of the NAADP binding protein(s) in mouse liver cytosol, one with an IC_{50} of 3.6 nM and 2.6 μM for the other. The fraction of the high affinity NAADP binding protein(s) was roughly 57% according to the non-linear regression analysis.

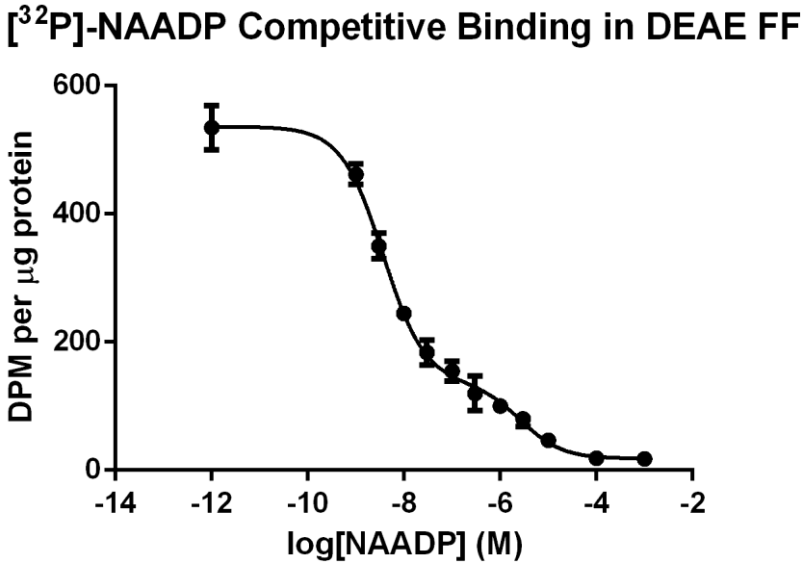

Figure 4.17. [^{32}P]-NAADP competitive binding curve in DEAE FF fractions.

Fractions collected from ion-exchange purification showed a similar [^{32}P]-NAADP binding profile as that of mouse liver cytosol (Figure 4.17). Nevertheless, DEAE column enriched the NAADP binding protein(s) as the total [^{32}P]-NAADP binding increased by approximately 200% per µg protein. The proportion of low affinity NAADP binding was also slightly reduced, as suggested by the non-linear regression that the fraction containing high affinity NAADP binding protein(s) increased from 57% to 77%. The IC_{50} was 3.7 nM for the high affinity site and 2.7 µM for the low affinity site.

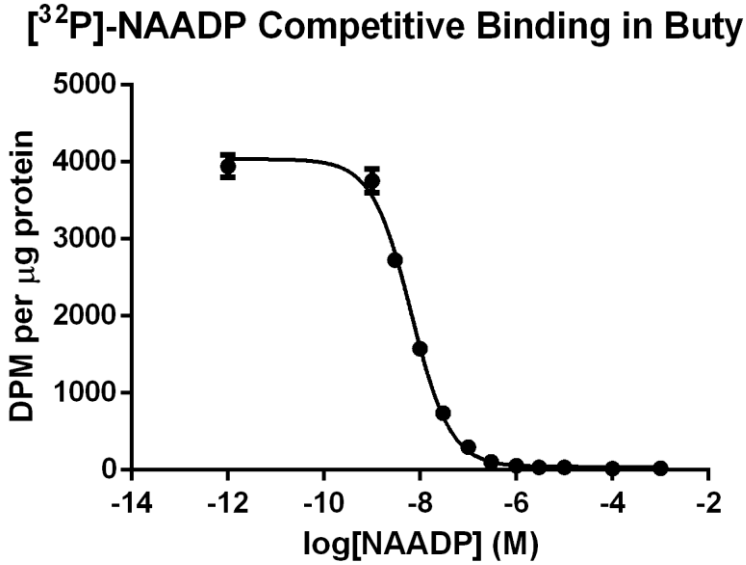

Figure 4.18. [^{32}P]-NAADP competitive binding curve in Butyl HP fractions.

The major achievement of adopting hydrophobic interaction chromatography was that it could further enrich the binding protein(s) as well as effectively eliminating the low affinity NAADP binding protein(s) population, as shown in Figure 4.18. The non-linear regression could no longer converge when a two-site homologous binding model was used, hence one-site homologous binding model was adopted for curve fitting instead. The IC_{50} of the Butyl HP fraction was approximately 6.5 nM. The Hill slope was -1.064 ± 0.04, suggesting the presence of a single homologous NAADP binding site.

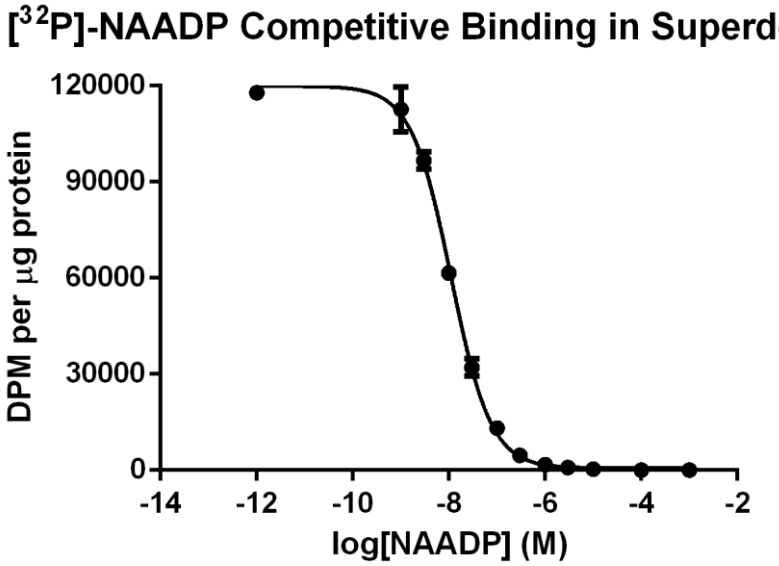

Figure 4.19. [^{32}P]-NAADP competitive binding curve in Superdex 200 fractions.

As the last step of the entire purification process, size-exclusion chromatography concentrated the high affinity NAADP binding protein(s) into a narrow molecular weight range, thus further reducing the protein contaminants in the collected fractions (Figure 4.19). The S200 enriched fractions had a 685-fold increase in DPM per µg protein compared to the liver cytosol input. However, its IC_{50} was about 11.1 nM, which was slightly increased compare to the IC_{50} of high affinity binding site of mouse liver cytosol mentioned above (3.6 nM). The Hill slope was calculated as -1.049 ± 0.04, which agreed with the result of HIC binding analysis.

The sequential chromatography purification achieved an astonishing enrichment of high affinity NAADP binding protein, which was calculated from the increase of B_{max} of high affinity fraction after each chromatography purification. The calculation of B_{max} is based on the Cheng and Pursoff equation (Cheng and Prusoff, 1973):

$$K_i = \frac{IC_{50}}{1 + \frac{[Radioligand]}{K_d}} \quad (1)$$

The [^{32}P]-NAADP binding assay is a homologous displacement assay. Hence it is assumed that the K_i of NAADP and K_d of [^{32}P]-NAADP are identical. The equation can therefore be transformed into the following:

$$K_i = K_d = IC_{50} - [Radioligand] \quad (2)$$

Since:

$$Specific\ Binding = \frac{B_{max} * [Radioligand]}{[Radioligand] + K_d} \quad (3)$$

Therefore, using data from the radioligand competitive binding this can be transformed into:

$$B_{max} = \frac{Specific\ Binding * (K_d + [Radioligand])}{[Radioligand]} \quad (4)$$

Because of Equation (2), Equation (4) can be transformed into:

$$B_{max} = \frac{Specific\ Binding * IC_{50}}{[Radioligand]} \quad (5)$$

Using Equation (5), the B_{max} of fractions collected from each chromatography purification were calculated and summarized in Table 5.2

Table 5.2. Summary of enrichment of high affinity NAADP binding protein by sequential chromatography.

Purification Step	***Fraction***	***Bmax (fmol/µg)***	***Enrichment (fold)***	***Cumulative Enrichment (fold)***
1	Cytosol	0.43	1	1
2	DEAE FF	1.43	3.34	3.34
3	Butyl HP	19.5	13.6	45.6
4	Superdex 200	992.8	50.8	2316.3

In summary, sequential chromatography successfully enriched the high affinity NAADP binding protein(s) by more than 2300-fold in comparison to the starting material, the mouse liver cytosol. However, one should take note that the calculation

listed above took IC_{50} into consideration, which gradually increased throughout as purification progressed. Through the elution profile of high affinity NAADP binding protein, one could speculate that it has the following two characteristics: 1. weak surface hydrophobicity as it eluted early in HIC gradient; 2. relatively low molecular weight since it eluted later than carbonic anhydrase standard, which is 29 kDa.

4.1.4. Discussion

This section discussed about the development of a tandem chromatography strategy to enrich high affinity NAADP binding protein(s).

The sequence of the chromatography was designed to minimize handling as well as speeding up the process. In IEX, proteins are eluted by increasing the ionic strength of the mobile phase whereas in HIC proteins are eluted using the opposite method. Hence performing IEX before HIC would waiver the extra desalting step if scheduled otherwise. Superdex 200 has a maximum loading volume of 200 µl. It would be unwise to perform size-exclusion chromatography at an early stage as the loading capacity of Superdex 200 would render the process extremely sluggish when large sample quantity is present. Therefore the final sequence of the chromatography was set to ion-exchange, hydrophobic interaction and size-exclusion chromatography.

The HIC performed with Butyl HP proved to be a huge success compared to the previous attempt using Phenyl FF (high substitution). Phenyl is a good choice of ligand for HIC since it offers not only hydrophobic but also π-π interaction due to its aromatic ring (Kennedy, 2001). The hydrophobicity of Phenyl FF is considered much higher than what Butyl HP could offer. However, higher hydrophobicity may not always be

beneficial. The failure of Phenyl FF to achieve separation of protein could be owing to the nature of cytosolic proteins used in this study, which presumably had low surface hydrophobicity on average. Thus a shorter alkyl-chain ligand, such as butyl, would be ideal for the satisfactory separation of cytosolic proteins thanks to its relatively lower hydrophobicity. Apart from the functional groups, these two columns also have different particle sizes. The Butyl HP column has an average particle size of 34 µm, which is considerably smaller than that of the Phenyl FF column (90 µm). A smaller particle size would increase efficiency of the column and therefore provide better resolution during separation. In summary, the factors mentioned above contributed to the successful separation in Butyl HP.

Isolation of NAADP binding protein(s) by Butyl HP also saw the separation of three groups of NAADP binding proteins, which were illustrated in Figure 4.9. Fractions 11 and 12 represented the population of high affinity NAADP binding protein(s) that was selected as the key focus of the chromatography purification. The second group of NAADP binding protein(s) is exemplified by fractions 13 and 14, which have high NAADP binding capacity but with rather low affinity. This is reminiscent of the low affinity NAADP binding proteins on the MEF membrane described in Chapter 3. On the other hand, although possessed of high affinity for NAADP, the third group of NAADP binding proteins such as those in fractions 15 and 16 was rather elusive as its presence was quite inconsistent between different mouse batches. This suggests that NAADP binding in those fractions could be from fragile protein complexes sensitive to handling, or could be a result of certain physiological events that took place in some animal batches. In short, the finding using Butyl HP suggested that multiple types of NAADP binding proteins may exist and could be involved in various physiological roles.

What is also worth noting is the increase of apparent IC_{50} throughout the purification. The IC_{50} of the Superdex 200 fractions was 11.1 nM, which was more than three times higher than the IC_{50} of the cytosol (3.6 nM). At a first glance, it seems that the lengthy chromatography purification, while being certainly effective in enriching the high affinity NAADP binding protein, caused a loss of NAADP affinity. However, one should bear in mind that IC_{50} is not a reflection of the true affinity but the concentration of inhibitor producing 50% inhibition (Cheng and Prusoff, 1973). As suggested by its definition, IC_{50} is also influenced by the receptor concentration. Assuming no radioligand depletion occurred during the binding assay, a rise in the receptor concentration would also increase the amount of inhibitor needed to achieve 50% inhibition, thus increase the apparent IC_{50} observed in the experiment. Therefore, the increase of IC_{50} in this study might indicate a surge in the high affinity NAADP binding protein, which requires more unlabelled NAADP to achieve a half-maximal displacement.

4.2. In-gel photoaffinity labelling of NAADP binding protein

4.2.1. Introduction

One of the greatest challenges in searching for NAADP binding protein(s) is that little is known about the its physical properties. This has become a hurdle in identifying the NAADP binding protein even using the MS results of a highly enriched fraction, since its size is unknown and one could only make speculation by names and mascot scores. In 2012, Lin-Moshier *et al.* used a synthetic probe, 5-azido-NAADP, to specifically label NAADP binding protein(s), and discovered that a 22/23kDa protein doublelet labelled by the probe in various cells and tissues showed high affinity towards NAADP (Lin-Moshier *et al.*, 2012). Labelling the NAADP binding protein in the gel using [^{32}P]-5-azido-NAADP will provide valuable information to pinpoint the potential candidates on the list.

The photoaffinity labelling of NAADP binding was carried out by incubating [^{32}P]-5-azido-NAADP in the presence or absence of non-radioactive NAADP, followed by UV irradiation to allow formation of covalent bonds between the azide group and the protein (Figure 4.20). Thus, all proteins that binds NAADP with specificity could be tagged with radioactive ^{32}P and the labelling could be blocked by binding competition in the presence of non-radioactive NAADP.

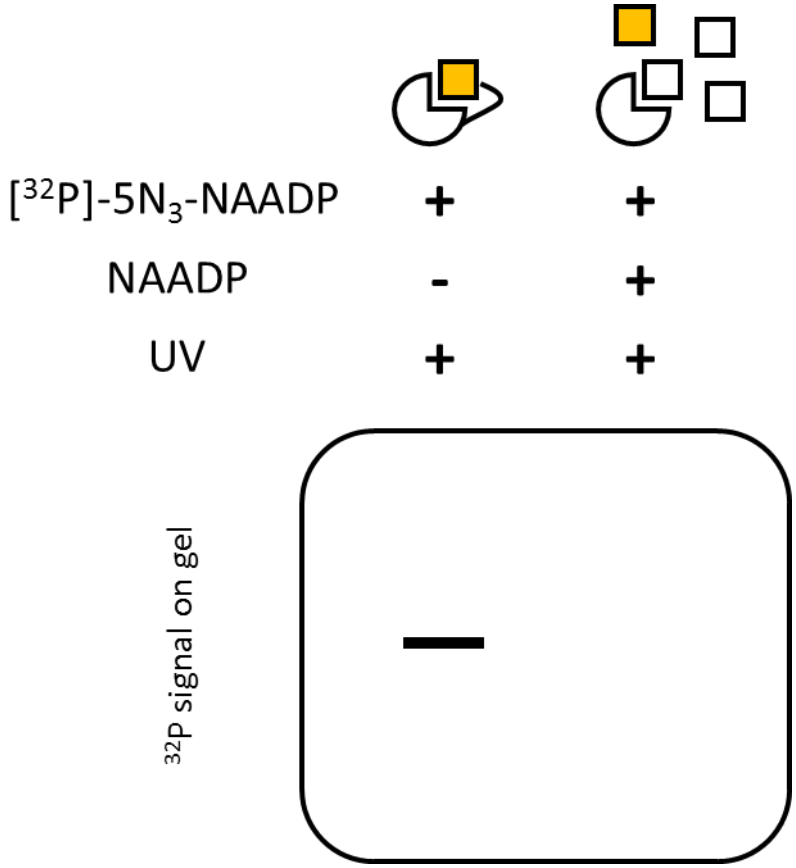

Figure 4.20. Principles of [^{32}P]-5-azido-NAADP photoaffinity labelling.

4.2.2 Photoaffinity labelling of NAADP binding protein in mouse tissues.

The preliminary photoaffinity labelling experiment was performed in bovine serum albumin and mouse liver, heart and brain homogenates to examine the selectivity of the labeling. As shown in Figure 4.21, mouse homogenates can be specifically labelled by the probe as the presence of NAADP blocked the radioactive signals in some bands. Although bovine serum albumin can also be labelled with [^{32}P]-5-azido-NAADP, the labelling cannot be displaced by 4 µM non-radioactive NAADP, which demonstrated the specificity of the photoaffinity labelling.

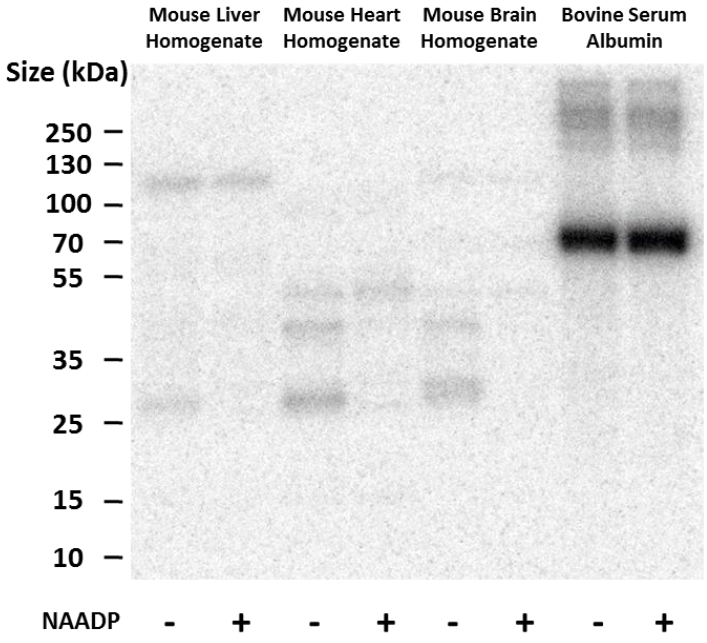

Figure 4.21. [^{32}P]-5-azido-NAADP photoaffinity labelling in bovine serum albumin and mouse tissues. "+" and "-" indicates that the sample was irradiated by 365 nm UV in the presence or absence of 4 µM non-radioactive NAADP.

To investigate whether the distribution of NAADP binding protein in cell compartments varies in different tissues, homogenates from mouse liver, heart and brain were separated into corresponding cytosol or membrane fractions and were

labelled with [^{32}P]-5-azido-NAADP. As shown in Figure 4.22-4.24, each tissue has a unique population of proteins that were labelled with ^{32}P. One specific band at around 27 kDa was labelled in all three tissue preparations. Another specific band at about 37 kDa was also labelled in all samples though less prominently in liver. What is worth noting is that compared to cytosol fraction, fewer bands were labelled in membrane fractions and the labelling intensity was overall much lower. These phenomena were also observed in other mammalian cell preparations (Lin-Moshier *et al.*, 2012).

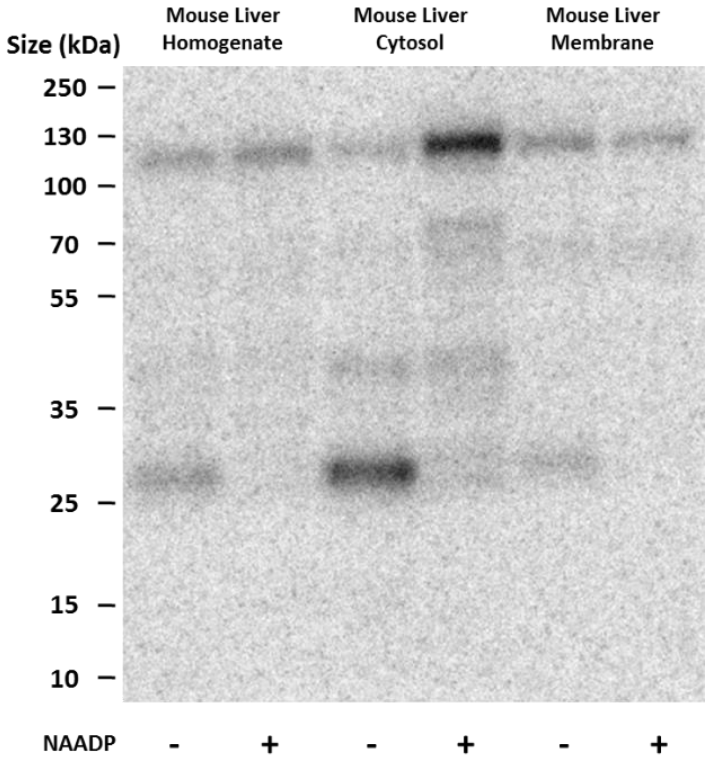

Figure 4.22. [^{32}P]-5-azido-NAADP photoaffinity labelling in mouse liver. "+" and "-" indicates that the sample was irradiated by 365 nm UV in the presence or absence of 4 µM non-radioactive NAADP.

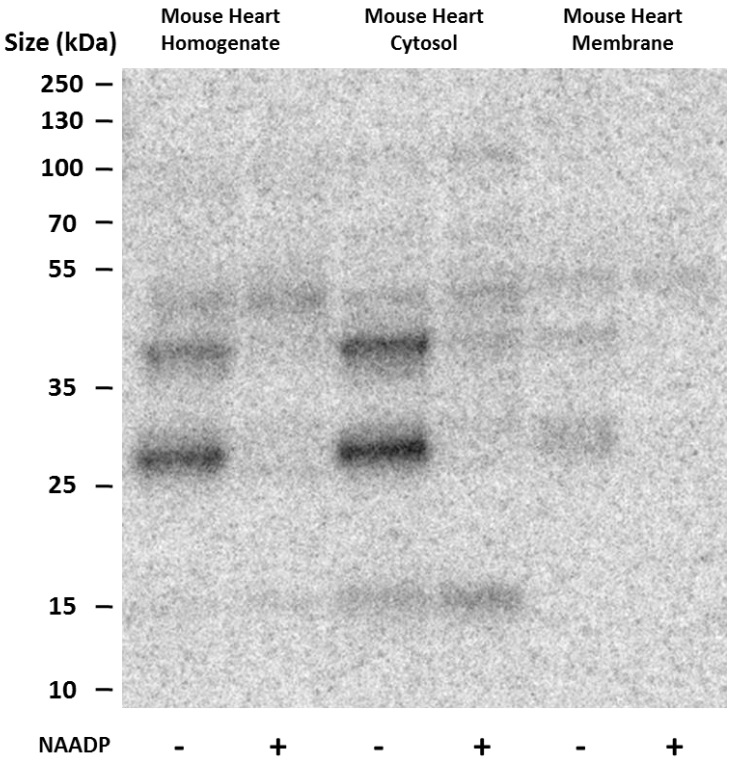

Figure 4.23. [^{32}P]-5-azido-NAADP photoaffinity labelling in mouse heart. "+" and "-" indicates that the sample was irradiated by 365 nm UV in the presence or absence of 4 µM non-radioactive NAADP.

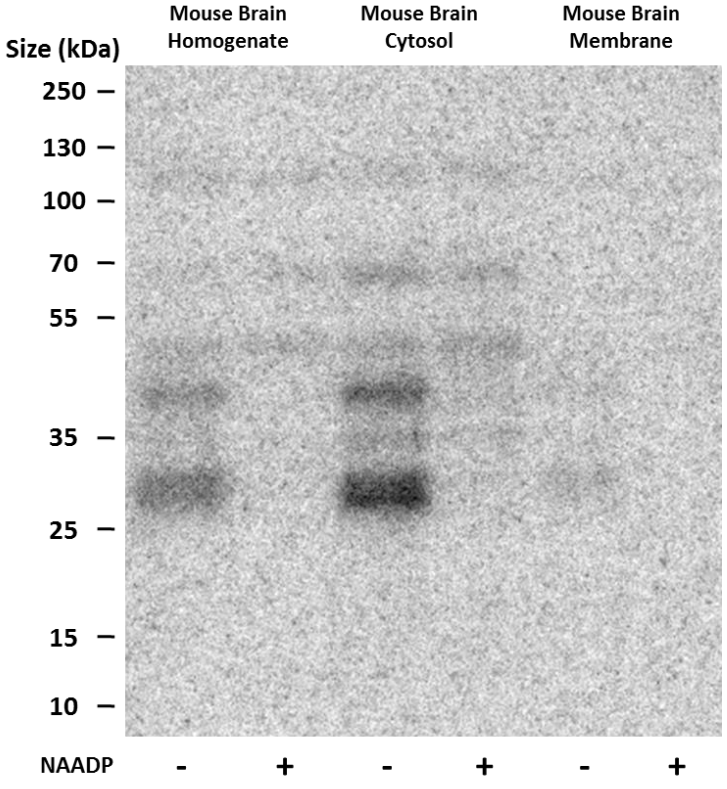

Figure 4.24. [^{32}P]-5-azido-NAADP photoaffinity labelling in mouse brain. "+" and "-" indicates that the sample was irradiated by 365 nm UV in the presence or absence of 4 µM non-radioactive NAADP.

4.2.3. Photoaffinity labelling of NAADP binding protein in chromatography-purified fractions

A photoaffinity labelling was performed in all collected fractions from chromatography purification to identify the protein population that was enriched by sequential chromatography. As shown in Figure 4.25, the ^{32}P intensity of the 27 kDa band increased substantially as the purification proceeds and radiolabelling could be displaced by 4 µM NAADP, which was consistent with the enrichment determined by [^{32}P]-NAADP binding assay.

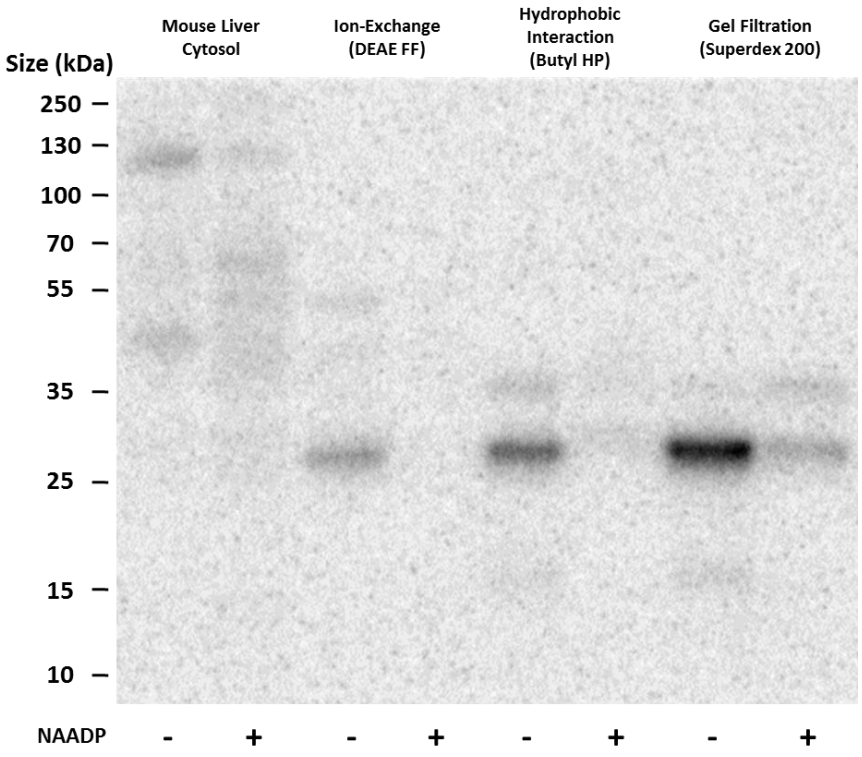

Figure 4.25. [^{32}P]-5-azido-NAADP photoaffinity labelling in chromatography fractions. "+" and "-" indicates that the sample was irradiated by 365 nm UV in the presence or absence of 4 µM non-radioactive NAADP.

Interestingly, the 27 kDa band identified in the photoaffinity labelling was also reported in the existing literature. Photoaffinity labelling in mouse pancreas homogenate performed by Lin-Moshier *et al.* revealed 4 specific bands that might

represent high affinity NAADP binding protein (Figure 4.26, band C-F). As shown in Figure 4.26, the specific band labelled in this study has an almost identical size to band D in mouse pancreas reported by Lin-Moshier *et al.* (2012).

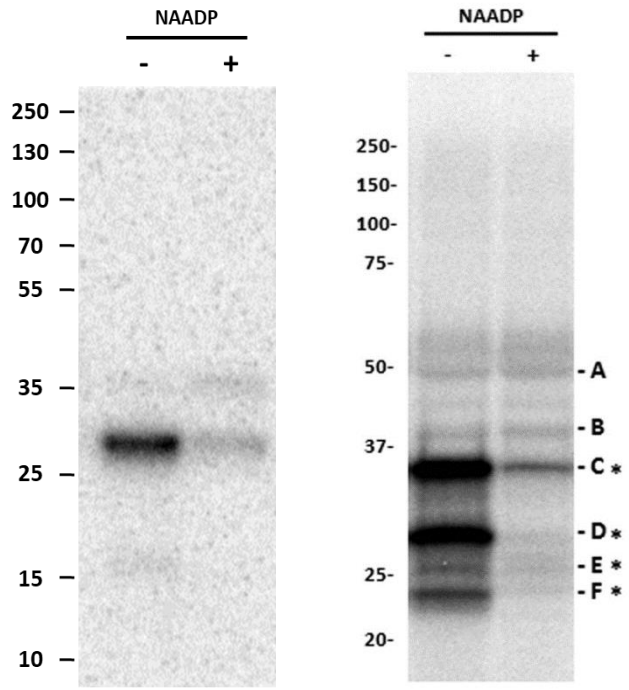

Figure 4.26. Photoaffinity labelling of in Superdex 200 fractions (left) and comparison with photoaffinity labelling of mouse pancreas homogenate by Lin-Moshier *et al.* (right). The NAADP concentration used for displacement was 4 µM and 10 µM for left and right gel, respectively. A 27 kDa band was found in both preparations.

4.2.4. Discussion

The synthesis of 5-azido-NAADP was a milestone in the journey of identifying the elusive NAADP binding protein as it finally allowed the visualization of NAADP binding protein(s). It has an IC_{50} of 18 ± 14 nM in sea urchin egg homogenate (Jain *et al.*, 2010) and its specificity has been readily tested in several systems, such as sea urchin egg homogenate, SKBR3 lysate, HEK293 lysate, Jurkat T-lymphocytes, mouse liver and pancreas homogenate (Walseth *et al.*, 2012a; Lin-Moshier *et al.*, 2012; Walseth *et al.*, 2012b; Ruas *et al.*, 2015). While overlapping of the radiolabelled protein population was observed, most reported preparations saw different sets of protein labelled by radioactive probes, indicating that multiple NAADP binding proteins may exist across species. Also, in this study, radiolabelling in mouse liver, heart and brain suggested that NAADP binding proteins in these tissues are predominately located in the cytosolic fraction. This was also seen in the SKBR3 whole cell lysate preparation (Lin-Moshier *et al.*, 2012) and concurred with the reported [^{32}P]-NAADP binding assay results in subcellular fractions of these tissues (Zhu, 2012). Those observations were in agreement with hypothesis that an intermediate cytosolic protein might be involved in NAADP signalling cascade since NAADP does not seem to directly bind to its proposed receptors (Calcraft *et al.*, 2009). It is worth noting that in Figure 4.22, the labelling of a 120 kDa band in mouse cytosol was increased in the presence of 4 μM unlabelled NAADP. Judging from the labelling profile of mouse liver homogenate and cytosol in Figure 4.22 and Figure 4.25, it can be deduced that this band contained noticeable level of low affinity NAADP binding. In addition, all samples were reduced by Lammeli buffer and boiled at 95 °C for 10 minutes, thus ruled out the possibility of

incompletion reduction of the sample. Therefore, the increase of the labelling intensity of this 120 kDa band in the presence of unlabelled NAADP is mostly like an artifact introduced by the addition of incorrect amount of labelling probe.

As demonstrated in the previous section, the enriched binding protein fraction had an IC_{50} of 11.1 nM as revealed by the [^{32}P]-NAADP binding assay. However, in photoaffinity labelling, 4 µM NAADP could not completely displace the ^{32}P signal of the presumed NAADP binding protein band (Figure 4.25). The UV wavelength for irradiation was 365 nm, which is not damaging to proteins (MacKinnon and Taunton, 2009) and therefore is unlikely to be the cause of affinity loss. It is worth mentioning that the intensity of UV lamp used for irradiation was very low (8W), hence the time of exposure was extended to compensate for the lack of UV intensity. However, prolonged exposure could have also given rise to the non-specific binding.

Interestingly, none of the photoaffinity labelling results in this study identified the 22/23 kDa band reported in existing literature (Walseth *et al.*, 2012b; Lin-Moshier *et al.*, 2012). This is believed to be more of a sensitivity or sample preparation issue than a problem with the probe. In this study, the [^{32}P]-5-azido-NAADP was synthesized through a two-step reaction. The critical functional groups, the ^{32}P and azido-group was integrated into the molecule in separate steps. Thus an erroneous reaction would result in no labelling in subsequent experiment, due to either no effective crosslinking functional group or no ^{32}P present. In addition, all intermediates and the final probe were verified by NMR. Therefore, the chances of having a failing probe is highly unlikely. What is worth mentioning is that during the synthesis of the probe a mistake in the published synthesis method was found. When describing the procedure of

collecting 5-azidonicotinic acid ethyl ester, Jain *et al.* stated that the product to be collected should be 'the golden oil' (Jain *et al.*, 2010). However, during the reproduction of column chromatography procedure, it was noticed that the final product, contrary to what was described in the literature, was a rather colorless fraction visually indistinguishable from the color of silica gel. This fraction eluted before the colored oil and had strong UV absorption owing to the nicotinic ring in the structure, whereas the oil fraction had no UV absorption at all.

There are two possible explanations for the absence of 22/23 kDa doublet labelling in this study: First of all, judging from the reported labelling profile of the 22/23 kDa doublet, the binding protein abundance within the doublet seems to be low since the ^{32}P intensity of the doublet was much lower than the other labelled bands. Unfortunately, the phosphor screen used to acquire the radiolabelled gel image in this study did not have the sufficient sensitivity to produce images of the highest resolution. Hence it is possible that 22/23 kDa was not visualized due to the sensitivity of the imaging equipment. Secondly, the chromatography purification was an unbiased approach to isolate high affinity NAADP binding protein(s) and the selection of the fractions to proceed was entirely based on their NAADP binding. Nevertheless, this also means that fractions with less prominent or reproducible NAADP binding, such as fraction 15 and 16 from Butyl HP slop gradient (Figure 4.9) were not taken into consideration since it was not realistic to perform a thorough investigation of every fraction. Yet one cannot deny the possibility of the existence of high affinity NAADP binding protein in those discarded fractions. Therefore it is also possible that the 22/23 kDa doublet was lost during the selection.

It is worth noting that the 22/23 kDa doublet, while certainly being more universal, was not the only high affinity NAADP binding protein that was labelled in the literature. For instance, in the right-side gel image in Figure 4.26, band D has been reported to have almost identical affinity and selectivity as the 22/23 kDa doublet (band F) and its ^{32}P intensity was much higher than that of band F (Lin-Moshier *et al.*, 2012). However, no update on band D has been reported in the past years, perhaps due to the fact that it was more tissue-specific. Interestingly, band D represented the protein population that was enriched by sequential chromatography in this study (Figure 4.25). This 27 kDa band may be another promising lead to unravel the identity of the NAADP binding protein(s).

4.3. Identification of NAADP binding proteins

4.3.1. Introduction

The previous section described the major discovery achieved through photoaffinity labelling in chromatography fractions, which provided crucial information on the size of the binding protein candidates. Based on those findings, a plan was conceived to identify the NAADP binding protein from the enriched fractions by the combined arms of mass spectrometry and docking simulation (Figure 4.27). Briefly, three batches of sample were purified and sent for mass spectrometry analysis. A size cut-off was applied to the results and shared candidates among three batches were subsequently tested by docking simulation to determine the candidates with the highest affinity to NAADP.

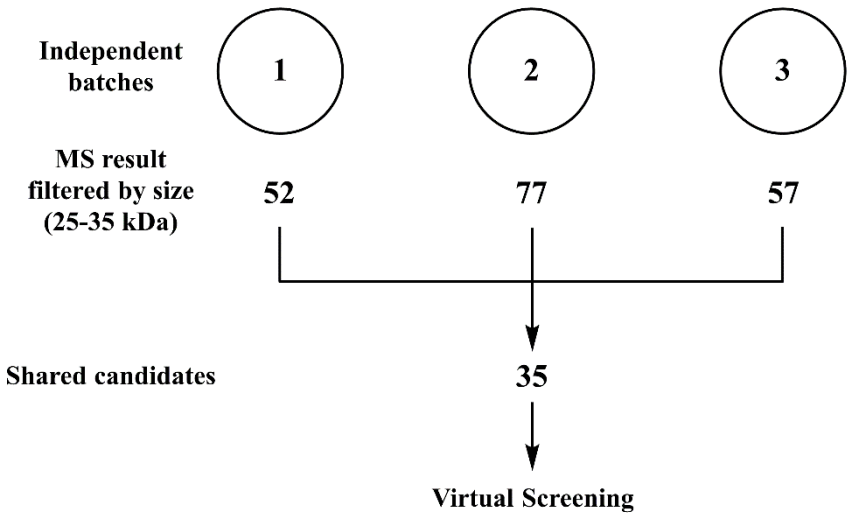

Figure 4.27. Schematics of MS-docking analysis of NAADP enriched fractions.

4.3.2. Mass spectrometry analysis of fractions from sequential chromatography purification

To identify the protein candidates from enriched fractions, three independent batches of NAADP enriched fractions were obtained from sequential chromatography and the presence and the enrichment of NAADP binding protein was confirmed by photoaffinity labelling. After that, these fractions were sent for mass spectrometry analysis at the Advanced Proteomics Facility, University of Oxford. As indicated by the photoaffinity labelling experiment, the protein band representing the NAADP binding protein has a size of approximately 27 kDa. To avoid inaccurate size predication from the potential discrepancy between theoretical and observed protein size due to migration anomaly and possible post-translational modification, the results were filtered by a wide range of 25-35 kDa. Since the profile of ^{32}P labelled band was identical in all three batches, it was reasonable to assume that potential candidates should be present in all batches. Thus the shortlisted candidates from each batch were compared to identify candidates that were shared and a final list of 35 NAADP binding protein candidates was generated.

Table 5.3. 35 NAADP binding protein candidates from mass spectrometry analysis.

Accession	Description	Mass	Sequence coverage	Score
sp|Q9WUK2-2|IF4H_MOUSE	Isoform Short of Eukaryotic translation initiation factor 4H OS=Mus musculus GN=Eif4h	25228	0.2	226
sp|P24472|GSTA4_MOUSE	Glutathione S-transferase A4 OS=Mus musculus GN=Gsta4 PE=1 SV=3	25547	0.05	17
sp|Q8BVI4|DHPR_MOUSE	Dihydropteridine reductase OS=Mus musculus GN=Qdpr PE=1 SV=2	25782	0.74	3444
sp|Q9WTP6-2|KAD2_MOUSE	Isoform 2 of Adenylate kinase 2, mitochondrial OS=Mus musculus GN=Ak2	25817	0.55	1693
tr|E0CXT5|E0CXT5_MOUSE	Disabled homolog 2 OS=Mus musculus GN=Dab2 PE=1 SV=1	26154	0.16	119

sp|P58044|IDI1_MOUSE	Isopentenyl-diphosphate Delta-isomerase 1 OS=Mus musculus GN=Idi1 PE=2 SV=1	26615	0.33	243
tr|Q8BH80|Q8BH80_MOUSE	Vesicle-associated membrane protein, associated protein B and C OS=Mus musculus GN=Vapb PE=1 SV=1	27129	0.12	73
tr|D3YYS7|D3YYS7_MOUSE	mRNA cap guanine-N7 methyltransferase (Fragment) OS=Mus musculus GN=Rnmt PE=1 SV=1	27366	0.05	49
sp|O09131|GSTO1_MOUSE	Glutathione S-transferase omega-1 OS=Mus musculus GN=Gsto1 PE=2 SV=2	27708	0.17	113
sp|O55060|TPMT_MOUSE	Thiopurine S-methyltransferase OS=Mus musculus GN=Tpmt PE=1 SV=1	27853	0.25	93
sp|Q8R1G2|CMBL_MOUSE	Carboxymethylenebutenolidase homolog OS=Mus musculus GN=Cmbl PE=2 SV=1	28226	0.21	64
sp|P51163|HEM4_MOUSE	Uroporphyrinogen-III synthase OS=Mus musculus GN=Uros PE=2 SV=1	28885	0.41	521
sp|P49312-2|ROA1_MOUSE	Isoform Short of Heterogeneous nuclear ribonucleoprotein A1 OS=Mus musculus GN=Hnrnpa1	28994	0.16	73
sp|P00920|CAH2_MOUSE	Carbonic anhydrase 2 OS=Mus musculus GN=Ca2 PE=1 SV=4	29129	0.05	15
tr|Q5ND50|Q5ND50_MOUSE	Adapter molecule crk OS=Mus musculus GN=Crk PE=1 SV=2	29380	0.07	153
sp|P16015|CAH3_MOUSE	Carbonic anhydrase 3 OS=Mus musculus GN=Ca3 PE=1 SV=3	29633	0.79	2076
sp|P40936|INMT_MOUSE	Indolethylamine N-methyltransferase OS=Mus musculus GN=Inmt PE=1 SV=1	30068	0.31	421
sp|Q9CQ01|RNT2_MOUSE	Ribonuclease T2 OS=Mus musculus GN=Rnaset2 PE=2 SV=1	30160	0.32	1013
sp|Q61166|MARE1_MOUSE	Microtubule-associated protein RP/EB family member 1 OS=Mus musculus GN=Mapre1 PE=1 SV=3	30168	0.09	38
sp|P48758|CBR1_MOUSE	Carbonyl reductase [NADPH] 1 OS=Mus musculus GN=Cbr1 PE=1 SV=3	30907	0.92	2991
sp|Q9DCN2-2|NB5R3_MOUSE	Isoform 2 of NADH-cytochrome b5 reductase 3 OS=Mus musculus GN=Cyb5r3	31757	0.44	837
sp|Q8CDN6|TXNL1_MOUSE	Thioredoxin-like protein 1 OS=Mus musculus GN=Txnl1 PE=2 SV=3	32616	0.06	123
sp|P17751|TPIS_MOUSE	Triosephosphate isomerase OS=Mus musculus GN=Tpi1 PE=1 SV=4	32684	0.64	1325
tr|Q3UW66|Q3UW66_MOUSE	Sulfurtransferase OS=Mus musculus GN=Mpst PE=1 SV=1	33305	0.51	1045
sp|Q9CPV4|GLOD4_MOUSE	Glyoxalase domain-containing protein 4 OS=Mus musculus GN=Glod4 PE=1 SV=1	33581	0.81	1430
sp|Q9Z130|HNRDL_MOUSE	Heterogeneous nuclear ribonucleoprotein D-like OS=Mus musculus GN=Hnrnpdl PE=1 SV=1	33709	0.34	279
tr|E9Q5D9|E9Q5D9_MOUSE	Insulin-like growth factor-binding protein 7 OS=Mus musculus GN=Igfbp7 PE=1 SV=1	33866	0.15	258
sp|Q64374|RGN_MOUSE	Regucalcin OS=Mus musculus GN=Rgn PE=1 SV=1	33899	0.04	49
sp|P47941|CRKL_MOUSE	Crk-like protein OS=Mus musculus GN=Crkl PE=1 SV=2	33923	0.15	67

tr|F6QCI0|F6QCI0_MOUSE	Protein Taf15 (Fragment) OS=Mus musculus GN=Taf15 PE=1 SV=1	33923	0.13	842
sp|P23589|CAH5A_MOUSE	Carbonic anhydrase 5A, mitochondrial OS=Mus musculus GN=Ca5a PE=1 SV=2	34450	0.11	152
tr|G5E8T9|G5E8T9_MOUSE	Hydroxyacyl glutathione hydrolase OS=Mus musculus GN=Hagh PE=1 SV=1	34538	0.57	1793
sp|Q9WUU7|CATZ_MOUSE	Cathepsin Z OS=Mus musculus GN=Ctsz PE=2 SV=1	34658	0.1	48
sp|Q9CYG7-2|TOM34_MOUSE	Isoform 2 of Mitochondrial import receptor subunit TOM34 OS=Mus musculus GN=Tomm34	34658	0.04	62
sp|Q61176|ARGI1_MOUSE	Arginase-1 OS=Mus musculus GN=Arg1 PE=1 SV=1	34957	0.08	90

The candidate list above is possibly by far the most concise list ever produced. Previous attempt using a suboptimal chromatography method yielded a list of more than 700 candidates and the size of the binding protein was unknown due to the absence of an effective labelling technique, rendering the identification of candidates almost impossible. Elimination of bulk contaminants by sequential chromatography combined with size prediction by photoaffinity labelling significantly reduced the number of the candidates to less than 5% of the previous trial. The small number of candidates would allow the subsequent implementation of individual protein docking simulation.

4.3.3. Virtual screening of NAADP binding proteins by AutoDock Vina and CLC Drug Discovery Workbench

Protein-ligand docking simulation is a powerful tool for screening potential binding partners of a protein, providing its speculative binding confirmation upon interaction and it has been used for high-throughput screening in the pharmaceutical companies in drug discovery. However, the accuracy of the prediction is less than perfect, which severely limits the reliability of the docking predication. Although state-of-art docking software normally could immaculately reproduce the ligand binding stats determined by X-ray crystallography, many could not provide accurate prediction of the binding affinity (Warren *et al.*, 2006). Hence in this study, two docking programs with different docking algorithms and scoring functions were employed to reduce the chance of false-positives or false-negatives. The programs of choice were AutoDock Vina and CLC Drug Discovery Workbench.

AutoDock Vina is one of the most popular docking programs and has improved average prediction accuracy over its predecessor AutoDock 4 (Trott and Olson, 2010). The scoring function of AutoDock Vina is a hybrid of knowledge-based potentials and empirical scoring functions, which was extracted from both conformation preference and experimentally determined affinity of the ligand-receptor complexes. The score is a sum of intermolecular and intramolecular contributions, and thus avoids the internally clashed structure which is often found in scoring functions that do not take internal constraints into account (Trott and Olson, 2010). AutoDock Vina employs the Iterated Local Search global optimizer as its optimization algorithm. This stochastic global optimizer is made of a mutation and a local optimization using the Broyden-

Fletcher-Goldfarb-Shanno (BFGS) method, which is a quasi-Newton method that uses both the value of the scoring function and its derivatives regarding the ligand (position, orientation, torsion, active rotatable bonds, flexible residues, etc.) (Trott and Olson, 2010).

CLC Drug Discovery Workbench is a drug design software distributed by Qiagen and is also capable of performing protein-ligand docking simulation. The docking score used is $PLANTS_{PLP}$ (Protein-Ligand Ant Colony Optimization System) score, an empirical scoring function based on some of the published scoring functions and force fields. PLP refers to Piecewise Linear Potential, which is adopted to model the steric complementarity of ligand and protein (Korb *et al.*, 2009). The score is a sum of the piecewise linear potential, ligand clash potential, ligand torsion potential and a site-directory quadratic potential. The local optimization algorithm used in the CLC Drug Discovery Workbench is the Simplex method (Nelder and Mead, 1965), which is an effective stochastic procedure that adapts itself to local landscape and contracts until the final minimum is reached.

These two docking programs are similar in algorithm hierarchy (global solution + local optimization) and both have stochastic local optimization algorithms. However, they are different in many other aspects. The scoring function of AutoDock Vina returns scores of the top 9 best docking conformation in affinity units, kcal/mol, as it benefits from the knowledge-based potential, whereas the scoring function in CLC would only return the score of the best docking confirmation in arbitrary unit. Although scoring functions of both programs are empirically based, or at least partly so, the types of interactions that contribute to the score and the weights that assigned to them were

not the same. The local optimization algorithms of the two programs also adopt a different strategy for minimization.

To initiate the docking simulation, X-ray crystallography structures of the candidates were downloaded from the European Bioinformatics Institute (EMBL-EBI) or Protein Data Bank (RCSB PDB). For protein candidates that did not have their crystallography structures available, substitutions from closely resembled homologous protein in other species were taken instead. The docking simulation was not performed on candidates without legitimate crystallography structures or suitable homologous protein structures, hence only 25 out of 35 candidates were eligible for simulation. The 3D structure of NAADP was obtained from PubChem. Docking simulation was carried out using a setting recommended by the relevant manuals. The search area of the simulation was selected to cover as much surface area of the protein as possible. For CLC Drug Discovery Workbench, a further ligand optimization was performed after acquiring the docking result. The summary of docking simulation is listed in Table 5.4. For both AutoDock Vina and CLC Drug Discovery Workbench, a more negative score suggests stronger binding.

Table 5.4. Docking results of NAADP binding protein candidates.

Mass	Description	PDB name	Sequence Similarity	Autodock Vina	CLC
25547	Glutathione S-transferase A4 OS=Mus musculus GN=Gsta4 PE=1 SV=3	1guk	59%	-8.1	-59.51
25782	Dihydropteridine reductase OS=Mus musculus GN=Qdpr PE=1 SV=2	1dhr	98%	-8.7	-67.92
25817	Isoform 2 of Adenylate kinase 2, mitochondrial OS=Mus musculus GN=Ak2	2c9y	94%	-8.4	-69.75
26154	Disabled homolog 2 OS=Mus musculus GN=Dab2 PE=1 SV=1	1m7e	[33-191]* 100%	-8.8	-65.88
26615	Isopentenyl-diphosphate Delta-isomerase 1 OS=Mus musculus GN=Idi1 PE=2 SV=1	2dho	87%	-8.3	-55.61
27708	Glutathione S-transferase omega-1 OS=Mus musculus GN=Gsto1 PE=2 SV=2	1eem	72%	-7.2	-58.67

27853	Thiopurine S-methyltransferase OS=Mus musculus GN=Tpmt PE=1 SV=1	2bzg	80%	-9.7	-79.34
28885	Uroporphyrinogen-III synthase OS=Mus musculus GN=Uros PE=2 SV=1	1jr2	78%	-6.9	-55.61
28994	Isoform Short of Heterogeneous nuclear ribonucleoprotein A1 OS=Mus musculus GN=Hnrnpa1	1u1r	100%	-7.9	-65.64
29129	Carbonic anhydrase 2 OS=Mus musculus GN=Ca2 PE=1 SV=4	4r5b	81%	-7.7	-56.11
29633	Carbonic anhydrase 3 OS=Mus musculus GN=Ca3 PE=1 SV=3	1z93	91%	-7.2	-59.27
30068	Indolethylamine N-methyltransferase OS=Mus musculus GN=Inmt PE=1 SV=1	2a14	58%	-7.3	-66.25
30160	Ribonuclease T2 OS=Mus musculus GN=Rnaset2 PE=2 SV=1	3t0o	[39-255]* 72%	-7.7	-68.52
30168	Microtubule-associated protein RP/EB family member 1 OS=Mus musculus GN=Mapre1 PE=1 SV=3	2r8u	96%	-6.4	-62.36
30907	Carbonyl reductase [NADPH] 1 OS=Mus musculus GN=Cbr1 PE=1 SV=3	1wma	89%	-10.4	-84.2
31757	Isoform 2 of NADH-cytochrome b5 reductase 3 OS=Mus musculus GN=Cyb5r3	1umk	[27-301]* 87%	-9.0	-94.44
32684	Triosephosphate isomerase OS=Mus musculus GN=Tpi1 PE=1 SV=4	2jk2	[55-299]* 96%	-6.9	-51.19
33305	Sulfurtransferase OS=Mus musculus GN=Mpst PE=1 SV=1	4jgt	84%	-9.1	-55.52
33581	Glyoxalase domain-containing protein 4 OS=Mus musculus GN=Glod4 PE=1 SV=1	3zi1	90%	-6.8	-64.46
33899	Regucalcin OS=Mus musculus GN=Rgn PE=1 SV=1	4gna	100%	-8.1	-69.48
33923	Crk-like protein OS=Mus musculus GN=Crkl PE=1 SV=2	2lqn	96%	-7.6	-70.16
34450	Carbonic anhydrase 5A, mitochondrial OS=Mus musculus GN=Ca5a PE=1 SV=2	1dmx	[53-299]* 98%	-8.8	-71.94
34538	Hydroxyacyl glutathione hydrolase OS=Mus musculus GN=Hagh PE=1 SV=1	1qh3	[50-309]* 91%	-8.8	-68.32
34658	Cathepsin Z OS=Mus musculus GN=Ctsz PE=2 SV=1	1deu	87%	-7.7	-60.43
34957	Arginase-1 OS=Mus musculus GN=Arg1 PE=1 SV=1	1d3v	94%	-6.8	-58.11

*: numbers in the brackets indicate the length of amino acid sequence of homologous protein with respect to that of the protein candidate.

Three outstanding candidates emerged in both docking programs: Thiopurine S-methyltransferase (TPMT), Carbonyl reductase [NADPH] 1 (CBR1) and Isoform 2 of NADH-cytochrome b5 reductase 3 (CYB5R3).

CBR1 has a board spectrum of substrate specificity and uses NADP as cofactor to facilitate its reductase activity. Figure 4.28 shows the overlay of docking results in hCBR1 crystallography structure with NADP. Docking simulations of both programs produced conformations of NAADP that highly resemble the experimentally determined conformation of NADP inside the cofactor binding pocket of CBR1.

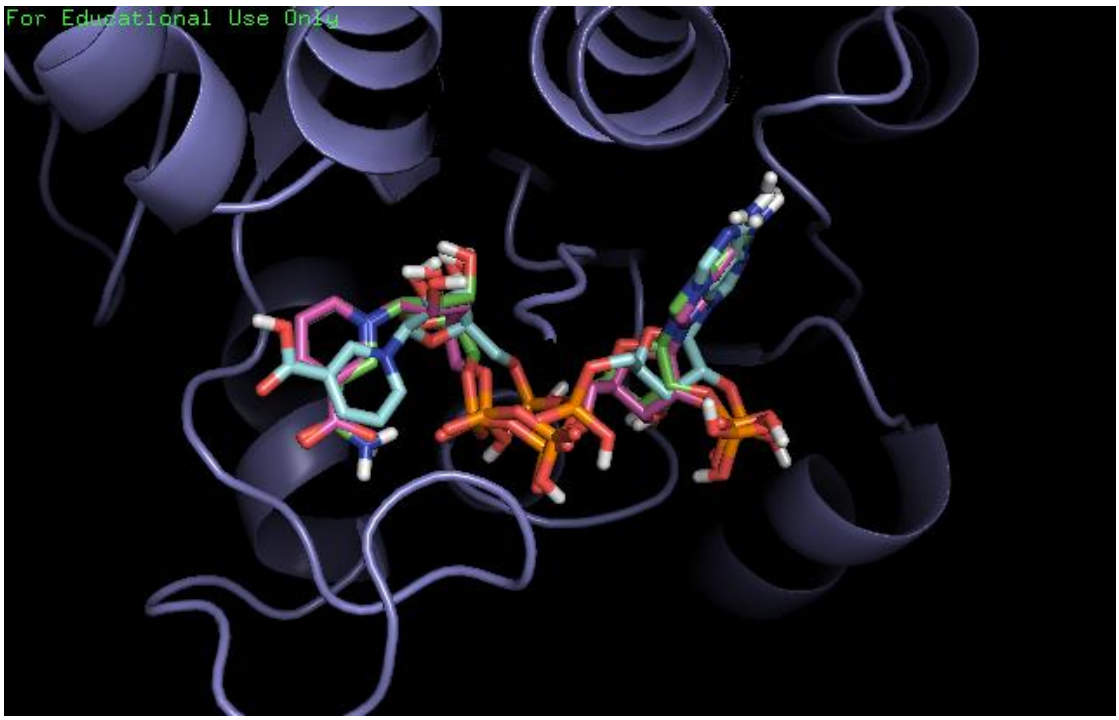

Figure 4.28. Human carbonyl reductase 1 (hCBR1) crystal structure with NADP and overlay of the best NAADP confirmations from docking results. The backbone of the ligands were highlighted in different colors to differentiate NADP (green) and docking results from AutoDock Vina (pink) and CLC Drug Discovery Workbench (cyan).

CYB5R3 is a NADH-dependent reductase that transfers the electrons of NADH to a variety of substrates via cofactor flavin adenine dinucleotide (FAD). The candidate revealed by MS is the soluble isoform, which can be found in mammalian erythrocytes (Passon and Hultquist, 1972) and is believed to be involved in methemoglobin reduction (Elahian *et al.*, 2014). Similarly, the docking simulation returned NAADP conformations that overlapped with the cofactor FAD (Figure 4.29).

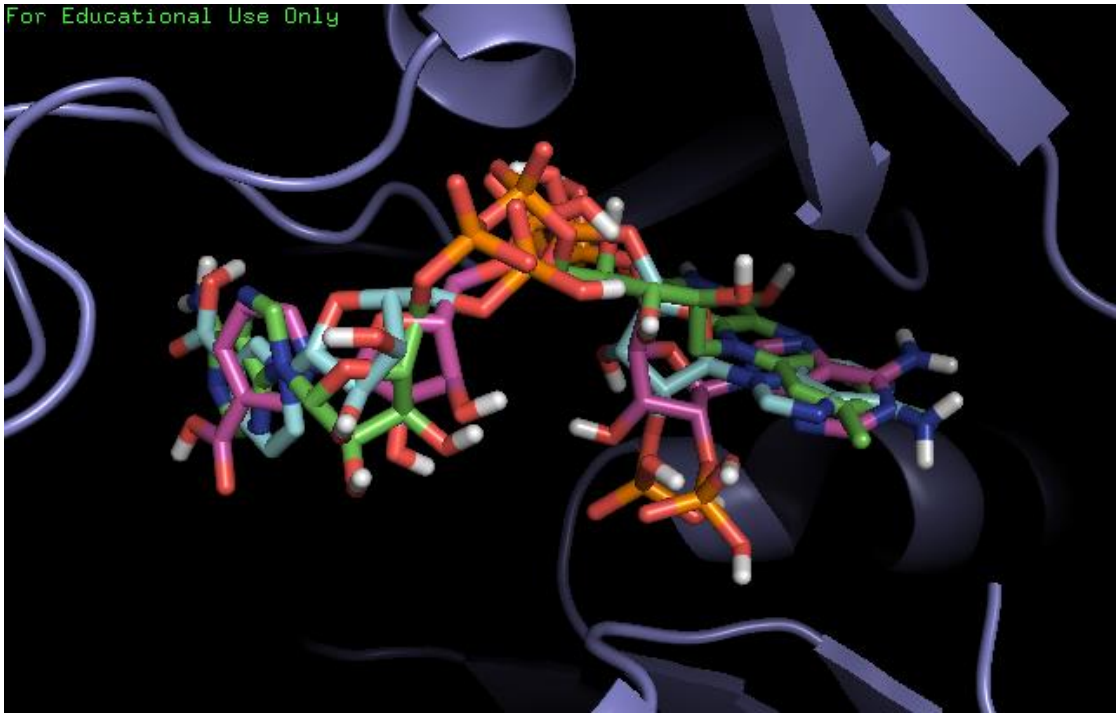

Figure 4.29. Human cytochrome b5 reductase 3 (hCYB5R3) crystal structure with FAD and overlay of the best NAADP confirmations from docking results. The backbone of the ligands were highlighted in different colors to differentiate FAD (green) and docking results from AutoDock Vina (pink) and CLC Drug Discovery Workbench (cyan).

Unlike the two reductases mentioned above, TPMT is a methyltransferase that catalyze the S-methylation of thiopurines and is typically involved in the detoxification of chemotherapy agents. The methylation catalyzed by TPMT requires the presence of a methyl donor, S-adenosyl-L-methionine (SAM) and currently there has been no evidence claiming the binding of common cofactors such as NAD or NADP to this protein. Nevertheless, the docking results in this study suggested that NAADP may bind to TPMT via the same binding pocket occupied by SAM as the speculative NAADP conformations from both programs showed partial overlapping over S-adenosyl-L-homocysteine (SAH), a by-product of the S-methylation and an inhibitor of hTPMT (Figure 4.30).

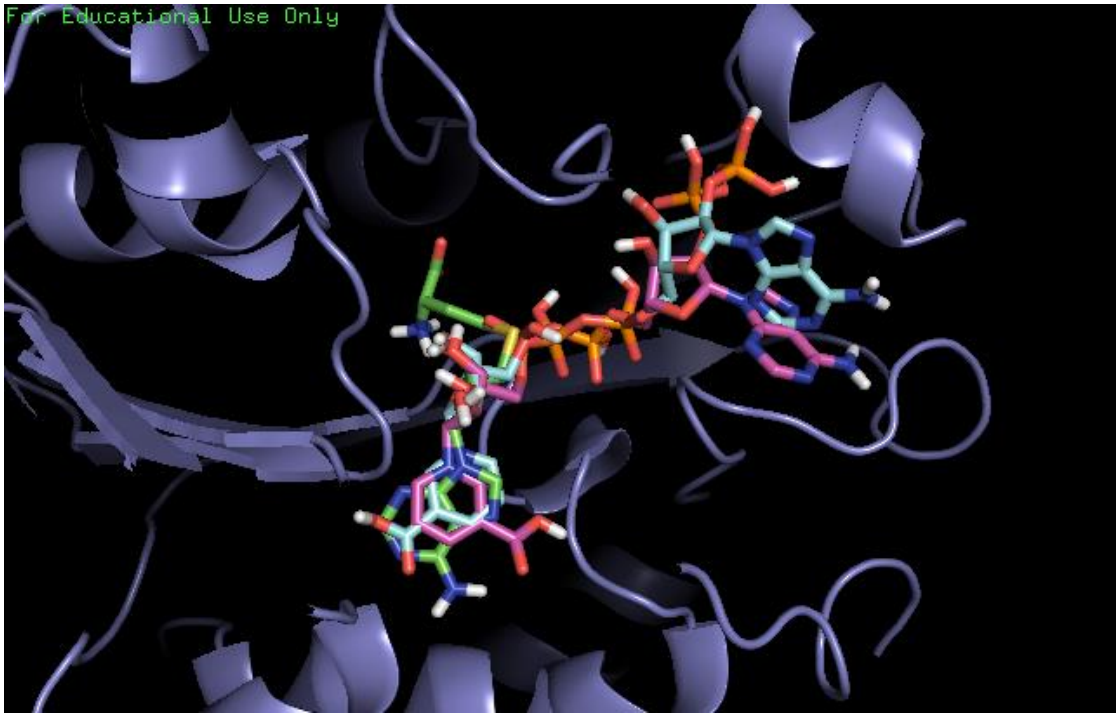

Figure 4.30. Human thiopurine S-methyltransferase (hTPMT) crystal structure with S-adenosyl-L-homocystine (SAH) and overlay of the best NAADP confirmations from docking results. The backbone of the ligands were highlighted in different colors to differentiate SAH (green) and docking results from AutoDock Vina (pink) and CLC Drug Discovery Workbench (cyan).

AutoDock Vina and CLC Drug Discovery Workbench both predicted that carbonyl reductase 1, cytochrome b5 reductase 3 and thiopurine methyltransferase could have potentially strong NAADP binding and the docking results were reasonable with respect to the speculative ligand conformations in protein crystallography structures. The sequences of these proteins were subsequently cloned for experimental validation of their affinity towards NAADP.

4.3.4. Discussion

In this section, a list of 35 protein candidates was acquired from mass spectrometry analysis. This is by far the shortest comprehensive list of NAADP binding protein candidates ever produced. The phosphor image plate used to visualize the radioactive signal in the gel has a detection limit of lower than 0.01 ng (Weiss *et al.*, 2009) whereas detection of a single protein in Liquid Chromatography-Mass Spectrometry (LC-MS) normally would require around nanogram levels of sample (Dr. Benjamin Thomas, personal communication). The sensitivity gap between these two techniques leads to the concern that the protein labelled by ^{32}P may not always be found in the subsequent MS analysis, since ^{32}P has a high emission energy of 1.7 MeV. This prompts the necessity of enriching the NAADP binding protein(s) from the crude sample to increase the chance of detection in MS analysis, especially given the fact that the LC-MS used for the analysis in this study only allowed 2 µg protein to be analyzed per run. Previously in 2012, Lin-Moshier sent the 22/23 kDa doublet for MS analysis and obtained a list of 22 candidates, which is listed in Table 5.5.

Table. 5.5. Protein candidates from the 22/23kDa doublet identified by MS.

(Adapted from Lin-Moshier, 2012)

#	Identified Proteins (22)	Acc. No.	MW
1	28 kDa heat- and acid-stable phosphoprotein	Q13442	21 kDa
2	60S ribosomal protein L10	P27635	25 kDa
3	60S ribosomal protein L13a	P40429	24 kDa
4	60S ribosomal protein L15	P61313	24 kDa
5	60S ribosomal protein L19	P84098	23 kDa
6	BAG family molecular chaperone regulator 2	O95816	24 kDa
7	COMM domain-containing protein 5	Q9GZQ3	25 kDa
8	Growth factor receptor-bound protein 2	P62993	25 kDa
9	GTP-binding nuclear protein Ran	P62826	24 kDa
10	Heat shock protein beta-1	P04792	23 kDa
11	Hypoxanthine-guanine phosphoribosyltransferase	P00492	25 kDa
12	Isoform 2 of Acyl-protein thioesterase 1	O75608	23 kDa
13	Isoform 2 of Protein-L-isoaspartate(D-aspartate) O-methyltransferase	P22061	25 kDa
14	Mps one binder kinase activator-like 1A	Q7L9L4	25 kDa
15	Neighbor of COX4	O43402	24 kDa
16	Peroxiredoxin-6	P30041	25 kDa
17	Prefoldin subunit 3	P61758	23 kDa
18	Proteasome subunit beta type-3	P49720	23 kDa
19	Ras-related protein Rab-11A	P62491	24 kDa
20	Ras-related protein Rab-14	P61106	24 kDa
21	Ras-related protein Rab-2A	P61019	24 kDa
22	Ras-related protein Rab-7a	P51149	23 kDa

One of the identified candidate from the list above, the Rab7a, was later shown to interact with the NAADP receptor TPC2 and plays a pivotal role in TPC2-dependent pigmentation defect as well as NAADP-induced calcium release (Lin-Moshier *et al.*, 2014). However, it has not been confirmed whether Rab7 binds NAADP. The demography of the candidates is very different between the list from Lin-Moshier and the one presented in this study. Apart from size variation, most of the candidates on our list were identified as enzymes and were quite well-characterized. This suggested that the enrichment by chromatography indeed aided the identification of NAADP binding protein(s) by MS. Moreover, the parallel MS analysis of enriched batches

helped to remove more than 30% of the random encounters, which made the docking simulation less arduous.

The recruitment of the ligand docking programs proved to be extremely useful in narrowing down the candidates even further. In drug discovery, docking simulation is a common high-throughput tool to screen for lead compounds of the receptor from the ligand library, in which the receptor is set as constant and the ligands are the variables. However, this is reversed in this study. The docking performed here used the ligand, NAADP, as the constant and docked with all the candidates, which were treated as the variables. Unlike conventional docking, which typically has one binding pocket set for all docking ligands, in this study each docking simulation had specific simulation domains setup for individual candidates. Although NAADP was used to dock all candidates, its conformation varied for each candidate as the programs treated marcobiomolecules as rigid objects and thus altered the ligand poses to achieve best ligand-receptor complex conformations. Therefore, the scores between candidates are technically not comparable since both NAADP and the candidates were treated as variables in this scenario. Nevertheless, the scores returned from the programs could still implicate the relative strength of binding between NAADP and candidates.

The initial consideration to have two docking programs working simultaneously was to reduce the bias that could be introduced by a single scoring function and search algorithm. This was proven necessary as the score distribution of the two programs used was quite different from each other. Since no benchmark of the affinity-score correspondence had been established in either program, the scores returned from

each program were compared within their dynamic range (i.e. all the tested candidates).

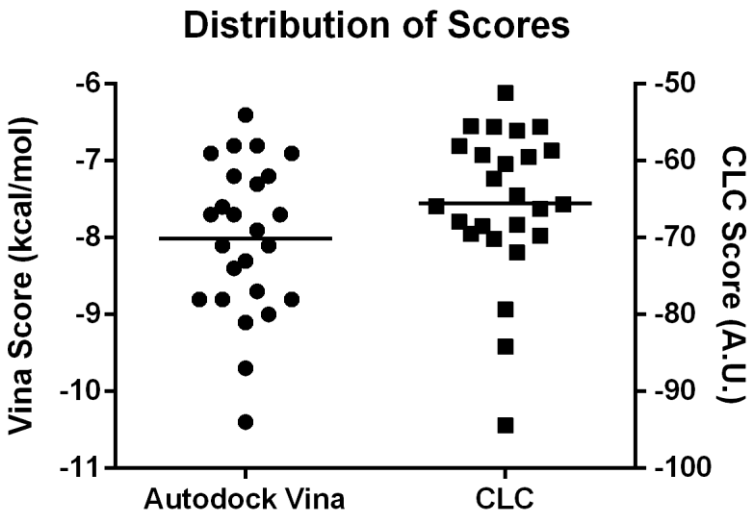

Figure 4.31. Distribution of docking scores of 25 candidates generated from AutoDock Vina and CLC Drug Discovery Workbench. The horizontal lines indicate the mean of each data set.

It is intriguing that although AutoDock Vina and CLC Drug Discovery Workbench use separate sets of scoring function and optimization algorithm, their docking results were highly similar in terms of ligand poses, yet the same pose would score differently in these two programs. As demonstrated in Figure 4.31, scores generated by AutoDock Vina were distributed in a more scattered pattern within the dynamic range whereas scores from CLC were clustered between -50 to -70 and the outliers were more distinctive than those in AutoDock Vina. Without the parallel comparison with the results from CLC, it would have been difficult to set the cut-off line for top hits by judging from the scores from AutoDock Vina alone. However, it was confirmed later that one out of three top hits predicted by CLC does not bind NAADP with high affinity. On the other hand, AutoDock Vina made accurate qualitative prediction on the strength of NAADP binding in two lowest scoring hits. The details will be discussed in

the following section. This again demonstrated the influence of scoring function and optimization algorithm on the score distribution and prediction accuracy.

In summary, the MS analysis provided a list with only 35 protein candidates thanks to the previous enrichment by chromatography and parallel batch strategy. Docking simulation of the 25 candidates with AutoDock Vina and CLC Drug Discovery Workbench further reduced the candidate number to only three, which was a decisive step forward to finally reveal the identity of NAADP binding protein. Due the unavailability of suitable protein crystal structures, 10 out of 35 candidates were not assessed by docking simulation. However, this does not rule out the possibility that those could be the long-sought NAADP binding proteins. Virtual screening should be carried out on those candidates once their crystallography structures are available to evaluate their candidacies.

4.4. Validation of NAADP binding protein candidates by label-free binding assays

4.4.1. Introduction

The original plan was to test the NAADP binding of the protein candidates experimentally using the radioligand binding assay. However, due to an unforeseen problem with our radiochemical suppliers, it was not possible to acquire ^{32}P with reasonable quality from any sources. As a result, the plan was compromised by replacing the radioligand binding assay with a non-radioactive ligand assay binding assay. The nature of the protein candidates, e.g. low molecular weight, anticipated high affinity binding, makes it difficult to employ Isothermal Titration Calorimetry (ITC) as the amount of protein required would be enormous (≈400 µg per assay). Therefore, we contacted our collaborators in the Chinese Academy of Sciences, Shanghai Branch to validate the candidates using label-free techniques: Bio-Layer Interferometry (BLI) and Micro-Scale Thermophoresis (MST).

4.4.2. Expression of protein candidates

Since the quality of protein is crucial for the success of the assays, it would be ideal to express the protein in Shanghai to ensure that the proteins are in the best condition suitable for the subsequent evaluation. The protein candidate sequences were sent to and expressed by Dr. Bin Meng at ShanghaiTech University. The protein candidates were expressed in E.Coli. with a 10x Histidine tag and a TEV cleavage site (ENLYFQS) in between the tag and protein sequence to allow cleavage of the histidine tag. The expressed protein was purified by sequential chromatography in FPLC. The *E. Coli* were lysed and his-tagged proteins were captured by immobilized metal affinity chromatography (IMAC). The captured proteins were eluted with imidazole gradient and then treated with TEV to cleave off the histidine tag. The TEV treated proteins were once again processed by IMC, but only proteins in the flow through were collected. Finally, the proteins were purified by ion-exchange chromatography and size-exclusion chromatography. Five recombinant proteins were purified through this process: apo-hCBR1, holo-hCBR1, apo-hCYB5R3, holo-hCYB5R3 and hTPMT. The SDS-PAGE profile of the purified protein candidates is shown in Figure 4.32. Additional chromatograms and SDS-PAGE profiles can be found in the Appendix.

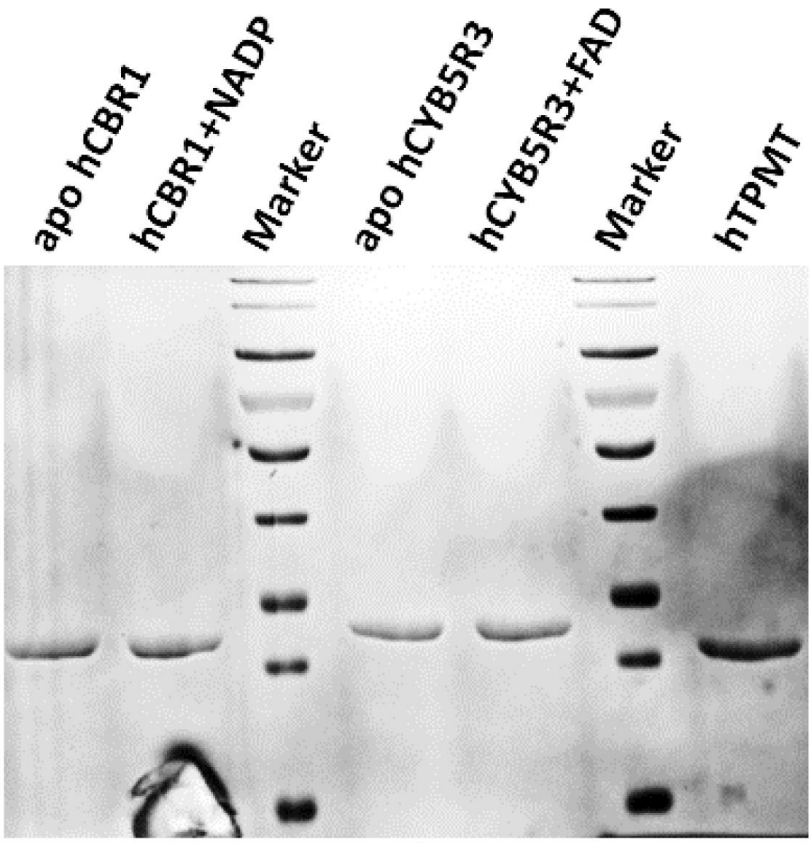

Figure 4.32. SDS-PAGE profile of FPLC purified recombinant binding protein candidates.

4.4.3. Validation of NAADP binding protein candidates by Bio-Layer Interferometry (BLI)

To validate the docking simulation results, the recombinant proteins were tested by bio-layer interferometry for their NAADP affinity. BLI is a label-free technique that measures the interaction of biomolecules via optical interference. Compared to Surface Plasmon Resonance (SPR), which is a similar technique, BLI is more solvent tolerant, faster and much cheaper to operate while able to produce data with almost equivalent quality.

According to the [^{32}P]-NAADP binding assay, the IC_{50} of NAADP in the enriched fraction is about 11.1 nM. However, photoaffinity labelling of [^{32}P]-5-azido-NAADP was not completely displaced in the presence of 4 µM NAADP. During preliminary scouting, a single-point measurement was taken using an NAADP concentration at 1.2 µM. For all five recombinant proteins, a modest response was observed with well resolved association and dissociation kinetics. A higher concentration of 120 µM NAADP was further tested in apo-hCBR1, holo-hCBR1 and hTPMT, which increased the response by roughly two-fold for all three proteins (Figure 4.33-4.37).

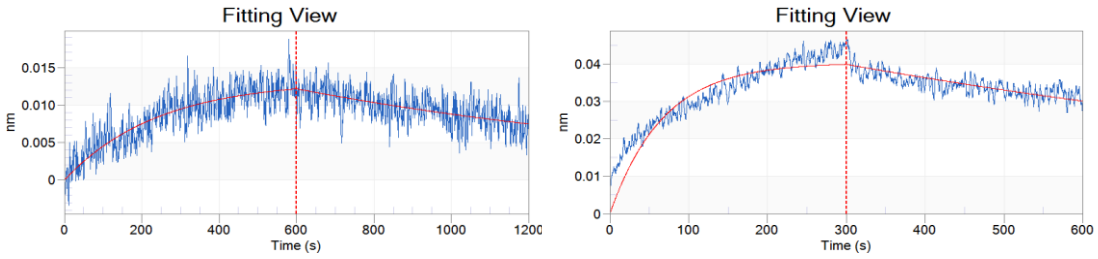

Figure 4.33. Binding kinetics of NAADP in apo-hCBR1. The left and right diagram shows binding kinetics of NAADP at 1.2 and 120 µM, respectively. K_d was calculated from rate constants K_{on} and K_{off} determined in the BLI experiment. At 1.2 and 120 µM NAADP concentration, the K_ds were calculated as 288 nM and 8.1 µM, respectively.

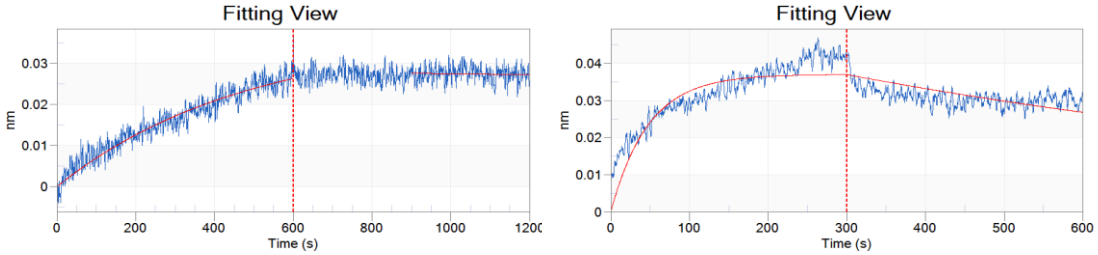

Figure 4.34. Binding kinetics of NAADP in holo-hCBR1. The left and right diagram shows binding kinetics of NAADP at 1.2 and 120 µM, respectively. K_d was calculated from rate constants K_{on} and K_{off} determined in the BLI experiment. At 1.2 and 120 µM NAADP concentration, the K_ds were calculated as 21.8 nM and 6.5 µM, respectively.

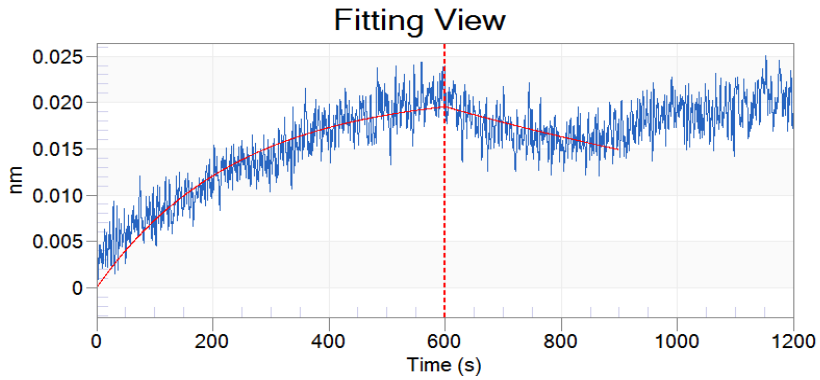

Figure 4.35. Binding kinetics of NAADP in apo-hCYB5R3. The left and right diagram shows binding kinetics of NAADP at 1.2 µM. K_d was calculated from rate constants K_{on} and K_{off} determined in the BLI experiment. The K_d was calculated as 330 nM.

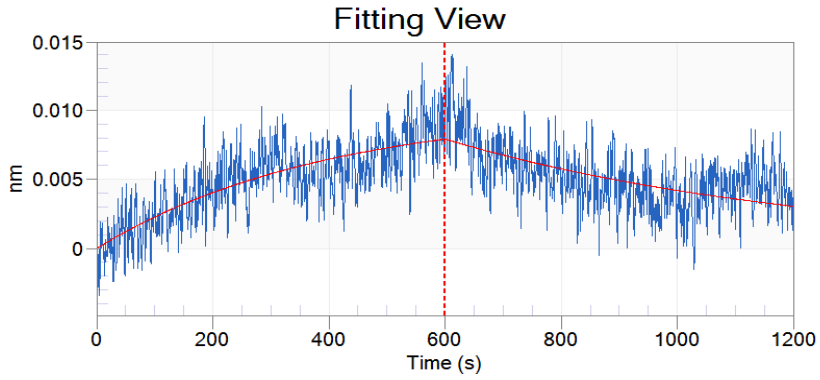

Figure 4.36. Binding kinetics of NAADP in holo-hCYB5R3. The left and right diagram shows binding kinetics of NAADP at 1.2 µM. K_d was calculated from rate constants K_{on} and K_{off} determined in the BLI experiment. The K_d was calculated as 2.0 µM.

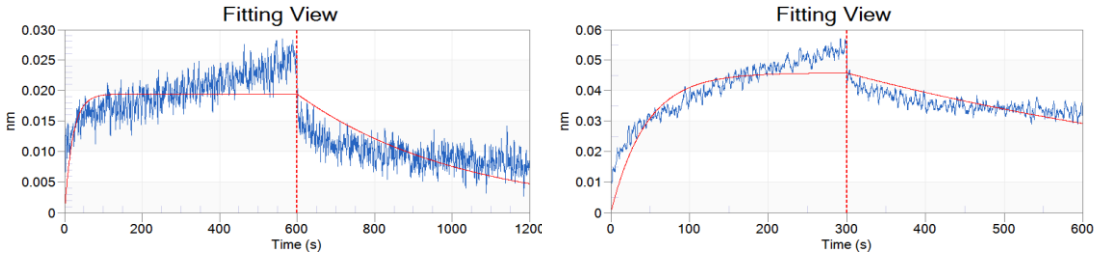

Figure 4.37. Binding kinetics of NAADP in hTPMT. The left and right diagram shows binding kinetics of NAADP at 1.2 and 120 µM, respectively. K_d was calculated from rate constants K_{on} and K_{off} determined in the BLI experiment. At 1.2 and 120 µM NAADP concentration, the K_ds were calculated as 63.7 nM and 8.5 µM, respectively.

Although the signal to noise ratio was improved, the calculated K_d was also higher when a higher NAADP concentration was used. To determine the suitable NAADP concentration gradient for BLI experiments, a serial of NAADP dilutions (480, 240, 120, 60, 30 µM) was tested on hTPMT. The maximal hTPMT response was achieved at 120 µM and hence this was used as the highest NAADP concentration for all subsequent BLI experiments (Figure 4.38). hTPMT was tested on an optimized NAADP concentration gradient (120, 60, 30, 15, 7.5 µM) and the K_d was calculated as 7.2 ± 2.9 µM (n=3) (Figure 4.38).

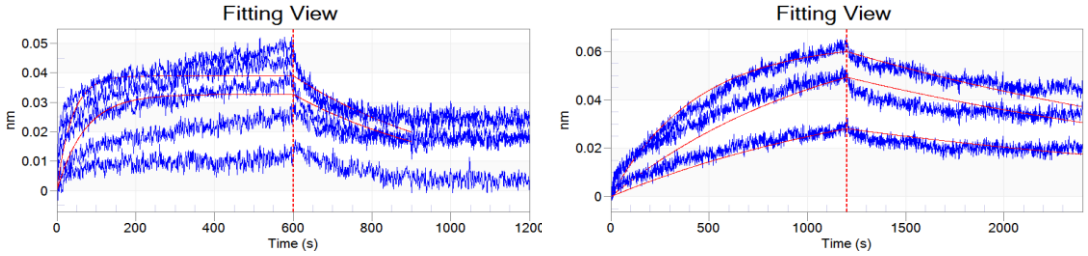

Figure 4.38. Optimization of NAADP concentration gradient in hTPMT. Left: BLI experiment using scouting NAADP gradient (480, 240, 120, 60, 30 µM). K_d=11.3 µM. Right: Representative BLI traces of optimized NAADP gradient (120, 60, 30, 15, 7.5 µM). K_d= 7.2 ± 2.9 µM (n=3)

Upon investigation of the data it became obvious that the signal was quite weak even with a refined ligand gradient. Although the signal from protein-small molecule interaction is in general weaker than protein-protein or protein-antibody interactions in BLI, the signal observed in this study was much lower than in the existing literature for similar scenarios (Zuo *et al.*, 2012; Xiao *et al.*, 2013). Since double referencing had already been used during the experiment to eliminate the signal from baseline drifting and non-specific binding of ligand to biosensor, another control experiment using heat-inactivated hTPMT was performed to determine the specificity of the signal.

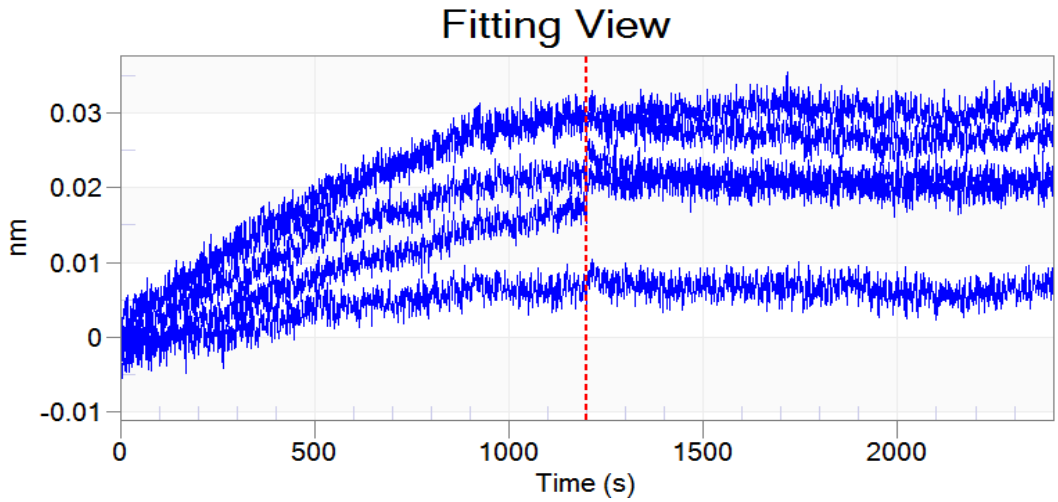

Figure 4.39. Binding kinetics of NAADP in heat-inactivated hTPMT using optimized NAADP gradient (120, 60, 30, 15, 7.5 µM).

As shown in Figure 4.39, in heat-inactivated hTPMT, the association of NAADP was almost comparable to that of the native protein whereas the dissociation was not detected. This combination of association and dissociation patterns is commonly interpreted as 'no-binding' in BLI as suggested by our collaborator. However, as K_d is equal to K_{off}/K_{on}, one could acquire very low K_d since the K_{off} would be extremely low in this 'no-binding' scenario, which in turn could be mistakenly interpreted as tight-binding between ligand and protein. In summary, the BLI experiment provided some useful insights into the NAADP affinity of the selected candidates and their respective binding kinetics. However, it was not possible to get a satisfactory competitive binding curve due to the sensitivity limitation of the technique. Also, since K_ds were calculated based on measured K_{on} and K_{off}, misinterpretation could occur in the case of no-binding. To overcome the limitation of BLI, a new technology was sought to confirm the BLI results.

4.4.4. Validation of NAADP binding protein candidates by Micro-Scale Thermophoresis (MST)

Micro-Scale Thermophoresis is a technique adapted from thermophoresis for the characterization of biomolecule interaction. It uses an infrared laser to heat up the sample, creating a temperature gradient and causing the fluorescent-coupled protein to migrate, which results in a change of local fluorescent intensity (Wienken *et al.*, 2010). The interaction between ligand and protein is measured using a ligand concentration gradient and the changes in fluorescent intensity would be recorded under infrared laser heating, which is similar to a conventional competitive binding assay but uses a different principle.

The aim of the first set of MST experiments was to measure the interaction between NAADP and protein candidates. A summary of the results is shown in Table 5.6. Of all the candidates tested, apo-hCBR1, holo-hCBR1 and hTPMT showed an affinity for NAADP.

Table 5.6. Summary of MST results

	Apo-hCBR1	Holo-hCBR1	Apo-hCYB5R3	Holo-hCYB5R3	hTPMT
NAADP affinity (µM)	80-190	≥ 4600	No binding	No binding	18
NADP affinity (µM)	560	N.T.*	N.T.*	N.T.*	No binding

*N.T.: Not tested

CBR1 is known to bind cofactor NADP. It is anticipated that CBR1 might bind NAADP as well since the structural variation is only limited to one functional group. MST revealed that both apo- and holo-hCBR1 (purified with or with or NADP) binds NAADP with different affinities. Apo-hCBR1 has a relatively lower K_d of 80-190 µM as determined by MST whereas the K_d of holo-hCBR1 is about 4.6 mM (Figure 4.40, Figure 4.41). During the experiment, it was observed that both protein did not reach 100%

occupancy even at millimolar NAADP concentration. This might affect the accuracy of K_d estimation by non-linear regression.

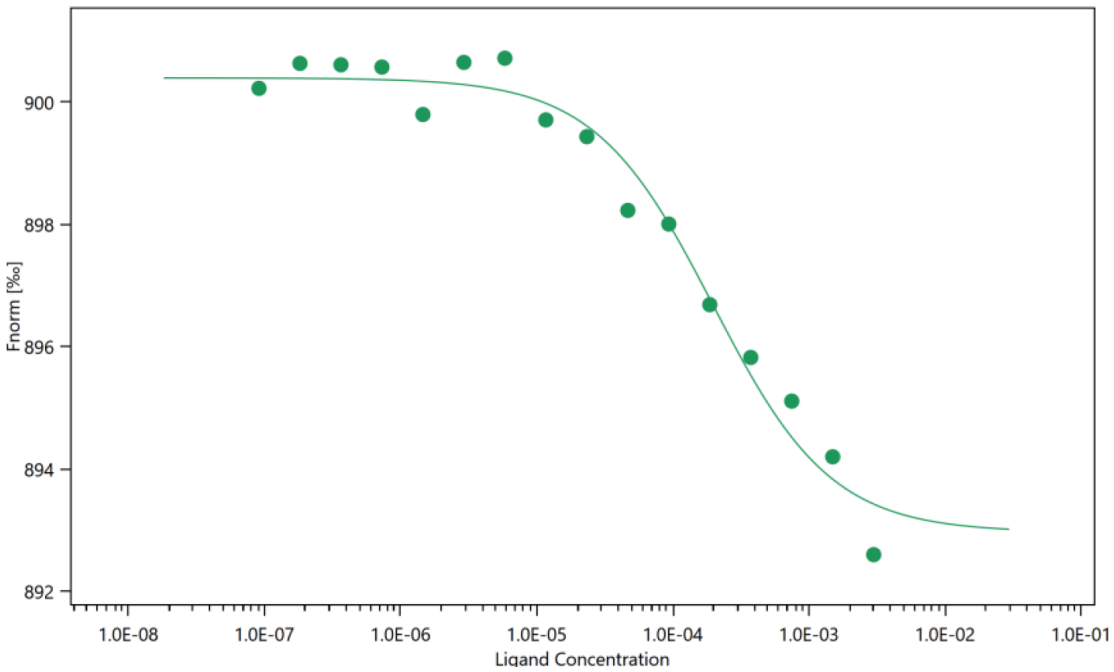

Figure 4.40. MST result of NAADP binding in apo-hCBR1. 200 nM fluorescent labelled protein was used for each point of the NAADP gradient from 91.6 nM to 3 mM. K_d≈ 80-190 µM.

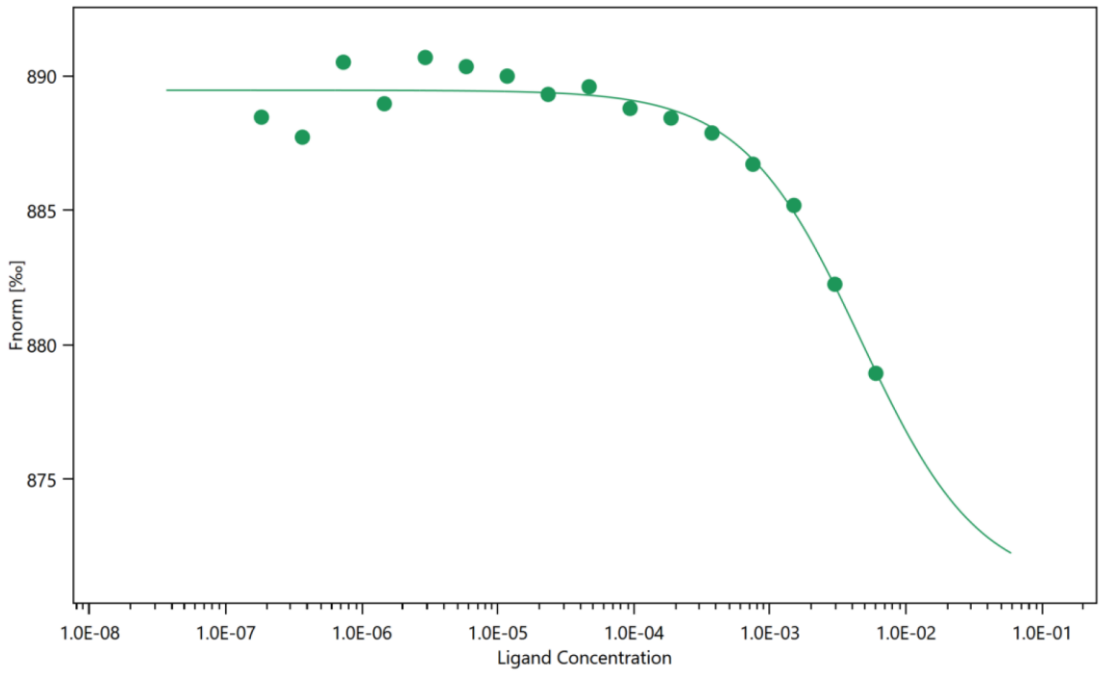

Figure 4.41. MST result of NAADP binding in holo-hCBR1. 100 nM fluorescent labelled protein was used for each point of the NAADP gradient from 183 nM to 6 mM. K_d≈ 4.6 mM.

The MST results of apo- and holo-hCYB5R3 are shown in Figure 4.42 and Figure 4.43. Although non-linear regression of both proteins could not be performed by the

analysis software as it did not recognize any distinctive binding patterns, the trend of fluorescent shift suggests that their NAADP affinities could be at millimolar range.

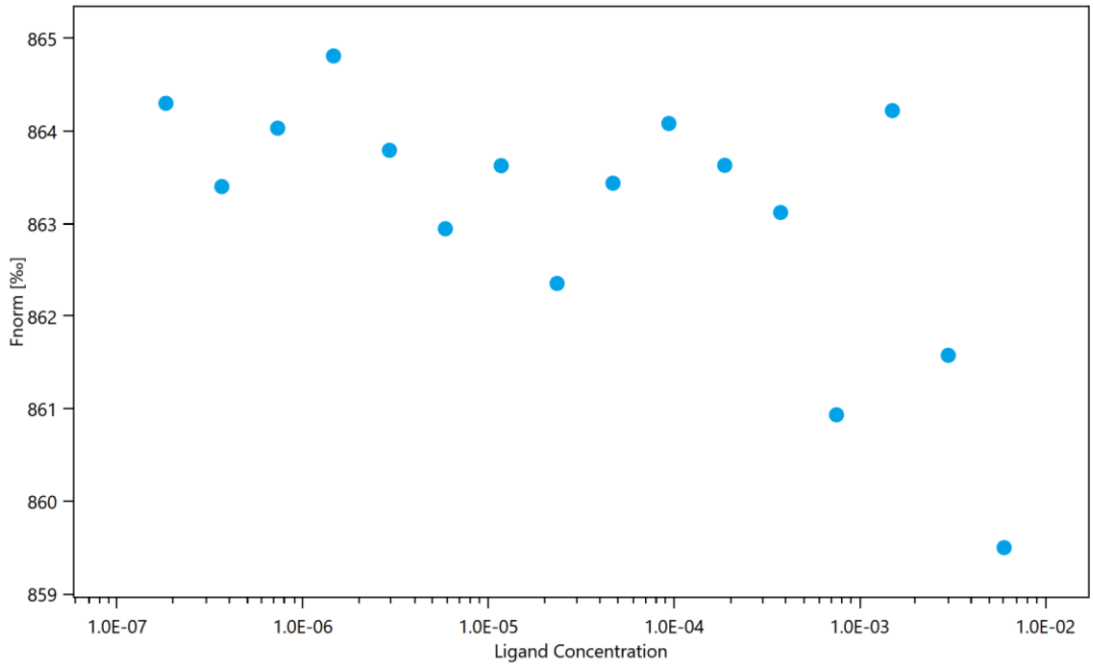

Figure 4.42. MST result of NAADP binding in apo-hCYB5R3. 100 nM fluorescent labelled protein was used for each point of the NAADP gradient from 183 nM to 6 mM. No binding observed.

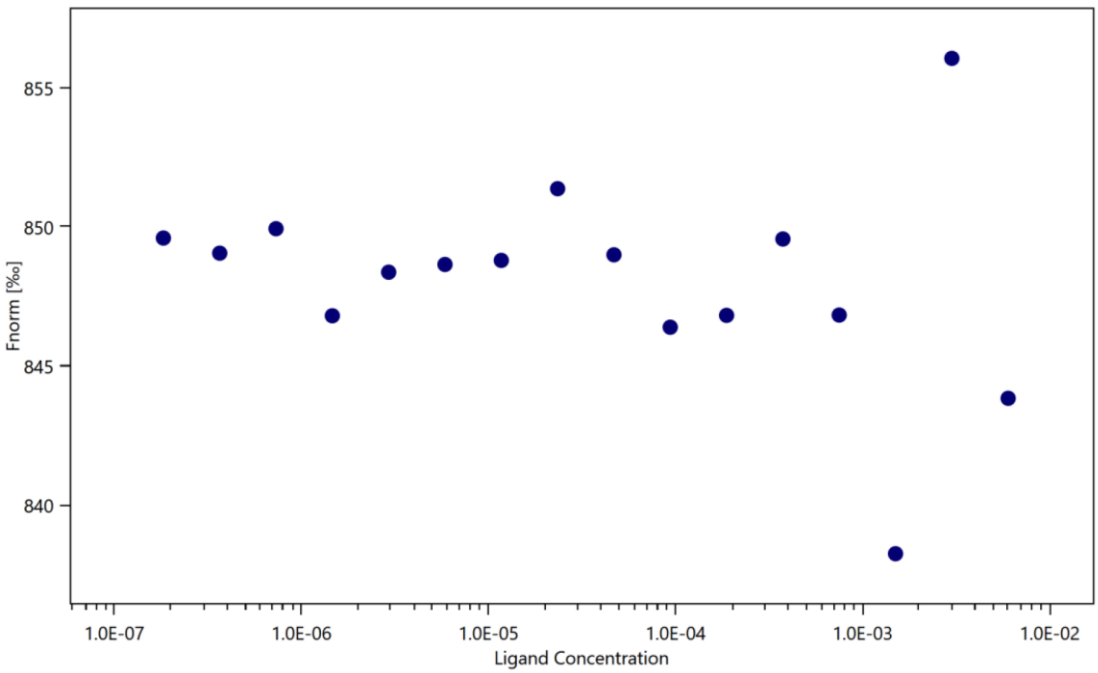

Figure 4.43. MST result of NAADP binding in holo-hCYB5R3. 100 nM fluorescent labelled protein was used for each point of the NAADP gradient from 183 nM to 6 mM. No binding observed.

TPMT catalyzes various reaction using SAM as methyl donor. The preceding docking simulation predicted TPMT has relatively high affinity to NAADP, which is in a

completely different class of its reported substrates. Nevertheless, hTPMT showed the highest affinity to NAADP among all the candidates tested, with a K_d of 18 µM.

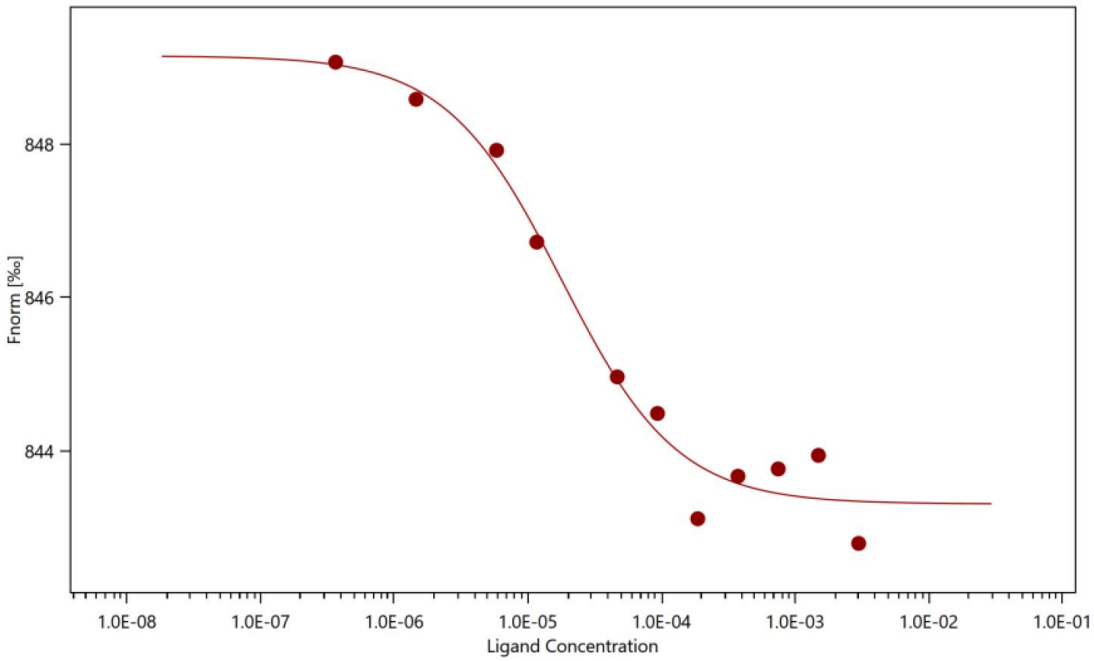

Figure 4.44. MST result of NAADP binding in hTPMT. 150 nM fluorescent labelled protein was used for each point of the NAADP gradient from 91.6 nM to 3000 µM. K_d= 18 µM.

In the second set of experiments, the affinity of apo-hCBR1 and hTPMT towards NADP was determined to evaluate if the candidate shows selectivity to NAADP. In apo-hCBR1, the affinity to NADP is similar to that of NAADP, suggesting that the interaction with NAADP could be rather promiscuous (Figure 4.45). On the hand, hTPMT demonstrated remarkable selectivity of NAADP over NADP, as no sign of specific binding was observed during the MST experiment (Figure 4.46).

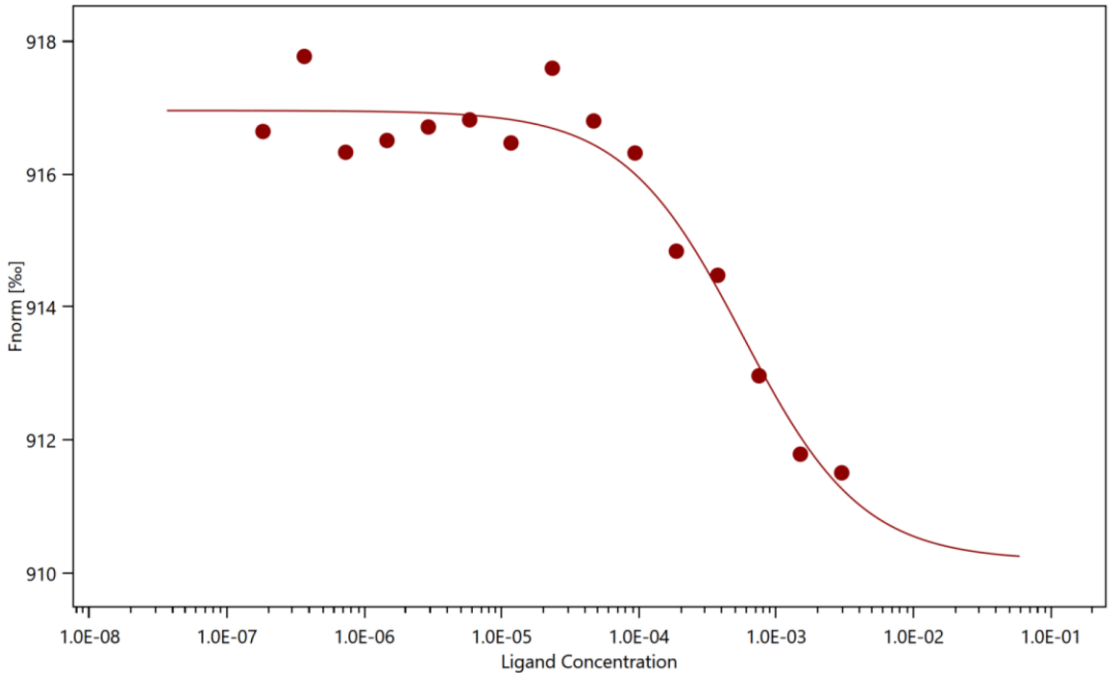

Figure 4.45. MST result of NADP binding in apo-hCBR1. 100 nM fluorescent labelled protein was used for each point of the NAADP gradient from 183 nM to 6 mM. $K_d \approx$ 0.56 mM.

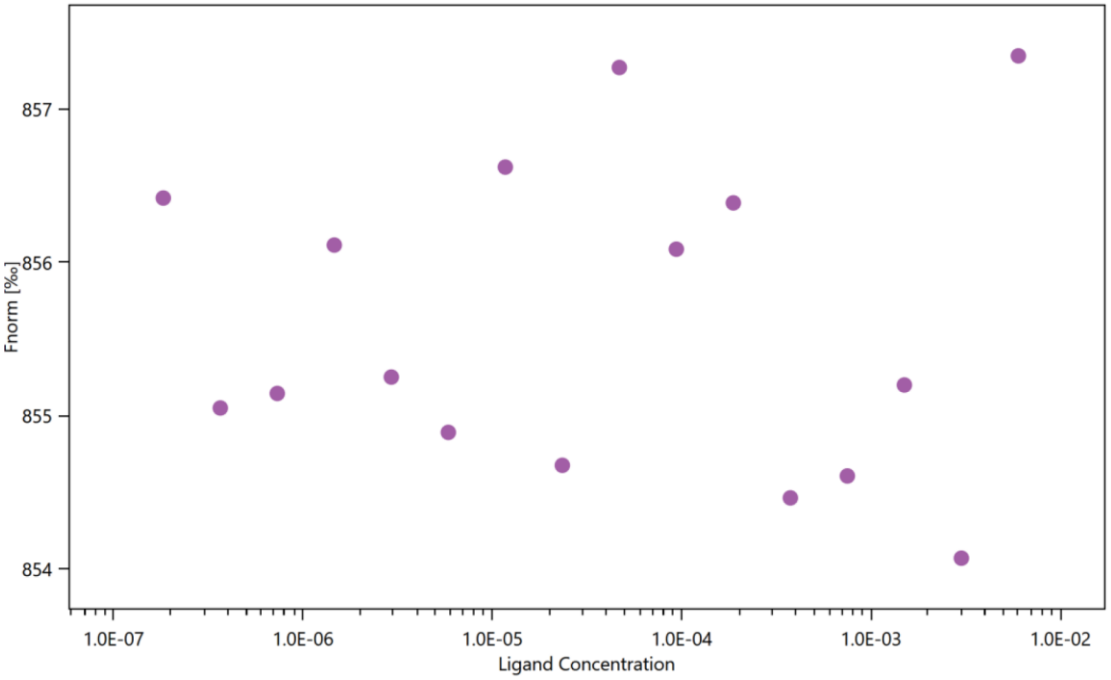

Figure 4.46. MST result of NADP binding in hTPMT. 100 nM fluorescent labelled protein was used for each point of the NAADP gradient from 183 nM to 6 mM. No binding observed.

In conclusion, two NAADP binding proteins, CBR1 and TPMT, were identified in this study, and TPMT showed outstanding selectivity to NAADP.

4.4.5. Discussion

This final section described the experimental validation of docking results and the identification of the NAADP binding proteins.

The initial attempt to validate docking results in BLI did not yield conclusive result due to the low signal to noise ratio despite the implementation of double referencing. In BLI, the optical interference induced by protein-small molecule interaction is very limited when compared with protein-protein or antibody-protein interaction, unless the ligand can elicit allosteric effect upon binding. For instance, the maximum optical interference observed in this study was around 0.055 nm in hTPMT with 120 µM NAADP, whereas binding of AMP kinase (AMPK) activator 991 to AMPK caused double the amount of wavelength shift at ligand concentration of 1.5 µM due to its allosteric effect (Xiao *et al.*, 2013). BLI measures both wavelength shift and kinetics of the shift, which provides information of the rate of association and dissociation. Low signal/noise ratio also hindered the accuracy of K_d prediction as BLI calculates the K_d from observed K_{on} and K_{off}, and would create pitfalls where a 'no-binding' scenario could be misinterpreted as high-affinity binding with low dissociation rate. Although BLI did not produce convincing results about the NAADP affinity of the candidates, it provided useful insight in the kinetics of NAADP binding. For example, the NAADP association in hTPMT was clearly faster than hCBR1, particularly at lower NAADP concentrations (Figure 4.33, Figure 4.37). This was also reflected in the later MST experiment in which hCBR1 struggled to reach 100% ligand occupancy (Figure 4.40). Normally, the increase in ligand concentration would drive the equilibrium towards

forming the ligand-protein complex. Failure to reach total occupancy at high NAADP concentration suggests that the NAADP affinity of hCBR1 could be relatively low.

In this study, three candidates showed unique binding profiles in MST: hCBR1 binds both NAADP and NADP whereas hCYB5R3 binds neither, and hTPMT binds NAADP only. In apo-hCBR1, NAADP and NADP binds with similar affinity, with K_d of 80-190 µM and 560 µM, respectively. On the other hand, in holo-hCBR1 where NADP was already embedded in the binding pocket, the K_d of NAADP increased substantially to 4.6 mM, suggesting that NAADP-hCBR1 complex was not favorable in comparison to NADP-hCBR1. This also indicates that hCBR1 does not discriminate NADP or NAADP since no selectivity for NAADP was observed.

In hCYB5R3, the K_d of NAADP is probably beyond millimolar scale as shown in MST results. This is in sharp contrast to the docking prediction, in which CYB5R3 scored the lowest among 25 candidates in CLC, suggesting a strong interaction with NAADP. The holo-hCYB5R3 used in this study contained tightly-bound FAD, a cofactor commonly seen in flavoproteins. NAADP shares some structural similarity to FAD, which explains the prediction of a strong interaction in docking. Some may argue that failure to reproduce the result experimentally could be owing to FAD being tightly bound to hCYB5R3 as a prosthetic group, yet crystallography evidence showed that FAD does not covalently bind to hCYB5R3 (Bando *et al.*, 2004). The case of hCYB5R3 reiterated the limitation of the docking prediction accuracy and the necessity of experimental validation.

hTPMT turned out to be the most promising NAADP binding protein candidate of all three, demonstrating its remarkable selectivity for NAADP and it had a lower K_d than the other NAADP binding protein candidate, hCBR1 (Figure 4.47).

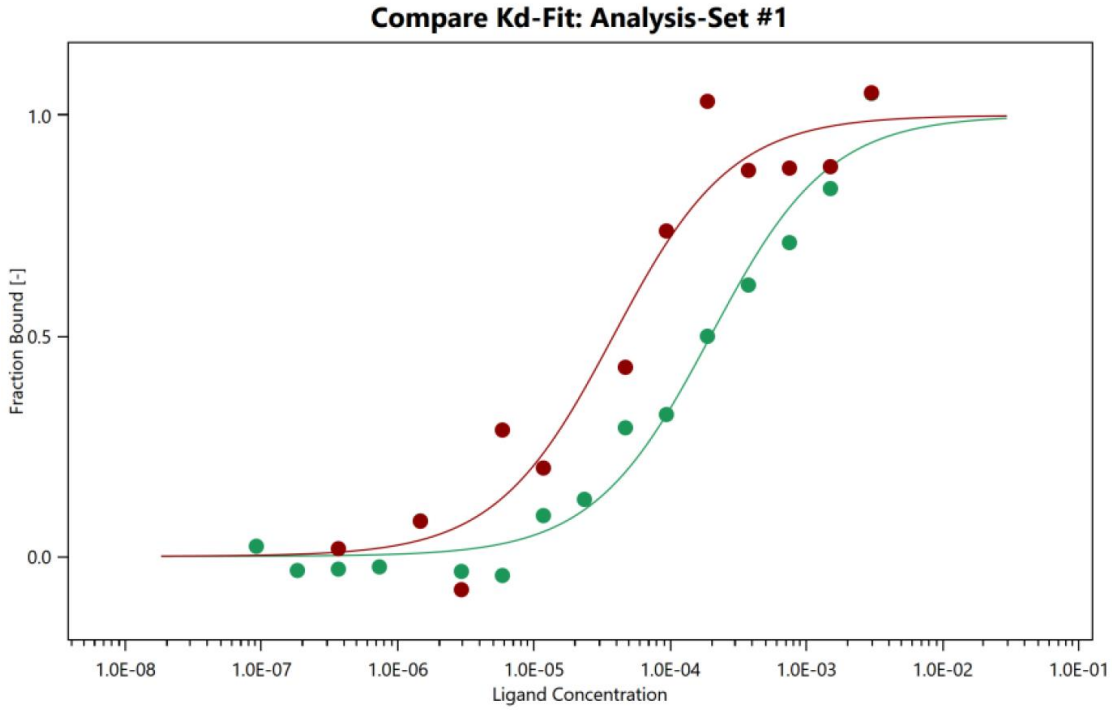

Figure 4.47. Overlay of MST results of NAADP binding in hTPMT (red) and hCBR1 (green).

The MST result showed that hTPMT had a K_d of 18 µM, which was similar to the K_d obtained from BLI (7.2 ± 2.9 µM). However, the K_ds measured by both MST and BLI were about 1000-fold higher than that in the ^{32}P radioligand binding assay (11.1 nM). Such discrepancy was also observed in the case of another second messenger cADPR: Glyceraldehyde 3-phosphate dehydrogenase was identified as a cADPR binding protein through photoaffinity labelling and SPR assay (Zhang *et al.*, 2017), yet its K_d (8.59 µM) was considerable higher than the affinity of cADPR binding site determined by [^{3}H]-cADPR binding assay (K_d=17 nM. Lee, 1991). One possible explanation for this is that other proteins might also be involved in the interaction between candidate proteins and NAADP, which means that the candidates could be functioning within a

larger protein complex rather than alone. Being devoid of their chaperones could hamper their ability to bind NAADP and result in a reduction of their NAADP affinity, though this is hypothetical and requires further investigation. Another likely cause for the affinity discrepancy could be the experimental method itself. Both BLI and MST requires pre-treatment of the sample, such as immobilization to biosensor or labelling with fluorescent indicators, often through non-specific methods. It could be anticipated that such treatments might exert unfavorable effect on the protein and cause a decrease of ligand affinity. As for TPMT, one possibility could be, as noted by our collaborator, that the recombinant hTPMT was probably purified with SAM or SAH judging from its high A254:A280 ratio (> 0.5, see Appendix Figure S11). Thus in both assays, the NAADP could be involved in the binding competition with SAM or SAH and the apparent K_d might increase as a result.

The structural variation between NADP and NAADP is only limited to the pyridinium moiety, thus it would be reasonable to presume that this single functional group difference would confer on NAADP its extraordinary potency and binding affinity. Here the significance of the functional group in NAADP with regard to binding will be discussed using the docking results from the simulation. The docking simulation, in addition to generating speculative ligand poses and predicting binding strength, also provides insight into the ligand-receptor interaction at the binding site. A previous investigation of TPMT crystal structure revealed that the TPMT inhibitor, SAH, binds to hTPMT via hydrogen bonds at Ile91, Ser134 and Ile135. Interestingly, our simulation showed that the pyridinium ring of NAADP is in the same binding cleft as the adenine ring of SAH (Figure 4.30), and analysis indicated that it also forms hydrogen bonds with Ile91, Cys133 and Ile 135, two of which are identical (Figure 4.48, Figure 4.49).

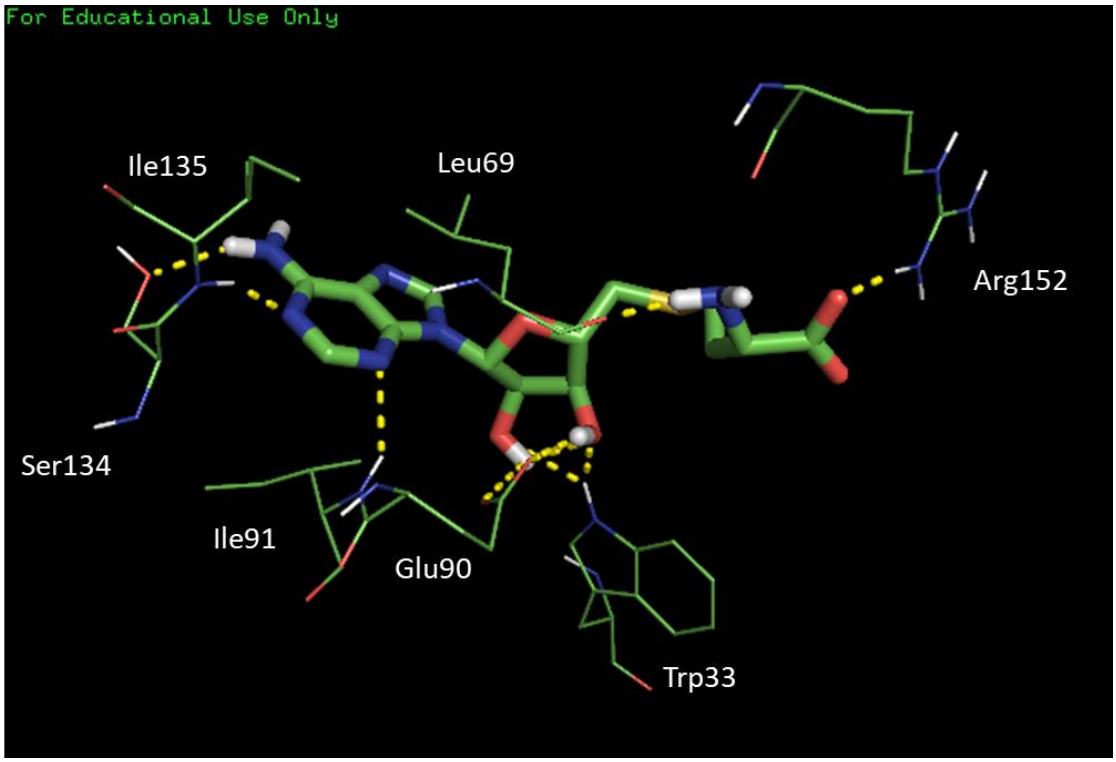

Figure 4.48. Direct polar interactions of SAH with TPMT. The adenine ring of SAH forms hydrogen bonds with Ile91, Ser134 and Ile135. The ribose ring forms polar contacts with Trp33 and Glu90. The homocysteine interacts with Leu69 and Arg152.

In addition, the ribose rings of SAH and NAADP interact with the same amino acids, Trp33 and Glu90. This could be the possible explanation for loss of binding affinity when the ribose ring was cleaved by periodate oxidation in the NAADP affinity column experiment mentioned previously (Figure 4.48, Figure 4.49).

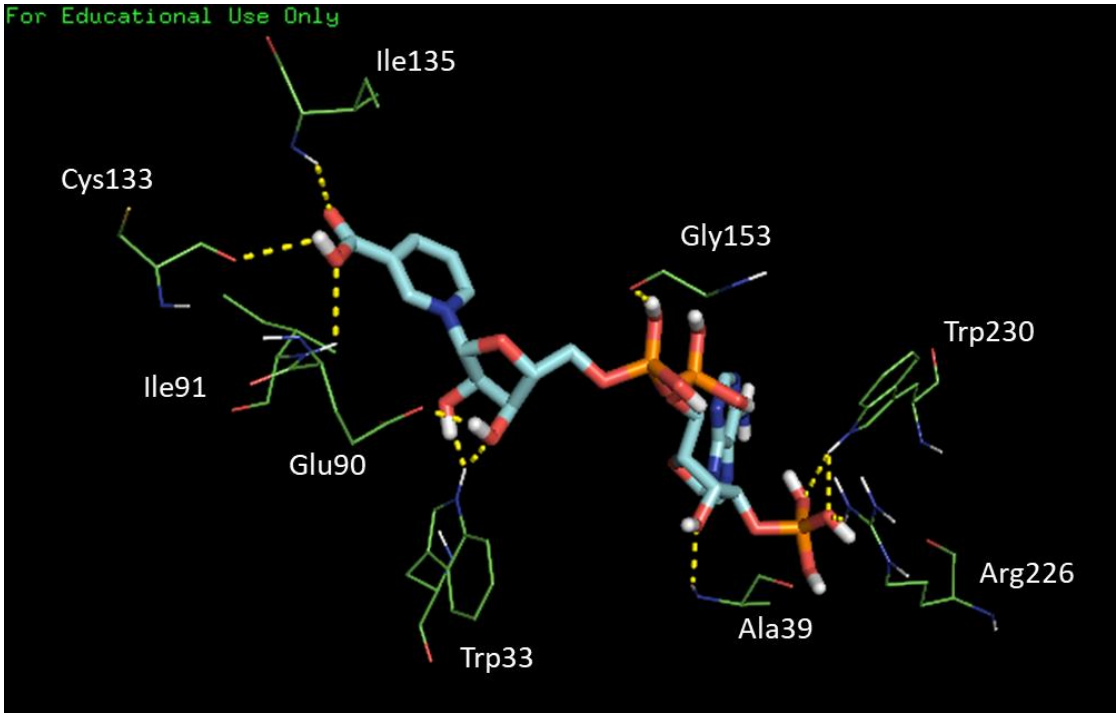

Figure 4.49. Speculative polar interactions of NAADP with TPMT. The carboxylic acid group of the nicotinic acid moiety forms hydrogen bonds with Ile91, Cys133 and Ile135. The pyridinium-ribose forms polar contacts with Trp33 and Glu90. The diphosphate bridge interacts with Gly153. The adenylyl ribose forms polar contact with Ala39 and the adenosyl 2'-phosphate contacts with Arg226 and Trp230.

The homocysteine moiety in SAH forms hydrogen bonds with Leu69, backbone and Arg152. While there is nothing equivalent to homocysteine in NAADP, the diphosphate bridge of NAADP has been demonstrated in the simulation to interact with Gly153, which is only one amino acid away from Arg152. Since SAM, the precursor of SAH, binds to TPMT at the same site, it would be sensible to speculate that the highly similar sets of amino acids residues that interact with SAM and NAADP could potentially be the reason for their comparable binding affinities in TPMT, whose K_d is about 2.2 ± 0.7 (Wennerstrand *et al.*, 2017) and 18 µM, respectively (Figure 4.48, Figure 4.49).

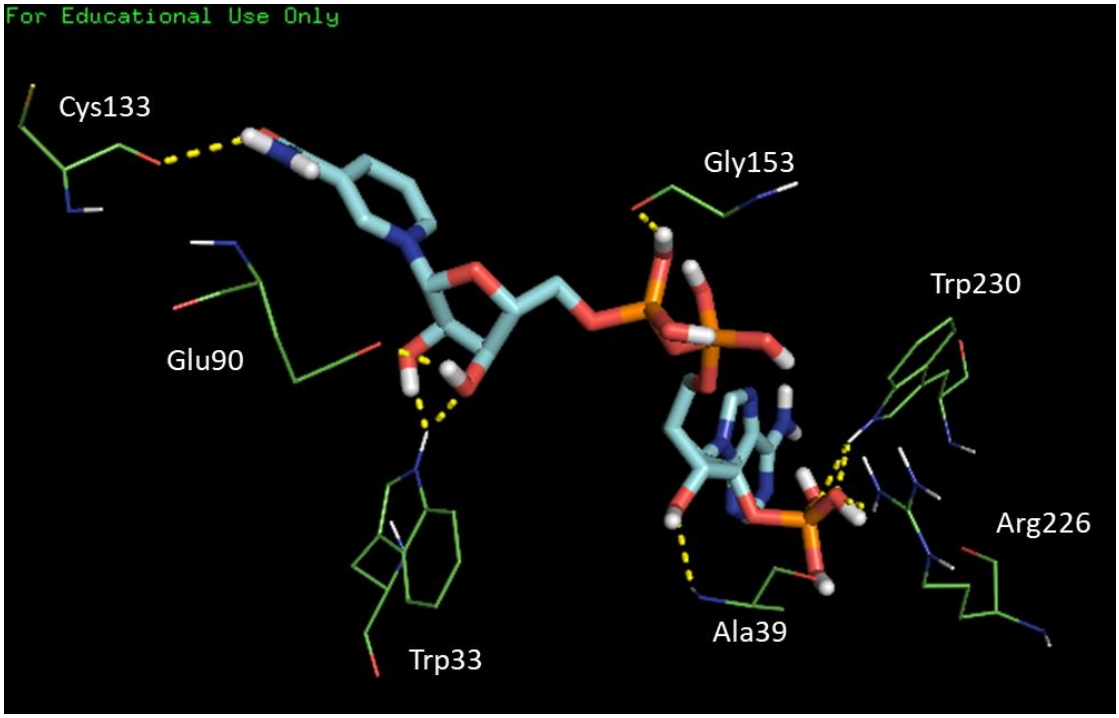

Figure 4.50. Speculative polar interactions of NADP with TPMT. The amide group of the nicotinamide moiety form a hydrogen bond with Cys133. The pyridinium-ribose forms polar contacts with Trp33 and Glu90. The diphosphate bridge interacts with Gly153. The adenylyl ribose forms polar contact with Ala39 and the adenosyl 2'-phosphate contacts with Arg226 and Trp230.

On the other hand, our docking simulation also revealed that NADP binds to hTPMT via a similar set of amino acid residues as NAADP. Their pyridinium-ribose both form polar contacts at Trp33 and Glu90. Also, both diphosphate bridges interact with hTPMT via Gly153. In addition, the adenosine 2'-phosphate in both NAADP and NADP forms hydrogen bonds at Arg226 and Trp230. Moreover, the adenylyl ribose ring of NAADP forms hydrogen bond with Ala39, which is the same for NADP as well. Although NAADP and NADP interacts with many residues that they both share, it is the difference at the pyridinium moiety that distinguishes the binding affinities of NAADP and NADP. As mentioned early, the nicotinic acid moiety of NAADP forms hydrogen bonds with hTPMT via Ile91, Cys133 and Ile 135. Although there is only one functional group difference, the nicotinamide moiety of NADP only forms contact with Cys133 and does not share any amino acid residues that interacts with SAH. Thus the

difference of hydrogen bonding might contribute to the distinct binding affinities of NAADP and NADP in hTPMT.

The number of hydrogen bonds could account for the binding affinity of NAADP. Additionally, the strength of the hydrogen bond is also another crucial determinant, which is dependent on the hydrogen bond forming capability of donor and acceptor. In a biological context, the interpretation of hydrogen bond regulation on ligand-receptor interaction is complicated by the fact that the hydrogen bonding process between ligand and receptor is constantly competed by the bulk of water molecules. It has been recently discovered that ligand-receptor interaction is only enhanced by hydrogen bonds when the hydrogen bonding capabilities of both donor and acceptor are significantly stronger or weaker than that of water, whereas strong-weak pairing would be interfered with water and result in the decrease of ligand binding affinity (Chen *et al.*, 2016). The substitution of amide to carboxyl group would result in a significant change in the hydrogen bond forming capability and therefore impact on the binding affinity of NAADP and NADP. Chen *et al.* used the computational chemistry approach to calculate the hydrogen bonding capability of different atoms from the free energy required to transfer atoms from water to hexadecane. According to their results, the hydrogen in the carboxylic acid group is a much stronger donor than the hydrogen in the amide group, whose hydrogen bonding capability are determined as 11.2 and 7.6, respectively. The acceptor capability of oxygen and donor capability of hydrogen in water are both determined as 7.02. Hence, the hydrogen in the carboxylic group of NAADP would form a strong hydrogen bond with the oxygen on the backbone of Cys133, which is a strong acceptor with an acceptor capability of 14.9 (Figure 4.51). On the other hand, the donor capability of hydrogen in the amide group of NADP (7.6)

is similar to the donor capability of hydrogen in water (7.02), thus the tendency to form a strong hydrogen bond with Cys133 would be ambiguous since the bonding would be largely affected by the competition of water.

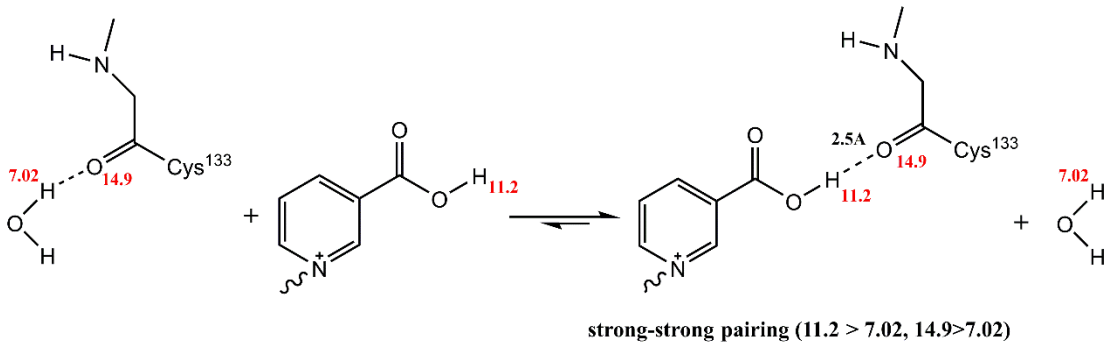

Figure 4.51. Hydrogen bond pairing between NAADP and Cys133 of hTPMT. The hydrogen bonding between NAADP and TPMT is expected to be competed with bulk water. The oxygen on Cys133 is a strong hydrogen acceptor (14.9), and is more likely to form hydrogen bond with the hydrogen on the carboxylic acid group of NAADP, which is a much stronger hydrogen donor (11.2) than the hydrogen in water (7.02).

Our docking simulation showed that the phosphate on the adenylyl ribose ring could be crucial for its recognition to the binding protein as the adenosyl phosphate of NAADP was shown to form polar contacts with multiple residues on hTPMT. This is consistent with the proposal from the existing literature that the 2'-phosphate on adenosine is an important determinant of binding affinity. It has been suggested that swapping the position of 2'-phosphate with an adjacent 3'-hydroxyl group, or forming 2,3-cyclic phosphate would cause a decrease in binding affinity (Lee and Aarhus, 1997). Lin-Moshier *et al.* also demonstrated in their photoaffinity labelling experiment that 10 µM NAADP effectively displaced the labelling of the 22/23 kDa doublet (2012). Using the same concentration, NADP could still cause displacement of labelling but to a lesser extent. On the other hand, removal of the 2'-phosphate would result in loss of affinity as 10 µM NAAD or NAD failed to displace the ^{32}P labelling of the doublet. Therefore, our finding concurs with the literature that the 2'-phosphate is paramount to the affinity of NAADP to its binding proteins.

Reports have suggested that modifications of the adenine moiety of NAADP would cause significant reduction of its affinity. Conversion of NAADP to NAIDP by modifying the 6-amino group of the adenine resulted in a 1000-fold less potent product (Trabbic *et al.*, 2012). Fluorescent analogs of NAADP, etheno-NAADP and etheno-aza-NAADP, both have 100-fold higher EC_{50} than NAADP in the sea urchin egg homogenate calcium release assay (Lee and Aarhus, 1998) due to the modification at the adenine moiety. The above pieces of evidence indicated the importance of the adenine moiety in NAADP for target recognition. However, the ligand conformation of NAADP from docking simulation showed that the adenine moiety does not form polar contacts with any residues of hTPMT and is positioned outside the binding pocket, which suggests that it may not be involved in determination of NAADP binding affinity in hTPMT. Co-crystallization of NAADP and TPMT should be performed to understand the binding conformation of NAADP in TPMT, and how the adenine moiety contributes to its affinity.

The discovery of 22/23 kDa doublet was the first direct evidence of the existence of NAADP binding protein(s) in mammalian cells. However, it also suggested that there might be multiple NAADP binding proteins. Indeed, in this study two distinct classes of NAADP were revealed: CBR1 represents the promiscuous binding protein that does not distinguish NADP and NAADP while TPMT is a member of highly selective NAADP binding proteins. CBR1 belongs to the short chain dehydrogenase/reductase family and has catalytic activity over a wide spectrum of endogenous and xenobiotic substrates (Matsunaga *et al.*, 2006), such as prostaglandin, steroid (Wermuth, 1981) and quinones (Wermuth *et al.*, 1986) as well as anthracyclin chemotherapy agents like daunorubicin and doxorubicin (Olson *et al.*, 2006; Gonzalez-Covarrubias *et al.*, 2007).

It depends on NADPH for its reductase activity and its activity can be modified by binding of glutathione and inhibited by flavonoids (Carlquist *et al.*, 2008). CBR1 is widely expressed in human tissue with high levels in liver, stomach, intestine, kidney and the central nervous system, which is consistent with its role of detoxification of reactive carbonyl compounds (Wirth and Wermuth, 1992). Interestingly, Billington *et al.* demonstrated that glucose-6-phosphate dehydrogenase can convert NAADP to NAADPH and that was independent of endogenous NADP levels (2004). In addition, NAADPH is far less effective than NAADP in evoking calcium release in sea urchin egg homogenate (Billington *et al.*, 2004), indicating that NAADPH might exert its physiological effects elsewhere. Our simulation and experimental data confirmed that CBR1 binds NAADP, suggesting that NAADPH might bind to CBR1 as well and serve as a reducing agent, which could also be regarded as a putative NAADP-salvage pathway. On the other hand, TPMT is a cytosolic enzyme that uses SAM to catalyze the S-methylation of thiopurine drugs, such as 6-mercaptopurine, thioguanine, and azathioprine (Stanulla *et al.*, 2005). Those drugs are inactive pro-drugs that require conversion into their active form thioguanine nucleotides (TGNs) via purine-salvage pathway to exert its therapeutic effect (Krynetski and Evans, 1998). TPMT is responsible for the S-methylation of the thiopurine drugs, a major pathway of thiopurine metabolism which prevents their further conversion into active metabolites (Coulthard and Hogarth, 2005). The cytotoxicity effect of thiopurine drugs is associated with intracellular concentration of TGNs, which is in an inverse correlation with TPMT activity (Lennard *et al.*, 1987). TPMT is widely distributed among human tissues with higher expression levels in liver and kidney, and the mutant TPMT alleles have been linked to reduced TPMT activity (Weinshilboum and Sladek,

1980; Krynetski et al., 1995; Otterness *et al.*, 1997; Collie-Duguid *et al.*, 1999), which could potentiate severe toxic effects and poor treatment outcome (Lennard *et al.*, 1989; Lennard, 1992). Since NAADP could not fulfil the role of SAM as a methyl donor, one could only speculate the effect of NAADP on TPMT and how that would modulate TPMT functionality.

It was revealed in our docking simulation that NAADP could be bound to TPMT at the same binding pocket as SAM. If this is true, one would wonder if any other SAM-dependent enzymes would potentially accept NAADP as substrates. Coincidentally, another SAM-binding protein, Indolethylamine N-methyltransferase (INMT), was also found in our candidate list. Yet its scores were poor in both docking programs. Through close examination of the SAH binding pocket, it was found that SAH binds to INMT with its homocysteine tail facing to the deep end of the binding pocket, whereas in TPMT the homocysteine tail faces outwards to the opening of the binding pocket. The binding conformation of SAH is a crucial factor in predicting the binding of NAADP. Although both NAADP and SAH have adenine moieties, the simulation suggested that the nicotinic acid moiety of the NAADP is in place of the adenine moiety of SAH to facilitate the intermolecular interaction. In addition, NAADP is essentially a much larger molecule than SAH. Thus, by checking the orientation of SAH one could predict if the NAADP would not fit into the binding pocket that harbours SAH. This hypothesis was tested in AutoDock Vina using crystal structures of DNA methyltransferases 1 (DNMT1) and protein arginine methyltransferases 5 (PRMT5), which are both SAM-dependent methyltransferases. Surprisingly, the docking scores for both structures were exceptionally low (-9.7 for both), suggesting possible strong interactions with NAADP. However, close examination of the simulated ligand poses identified

structural clashes within PRMT5. Also, a speculative NAADP conformation in DNMT1 did not see substantial overlap with the SAM, thus the accuracy of the docking result could be questionable. Yet still, it would be interesting to see whether the binding of SAM or SAH can be competed by NAADP in other SAM-dependent proteins.

Finally, this concluding section marks the end of this study. Of all the three candidates that had been experimentally tested, TPMT and CBR1 emerged as NAADP binding proteins. TPMT demonstrated its outstanding selectivity for NAADP in MST experiments, and became the first binding protein to have been ever reported that is exclusively selective for NAADP. This sets the stage for further investigation that would increase our understanding of the NAADP signalling pathway.

Chapter 5 General discussion

As a relatively new member of the second messenger family, NAADP has been regarded as the most potent Ca^{2+} mobilizing second messenger that targets acidic organelles with a distinct mechanism of action. There is no doubt that NAADP regulates many key physiological events through NAADP-induced Ca^{2+} release, yet how NAADP works at a molecular level remains unclear. The two-pore channels (TPCs) have been proposed as NAADP receptors and have been shown to play an indispensable role in NAADP-mediated Ca^{2+} responses (Calcraft *et al.*, 2009; Ruas *et al.*, 2015). However, it has been recognized that NAADP may not directly bind to TPCs and may require an accessory protein to mediate its Ca^{2+}-release effect (Calcraft *et al.*, 2009). Since then, the search for TPC interactors that bind NAADP with high affinity has been the major focus of the entire field. Nevertheless, so far neither structural mapping of potential NAADP binding sites on TPCs nor NAADP binding to identified TPC interactors (i.e. Hax-1, Rab7a, etc.) has been reported. Some of the high affinity NAADP binding protein populations have been discovered by photoaffinity labelling and their association with TPCs was established (Walseth *et al.*, 2012a; Walseth *et al.*,

2012b; Lin-Moshier *et al.*, 2012). Based on these pieces of evidence, a general chemistry-based approach was adopted in an attempt to isolate high-affinity NAADP binding protein(s) and was described in Chapter 3. Crosslinking was performed in WT and DKO MEFs, which have been previously shown to possess robust responsiveness to NAADP (Ruas *et al.*, 2015). Surprisingly, the majority of NAADP binding in MEFs was located on the membrane fraction, which is in sharp contrast to the existing evidence showing that NAADP primarily binds to cytosolic proteins in other studies (Lin-Moshier *et al.*, 2012). Even though NAADP-induced Ca^{2+} release is robust in MEFs, no high affinity NAADP binding site could be detected and most of the binding on MEF membranes was non-specific. The low affinity binding of NAADP seems to be contradictory to the remarkable NAADP responsiveness of MEFs since it is generally believed that high affinity NAADP binding is essential for NAADP-induced Ca^{2+} signalling. It is possible that the abundance of the high affinity binding protein(s) is not critical for NAADP response due to the extremely high potency of NAADP. Alternatively, the great efficacy of a high affinity binding protein may counterbalance its low abundance. Together with other reported NAADP binding profiles, such as HEK293, SKBR3, Jurkat T cells, mouse and rabbit tissues, etc. (Patel *et al.*, 2000; Bak *et al.*, 2001; Masgrau *et al.*, 2003; Calcraft *et al.*, 2009; Walseth *et al.*, 2012b; Lin-Moshier *et al.*, 2012), the case of MEFs suggests complexity and high variability of NAADP binding in mammalian systems.

The second part of Chapter 3 explored the effectiveness of the NAADP affinity column in capturing the high affinity binding protein(s) from mouse liver cytosol. A similar approach was previously adopted by Billington *et al.* to investigate NAADP protein in sea urchin egg homogenate (2004), and discovered that glucose-6-phosphate

dehydrogenase (G6PD) and 6-phosphogluconate dehydrogenase can be eluted from the affinity column using NAADP. G6PD had also been demonstrated to reduce NAADP into a less effective Ca^{2+}-mobilizing compound, NAADPH, which could be a potential pathway of NAADP inactivation (Billington *et al.*, 2004). In the present study, the NAADP affinity column was not able to isolate any high affinity binding proteins successfully. As demonstrated by SDS-PAGE, the specific band can only be displaced by excessive amount (500 µM) of NAADP or NADP. No significant displacement was observed in the presence of NAADP or NADP up to 10 µM, suggesting that the specific band was likely to bind NAADP with low affinity. Two factors may contribute to the unsuccessful implementation of an NAADP affinity column in this study. First, the mouse liver cytosol used to conduct the affinity pull-down has lower NAADP binding affinity than sea urchin egg homogenate. Hence it would be more difficult to isolate high affinity binding protein(s) when a modified NAADP, presumably with a weaker interaction with the binding protein, is used as the bait ligand. Second, Chapter 4 demonstrated that the identified NAADP binding protein TPMT forms polar contacts with the hydroxyl groups of the pyridinium-ribose, suggesting their importance in NAADP recognition. The NAADP affinity column prepared in this study used periodate to oxidize NAADP, which cleaves the cis-glycol group and convert the hydroxyl group to aldehydes for subsequent immobilization. One could anticipate that such procedure would cause the loss of recognition sites and introduce steric occlusion that decreases the affinity of NAADP to its prospective binding proteins.

Chapter 4 described a strategy to identify high affinity NAADP binding protein using the combination of several techniques. It has been acknowledged that the abundance of certain high affinity binding proteins could be too low to be identified by mass

spectrometry (Yaping Lin-Moshier, 2012). Therefore, it is paramount to enrich NAADP binding protein to increase the chance of identification. The first part of Chapter 4 detailed the optimization of a sequential chromatography, which successfully achieved a more than 2300-fold enrichment of high affinity NAADP binding proteins. What is most interesting is that the choice of chromatography in this study coincided with the historical records of chromatographic purification used to isolate TPMT and CBR1 (Woodson and Weinshilboum, 1983; Usami *et al.*, 2001), which were identified as the NAADP binding proteins at the end of Chapter 4. The results from HIC suggested that multiple NAADP binding protein populations were present in mouse liver and could be separated by their surface hydrophobicity. As shown in Figure 4.8, the second peak from the left eluted early and bound NAADP with high affinity, indicating that the surface of high affinity NAADP binding proteins is weakly hydrophobic. The third peak from the left represented the low affinity NAADP binding proteins and had higher surface hydrophobicity. Although the fourth peak also possessed high affinity for NAADP, the binding profile varied significantly between batches, suggesting that these may consist of transient NAADP binding complexes. An earlier attempt at mouse liver cytosol separation by SEC also showed that low affinity binding proteins are larger than the high affinity ones (data not shown). These observations, together with the photolabelling of NAADP binding protein described later in Chapter 4, were in agreement with reports of NAADP binding profiles in other systems (Walseth *et al.*, 2012a; Lin-Moshier *et al.*, 2012; Walseth *et al.*, 2012b; Ruas *et al.*, 2015), suggesting that multiple NAADP binding proteins are present, and that low affinity binding proteins are physically different from the high affinity ones.

In this study, the photoaffinity labelling of binding protein in chromatographically purified fractions was the most critical step in the identification of high affinity binding protein. Visualization of high affinity binding protein in enriched fractions by [^{32}P]-5-azido-NAADP, demonstrated in Figure 4.25, revealed that putative high affinity binding protein has an approximate size of 27 kDa, and its enrichment by chromatography process was also visualized on the SDS-PAGE gel that was consistent with the enrichment index determined by [^{32}P]-NAADP binding assay in Chapter 4. Additionally, the 27 kDa band was also discovered by Lin-Moshier *et al.* in the photoaffinity labelling of mouse pancreas and was demonstrated to be another population of high affinity NAADP binding protein other than the 22/23 kDa doublet (2012). Perhaps the most controversial part of the photolabelling profile is the absence of the signature 22/23 kDa doublet previously shown to be widely expressed in different mammalian cells and tissue preparations (Walseth *et al.*, 2012b; Lin-Moshier *et al.*, 2012). Since the doublet labelling was also missing in mouse liver, heart, and brain crude homogenate and the overall resolution was not that satisfactory, we believed that the limitation of imaging equipment sensitivity might be main reason for this problem, especially given the fact that the labelling intensity of the doublet was already low in the existing literature reports (Walseth *et al.*, 2012b; Lin-Moshier *et al.*, 2012). However, one cannot exclude the possibility that the doublet could have been lost during the sequential chromatography, which focused on the isolation and enrichment of fractions with prominent NAADP binding.

Based on the photoaffinity labelling profile of the enriched fraction, MS analysis detected only 35 proteins within the range (25-35 kDa) of the 27 kDa band. The 35 candidates were subsequently analyzed by docking simulation. It should be noted that

the accuracy of the docking results is subject to a few constraints. The availability of reliable target protein crystal structure is most critical for docking simulation. In this study, 10 candidates could not participate in the virtual screen due to the lack of suitable protein structures. Second, the scoring function of the docking program would also impact the interpretation of results. This has been illustrated by the comparison of docking results between AutoDock Vina and CLC Drug Discovery Workbench. Both programs adopt weighted scoring functions, which in general perform better than the consensus scoring function since the weights given to each interaction are extrapolated from their coefficient of regression (Chen, 2015). Despite both using weighted scoring functions, these two programs have different weights assigned (Korb *et al.*, 2009; Trott and Olson, 2010), hence result in their unique distribution of docking scores (Figure 4.31) which influenced the subsequent selection of top hits. Another factor that could affect the accuracy of the docking comes from the docking itself. The docking simulation only considers the affinity of interaction in the event of binding but does not take other crucial factors, such as how the ligand reaches the designated binding pocket and how stable is the protein-ligand complex in the presence of solvent, into account. Therefore, the molecular dynamics (MD), which simulates the movement of protein-ligand complex within a certain amount of time, is commonly used to validate the result of docking. In this study, MD validation could not be implemented due to the limited processing power available, which means that 6 hours is required to complete a one-nanosecond MD simulation. However, MD simulation should be performed to validate the result of docking in the future once sufficient calculation power is available.

The final section of Chapter 4 discussed the experimental validation of the high affinity NAADP binding protein candidates. NAADP binding of three candidates were determined by BLI and MST. The BLI experiment on NAADP binding affinity of the candidates could not yield convincing results due to a low signal-to-noise ratio. However, it provided valuable information on the NAADP binding kinetics of three candidates. Association of NAADP with TPMT was much faster than that in CBR1, especially at low NAADP concentrations (Figure 4.33, Figure 4.37), which suggested that TPMT could have higher NAADP affinity than CBR1 and this was confirmed later in the MST experiments. The MST results indicated that TPMT is a highly selective NAADP binding protein which does not show apparent affinity to NADP, while CBR1 has relatively lower affinity for NAADP and binds NADP with almost equivalent affinity. Although these proteins were shown to bind NAADP, their affinities for NAADP were lower than expected. MST determination of NAADP binding (Figure 4.40, Figure 4.44) showed that TPMT has a K_d of 18 µM, while the K_d of CBR1 is around 80-190 µM, both K_ds (ie. high affinity and low affinity) being at least 1000-fold higher than that of the high affinity NAADP binding site determined in the early section of Chapter 4 and from other published reports (Calcraft *et al.*, 2009; Walseth *et al.*, 2012b; Lin-Moshier *et al.*, 2012; Ruas *et al.*, 2015). Moreover, in the first part of Chapter 4, the Hill Slopes of [^{32}P]-NAADP competitive binding curve in HIC and SEC fractions were calculated as -1.064 ± 0.04 and -1.049 ± 0.04, respectively. This suggests that only one homologous binding site is present in those fractions, which is not consistent with the results of MST validation since TPMT and CBR1 have apparently different affinities for NAADP (Figure 4.47). A similar contradiction was reported in the case of a recently identified cADPR-binding protein, glyceraldehyde 3-phosphate dehydrogenase, as its K_d for

cADPR (8.59 μM) was much higher than the affinity of the cADPR binding site (K_d=17 nM) determined by [^{3}H]-cADPR (Lee, 1991; Zhang *et al.*, 2017). It was suspected that the fluorescent labelling and biotin coupling, mandatory procedures of protein modification required for corresponding techniques, could be the cause of the affinity discrepancy. Evidence came from the first section of Chapter 3, in which a significant reduction of NAADP binding on MEF membranes was observed after the treatment with amine-reactive non-selective crosslinker DSP. In BLI, either protein or ligand must be coupled to biosensor to initiate measurement. In this study, the candidates were first biotinylated by NHS-based biotin before BLI measurement, which reacts with the available primary amines on the cell surface. Similarly, in MST, the candidates were coupled with NHS-based fluorescent dye before the experiment. Those probes used in BLI and MST react in the same way as the DSP crosslinker and as DSP was found to interfere NAADP binding, one could anticipate that those probes would probably have similar effects on the binding protein candidates. Other explanations of relatively low NAADP affinity of the candidates includes possible loss of their binding partners that are essential for their NAADP binding.

Given the low NAADP affinity of apo-CBR1 and that NADP-bound holo-CBR1 has even lower affinity for NAADP ($K_d \approx$ 4.6 mM), the identity of CBR1 as a high-affinity NAADP binding protein remains questionable. On the other hand, the superb NAADP selectivity of TPMT makes it a more likely candidate for a high-affinity binding protein. Chapter 4 also investigated the residues in TPMT that interact with NAADP to identify determinants of NAADP selectivity and potency. It was revealed that NAADP interacts with a similar set of residues as SAH, a naturally occurring TPMT inhibitor, which explained the NAADP affinity of TPMT. Several key structural determinants of NAADP

activity, such as nicotinic acid moiety, 2'-phosphate on ADP-ribose and the adenine moiety (Lee and Aarhus, 1995; Lee *et al.*, 1997; Lee and Aarhus, 1997; Billington *et al.*, 2004; Billington *et al.*, 2005; Jain *et al.* 2010; Trabbic *et al.*, 2012), were also found to form polar contacts with TPMT residues. Interestingly, the pyridinium-ribose was found to form hydrogen bonds with TPMT residues, suggesting its importance in NAADP recognition and this could provide the explanation for the loss of binding affinity observed in the case of oxidized NAADP (Yee, 2002). On the other hand, docking simulation of the NADP-TPMT interaction showed that NADP forms hydrogen bonds with TPMT through mostly the same residues with NAADP but no obvious binding was detected in the MST experiment. Only a single functional group difference lies between NAADP and NADP and that could be the key component responsible for the unique properties of NAADP. According to a recently proposed theory, hydrogen bonding only enhances ligand-receptor interaction when both donor and acceptor have significantly stronger or weaker hydrogen bonding capability than that of water, whereas strong-weak pairing would result in the decrease of ligand binding affinity (Chen *et al.*, 2016). Using the hydrogen bonding capability data calculated from computational modelling (Chen *et al.*, 2016), it was found that the carboxyl group of the NAADP is a much stronger hydrogen donor than the amide group of NADP (11.2 vs 7.6). Docking simulation showed that the carboxyl group of NAADP and the amide group of NADP both form hydrogen bond with oxygen on the backbone of Cys133 in TPMT, which is a significantly stronger hydrogen acceptor than water (14.9 vs 7.02). Hence, it became obvious that hydrogen bonding of carboxyl-Cys133 would increase the binding affinity of NAADP, whereas the amide-Cys133 hydrogen bond would

decrease the NADP affinity to TPMT. Therefore, the disparity of NAADP and NADP binding affinity could be explained by a novel hydrogen bonding theory.

Identification of TPMT and CBR1 as NAADP binding proteins marks the end of this study, however, this is only a start for the further investigation into the NAADP signalling pathway. First, a few more experiments should be performed to consolidate the identity of TPMT as a selective NAADP binding protein. The NAADP binding affinity of TPMT and CBR1 should be confirmed by the [^{32}P]-NAADP binding assay as this can be done without modifying the protein, and the homologous binding of radiolabeled NAADP would also ensure the reliability of the assay. It would be interesting to see whether the TPMT substrate SAM can compete with NAADP for high affinity binding sites in other mammalian systems. Co-crystallization of TPMT with NAADP should also be carried out if possible to determine the binding conformation of NAADP for TPMT.

The purpose of finding the NAADP binding protein(s) is to identify the missing link between NAADP and its effectors of Ca^{2+} release, the TPCs. So far there is no report of TPMT being part of the TPC complex. Thus, priority should be given to investigation into potential interaction between TPMT and TPCs. The focus of further investigation should be whether TPMT binds to TPCs, whether the presence of NAADP can increase the transient interaction between TPMT and TPCs, and whether TPMT and TPC-TPMT interactivity are both essential for NAADP-induced Ca^{2+} release. Currently, a TPMT-equivalent protein has not been reported in sea urchin, which has been regarded as the golden standard of the NAADP-induced Ca^{2+} responses. Thus, generation of a TPMT knockout animal model would be beneficial for the investigation suggested above. Finally, TPMT is characterized as a detoxification enzyme responsible for a

SAM-dependent metabolism pathway for the thiopurine drugs that are commonly used as chemotherapy agents (Lennard *et al.*, 1989; Coulthard and Hogarth, 2005). The functional significance of TPMT-NAADP complex remains unclear as NAADP could not substitute for the role of SAM as a methyl donor. It would be intriguing to test whether TPMT has catalytic activity for NAADP as well. Furthermore, experiments should be carried out to check how NAADP would affect the interaction of TPMT with other binding partners, which might identify the hidden targets of NAADP signalling. Finally, inspired by the identity of TPMT as a SAM-binding protein, one would wonder whether other SAM-dependent proteins would be targets of NAADP as well. SAM is the second most utilized enzyme substrate and a hugely preferred methyl donor of methyltransferases (Schubert *et al.*, 2003). The SAM-dependent methylation is involved in numerous crucial physiological processes, such as biosynthesis, detoxification, signal transduction and epigenetic regulation, etc. (Martin and McMillan, 2002; Loenen, 2006). In this study, two SAM-dependent methyltransferases, DNA methyltransferases 1 (DNMT1) and protein arginine methyltransferases 5 (PRMT5), were tested by AutoDock Vina for their NAADP binding affinities. These two enzymes are responsible for the epigenetic regulation of gene transcription (Copeland *et al.*, 2009). Although the results did not suggest a promising NAADP interaction, this does not rule out the possibility that other SAM-dependent proteins might have affinity for NAADP, which could be the opportunity to discovery novel NAADP functionality.

In conclusion, TPMT and CBR1 have been identified as NAADP binding proteins through a rational combination of various techniques, which is a great addition to our understanding of the molecular mechanism of NAADP. TPMT demonstrated high

selectively to NAADP, which makes it a more likely candidate for a high-affinity NAADP binding protein. Further investigation is needed to provide more evidence of TPMT being an essential element of the NAADP signalling pathway.

Appendix

Purification of NAADP binding protein candidates was performed by Dr. Bin Meng from ShanghaiTech University and the rationale was illustrated in Figure 2.5. The chromatography purification of each candidate is detailed below.

S1. hCBR1

S1.1. IMAC of hCBR1

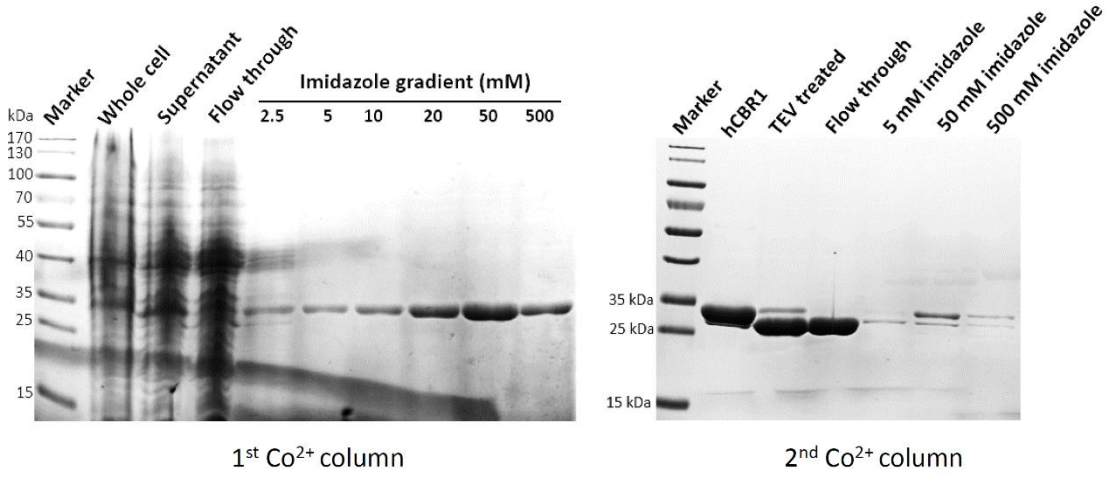

Figure S1. IMAC profile of recombinant hCBR1. IMAC purification of recombinant hCBR1 in 50 mM HEPES, 500 mM NaCl, 10% glycerol, pH 7.8 was performed by TALON metal affinity column. Proteins bound to the columns were eluted by increasing concentration of imidazole. In the first IMAC purification (left), proteins eluted within 20-500 mM imidazole gradient were collected. In second IMAC purification (right), only flow through was collected.

S1.2. IEX of hCBR1

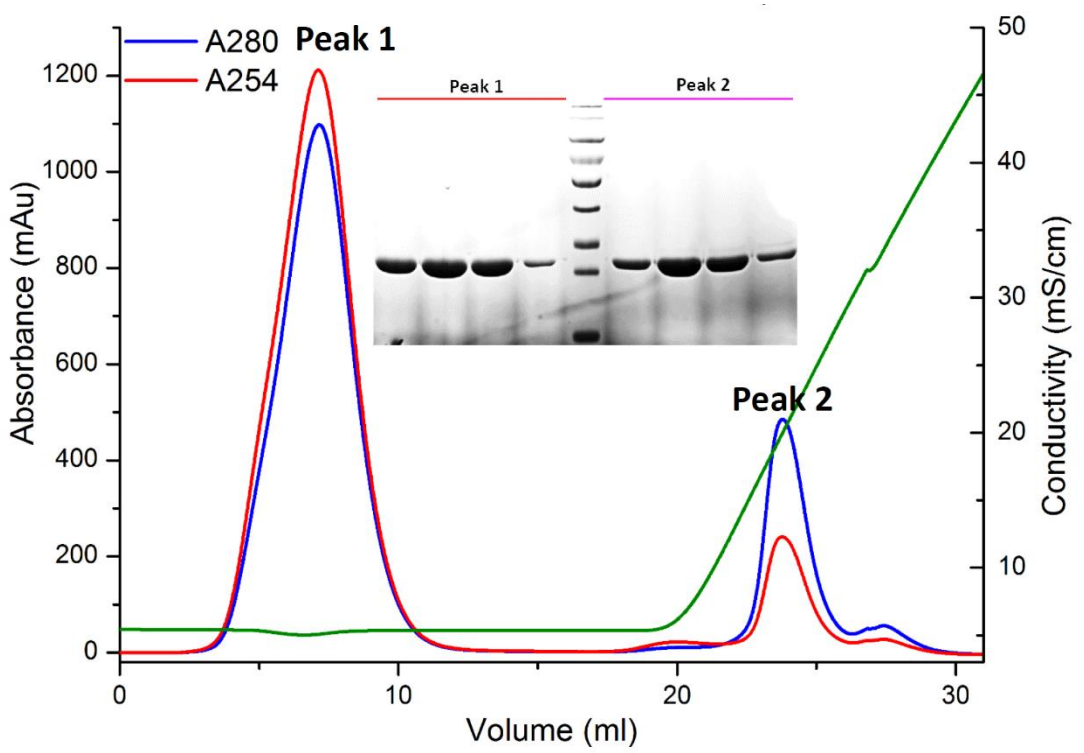

Figure S2. IEX profile of IMAC purified recombinant hCBR1. The IEX purification was carried out in HiTrap Heparin FF column using following buffers: Buffer A: 50 mM HEPES, 50 mM NaCl, 10% glycerol, pH 7.8; Buffer B: 50 mM HEPES, 1 M NaCl, 10% glycerol, pH 7.8. Proteins were eluted using a slope gradient. Peak 1 represents hCBR1 complexes with small molecules (holo-hCBR1), presumably NADP, as its A254 is higher than A280. Peak 2 is hCBR1 with no small molecules or nucleic acid bound (apo-hCBR1).

S1.3. SEC of holo-hCBR1

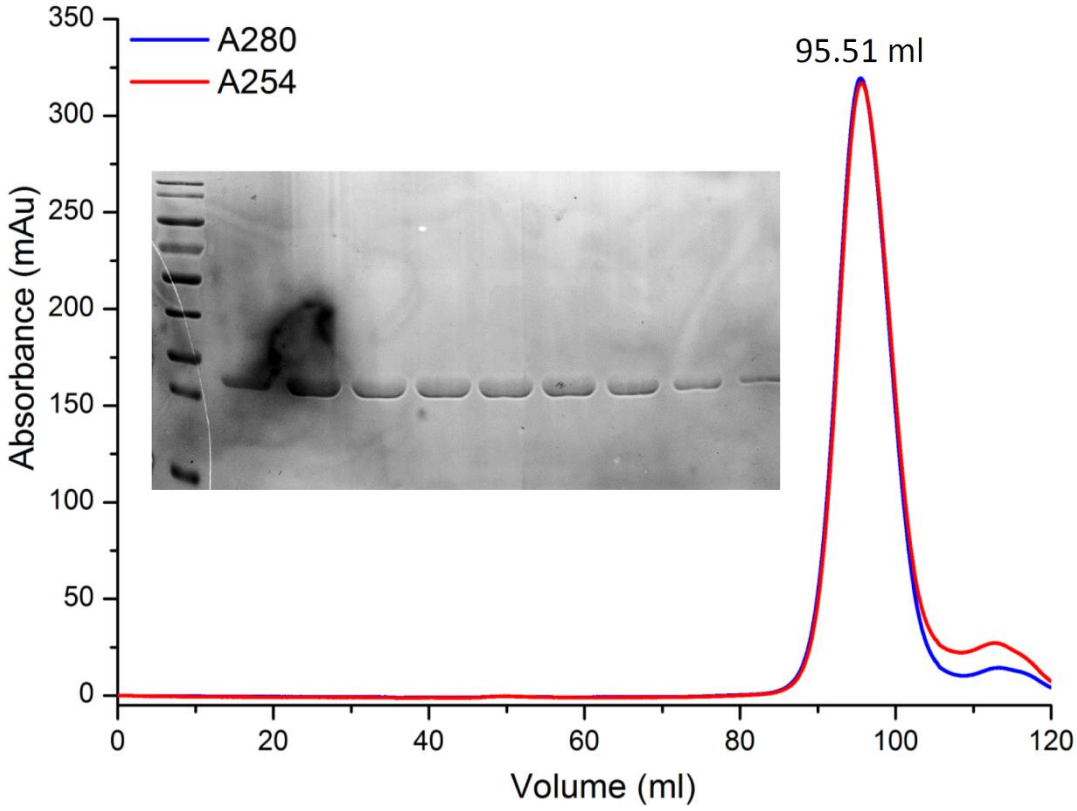

Figure S3. SEC profile of holo-hCBR1. The SEC purification was performed in HiLoad 10/600 Superdex 200. Proteins were eluted by isocratic elution using 50 mM HEPES, 500 mM NaCl, 10% glycerol, pH 7.8.

S1.4. SEC of apo-hCBR1

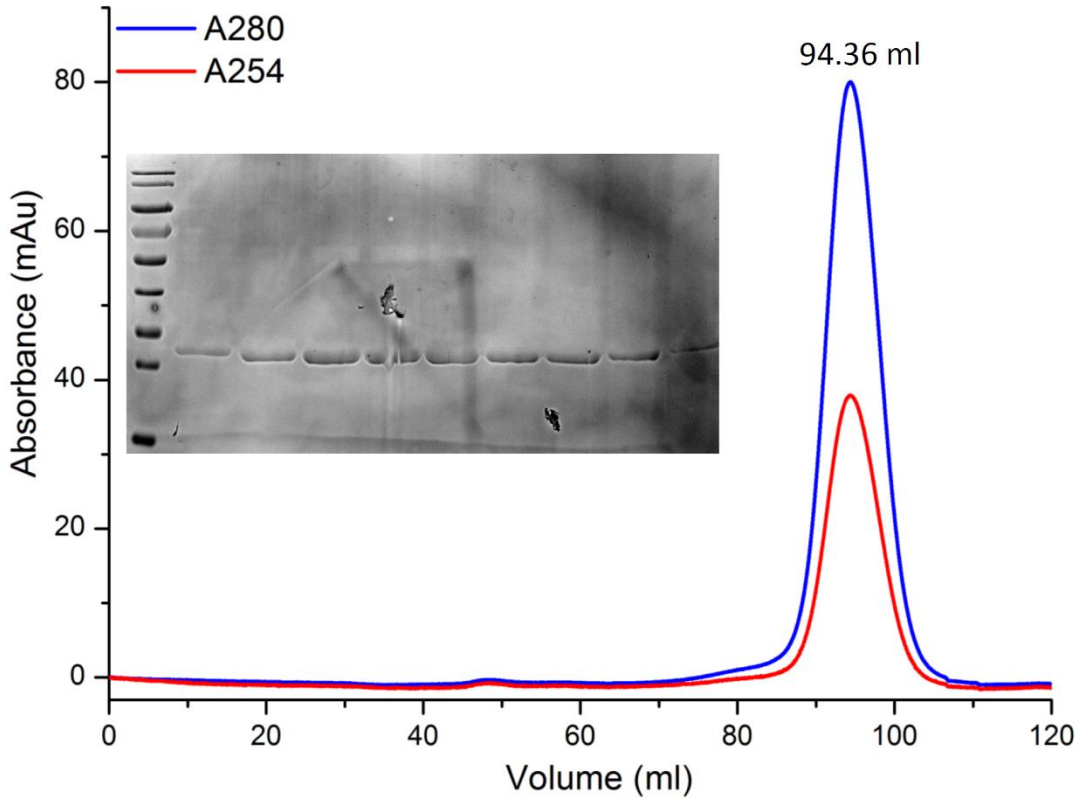

Figure S4. SEC profile of apo-hCBR1. The SEC purification was performed in HiLoad 10/600 Superdex 200. Proteins were eluted by isocratic elution using 50 mM HEPES, 500 mM NaCl, 10% glycerol, pH 7.8.

S2. hCYB5R3

S2.1. IMAC of hCYB5R3

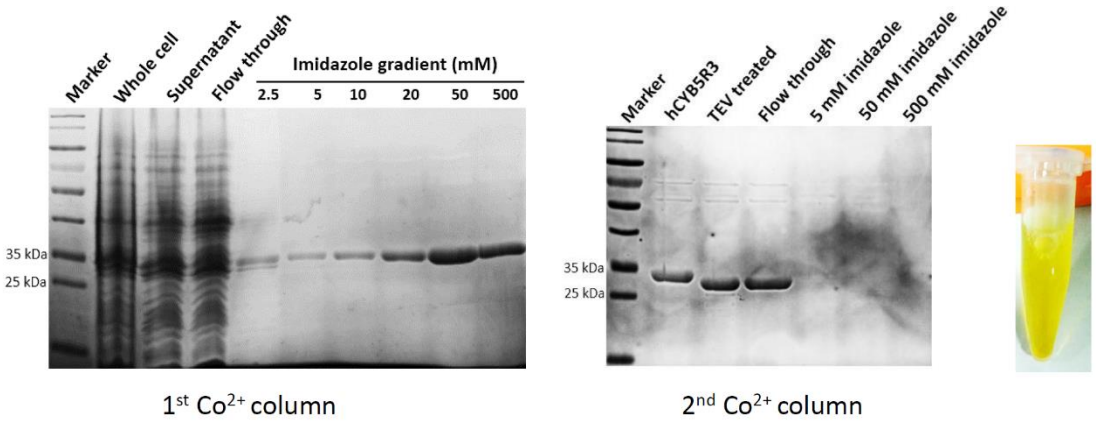

Figure S5. IMAC profile of recombinant hCYB5R3. IMAC purification of recombinant hCYB5R3 in 50 mM HEPES, 500 mM NaCl, 10% glycerol, pH 7.8 was performed by TALON metal affinity column. Proteins bound to the columns were eluted by increasing concentration of imidazole. In the first IMAC purification (left), proteins eluted within 20-500 mM imidazole gradient were collected. In second IMAC purification (right), only flow through was collected. The IMAC purified fractions had a yellow color due to the ability of hCYB5R3 to capture FAD from the culture medium.

S2.2. IEX of hCYB5R3

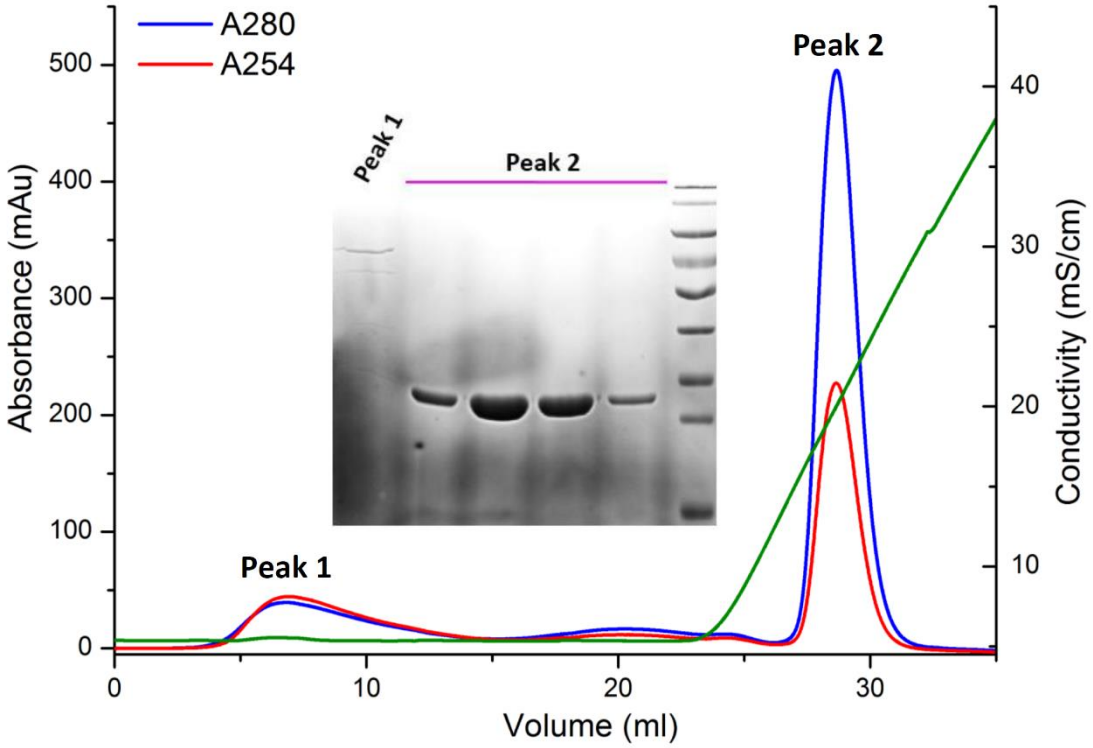

Figure S6. IEX profile of IMAC purified recombinant hCYB5R3. The IEX purification was carried out in HiTrap Heparin FF column using following buffers: Buffer A: 50 mM HEPES, 50 mM NaCl, 10% glycerol, pH 7.8; Buffer B: 50 mM HEPES, 1 M NaCl, 10% glycerol, pH 7.8. Proteins were eluted using a slope gradient. Peak 1 represents hCYB5R3 complexes with FAD (holo-hCYB5R3). Peak 2 is hCYB5R3 without FAD (apo-hCYB5R3).

S2.3. SEC of apo-hCYB5R3

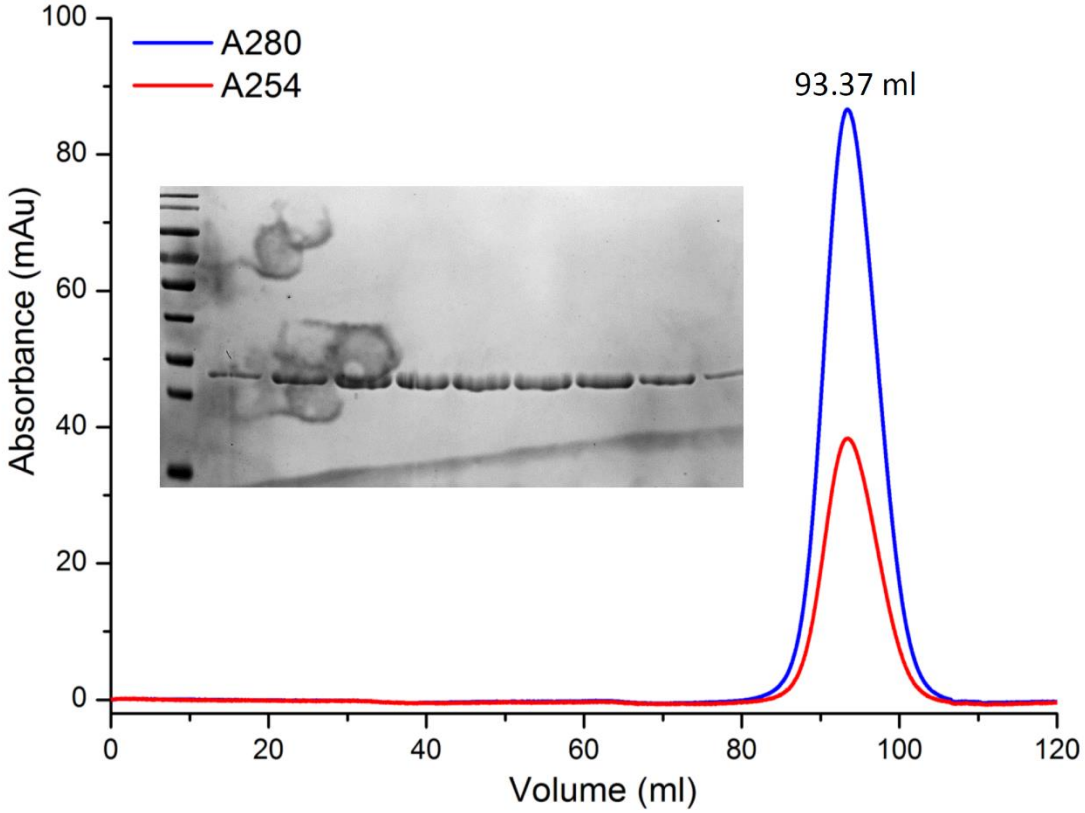

Figure S7. SEC profile of apo-hCYB5R3. The SEC purification was performed in HiLoad 10/600 Superdex 200. Proteins were eluted by isocratic elution using 50 mM HEPES, 500 mM NaCl, 10% glycerol, pH 7.8. The fractions collected were colorless, suggesting the absence of a bound cofactor (FAD).

S2.4. SEC of holo-hCYB5R3

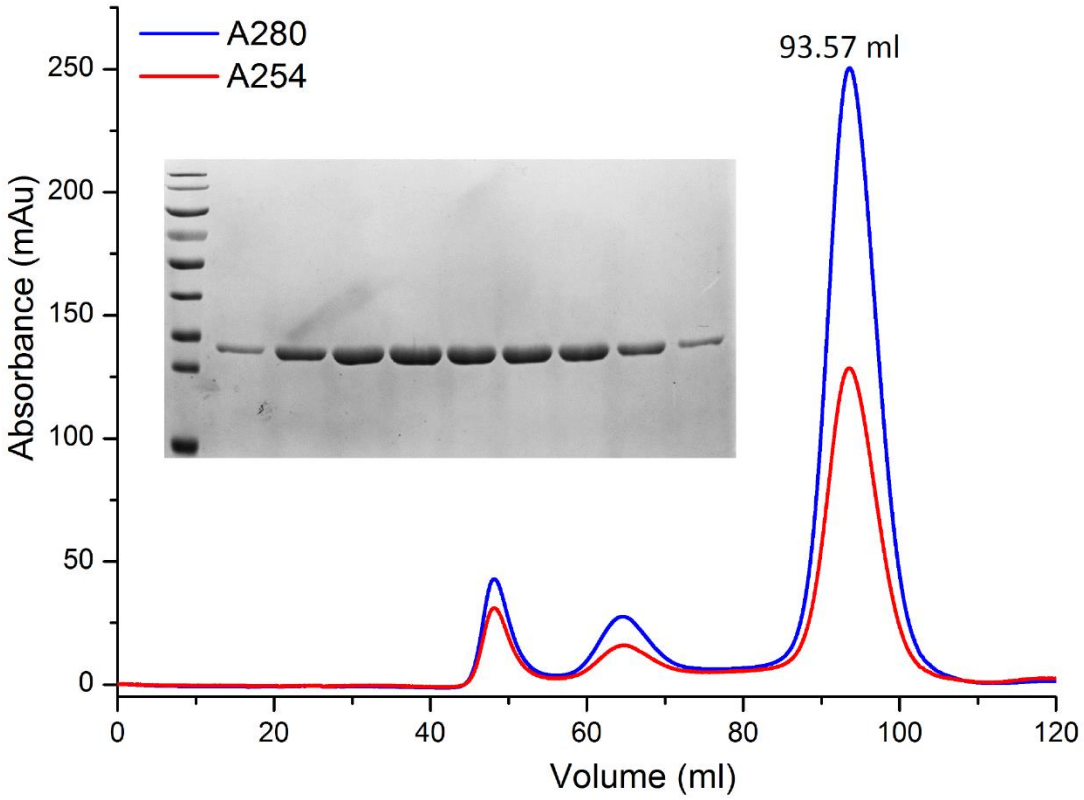

Figure S8. SEC profile of holo-hCYB5R3. The SEC purification was performed in HiLoad 10/600 Superdex 200. Proteins were eluted by isocratic elution using 50 mM HEPES, 500 mM NaCl, 10% glycerol, pH 7.8. The fractions collected around 93.57 ml were yellow, indicating that the proteins were purified with FAD.

S3. hTPMT

S3.1. IMAC of hTPMT

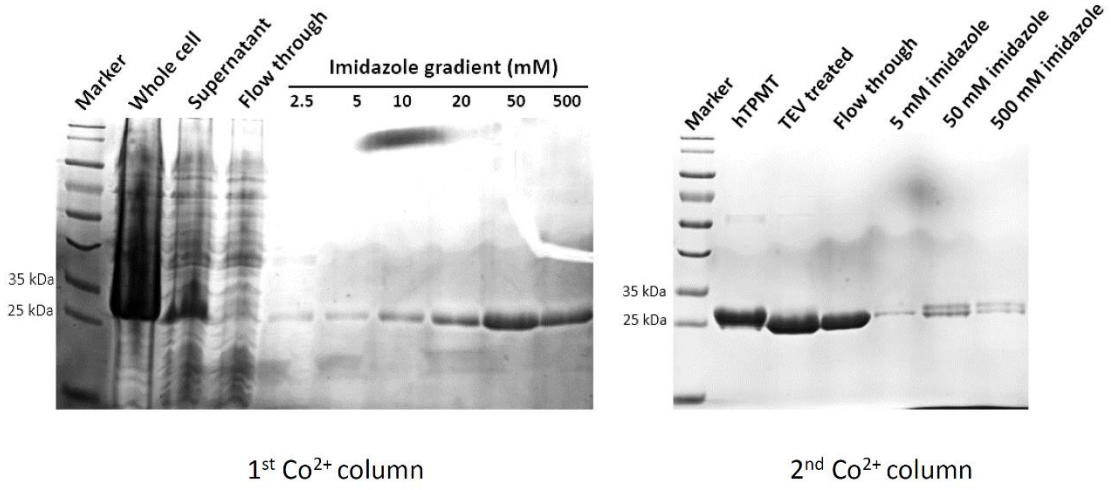

Figure S9. IMAC profile of recombinant hTPMT. IMAC purification of recombinant hTPMT in 50 mM HEPES, 500 mM NaCl, 10% glycerol, pH 7.8 was performed by TALON metal affinity column. Proteins bound to the columns were eluted by increasing concentration of imidazole. In the first IMAC purification (left), proteins eluted within 20-500 mM imidazole gradient were collected. In second IMAC purification (right), only flow through was collected.

S3.2. IEX of hTPMT

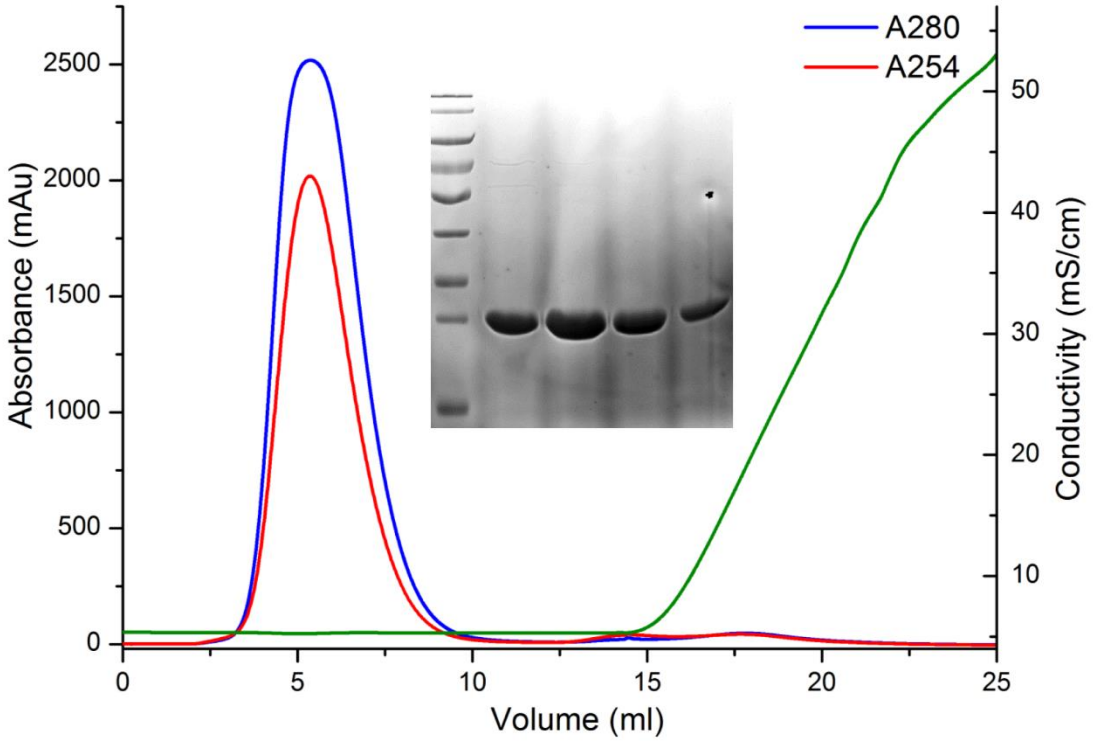

Figure S10. IEX profile of IMAC purified recombinant hTPMT. The IEX purification was carried out in HiTrap Heparin FF column using following buffers: Buffer A: 50 mM HEPES, 50 mM NaCl, 10% glycerol, pH 7.8; Buffer B: 50 mM HEPES, 1 M NaCl, 10% glycerol, pH 7.8. Proteins were eluted using a slope gradient. The IEX purified hTPMT should contain S-adenosyl-L-methionine (SAM) or S-adenosyl-L-homocysteine (SAH) as its A254/A280 > 0.5.

S3.3. SEC of hTPMT

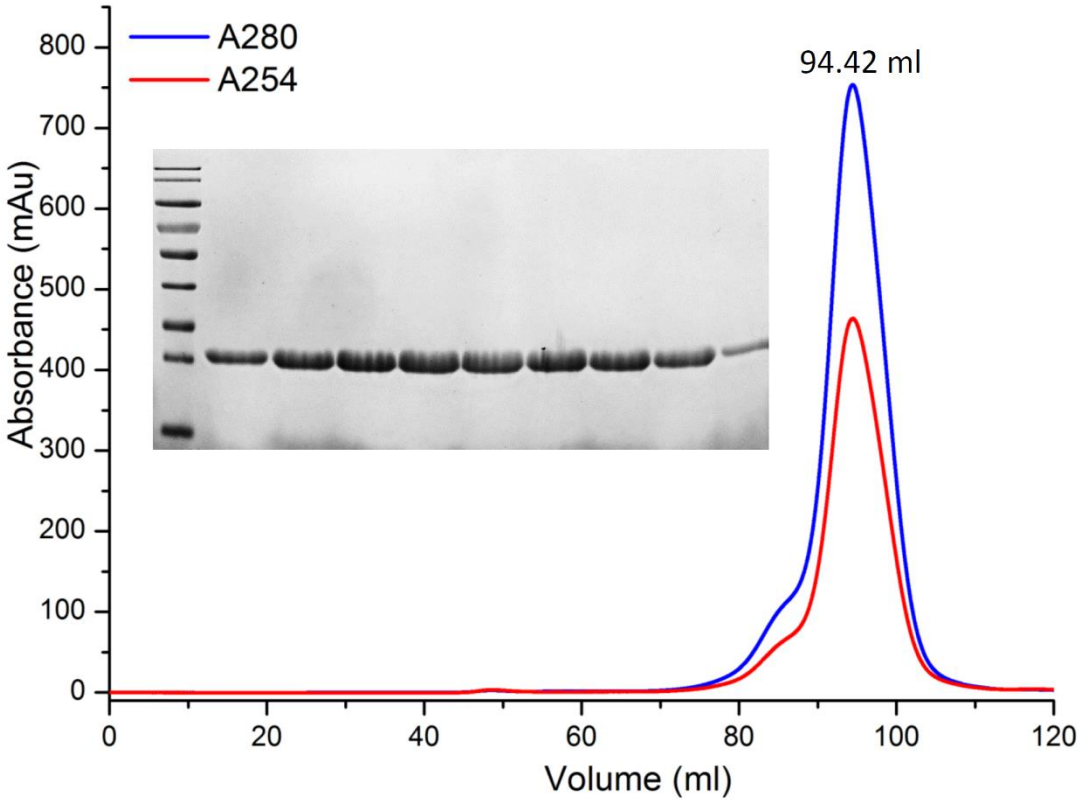

Figure S11. SEC profile of holo-hTPMT. The SEC purification was performed in HiLoad 10/600 Superdex 200. Proteins were eluted by isocratic elution using 50 mM HEPES, 500 mM NaCl, 10% glycerol, pH 7.8.

References

Aarhus, R., D. M. Dickey, R. M. Graeff, K. R. Gee, T. F. Walseth and H. C. Lee (1996). "Activation and inactivation of Ca2+ release by NAADP+." J Biol Chem **271**(15): 8513-8516.

Aarhus, R., R. M. Graeff, D. M. Dickey, T. F. Walseth and H. C. Lee (1995). "ADP-ribosyl cyclase and CD38 catalyze the synthesis of a calcium-mobilizing metabolite from NADP." J Biol Chem **270**(51): 30327-30333.

Ali, R. A., T. Zhelay, C. J. Trabbic, T. F. Walseth, J. T. Slama, D. R. Giovannucci and K. A. Wall (2014). "Activity of nicotinic acid substituted nicotinic acid adenine dinucleotide phosphate (NAADP) analogs in a human cell line: Difference in specificity between human and sea urchin NAADP receptors." Cell Calcium **55**(2): 93-103.

Bak, J., R. A. Billington, G. Timar, A. C. Dutton and A. A. Genazzani (2001). "NAADP receptors are present and functional in the heart." Curr Biol **11**(12): 987-990.

Bak, J., P. White, G. Timar, L. Missiaen, A. A. Genazzani and A. Galione (1999). "Nicotinic acid adenine dinucleotide phosphate triggers Ca2+ release from brain microsomes." Curr Biol **9**(14): 751-754.

Bando, S., T. Takano, T. Yubisui, K. Shirabe, M. Takeshita and A. Nakagawa (2004). "Structure of human erythrocyte NADH-cytochrome b5 reductase." Acta Crystallogr D Biol Crystallogr **60**(Pt 11): 1929-1934.

Bargal, R., N. Avidan, E. Ben-Asher, Z. Olender, M. Zeigler, A. Frumkin, A. Raas-Rothschild, G. Glusman, D. Lancet and G. Bach (2000). "Identification of the gene causing mucolipidosis type IV." Nature Genetics **26**(1): 118-121.

Beck, A., M. Kolisek, L. A. Bagley, A. Fleig and R. Penner (2006). "Nicotinic acid adenine dinucleotide phosphate and cyclic ADP-ribose regulate TRPM2 channels in T lymphocytes." FASEB J **20**(7): 962-964.

Berg, I., B. V. Potter, G. W. Mayr and A. H. Guse (2000). "Nicotinic acid adenine dinucleotide phosphate (NAADP(+)) is an essential regulator of T-lymphocyte Ca(2+)-signaling." J Cell Biol **150**(3): 581-588.

Berridge, G., R. Cramer, A. Galione and S. Patel (2002). "Metabolism of the novel Ca(2+)-mobilizing messenger nicotinic acid-adenine dinucleotide phosphate via a 2 '-specific Ca(2+)-dependent phosphatase." Biochemical Journal **365**: 295-301.

Berridge, M. J., M. D. Bootman and H. L. Roderick (2003). "Calcium signalling: dynamics, homeostasis and remodelling." Nat Rev Mol Cell Biol **4**(7): 517-529.

Bezprozvanny, I., J. Watras and B. E. Ehrlich (1991). "Bell-shaped calcium-response curves of Ins(1,4,5)P3- and calcium-gated channels from endoplasmic reticulum of cerebellum." Nature **351**(6329): 751-754.

Billington, R. A. and A. A. Genazzani (2000). "Characterization of NAADP(+) binding in sea urchin eggs." Biochemical and Biophysical Research Communications **276**(1): 112-116.

Billington, R. A. and A. A. Genazzani (2007). "PPADS is a reversible competitive antagonist of the NAADP receptor." Cell Calcium **41**(6): 505-511.

Billington, R. A., A. Ho and A. A. Genazzani (2002). "Nicotinic acid adenine dinucleotide phosphate (NAADP) is present at micromolar concentrations in sea urchin spermatozoa." J Physiol **544**(Pt 1): 107-112.

Billington, R. A., J. W. Thuring, S. J. Conway, L. Packman, A. B. Holmes and A. A. Genazzani (2004). "Production and characterization of reduced NAADP (nicotinic acid-adenine dinucleotide phosphate)." Biochem J **378**(Pt 1): 275-280.

Billington, R. A., G. C. Tron, S. Reichenbach, G. Sorba and A. A. Genazzani (2005). "Role of the nicotinic acid group in NAADP receptor selectivity." Cell Calcium **37**(1): 81-86.

Blaustein, M. P. and W. J. Lederer (1999). "Sodium calcium exchange: Its physiological implications." Physiological Reviews **79**(3): 763-854.

Bobbitt, J. M. (1956). "Periodate Oxidation of Carbohydrates." Advances in Carbohydrate Chemistry **11**: 1-41.

Brailoiu, E., D. Churamani, X. Cai, M. G. Schrlau, G. C. Brailoiu, X. Gao, R. Hooper, M. J. Boulware, N. J. Dun, J. S. Marchant and S. Patel (2009). "Essential requirement for two-pore channel 1 in NAADP-mediated calcium signaling." J Cell Biol **186**(2): 201-209.

Brailoiu, E., D. Churamani, V. Pandey, G. C. Brailoiu, F. Tuluc, S. Patel and N. J. Dun (2006). "Messenger-specific role for nicotinic acid adenine dinucleotide phosphate in neuronal differentiation." Journal of Biological Chemistry **281**(23): 15923-15928.

Brailoiu, E., J. L. Hoard, C. M. Filipeanu, G. C. Brailoiu, S. L. Dun, S. Patel and N. J. Dun (2005). "Nicotinic acid adenine dinucleotide phosphate potentiates neurite outgrowth." J Biol Chem **280**(7): 5646-5650.

Brailoiu, E., T. Rahman, D. Churamani, D. L. Prole, G. C. Brailoiu, R. Hooper, C. W. Taylor and S. Patel (2010). "An NAADP-gated two-pore channel targeted to the plasma membrane uncouples triggering from amplifying Ca2+ signals." J Biol Chem **285**(49): 38511-38516.

Brailoiu, G. C., E. Brailoiu, R. Parkesh, A. Galione, G. C. Churchill, S. Patel and N. J. Dun (2009). "NAADP-mediated channel 'chatter' in neurons of the rat medulla oblongata." Biochem J **419**(1): 91-97, 92 p following 97.

Burnashev, N. (1998). "Calcium permeability of ligand-gated channels." Cell Calcium **24**(5-6): 325-332.

Calcraft, P. J., M. Ruas, Z. Pan, X. Cheng, A. Arredouani, X. Hao, J. Tang, K. Rietdorf, L. Teboul, K. T. Chuang, P. Lin, R. Xiao, C. Wang, Y. Zhu, Y. Lin, C. N. Wyatt, J. Parrington, J. Ma, A. M. Evans, A. Galione and M. X. Zhu (2009). "NAADP mobilizes calcium from acidic organelles through two-pore channels." Nature **459**(7246): 596-600.

Cancela, J. M., G. C. Churchill and A. Galione (1999). "Coordination of agonist-induced Ca2+-signalling patterns by NAADP in pancreatic acinar cells." Nature **398**(6722): 74-76.

Cang, C., Y. Zhou, B. Navarro, Y. J. Seo, K. Aranda, L. Shi, S. Battaglia-Hsu, I. Nissim, D. E. Clapham and D. Ren (2013). "mTOR regulates lysosomal ATP-sensitive two-pore Na(+) channels to adapt to metabolic state." Cell **152**(4): 778-790.

Carafoli, E. (1991). "Calcium-Pump of the Plasma-Membrane." Physiological Reviews **71**(1): 129-153.

Carlquist, M., T. Frejd and M. F. Gorwa-Grausund (2008). "Flavonoids as inhibitors of human carbonyl reductase 1." Chemico-Biological Interactions **174**(2): 98-108.

Carta, G. and A. Jungbauer (2010). Protein chromatography : process development and scale-up. Weinheim, Wiley-VCH.

Chen, D. L., N. Oezguen, P. Urvil, C. Ferguson, S. M. Dann and T. C. Savidge (2016). "Regulation of protein-ligand binding affinity by hydrogen bond pairing." Science Advances **2**(3).

Chen, Y. C. (2015). "Beware of docking!" Trends in Pharmacological Sciences **36**(2): 78-95.

Cheng, J. F., A. N. K. Yusufi, M. A. Thompson, E. N. Chini and J. P. Grande (2001). "Nicotinic acid adenine dinucleotide phosphate: A new Ca2+ releasing agent in kidney." Journal of the American Society of Nephrology **12**(1): 54-60.

Cheng, Y. and W. H. Prusoff (1973). "Relationship between Inhibition Constant (K1) and Concentration of Inhibitor Which Causes 50 Per Cent Inhibition (I50) of an Enzymatic-Reaction." Biochemical Pharmacology **22**(23): 3099-3108.

Chini, E. N., K. W. Beers and T. P. Dousa (1995). "Nicotinate adenine dinucleotide phosphate (NAADP) triggers a specific calcium release system in sea urchin eggs." J Biol Chem **270**(7): 3216-3223.

Chini, E. N. and T. P. Dousa (1995). "Enzymatic-Synthesis and Degradation of Nicotinate Adenine-Dinucleotide Phosphate (Naadp), a Ca2+-Releasing Agonist, in Rat-Tissues." Biochemical and Biophysical Research Communications **209**(1): 167-174.

Churamani, D., R. Hooper, T. Rahman, E. Brailoiu and S. Patel (2013). "The N-terminal region of two-pore channel 1 regulates trafficking and activation by NAADP." Biochemical Journal **453**: 147-151.

Churchill, G. C. and A. Galione (2001). "NAADP induces Ca2+ oscillations via a two-pool mechanism by priming IP3- and cADPR-sensitive Ca2+ stores." Embo Journal **20**(11): 2666-2671.

Churchill, G. C. and A. Galione (2001). "Prolonged inactivation of nicotinic acid adenine dinucleotide phosphate-induced Ca2+ release mediates a spatiotemporal Ca2+ memory." J Biol Chem **276**(14): 11223-11225.

Churchill, G. C., J. S. O'Neill, R. Masgrau, S. Patel, J. M. Thomas, A. A. Genazzani and A. Galione (2003). "Sperm deliver a new second messenger: NAADP." Curr Biol **13**(2): 125-128.

Churchill, G. C., Y. Okada, J. M. Thomas, A. A. Genazzani, S. Patel and A. Galione (2002). "NAADP mobilizes Ca(2+) from reserve granules, lysosome-related organelles, in sea urchin eggs." Cell **111**(5): 703-708.

Clapham, D. E. (2007). "Calcium signaling." Cell **131**(6): 1047-1058.

Clapper, D. L., T. F. Walseth, P. J. Dargie and H. C. Lee (1987). "Pyridine nucleotide metabolites stimulate calcium release from sea urchin egg microsomes desensitized to inositol trisphosphate." J Biol Chem **262**(20): 9561-9568.

Collie-Duguid, E. S. R., S. C. Pritchard, R. H. Powrie, J. Sludden, D. A. Collier, T. Li and H. L. McLeod (1999). "The frequency and distribution of thiopurine methyltransferase alleles in Caucasian and Asian populations." Pharmacogenetics **9**(1): 37-42.

Copeland, R. A., M. E. Solomon and V. M. Richon (2009). "Protein methyltransferases as a target class for drug discovery." Nature Reviews Drug Discovery **8**(9): 724-732.

Coulthard, S. and L. Hogarth (2005). "The thiopurines: An update." Investigational New Drugs **23**(6): 523-532.

Dammermann, W. and A. H. Guse (2005). "Functional ryanodine receptor expression is required for NAADP-mediated local Ca2+ signaling in T-lymphocytes." J Biol Chem **280**(22): 21394-21399.

Dammermann, W., B. Zhang, M. Nebel, C. Cordiglieri, F. Odoardi, T. Kirchberger, N. Kawakami, J. Dowden, F. Schmid, K. Dornmair, M. Hohenegger, A. Flugel, A. H. Guse and B. V. Potter (2009). "NAADP-mediated Ca2+ signaling via type 1 ryanodine receptor in T cells revealed by a synthetic NAADP antagonist." Proc Natl Acad Sci U S A **106**(26): 10678-10683.

Dellis, O., S. G. Dedos, S. C. Tovey, Taufiq-Ur-Rahman, S. J. Dubel and C. W. Taylor (2006). "Ca2+ entry through plasma membrane IP3 receptors." Science **313**(5784): 229-233.

Dickey, D. M., R. Aarhus, T. F. Walseth and H. C. Lee (1998). "Thio-NADP is not an antagonist of NAADP." Cell Biochem Biophys **28**(1): 63-73.

Dickinson, G. D. and S. Patel (2003). "Modulation of NAADP (nicotinic acid-adenine dinucleotide phosphate) receptors by K+ ions: evidence for multiple NAADP receptor conformations." Biochem J **375**(Pt 3): 805-812.

Dong, X. P., D. B. A. Shen, X. Wang, T. Dawson, X. R. Li, Q. Zhang, X. P. Cheng, Y. L. Zhang, L. S. Weisman, M. Delling and H. X. Xu (2010). "PI(3,5)P-2 controls membrane trafficking by direct activation of mucolipin Ca2+ release channels in the endolysosome." Nature Communications **1**.

Dowden, J., G. Berridge, C. Moreau, M. Yamasaki, G. C. Churchill, B. V. Potter and A. Galione (2006). "Cell-permeant small-molecule modulators of NAADP-mediated Ca2+ release." Chem Biol **13**(6): 659-665.

Dubyak, G. R. and C. Elmoatassim (1993). "Signal-Transduction Via P2-Purinergic Receptors for Extracellular Atp and Other Nucleotides." American Journal of Physiology **265**(3): C577-C606.

Ehrlich, B. E. and J. Watras (1988). "Inositol 1,4,5-trisphosphate activates a channel from smooth muscle sarcoplasmic reticulum." Nature **336**(6199): 583-586.

Elahian, F., Z. Sepehrizadeh, B. Moghimi and S. A. Mirzaei (2014). "Human cytochrome b5 reductase: structure, function, and potential applications." Critical Reviews in Biotechnology **34**(2): 134-143.

Foskett, J. K., C. White, K. H. Cheung and D. O. D. Mak (2007). "Inositol trisphosphate receptor Ca2+ release channels." Physiological Reviews **87**(2): 593-658.

Galione, A., H. C. Lee and W. B. Busa (1991). "Ca(2+)-induced Ca2+ release in sea urchin egg homogenates: modulation by cyclic ADP-ribose." Science **253**(5024): 1143-1146.

Gambara, G., R. A. Billington, M. Debidda, A. D'Alessio, F. Palombi, E. Ziparo, A. A. Genazzan and A. Filippini (2008). "NAADP-induced Ca(2+) signaling in response to endothelin is via the receptor subtype B and requires the integrity of lipid rafts/caveolae." Journal of Cellular Physiology **216**(2): 396-404.

Genazzani, A. A., R. M. Empson and A. Galione (1996). "Unique inactivation properties of NAADP-sensitive Ca2+ release." J Biol Chem **271**(20): 11599-11602.

Genazzani, A. A. and A. Galione (1996). "Nicotinic acid-adenine dinucleotide phosphate mobilizes Ca2+ from a thapsigargin-insensitive pool." Biochem J **315 (Pt 3)**: 721-725.

Gerasimenko, J. V., Y. Maruyama, K. Yano, N. J. Dolman, A. V. Tepikin, O. H. Petersen and O. V. Gerasimenko (2003). "NAADP mobilizes Ca2+ from a thapsigargin-sensitive store in the nuclear envelope by activating ryanodine receptors." J Cell Biol **163**(2): 271-282.

Gerasimenko, J. V., M. Sherwood, A. V. Tepikin, O. H. Petersen and O. V. Gerasimenko (2006). "NAADP, cADPR and IP3 all release Ca2+ from the endoplasmic reticulum and an acidic store in the secretory granule area." J Cell Sci **119**(Pt 2): 226-238.

Gomez-Suaga, P., B. Luzon-Toro, D. Churamani, L. Zhang, D. Bloor-Young, S. Patel, P. G. Woodman, G. C. Churchill and S. Hilfiker (2012). "Leucine-rich repeat kinase 2 regulates autophagy through a calcium-dependent pathway involving NAADP." Human Molecular Genetics **21**(3): 511-525.

Gonzalez-Covarrubias, V., D. Ghosh, S. S. Lakhman, L. Pendyala and J. G. Blanco (2007). "A functional genetic polymorphism on human carbonyl reductase 1 (CBR1 V88I) impacts on catalytic activity and NADPH binding affinity." Drug Metabolism and Disposition **35**(6): 973-980.

Graeff, R., Q. Liu, I. A. Kriksunov, Q. Hao and H. C. Lee (2006). "Acidic residues at the active sites of CD38 and ADP-ribosyl cyclase determine nicotinic acid adenine dinucleotide phosphate (NAADP) synthesis and hydrolysis activities." J Biol Chem **281**(39): 28951-28957.

Gurtovenko, A. A. and J. Anwar (2007). "Modulating the structure and properties of cell membranes: the molecular mechanism of action of dimethyl sulfoxide." J Phys Chem B **111**(35): 10453-10460.

Haller, T., P. Dietl, P. Deetjen and H. Volkl (1996). "The lysosomal compartment as intracellular calcium store in MDCK cells: A possible involvement in InsP(3)-mediated Ca2+ release." Cell Calcium **19**(2): 157-165.

Hohenegger, M., J. Suko, R. Gscheidlinger, H. Drobny and A. Zidar (2002). "Nicotinic acid-adenine dinucleotide phosphate activates the skeletal muscle ryanodine receptor." Biochemical Journal **367**: 423-431.

Howard, M., J. C. Grimaldi, J. F. Bazan, F. E. Lund, L. Santos-Argumedo, R. M. Parkhouse, T. F. Walseth and H. C. Lee (1993). "Formation and hydrolysis of cyclic ADP-ribose catalyzed by lymphocyte antigen CD38." Science **262**(5136): 1056-1059.

Ishibashi, K., M. Suzuki and M. Imai (2000). "Molecular cloning of a novel form (two-repeat) protein related to voltage-gated sodium and calcium channels." Biochem Biophys Res Commun **270**(2): 370-376.

Iwai, M., T. Michikawa, I. Bosanac, M. Ikura and K. Mikoshiba (2007). "Molecular basis of the isoform-specific ligand-binding affinity of inositol 1,4,5-trisphosphate receptors." J Biol Chem **282**(17): 12755-12764.

Jain, P., J. T. Slama, L. A. Perez-Haddock and T. F. Walseth (2010). "Nicotinic acid adenine dinucleotide phosphate analogues containing substituted nicotinic acid: effect of modification on Ca(2+) release." J Med Chem **53**(21): 7599-7612.

Jha, A., M. Ahuja, S. Patel, E. Brailoiu and S. Muallem (2014). "Convergent regulation of the lysosomal two-pore channel-2 by Mg2+, NAADP, PI(3,5) P2 and multiple protein kinases." Embo Journal **33**(5): 501-511.

Kashir, J., B. Heindryckx, C. Jones, P. De Sutter, J. Parrington and K. Coward (2010). "Oocyte activation, phospholipase C zeta and human infertility." Hum Reprod Update **16**(6): 690-703.

Kennedy, R. M. (2001). "Hydrophobic-Interaction Chromatography." Current Protocols in Protein Science **Unit 8.4**.

Kinnear, N. P., F. X. Boittin, J. M. Thomas, A. Galione and A. M. Evans (2004). "Lysosome-sarcoplasmic reticulum junctions - A trigger zone for calcium signaling by nicotinic acid adenine dinucleotide phosphate and endothelin-1." Journal of Biological Chemistry **279**(52): 54319-54326.

Kinnear, N. P., C. N. Wyatt, J. H. Clark, P. J. Calcraft, S. Fleischer, L. H. Jeyakumar, G. F. Nixon and A. M. Evans (2008). "Lysosomes co-localize with ryanodine receptor subtype 3 to form a trigger zone for calcium signalling by NAADP in rat pulmonary arterial smooth muscle." Cell Calcium **44**(2): 190-201.

Kirichok, Y., G. Krapivinsky and D. E. Clapham (2004). "The mitochondrial calcium uniporter is a highly selective ion channel." Nature **427**(6972): 360-364.

Kobayashi, S., A. V. Somlyo and A. P. Somlyo (1988). "Heparin inhibits the inositol 1,4,5-trisphosphate-dependent, but not the independent, calcium release induced by guanine nucleotide in vascular smooth muscle." Biochem Biophys Res Commun **153**(2): 625-631.

Kolisek, M., A. Beck, A. Fleig and R. Penner (2005). "Cyclic ADP-ribose and hydrogen peroxide synergize with ADP-ribose in the activation of TRPM2 channels." Molecular Cell **18**(1): 61-69.

Korb, O., T. Stutzle and T. E. Exner (2009). "Empirical scoring functions for advanced protein-ligand docking with PLANTS." J Chem Inf Model **49**(1): 84-96.

Krynetski, E. Y. and W. E. Evans (1998). "Pharmacogenetics of cancer therapy: getting personal." Am J Hum Genet **63**(1): 11-16.

Krynetski, E. Y., J. D. Schuetz, A. J. Galpin, C. H. Pui, M. V. Relling and W. E. Evans (1995). "A Single-Point Mutation Leading to Loss of Catalytic Activity in Human Thiopurine S-Methyltransferase." Proceedings of the National Academy of Sciences of the United States of America **92**(4): 949-953.

Lam, A. K. M., A. Galione, F. A. Lai and S. Zissimopoulos (2013). "Hax-1 identified as a two-pore channel (TPC)-binding protein." Febs Letters **587**(23): 3782-3786.

Lambrecht, G., K. Braun, S. Damer, M. Ganso, C. Hildebrandt, H. Ullmann, M. U. Kassack and P. Nickel (2002). "Structure-activity relationships of suramin and pyridoxal-5 '-phosphate derivatives as P2 receptor antagonists." Current Pharmaceutical Design **8**(26): 2371-2399.

Lamed, R., Y. Levin and M. Wilchek (1973). "Covalent Coupling of Nucleotides to Agarose for Affinity Chromatography." Biochimica Et Biophysica Acta **304**(2): 231-235.

Lange, I., S. Yamamoto, S. Partida-Sanchez, Y. Mori, A. Fleig and R. Penner (2009). "TRPM2 Functions as a Lysosomal Ca2+-Release Channel in beta Cells." Science Signaling **2**(71).

Langhorst, M. F., N. Schwarzmann and A. H. Guse (2004). "Ca2+ release via ryanodine receptors and Ca2+ entry: major mechanisms in NAADP-mediated Ca2+ signaling in T-lymphocytes." Cell Signal **16**(11): 1283-1289.

Lanner, J. T., D. K. Georgiou, A. D. Joshi and S. L. Hamilton (2010). "Ryanodine receptors: structure, expression, molecular details, and function in calcium release." Cold Spring Harb Perspect Biol **2**(11): a003996.

Laver, D. R., K. R. Eager, L. Taoube and G. D. Lamb (2000). "Effects of cytoplasmic and luminal pH on Ca(2+) release channels from rabbit skeletal muscle." Biophys J **78**(4): 1835-1851.

Ledbetter, M. W., J. K. Preiner, C. F. Louis and J. R. Mickelson (1994). "Tissue Distribution of Ryanodine Receptor Isoforms and Alleles Determined by Reverse Transcription-Polymerase Chain-Reaction." Journal of Biological Chemistry **269**(50): 31544-31551.

Lee, H. C. (1991). "Specific Binding of Cyclic Adp-Ribose to Calcium-Storing Microsomes from Sea-Urchin Eggs." Journal of Biological Chemistry **266**(4): 2276-2281.

Lee, H. C. and R. Aarhus (1991). "Adp-Ribosyl Cyclase - an Enzyme That Cyclizes Nad+ into a Calcium-Mobilizing Metabolite." Cell Regulation **2**(3): 203-209.

Lee, H. C. and R. Aarhus (1995). "A derivative of NADP mobilizes calcium stores insensitive to inositol trisphosphate and cyclic ADP-ribose." J Biol Chem **270**(5): 2152-2157.

Lee, H. C. and R. Aarhus (1997). "Structural determinants of nicotinic acid adenine dinucleotide phosphate important for its calcium-mobilizing activity." Journal of Biological Chemistry **272**(33): 20378-20383.

Lee, H. C. and R. Aarhus (1998). "Fluorescent analogs of NAADP with calcium mobilizing activity." Biochimica Et Biophysica Acta-General Subjects **1425**(1): 263-271.

Lee, H. C. and R. Aarhus (2000). "Functional visualization of the separate but interacting calcium stores sensitive to NAADP and cyclic ADP-ribose." J Cell Sci **113 Pt 24**: 4413-4420.

Lee, H. C., R. Aarhus, K. R. Gee and T. Kestner (1997). "Caged nicotinic acid adenine dinucleotide phosphate - Synthesis and use." Journal of Biological Chemistry **272**(7): 4172-4178.

Lennard, L. (1992). "The Clinical-Pharmacology of 6-Mercaptopurine." European Journal of Clinical Pharmacology **43**(4): 329-339.

Lennard, L., J. A. Vanloon, J. S. Lilleyman and R. M. Weinshilboum (1987). "Thiopurine Pharmacogenetics in Leukemia - Correlation of Erythrocyte Thiopurine Methyltransferase Activity and 6-Thioguanine Nucleotide Concentrations." Clinical Pharmacology & Therapeutics **41**(1): 18-25.

Lennard, L., J. A. Vanloon and R. M. Weinshilboum (1989). "Pharmacogenetics of Acute Azathioprine Toxicity - Relationship to Thiopurine Methyltransferase Genetic-Polymorphism." Clinical Pharmacology & Therapeutics **46**(2): 149-154.

Lewis, R. S. (2007). "The molecular choreography of a store-operated calcium channel." Nature **446**(7133): 284-287.

Lin-Moshier, Y. (2012). Investigation of proteins that interact with NAADP-Gated two-pore channels. Ph.D. dissertation, University of Minnesota.

Lin-Moshier, Y., M. V. Keebler, R. Hooper, M. J. Boulware, X. Liu, D. Churamani, M. E. Abood, T. F. Walseth, E. Brailoiu, S. Patel and J. S. Marchant (2014). "The Two-pore channel (TPC) interactome unmasks isoform-specific roles for TPCs in endolysosomal morphology and cell pigmentation." Proc Natl Acad Sci U S A.

Lin-Moshier, Y., T. F. Walseth, D. Churamani, S. M. Davidson, J. T. Slama, R. Hooper, E. Brailoiu, S. Patel and J. S. Marchant (2012). "Photoaffinity labeling of nicotinic acid adenine dinucleotide phosphate (NAADP) targets in mammalian cells." J Biol Chem **287**(4): 2296-2307.

Lloyd-Evans, E., A. J. Morgan, X. He, D. A. Smith, E. Elliot-Smith, D. J. Sillence, G. C. Churchill, E. H. Schuchman, A. Galione and F. M. Platt (2008). "Niemann-Pick disease type C1 is a sphingosine storage disease that causes deregulation of lysosomal calcium." Nat Med **14**(11): 1247-1255.

Lloyd-Evans, E., H. Waller-Evans, K. Peterneva and F. M. Platt (2010). "Endolysosomal calcium regulation and disease." Biochem Soc Trans **38**(6): 1458-1464.

Loenen, W. A. M. (2006). "S-adenosylmethionine: jack of all trades and master of everything?" Biochemical Society Transactions **34**: 330-333.

Low, A., H. G. Faulhammer and M. Sprinzl (1992). "Affinity labeling of GTP-binding proteins in cellular extracts." FEBS Lett **303**(1): 64-68.

Macgregor, A., M. Yamasaki, S. Rakovic, L. Sanders, R. Parkesh, G. C. Churchill, A. Galione and D. A. Terrar (2007). "NAADP controls cross-talk between distinct Ca2+ stores in the heart." Journal of Biological Chemistry **282**(20): 15302-15311.

Mackinnon, A. L. and J. Taunton (2009). "Target Identification by Diazirine Photo-Cross-linking and Click Chemistry." Curr Protoc Chem Biol **1**: 55-73.

Marks, A. R., P. Tempst, K. S. Hwang, M. B. Taubman, M. Inui, C. Chadwick, S. Fleischer and B. Nadal-Ginard (1989). "Molecular cloning and characterization of the ryanodine receptor/junctional channel complex cDNA from skeletal muscle sarcoplasmic reticulum." Proc Natl Acad Sci U S A **86**(22): 8683-8687.

Martin, J. L. and F. M. McMillan (2002). "SAM (dependent) I AM: the S-adenosylmethionine-dependent methyltransferase fold." Current Opinion in Structural Biology **12**(6): 783-793.

Masgrau, R., G. C. Churchill, A. J. Morgan, S. J. Ashcroft and A. Galione (2003). "NAADP: a new second messenger for glucose-induced Ca2+ responses in clonal pancreatic beta cells." Curr Biol **13**(3): 247-251.

Matsunaga, T., S. Shintani and A. Hara (2006). "Multiplicity of mammalian reductases for xenobiotic carbonyl compounds." Drug Metab Pharmacokinet **21**(1): 1-18.

Mitchell, K. J., F. A. Lai and G. A. Rutter (2003). "Ryanodine receptor type I and nicotinic acid adenine dinucleotide phosphate receptors mediate Ca2+ release from insulin-containing vesicles in living pancreatic beta-cells (MIN6)." Journal of Biological Chemistry **278**(13): 11057-11064.

Mojzisova, A., O. Krizanova, L. Zacikova, V. Kominkova and K. Ondrias (2001). "Effect of nicotinic acid adenine dinucleotide phosphate on ryanodine calcium release channel in heart." Pflugers Archiv-European Journal of Physiology **441**(5): 674-677.

Moreschi, I., S. Bruzzone, N. Bodrato, C. Usai, L. Guida, R. A. Nicholas, M. U. Kassack, E. Zocchi and A. De Flora (2008). "NAADP+ is an agonist of the human P2Y11 purinergic receptor." Cell Calcium **43**(4): 344-355.

Morgan, A. J. and A. Galione (2007). "Fertilization and nicotinic acid adenine dinucleotide phosphate induce pH changes in acidic Ca(2+) stores in sea urchin eggs." J Biol Chem **282**(52): 37730-37737.

Naylor, E., A. Arredouani, S. R. Vasudevan, A. M. Lewis, R. Parkesh, A. Mizote, D. Rosen, J. M. Thomas, M. Izumi, A. Ganesan, A. Galione and G. C. Churchill (2009). "Identification of a chemical probe for NAADP by virtual screening." Nature Chemical Biology **5**(4): 220-226.

Nelder, J. A. and R. Mead (1965). "A Simplex-Method for Function Minimization." Computer Journal **7**(4): 308-313.

Newton, C. L., G. A. Mignery and T. C. Sudhof (1994). "Co-expression in vertebrate tissues and cell lines of multiple inositol 1,4,5-trisphosphate (InsP3) receptors with distinct affinities for InsP3." J Biol Chem **269**(46): 28613-28619.

Noguchi, N., S. Takasawa, K. Nata, A. Tohgo, I. Kato, F. Ikehata, H. Yonekura and H. Okamoto (1997). "Cyclic ADP-ribose binds to FK506-binding protein 12.6 to release Ca2+ from islet microsomes." J Biol Chem **272**(6): 3133-3136.

Olson, L. E., D. Bedja, S. J. Alvey, A. J. Cardounel, K. L. Gabrielson and R. H. Reeves (2003). "Protection from doxorubicin-induced cardiac toxicity in mice with a null allele of carbonyl reductase 1." Cancer Research **63**(20): 6602-6606.

Otterness, D., C. Szumlanski, L. Lennard, B. Klemetsdal, J. Aarbakke, J. O. Park-Hah, H. Iven, K. Schmiegelow, E. Branum, J. O'Brien and R. Weinshilboum (1997). "Human thiopurine methyltransferase pharmacogenetics: gene sequence polymorphisms." Clin Pharmacol Ther **62**(1): 60-73.

Pankratov, Y. and U. Lalo (2014). "Calcium permeability of ligand-gated Ca2+ channels." European Journal of Pharmacology **739**: 60-73.

Passon, P. G. and D. E. Hultquist (1972). "Soluble Cytochrome-B5 Reductase from Human Erythrocytes." Biochimica Et Biophysica Acta **275**(1): 62-+.

Patel, S., G. C. Churchill, T. Sharp and A. Galione (2000). "Widespread distribution of binding sites for the novel Ca2+-mobilizing messenger, nicotinic acid adenine dinucleotide phosphate, in the brain." J Biol Chem **275**(47): 36495-36497.

Peiter, E., F. J. Maathuis, L. N. Mills, H. Knight, J. Pelloux, A. M. Hetherington and D. Sanders (2005). "The vacuolar Ca2+-activated channel TPC1 regulates germination and stomatal movement." Nature **434**(7031): 404-408.

Perraud, A. L., A. Fleig, C. A. Dunn, L. A. Bagley, P. Launay, C. Schmitz, A. J. Stokes, Q. Q. Zhu, M. J. Bessman, R. Penner, J. P. Kinet and A. M. Scharenberg (2001). "ADP-ribose gating of the calcium-permeable LTRPC2 channel revealed by Nudix motif homology." Nature **411**(6837): 595-599.

Pinton, P., T. Pozzan and R. Rizzuto (1998). "The Golgi apparatus is an inositol 1,4,5-trisphosphate-sensitive Ca2+ store, with functional properties distinct from those of the endoplasmic reticulum." Embo Journal **17**(18): 5298-5308.

Piper, R. C. and J. P. Luzio (2004). "CUPpling calcium to lysosomal biogenesis." Trends Cell Biol **14**(9): 471-473.

Pitt, S. J., T. M. Funnell, M. Sitsapesan, E. Venturi, K. Rietdorf, M. Ruas, A. Ganesan, R. Gosain, G. C. Churchill, M. X. Zhu, J. Parrington, A. Galione and R. Sitsapesan (2010). "TPC2 Is a Novel NAADP-sensitive Ca2+ Release Channel, Operating as a Dual Sensor of Luminal pH and Ca2+." Journal of Biological Chemistry **285**(45): 35039-35046.

Pitt, S. J., A. K. Lam, K. Rietdorf, A. Galione and R. Sitsapesan (2014). "Reconstituted human TPC1 is a proton-permeable ion channel and is activated by NAADP or Ca2+." Sci Signal **7**(326): ra46.

Pryor, P. R., F. Reimann, F. M. Gribble and J. P. Luzio (2006). "Mucolipin-1 is a lysosomal membrane protein required for intracellular lactosylceramide traffic." Traffic **7**(10): 1388-1398.

Qureshi, O. S., A. Paramasivam, J. C. H. Yu and R. D. Murrell-Lagnado (2007). "Regulation of P2X(4) receptors by lysosomal targeting, glycan protection and exocytosis." Journal of Cell Science **120**(21): 3838-3849.

Ramsey, I. S., M. Delling and D. E. Clapham (2006). "An introduction to TRP channels." Annual Review of Physiology **68**: 619-647.

Ringer, S. (1883). "A third contribution regarding the Influence of the Inorganic Constituents of the Blood on the Ventricular Contraction." J Physiol **4**(2-3): 222-225.

Rosen, D., A. M. Lewis, A. Mizote, J. M. Thomas, P. K. Aley, S. R. Vasudevan, R. Parkesh, A. Galione, M. Izumi, A. Ganesan and G. C. Churchill (2009). "Analogues of the Nicotinic Acid Adenine Dinucleotide Phosphate (NAADP) Antagonist Ned-19 Indicate Two Binding Sites on the NAADP Receptor." Journal of Biological Chemistry **284**(50): 34930-34934.

Ross, C. A., J. Meldolesi, T. A. Milner, T. Satoh, S. Supattapone and S. H. Snyder (1989). "Inositol 1,4,5-trisphosphate receptor localized to endoplasmic reticulum in cerebellar Purkinje neurons." Nature **339**(6224): 468-470.

Ruas, M., L. C. Davis, C. C. Chen, A. J. Morgan, K. T. Chuang, T. F. Walseth, C. Grimm, C. Garnham, T. Powell, N. Platt, F. M. Platt, M. Biel, C. Wahl-Schott, J. Parrington and A. Galione (2015). "Expression of Ca2+-permeable two-pore channels rescues NAADP signalling in TPC-deficient cells." EMBO J.

Ruas, M., K. Rietdorf, A. Arredouani, L. C. Davis, E. Lloyd-Evans, H. Koegel, T. M. Funnell, A. J. Morgan, J. A. Ward, K. Watanabe, X. Cheng, G. C. Churchill, M. X. Zhu, F. M. Platt, G. M. Wessel, J. Parrington and A. Galione (2010). "Purified TPC isoforms form NAADP receptors with distinct roles for Ca(2+) signaling and endolysosomal trafficking." Curr Biol **20**(8): 703-709.

Rybalchenko, V., M. Ahuja, J. Coblentz, D. Churamani, S. Patel, K. Kiselyov and S. Muallem (2012). "Membrane potential regulates nicotinic acid adenine dinucleotide phosphate (NAADP) dependence of the pH- and Ca2+-sensitive organellar two-pore channel TPC1." J Biol Chem **287**(24): 20407-20416.

Sano, Y., K. Inamura, A. Miyake, S. Mochizuki, H. Yokoi, H. Matsushime and K. Furuichi (2001). "Immunocyte Ca2+ influx system mediated by LTRPC2." Science **293**(5533): 1327-1330.

Schmid, F., S. Bruhn, K. Weber, H. W. Mittrucker and A. H. Guse (2011). "CD38: A NAADP degrading enzyme." Febs Letters **585**(22): 3544-3548.

Schmid, F., R. Fliegert, T. Westphal, A. Bauche and A. H. Guse (2012). "Nicotinic Acid Adenine Dinucleotide Phosphate (NAADP) Degradation by Alkaline Phosphatase." Journal of Biological Chemistry **287**(39): 32525-32534.

Schubert, H. L., R. M. Blumenthal and X. D. Cheng (2003). "Many paths to methyltransfer: a chronicle of convergence." Trends in Biochemical Sciences **28**(6): 329-335.

Smith, A. L., D. B. Friedman, H. Yu, R. H. Carnahan and A. B. Reynolds (2011). "ReCLIP (reversible cross-link immuno-precipitation): an efficient method for interrogation of labile protein complexes." PLoS One **6**(1): e16206.

Smith, J. S., T. Imagawa, J. J. Ma, M. Fill, K. P. Campbell and R. Coronado (1988). "Purified Ryanodine Receptor from Rabbit Skeletal-Muscle Is the Calcium-Release Channel of Sarcoplasmic-Reticulum." Journal of General Physiology **92**(1): 1-26.

Stanulla, M., E. Schaeffeler, T. Flohr, G. Cario, A. Schrauder, M. Zimmermann, K. Welte, W. D. Ludwig, C. R. Bartram, U. M. Zanger, M. Eichelbaum, M. Schrappe and M. Schwab (2005). "Thiopurine methyltransferase (TPMT) genotype and early treatment response to mercaptopurine in childhood acute lymphoblastic leukemia." Jama-Journal of the American Medical Association **293**(12): 1485-1489.

States, D. J., T. F. Walseth and H. C. Lee (1992). "Similarities in amino acid sequences of Aplysia ADP-ribosyl cyclase and human lymphocyte antigen CD38." Trends Biochem Sci **17**(12): 495.

Stehno-Bittel, L., A. Luckhoff and D. E. Clapham (1995). "Calcium release from the nucleus by InsP3 receptor channels." Neuron **14**(1): 163-167.

Sun, L. (2016). Interactions between Human Two-pore Channels and Nonaspanin Proteins. Master thesis, University of Minnesota.

Supattapone, S., P. F. Worley, J. M. Baraban and S. H. Snyder (1988). "Solubilization, Purification, and Characterization of an Inositol Trisphosphate Receptor." Journal of Biological Chemistry **263**(3): 1530-1534.

Takeshima, H., S. Nishimura, T. Matsumoto, H. Ishida, K. Kangawa, N. Minamino, H. Matsuo, M. Ueda, M. Hanaoka, T. Hirose and et al. (1989). "Primary structure and expression from complementary DNA of skeletal muscle ryanodine receptor." Nature **339**(6224): 439-445.

Taylor, C. W., A. A. Genazzani and S. A. Morris (1999). "Expression of inositol trisphosphate receptors." Cell Calcium **26**(6): 237-251.

Thrower, E. C., R. E. Hagar and B. E. Ehrlich (2001). "Regulation of Ins(1,4,5)P-3 receptor isoforms by endogenous modulators." Trends in Pharmacological Sciences **22**(11): 580-586.

Trabbic, C., T. Walseth and J. Slama (2012). "Synthesis, Biochemical Activity, and Structure-Activity Relationship Among Nicotinic Acid Adenine Dinucleotide Phosphate (NAADP) Analogs." Messenger.

Trott, O. and A. J. Olson (2010). "Software News and Update AutoDock Vina: Improving the Speed and Accuracy of Docking with a New Scoring Function, Efficient Optimization, and Multithreading." Journal of Computational Chemistry **31**(2): 455-461.

Usami, N., K. Kitahara, S. Ishikura, M. Nagano, S. Sakai and A. Hara (2001). "Characterization of a major form of human isatin reductase and the reduced metabolite." European Journal of Biochemistry **268**(22): 5755-5763.

Vasilescu, J., X. C. Guo and J. Kast (2004). "Identification of protein-protein interactions using in vivo cross-linking and mass spectrometry." Proteomics **4**(12): 3845-3854.

Wall, P. E. (2005). Thin-layer chromatography : a modern practical approach. Cambridge, Royal Society of Chemistry.

Walseth, T. F., R. Aarhus, J. A. Kerr and H. C. Lee (1993). "Identification of Cyclic Adp-Ribose-Binding Proteins by Photoaffinity-Labeling." Journal of Biological Chemistry **268**(35): 26686-26691.

Walseth, T. F., Y. Lin-Moshier, P. Jain, M. Ruas, J. Parrington, A. Galione, J. S. Marchant and J. T. Slama (2012). "Photoaffinity labeling of high affinity nicotinic acid adenine dinucleotide phosphate (NAADP)-binding proteins in sea urchin egg." J Biol Chem **287**(4): 2308-2315.

Walseth, T. F., Y. Lin-Moshier, K. Weber, J. S. Marchant, J. T. Slama and A. H. Guse (2012). "Nicotinic Acid Adenine Dinucleotide 2'-Phosphate (NAADP) Binding Proteins in T-Lymphocytes." Messenger (Los Angel) **1**(1): 86-94.

Wang, X., X. Zhang, X. P. Dong, M. Samie, X. Li, X. Cheng, A. Goschka, D. Shen, Y. Zhou, J. Harlow, M. X. Zhu, D. E. Clapham, D. Ren and H. Xu (2012). "TPC proteins are phosphoinositide-activated sodium-selective ion channels in endosomes and lysosomes." Cell **151**(2): 372-383.

Warren, G. L., C. W. Andrews, A. M. Capelli, B. Clarke, J. LaLonde, M. H. Lambert, M. Lindvall, N. Nevins, S. F. Semus, S. Senger, G. Tedesco, I. D. Wall, J. M. Woolven, C. E. Peishoff and M. S. Head (2006). "A critical assessment of docking programs and scoring functions." Journal of Medicinal Chemistry **49**(20): 5912-5931.

Weinshilboum, R. M. and S. L. Sladek (1980). "Mercaptopurine Pharmacogenetics - Monogenic Inheritance of Erythrocyte Thiopurine Methyltransferase Activity." American Journal of Human Genetics **32**(5): 651-662.

Weiss, W., F. Weiland and A. Gorg (2009). "Protein detection and quantitation technologies for gel-based proteome analysis." Methods Mol Biol **564**: 59-82.

Wennerstrand, P., A. Blissing and L. G. Martensson (2017). "In Vitro Protein Stability of Two Naturally Occurring Thiopurine S-Methyltransferase Variants: Biophysical Characterization of TPMT*6 and TPMT*8." Acs Omega **2**(8): 4991-4999.

Wermuth, B. (1981). "Purification and Properties of an Nadph-Dependent Carbonyl Reductase from Human-Brain - Relationship to Prostaglandin 9-Ketoreductase and Xenobiotic Ketone Reductase." Journal of Biological Chemistry **256**(3): 1206-1213.

Wermuth, B., K. L. Platts, A. Seidel and F. Oesch (1986). "Carbonyl reductase provides the enzymatic basis of quinone detoxication in man." Biochem Pharmacol **35**(8): 1277-1282.

Wienken, C. J., P. Baaske, U. Rothbauer, D. Braun and S. Duhr (2010). "Protein-binding assays in biological liquids using microscale thermophoresis." Nat Commun **1**: 100.

Wilchek, M. and R. Lamed (1974). "Immobilized nucleotides for affinity chromatography." Methods Enzymol **34**: 475-479.

Wilson, H. L. and A. Galione (1998). "Differential regulation of nicotinic acid-adenine dinucleotide phosphate and cADP-ribose production by cAMP and cGMP." Biochem J **331 (Pt 3)**: 837-843.

Wirth, H. and B. Wermuth (1992). "Immunohistochemical localization of carbonyl reductase in human tissues." J Histochem Cytochem **40**(12): 1857-1863.

Woodson, L. C. and R. M. Weinshilboum (1983). "Human-Kidney Thiopurine Methyltransferase - Purification and Biochemical-Properties." Biochemical Pharmacology **32**(5): 819-826.

Xiao, B., M. J. Sanders, D. Carmena, N. J. Bright, L. F. Haire, E. Underwood, B. R. Patel, R. B. Heath, P. A. Walker, S. Hallen, F. Giordanetto, S. R. Martin, D. Carling and S. J. Gamblin (2013). "Structural basis of AMPK regulation by small molecule activators." Nature Communications **4**.

Xu, H. and D. Ren (2015). "Lysosomal physiology." Annu Rev Physiol **77**: 57-80.

Yamaguchi, S., A. Jha, Q. Li, A. A. Soyombo, G. D. Dickinson, D. Churamani, E. Brailoiu, S. Patel and S. Muallem (2011). "Transient receptor potential mucolipin 1 (TRPML1) and two-pore channels are functionally independent organellar ion channels." J Biol Chem **286**(26): 22934-22942.

Yamasaki, M., R. Masgrau, A. J. Morgan, G. C. Churchill, S. Patel, S. J. Ashcroft and A. Galione (2004). "Organelle selection determines agonist-specific Ca2+ signals in pancreatic acinar and beta cells." J Biol Chem **279**(8): 7234-7240.

Yee, L. (2002). Characterization of Nicotinic Acid Adenine Dinucleotide Phosphate Signaling System. Master thesis, University of Minnesota.

Yu, X., S. Carroll, J. L. Rigaud and G. Inesi (1993). "H+ countertransport and electrogenicity of the sarcoplasmic reticulum Ca2+ pump in reconstituted proteoliposomes." Biophys J **64**(4): 1232-1242.

Zalk, R., S. E. Lehnart and A. R. Marks (2007). "Modulation of the ryanodine receptor and intracellular calcium." Annual Review of Biochemistry **76**: 367-385.

Zhang, F., S. Jin, F. Yi and P. L. Li (2009). "TRP-ML1 functions as a lysosomal NAADP-sensitive Ca2+ release channel in coronary arterial myocytes." J Cell Mol Med **13**(9B): 3174-3185.

Zhang, F. and P. L. Li (2007). "Reconstitution and characterization of a nicotinic acid adenine dinucleotide phosphate (NAADP)-sensitive Ca2+ release channel from liver Lysosomes of rats." Journal of Biological Chemistry **282**(35): 25259-25269.

Zhang, F., M. Xu, W. Q. Han and P. L. Li (2011). "Reconstitution of lysosomal NAADP-TRP-ML1 signaling pathway and its function in TRP-ML1(-/-) cells." American Journal of Physiology-Cell Physiology **301**(2): C421-C430.

Zhang, F., G. Zhang, A. Y. Zhang, M. J. Koeberl, E. Wallander and P. L. Li (2006). "Production of NAADP and its role in Ca2+ mobilization associated with lysosomes in coronary arterial myocytes." Am J Physiol Heart Circ Physiol **291**(1): H274-282.

Zhang, K., W. Sun, L. Huang, K. Zhu, F. Pei, L. Zhu, Q. Wang, Y. Lu, H. Zhang, H. Jin, L. H. Zhang, L. Zhang and J. Yue (2017). "Identifying Glyceraldehyde 3-Phosphate Dehydrogenase as a

Cyclic Adenosine Diphosphoribose Binding Protein by Photoaffinity Protein-Ligand Labeling Approach." J Am Chem Soc **139**(1): 156-170.

Zhu, D. (2012). Characterization of Nicotinic Acid Adenine Dinucleotide Phosphate (NAADP) Binding Protein. Master dissertation, University of Oxford.

Zhu, M. X., J. J. Ma, J. Parrington, A. Galione and A. M. Evans (2010). "TPCs: Endolysosomal channels for Ca2+ mobilization from acidic organelles triggered by NAADP." Febs Letters **584**(10): 1966-1974.

Zong, X., M. Schieder, H. Cuny, S. Fenske, C. Gruner, K. Rotzer, O. Griesbeck, H. Harz, M. Biel and C. Wahl-Schott (2009). "The two-pore channel TPCN2 mediates NAADP-dependent Ca(2+)-release from lysosomal stores." Pflugers Arch **458**(5): 891-899.

Zuo, T., D. L. Liu, W. Lv, X. D. Wang, J. W. Wang, M. Y. Lv, W. L. Huang, J. X. Wu, H. H. Zhang, H. W. Jin, L. R. Zhang, W. Kong and X. H. Yu (2012). "Small-Molecule Inhibition of Human Immunodeficiency Virus Type 1 Replication by Targeting the Interaction between Vif and ElonginC." Journal of Virology **86**(10): 5497-5507.